STUDIES OF THE DEFECTS IN SINGLE CRYSTALS OF SODIUM CHLORIDE

Thesis

submitted for the degree of

DOCTOR OF PHILOSOPHY

of the

University of Kent at Canterbury

by

Neil Brown, B.Sc. (Glasgow)

September, 1967.

ACKNOWLEDGEMENTS

I should like to express my appreciation and thanks to my supervisor, Dr. I.M. Hoodless, for his constant help and guidance throughout the course of this work.

I am also indebted to the Science Research Council for the award of a Research Studentship, which provided me with financial support for the period during which this work was done.

ABSTRACT

Measurements of ionic conductance in divalent cation-doped single crystals of NaCl have been used to investigate the impurity-cation vacancy association in these crystals. The measurements were made over the temperature range 150° - 650°C on crystals of NaCl doped with Mg^{2+}, Mn^{2+}, Ca^{2+}, Sr^{2+}, Pb^{2+} and Ba^{2+} impurity ions. Four regions of ionic conductance have been observed; these correspond to an intrinsic region (I), an impurity-induced free vacancy region (II), an association region (III) and an impurity precipitation region (IV).

The conductivity results in regions II and III have been analysed in terms of the Lidiard association theory, and enthalpies of association of 0.31 eV, 0.28 eV, 0.30 eV, 0.53 eV, 0.56 eV and 0.79 eV have been obtained for Mg^{2+}, Mn^{2+}, Ca^{2+}, Sr^{2+}, Pb^{2+} and Ba^{2+} impurity-cation vacancy complexes respectively. A theoretical calculation of the binding energy of the Ba^{2+}-cation vacancy complex has been made and this result, along with the results of previous theoretical calculations, indicates that the enthalpy of association should increase as the impurity ion size increases. The enthalpies of association deduced from the conductance

measurements are in agreement with this theoretical prediction for impurity ions which are larger than the Na^+ ion. With the smaller impurity ions however, there is little change in the enthalpy of association with change in impurity ion size. It is suggested that in the case of large impurity ions a cation vacancy situated in the nearest-neighbour position to the impurity will substantially reduce the lattice distortion and hence form the more stable complex. On the other hand, the contraction of the lattice surrounding a small impurity ion may favour the cation vacancy in the next-nearest-neighbour position. Therefore, for small impurity ions, next-nearest-neighbour association may become significant.

A detailed study of the association reactions in the $NaCl-MnCl_2$ system has been made from ionic conductance, Mn^{54} impurity-diffusion and electron spin resonance measurements. The enthalpy of association, as determined from the conductance and impurity-diffusion studies, is 0.28 eV and 0.33 eV respectively. The agreement of the values obtained by the different methods is much better than has previously been observed for other impurity ions, and it is suggested that the discrepancies observed in earlier work are due to the effect of next-nearest-neighbour interactions. The

electron spin resonance measurements on the $NaCl-MnCl_2$ system indicate that the nearest-neighbour complex is slightly more stable than the next-nearest-neighbour complex, and the conductance and impurity-diffusion measurements confirm this.

The entropy of formation of complexes has been examined from the ionic conductance and impurity diffusion data. The inference is that the entropy of formation of the larger impurity ion complexes is positive while for the smaller impurity ion complexes it is negative. A possible explanation, in terms of close-range exponential repulsions and lattice dilations, is proposed assuming that the entropy of formation depends only on the lattice frequencies before and after formation of the complex.

The conductance measurements have also been used to study the solubility of the impurities in the NaCl lattice. Energies of solution of 1.44 eV, 0.92 eV, 1.28 eV, 1.80 eV, 1.90 eV and 2.00 eV have been obtained for the solubilities of Mg^{2+}, Mn^{2+}, Ca^{2+}, Sr^{2+}, Pb^{2+} and Ba^{2+} impurity ions respectively. The results show that impurity ion size is a more important factor than impurity ion polarisability in determining the solubility. The relatively low solubility of ions which are appreciably different in size from the Na^{+} ion can be explained in

terms of the lattice distortion due to the misfit of these impurity ions.

The energy for formation of a Schottky defect and the energy for mobility of a cation vacancy have also been determined from the measurements of ionic conductance. A value of 2.20 eV was obtained for the energy for formation of a Schottky defect, and this is in good agreement with the results of other workers. The energy for mobility of a cation vacancy was found to be 0.76 eV, a value which compares favourably with the results reported here of some studies of Na^{+} ion self-diffusion on 'pure' and Ca^{2+}-doped crystals of NaCl.

CONTENTS

CHAPTER I

INTRODUCTION

1.1. The Nature of Defects in Ionic Solids

Any compound in which the arrangement of the constituent atoms or ions is not completely regular is said to be non-ideal or defective. No crystal structure is perfect and at temperatures above the absolute zero, it is thermodynamically necessary for a crystal lattice to contain defects. The concept of an ionic crystal as a perfectly-ordered array of ions denies the interpretation of many well-known phenomena in the solid state, and it is in fact the presence of these defects and their ability to move through the crystal lattice which accounts for many of the physical and chemical properties of solids.

Two important groups of imperfection can be distinguished in ionic crystals:

(a) Point or lattice defects.

(b) Gross defects.

The former, as their name implies, usually involve individual lattice positions and their sphere of influence is restricted to the ions in the immediate neighbourhood of the defect. The principal defects of this type are vacant lattice sites, interstitial ions or impurity atoms in lattice positions.

On the other hand, gross defects, which may be sub-divided into surface and line defects, are imperfections which involve the misalignment of relatively large numbers of atoms or ions. There are two types of surface defect, external and internal. The former is associated with the disorder represented by the discontinuity at the surface while the latter occurs when the crystal lattice changes from one orientation to another, that is when there is a misorientation of two crystal grains. Line defects have an appreciable extension in one dimension and are generally referred to as dislocations. They are particularly important in determining the mechanical properties of solids.

The effects of point and gross defects can be studied separately by using good quality single crystals and powdered compacts of a crystalline solid respectively. Ionic crystals lend themselves to this study, and the alkali halides in particular have played an important part in the development of the theory of point defects.

1.2. Thermally Created Point Defects in Ionic Crystals

There are two types of thermodynamic defect in ionic crystals: (i) Schottky defects[1] and (ii) Frenkel defects[2].

A Schottky defect consists of a vacant cation site and a vacant anion site; the two missing ions are considered to have migrated to the surface of the crystal. Thus, both the

cation and anion lattices are incomplete, Fig. 1.

A Frenkel defect consists of a vacant lattice site, with the ion which should have ideally occupied that site occupying an interstitial position in the lattice, Fig. 2. If Frenkel defects are present, an incomplete cation lattice will be more common than an incomplete anion lattice, since cations are in general smaller than anions and hence can be more easily squeezed into the alternative interstitial positions.

Although any crystal contains both types of defect, one type normally predominates. Frenkel defects are more easily formed in those compounds in which the constituent ions are easily distorted. Such compounds are formed by strongly polarising cations and easily polarisable anions, and are thus compounds of appreciable covalent character. They are also more likely where there is an appreciable difference in size between the cation and the anion.

In most of the alkali halides there is not a great disparity in size between cation and anion, and polarisation is not appreciable since the cations have inert gas type of electronic configurations, so that these crystals contain Schottky defects almost exclusively.

Vacancies represent places where the lattice cohesion is lost so that they must require energy for their formation. To squeeze an ion into an interstitial position likewise must require energy. The concentration of these defects in

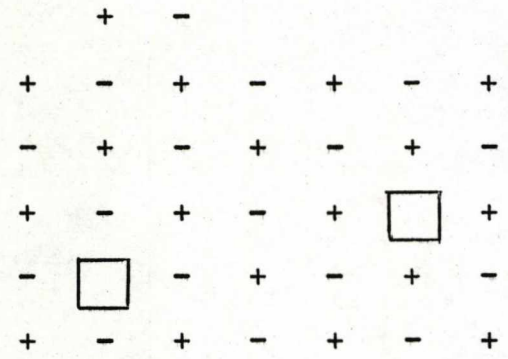

Fig. 1. - Schottky Defect.

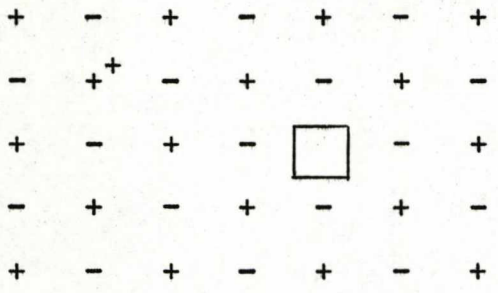

Fig. 2. - Frenkel Defect.

conditions of thermal equilibrium will thus be governed by a Boltzmann exponential factor, and can be calculated as a function of temperature from normal thermodynamic considerations. The calculation takes the following form for the determination of the equilibrium vacancy concentration in an ionic crystal containing Schottky defects.

Consider the crystal to contain N anions and cations and suppose there are n Schottky defects present at a particular temperature T. The presence of these Schottky defects increases the configurational entropy of the crystal, according to the Boltzmann relationship, by an amount,

$$\Delta S = k \ln \left[\frac{N!}{(N-n)!\, n!}\right]^2 \qquad (1.1)$$

The increase in internal energy is nW, where W is the free energy of formation of one Schottky defect. Hence, since $\Delta G = \Delta H - T\Delta S$,

$$\Delta G = \Delta G_o + nW - kT \ln \left[\frac{N!}{(N-n)!\, n!}\right]^2 \qquad (1.2)$$

The additional term nW is linear in n, since the assumption is that there is no interaction among the defects. The general equation of equilibrium is

$$\partial G = 0 \qquad (1.3)$$

so that by minimising ΔG with respect to n, and applying Stirling's approximation, equation (12) becomes

$$\left[\frac{\partial(\Delta G)}{\partial n}\right]_{P,T} = W - kT \ln \left[\frac{N-n}{n}\right]^2 = 0 \qquad (1.4)$$

$$\therefore \left[\frac{N-n}{n}\right]^2 = \exp(W/kT) \qquad (1.5)$$

Since the extent of Schottky disorder is usually small, that is, N-n = N, equation (15) reduces to

$$\left(\frac{n}{N}\right)^2 = \exp(-W/kT) \qquad (1.6)$$

or

$$n = N \exp(-W/2kT) \qquad (1.7)$$

A similar type of derivation for Frenkel disorder gives

$$\frac{n}{(N.N_i)^{\frac{1}{2}}} = \exp(-W/2kT) \qquad (1.8)$$

The derivation is simplified since it has not taken into account the effects of the lattice vibrations and thermal expansion of the crystal, upon the formation energy of the defects. As the temperature rises, thermal expansion leads to a decrease W which can be represented as,

$$W_T = W_o + \alpha V_o T(dW/dV) \qquad (1.9)$$

where W_o and V_o are respectively the energy to form a defect and the volume of the crystal at 0^oK; α is the coefficient of thermal expansion for the crystal.

The presence of defects produces changes in the vibrational frequency of the ions. The correction for this introduces a pre-exponential factor, γ, which is given by

$$\gamma = (\frac{\nu}{\nu'})^x \qquad (1.10)$$

where ν is the normal lattice frequency, ν' is the frequency of an ion adjacent to a defect and x is the number of nearest neighbour ions.

Equation (1.7) now becomes

$$n = \gamma BN \exp(-W/2kT) \qquad (1.11)$$

where $$B = \exp(-\frac{\alpha V_o}{2k} \cdot \frac{dW}{dV})$$

In ionic crystals, the pre-exponential factor, γ, can have a value between 10 and 10^4 for Schottky defects, but it is several orders of magnitude smaller for Frenkel defects[3].

1.3. Gross Defects

Gross defects result in a dislocation network within a crystal. They can extend over many lattice spacings and are not confined to one particular site. Fundamentally, they are non-equilibrium states unlike the normal thermodynamic point defect. Dislocations of two kinds can be produced; these are

(i) Screw dislocations,

and (ii) Edge dislocations.

A crystal containing a screw dislocation is not made up of parallel atomic planes arranged one above the other. It is in fact a single atomic plane built up in the form of a spiral. A screw dislocation may be thought of as being produced by the displacing of one part of a crystal, usually one atomic spacing, relative to the remainder of the crystal, the displacement terminating within the crystal, Fig. 3. They are of extreme importance in connection with crystal growth from the vapour or solution[4]. In these cases crystal growth is a result of supersaturation and of the conditions on the surface of the growing crystal. It is difficult to imagine a continuous growth process without the presence of a screw dislocation. In order for atoms deposited on the surface to be firmly bound, the surface must contain steps, since at the corners of these steps they can be bound by two or more atoms. A crystal without dislocations may have such steps on its faces, however, these will gradually become filled up, so that the surface of the crystal ultimately becomes flat and unsuitable for further growth. If the crystal has a screw dislocation continuous growth becomes possible, since as new material is deposited, the step simply rotates but never disappears.

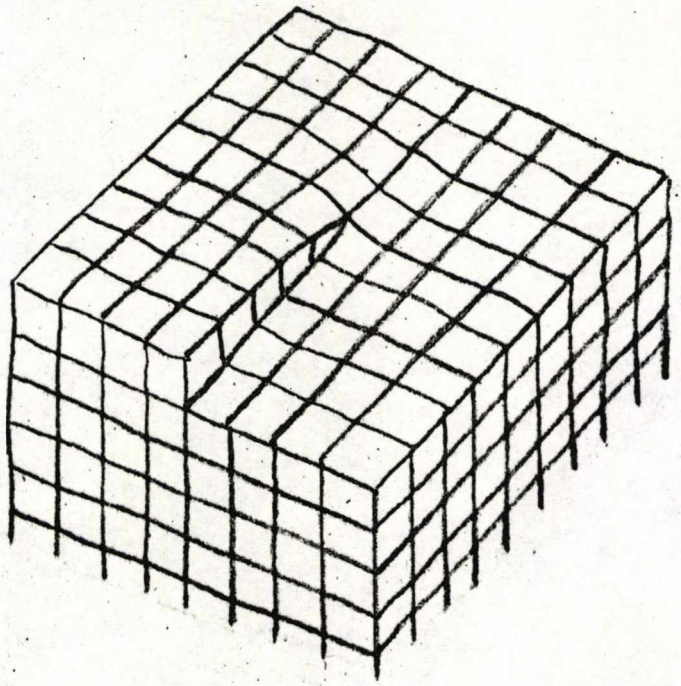

Fig. 3. - Screw Dislocation.

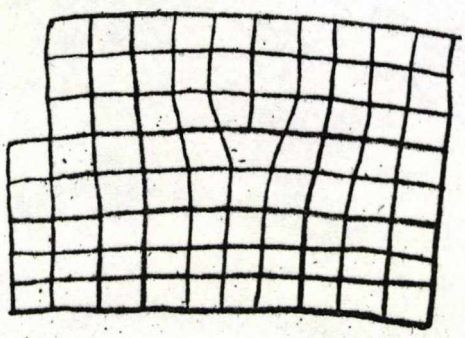

Fig. 4. - Edge Dislocation.

Edge dislocations arise by the introduction of an extra plane of atoms part way into the crystal, Fig. 4. The internal boundary of this extra plane of atoms forms the dislocation line, which is not necessarily a straight line since jump to an adjacent slip-plane is possible. The point at which the jump is made is called a "jog", and since these may be charged[3], they determine to a large extent the properties of the edge dislocation.

The movement of dislocations can have a marked effect on the concentration of defects in a crystal. The charged nature of dislocation jogs restricts the type of movement and to preserve electroneutrality a moving dislocation produces Schottky defects in an ionic crystal. Moreover, a stationary dislocation can affect the local concentration of point defects, since it can act as a source or sink for point defects.

Schottky and Frenkel defects can be formed at surfaces, grain boundaries or dislocation jogs and since the energies of formation of each component of the defect pair are different, the thermal equilibrium concentrations of each will also be unequal[5,6]. For example, in NaCl sodium ion vacancies are more easily formed than chlorine ion vacancies. As the temperature is raised, sodium ion vacancies having the lower activation energy for movement, will be emitted into the crystal leaving a net charge on the internal surface. The resulting space charge acts to

prevent any further movement of sodium ion vacancies and encourages the chlorine ion vacancies to move. Each edge dislocation therefore has a space charge layer associated with it, the excess of anion vacancies around the dislocation being balanced by an excess of cation vacancies situated in the bulk of the crystal. The magnitude and width of the space charge layer depends on temperature and the difference in formation energies of anion and cation vacancies. The width of the space charge layer in NaCl has been estimated to be 2.2×10^{-5} cm at $600^{\circ}K$ and 1.3×10^{-6} cm at $900^{\circ}K$[5]. At lower temperatures these boundary effects are significant, and can play an important role in ion migration.

1.4. Impurity Created Defects

When a divalent metal impurity ion is incorporated into an alkali halide such as NaCl it can enter the lattice substitutionally[7]. Since the crystal must be electrically neutral, each divalent impurity ion replaces two sodium ions with the result that a concentration of positive ion vacancies, equal to the concentration of impurity ions, is introduced into the crystal. These impurity created vacancies will be very important particularly at low temperatures where the concentrations of thermally created Schottky defects is low.

Equation (17) can be rewritten in the form

$$x_1 x_2 = \text{constant} = x_o^2 \qquad (1.12)$$

where x_1 and x_2 are the mole fractions of positive and negative ion vacancies respectively, and x_o is the mole fraction of thermal vacancies in a pure crystal. The effect of adding a mole fraction c of divalent impurity is to produce an equal number of cation vacancies. Then for electroneutrality

$$x_1 = x_2 + c \qquad (1.13)$$

Equation (1.12) then becomes

$$x_1(x_1 - c) = x_o^2$$

$$x_1 = \frac{c}{2}[1 + (1 + 4x_o^2/c^2)] \qquad (1.14)$$

This relationship shows the change from intrinsic conduction at high temperatures where $x_o >> c$, to impurity controlled conduction at low temperatures where $x_o << c$.

Divalent cation impurities in substitutional solution may also have an effect on space charge layers in the crystal. At lower temperatures the impurity ions tend to move towards dislocations, which can act as

nucleation sites or centres for precipitation. The presence of divalent impurities at the electrically charged dislocations will reduce the magnitude of the space charge, and possibly even reverse the charge[6].

1.5. Transport Processes in Ionic Crystals

The concept of an ionic crystal as a perfectly ordered array of ions denies the interpretation of many well-known phenomena in the solid state. Transport of charge depends upon the existence of structural imperfections, and their ability to move through the lattice.

The mechanism by which an ionic crystal carries an electric current, for example, is such that as one ion moves into a vacancy situated nearby, it leaves its own site vacant, so that a second ion in its turn can move into the site left vacant. This process is continued by further ions so that the net result is transport of charge throughout the entire crystal.

Experimental investigations of ion movement in ionic crystals revolve around two closely related techniques. The self-diffusion of ions may be studied using radioactive isotopes of the diffusing species in tracer concentrations, and the measurement of ionic conductivity and transport of charge can also provide information on the concentration and mobility of defects.

In an ionic crystal containing Schottky defects the electrical conductivity, σ, is of the form

$$\sigma = n_1 q_1 \mu_1 + n_2 q_2 \mu_2 \qquad (1.15)$$

where n_1 and n_2 represent the number of cation and anion vacancies per cc., q is the electronic charge on the ions and μ_1 and μ_2 are the cation and anion mobilities respectively. Transport number measurements pioneered by Tubandt[8] have shown that for a number of alkali halides, in particular LiCl, NaCl and KCl, the conductivity is almost totally cationic except at temperatures near the melting point. Equation (1.15), when applied to an alkali halide such as NaCl, can therefore be reduced to

$$\sigma = n_1 q_1 \mu_1 \qquad (1.16)$$

This equation may be expanded by introducing the equation for the ion mobility[9],

$$\mu = (\nu a^2 \frac{Cq}{kT}) \exp(-U/kT) \qquad (1.17)$$

where ν is the lattice vibrational frequency, $\underline{a}$ is the anion-cation distance and C is a thermal expansion correction term to the height of the energy barrier for mobility, U. Substituting equations (1.17) and (1.11) into (1.16) gives

$$\sigma = \frac{\gamma BCN\, a^2 q^2 \nu}{kT} \exp(-(U + W/2)/kT) \qquad (1.18)$$

The corresponding expression for the diffusion coefficient is given by

$$D = \gamma BC\sqrt{a^2} \exp(-(U + W/2)/kT) \qquad (1.19)$$

Hence, a plot of $\log_{10}\sigma$ or $\log_{10}D$ against $1/T$ should give a straight line, the gradient of which is $-(U + W/2)/2.3R$.

In practice, at least four ranges of conduction are observed over the temperature range $0^{\circ}C$-melting point, Fig. 5. These have been labelled according to the Dreyfus and Nowick[10] notation. Regions III and IV will be discussed in more detail later. Region I is an intrinsic property of the crystal in that it is reproducible and independent of the previous history of the specimen. According to the theory given above, the slope in this range will be $-(U + W/2)/2.3R$. Region II is not reproducibl and depends on the concentration of aliovalent impurities which are unavoidably incorporated in the crystal lattice.

U, the activation energy for mobility, can be evaluated directly from the low temperature or extrinsic range, since the concentration of impurity-created vacancie greatly exceeds the concentration of thermodynamic point defects. The variation of extrinsic conductivity or diffusion is therefore a function only of the increasing mobility of the ions. Hence, by combining the results of the slopes of the two regions, a value for W, the activatio

Conductivity - Temperature Relationship

for NaCl.

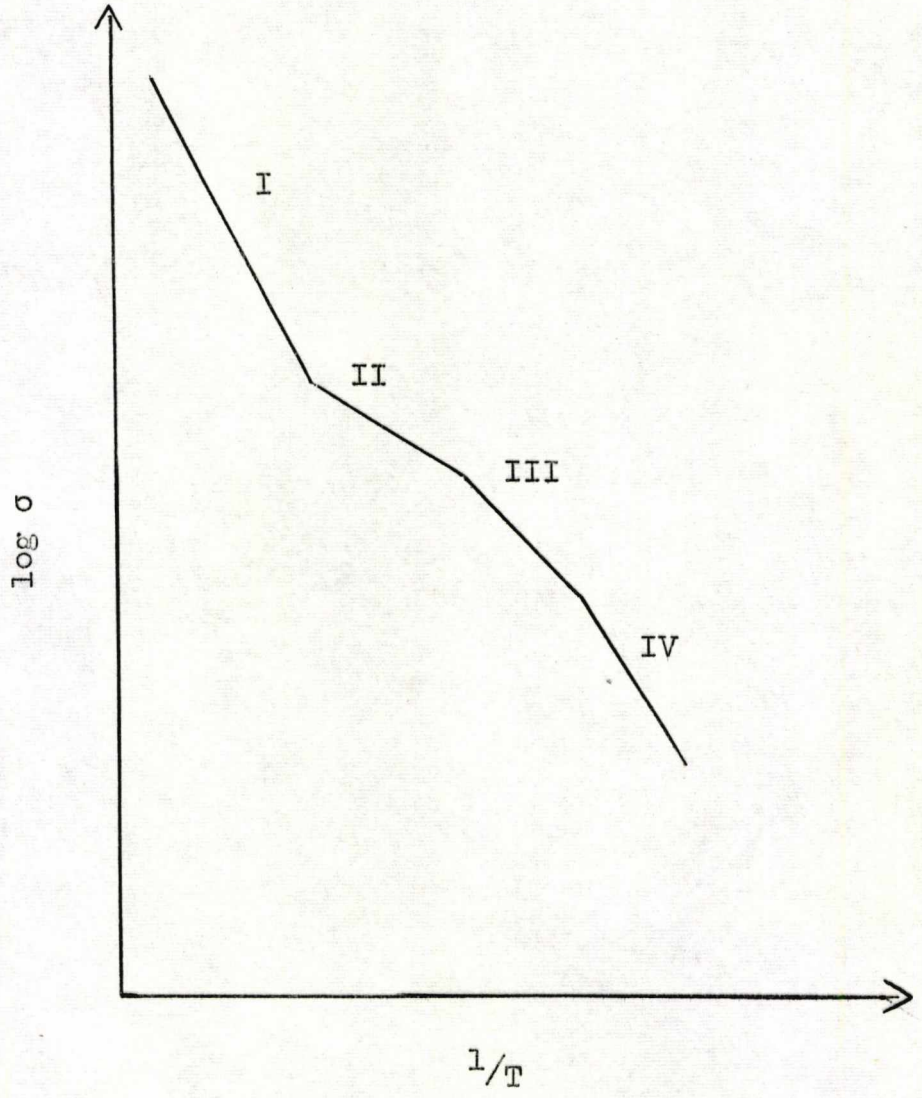

Fig. 5

Comparitive measurements of ionic conduction and diffusion in the same system are very important. Since ionic conduction is essentially diffusion under an applied field, a relationship between the mobility of a species and its diffusion coefficient can be deduced from equations (1.18) and (1.19), that is

$$\sigma/D = \frac{Nq\mu}{D} = \frac{Nq^2}{kT} \qquad (1.20)$$

This is known as the Nernst-Einstein relation. For comparison of ionic conduction and tracer diffusion the relationship must be amended. The tracer ions are distinguishable from the host ions of the crystal, and, since they are employed in very small concentrations, statistical correlations may arise between the directions of successive jumps of the radioisotope. By introducing a correlation factor, 'f', into equation (1.20) these effects can be allowed for,

$$\frac{\sigma f}{D} = \frac{Nq^2}{kT} \qquad (1.21)$$

In principle, the evaluation of 'f' allows the mechanism of self-diffusion to be determined. In self-diffusion, where the difference in jump frequency between the radioactive isotope and the corresponding host ion can be neglected, 'f' is found to be a pure number less than one. For example, self-diffusion via vacancy pairs in NaCl has an 'f' value of 0.475 whereas for single vacancies it is 0.781.

The experimental verification of equation (1.21) however is difficult owing to uncertainties in the measurement of conductivity and diffusion. Values of 'f' obtained are not precise enough to allow a definite mechanism to be assigned to a particular defect process, in the majority of cases.

From results of conductivity and diffusion studies on NaCl, NaBr[11] and KCl[12] crystals, it was shown that the Einstein relation was valid for self-diffusion measurements made in the region of intrinsic conduction, (Region I). However, at the lower temperatures, region II, it was found that the measured diffusion coefficients were larger than those calculated from the conductivity measurements. This can only be explained in terms of the existence of some neutral defect species, which can contribute to the diffusion without taking part in the conductivity.

Further evidence of the presence of neutral species contributing to diffusion has been obtained by measurements of tracer diffusion in the presence of an applied electric field[13]. The diffusion profile then migrates through the crystal with a velocity μE, where E is the applied electric field. In this way the Nernst-Einstein relationship has been verified for monovalent ions in NaCl. However, for divalent and trivalent cations it was found

that the ratio μ/D, eqn (1.20), was much less than predicted. The results indicate an increased mobility of the aliovalent ions, but no corresponding increase in charge transport.

1.6. Vacancy Pairs

One possible neutral defect is known as the vacancy pair. A cation vacancy, being a missing positive charge, carries an effective negative charge in the lattice. It will experience a Coulombic attraction to the effective positive charge of an anion vacancy and may pair off with it to form a double vacancy, Fig. 6. The concentration of these vacancy pairs, x_p, in a sodium chloride type lattice is given by

$$x_p = 6 \exp(-g/kT) \qquad (1.23)$$

where g is the free energy of formation of a vacancy pair, and 6 is the number of possible orientations of the vacancy pair in the lattice. The concentration of vacancy pairs is dependent only on the product concentrations of cation and anion vacancies, $x_1 x_2$, and hence is unaffected by changes in x_1 and x_2 due to the presence of divalent impurities.

Ionic movement via vacancy pairs might be expected to have a lower activation energy than that via single vacancies, since one of the two 'barrier' ions is now missing and moreover the defect is uncharged.

Early calculations indicated that the process did indeed have a considerably lower activation energy than that for movement via single vacancies. Recently, however, good agreement between theoretical and measured values for the mobility of single vacancies have been obtained using the Born-Mayer-Verwey repulsion potential[14]. When this type of calculation is applied to the mobility of vacancy pairs, significantly higher energies are obtained than had previously been supposed, Table 1.

Table 1.

Activation Energies for Movement via Single Vacancies and Vacancy Pairs

	Single Vacancies E (eV)	Vacancy Pairs E (eV)
NaCl - Na^+	0.87	1.46
- Cl^-	1.11	1.27
KCl - K^+	1.13	1.30
- Cl^-	1.18	1.15

These calculations indicate therefore that vacancy pairs are not highly mobile in the alkali halides. Correlation effects in vacancy pair diffusion make certain that the higher of the two activation energies controls the rate of diffusion. Consequently, the vacancy pair should be much more important in the diffusion of the

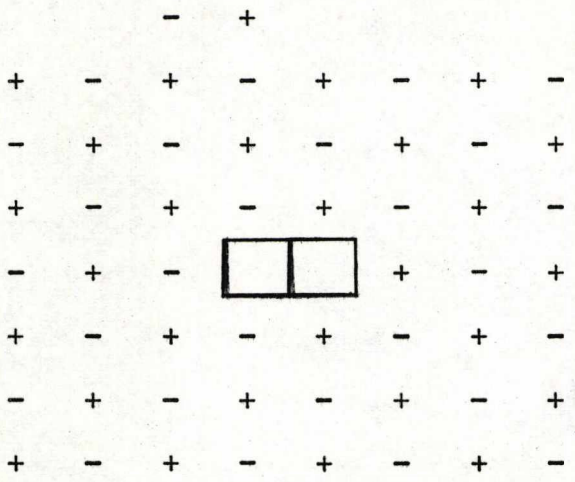

Fig. 6. – Vacancy Pair

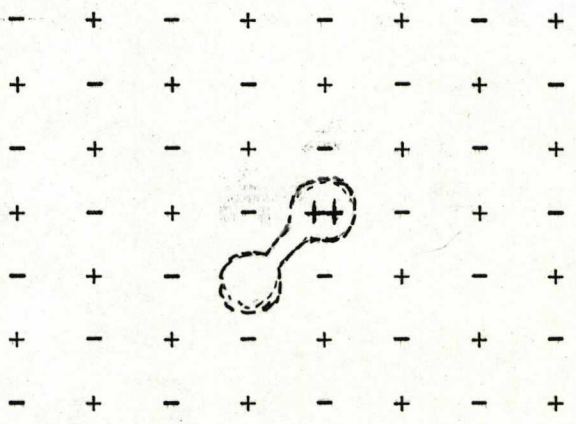

Fig. 7. – Impurity – Vacancy Complex.

less mobile species, i.e. the anion, in NaCl. This has been confirmed by recent measurements in NaCl and KCl crystals doped with divalent cations[15,16,17]. On the other hand, the significance of vacancy pairs in cation transport should be negligible.

1.7. Divalent Impurity-Vacancy Complexes

The other possibility of a neutral defect which contributes to diffusion but not conductivity is the associated divalent impurity-vacancy complex, Fig. 7. In the NaCl type of crystal the complex can move through the lattice by a sequence of jumps in which the divalent cation impurity exchanges places with the vacancy and the vacancy jumps around the impurity ion from one associated position to another. It is these latter jumps which could produce the increase in measured diffusion coefficient over the calculated value.

If all but nearest neighbour interactions are neglected the equilibrium between the complexes, impurity cations and free cation vacancies is given by[18],

$$\frac{x_k}{x_1(C - x_k)} = Z \exp(Wa/kT) \qquad (1.24)$$

where x_k is the mole fraction of complexes, Z is the number of distinct orientations of the complex and Wa is the free energy of association. Values of Wa are in the region of

0.4 eV so that at low temperatures there should be an appreciable concentration of these complexes.

The complexes result from the electrostatic attraction that exists between the excess positive charge of the impurity ion and the virtual negative charge of the cation vacancy. Various states of association, corresponding to various distances of the two interacting defects, are possible. The ground state of these complexes has the cation vacancy occupying a nearest-neighbour sodium ion site to the divalent impurity ion. The first excited state, or next-nearest-neighbour complex, has the cation vacancy located at a distance $2r_o$ from the impurity ion, where r_o is the anion-cation separation. Complexes involving large distances, that is, greater than twice the interionic distance, are unlikely to exist at the lower temperatures of the extrinsic range, because of the rapid increase in potential energy with distance. However, theoretical calculations[19] show that the binding energies of the nearest-neighbour and next-nearest-neighbour complexes are almost equal. This is almost certainly due to the absence of a polarisable Cl^- ion between the impurity and nearest-neighbour vacancy reducing the binding energy of the complex to about the same as that for the next-nearest-neighbour complex.

A difference in size between the divalent cation impurity and the host cation should promote the formation of complexes, since a vacancy in the nearest-neighbour position should help to relieve the local stress surrounding the impurity ion.

The effect of complex formation would be to lower the concentration of free cation vacancies which contribute to the ionic conductivity of the crystal. Since large deviations from the Nernst-Einstein relation have only been observed in the extrinsic or impurity range in NaCl, NaBr[11] and KCl[12] crystals, it is generally assumed that the associated impurity-cation vacancy complex is the species responsible for the extra diffusion in this range.

Complexes will contribute differently to any physical property being measured than will isolated defects. It is therefore essential, in order to interpret the experiments properly, to know the type and concentration of complexes present. Information about association has been obtained from the application of various experimental techniques to the problem.

1.8. Experimental Evidence of Association in NaCl

Experimental evidence of association has been cited in the literature from measurements of ionic conductivity, impurity diffusion, dielectric loss and electron spin resonance in NaCl crystals.

(a) Ionic Conductivity

As has been stated earlier, conductivity measurements[10] have been made on NaCl crystals over the temperature range $0^{o}C$ to the melting point. At high temperatures (region I) the crystal behaves as a pure crystal, but at lower temperatures impurity effects predominate. Region II, previously discussed, is the conductance range corresponding to impurity-induced free vacancies. At still lower temperatures the conductivity is further complicated by the presence of the impurity-vacancy complexes (region III) and the onset of an impurity precipitation range (region IV). The activation energies of regions III and IV are given by $(U + Wa/2)eV$ and $(U + h_s/2)eV$, where Wa is the free energy of association and h_s is the solubility energy.

The measurements show that in the impurity controlled extrinsic region, the conductivity is not a linear function of the impurity concentration. This is due to the formation of complexes and the presence of impurity as precipitate at crystal imperfections. The transition from complexes to

precipitate may involve an intermediate state. As the temperature is lowered clustering of the complexes could lead to the formation of higher aggregates. These large conglomerates may then act as nucleation centres for precipitation.

Comparison of the conductance measurements with those from self-diffusion in NaCl indicate significant overlap of these regions (II,III and IV). Although it is possible to determine approximate values of the association energy, Wa, and the solubility energy, h_s, from the slope of the $\log_{10}\sigma$ versus 1/T plot, accurate estimations require a more detailed analysis and the measurement of conductance over a wide range of impurity concentrations. Lidiard[18] has developed a theory of ionic conductivity taking into account the effect of impurity-vacancy complexes, this will be summarised in a later section.

It should be noted that the conductivity is affected only by the amount of impurity dissolved substitutionally in the crystal. Precipitated impurity forms a separate phase and has no effect on the concentration of vacancies in the crystal. At equilibrium, there is therefore a maximum conductivity which can be reached at any particular temperature corresponding to the maximum value of the free vacancy concentration as determined by the impurity solubility.

(b) Impurity Diffusion

Experiments on impurity diffusion can yield information about complexes by measuring the diffusion as a function of impurity concentration and temperature. Lidiard[18] has developed an equation which relates the impurity diffusion coefficient to the degree of association. According to the theory, the diffusion coefficient should be proportional to the concentration at low concentrations, but tend towards a constant value at high concentrations of impurity. Treating the association reaction as a chemical equilibrium leads to a mass action constant, and a free energy of association. This approach has been used to determine the association energies of Zn^{2+} [33], Ca^{2+} and Cd^{2+} [34], and Mn^{2+} [35] in NaCl.

(c) Dielectric Loss[20,21,22,23,24]

Information about association can also be obtained from measurements of dielectric loss. Since the impurity-vacancy complex is an electric dipole, its energy depends upon its orientation with respect to an applied electric field. If an a.c. electric field is applied to a crystal preferential reorientation of the complexes takes place producing an alternating current lagging in phase behind the field. This gives rise to a Debye loss peak, which has a characteristic maximum when the frequency of

the applied electric field is equal to the rate of reorientation of the impurity-vacancy complex.

(d) Electron Spin Resonance[25]

Until the application of electron spin resonance to the study of association, the precise interpretation of data obtained from dielectric loss experiments proved difficult since the exact concentration and type of complexes was not known. With the information available from electron spin resonance measurements it is possible to make a complete analysis of the loss peaks, when the impurity is a paramagnetic ion, such as Mn^{2+}.

The types of impurity-vacancy complex present can be readily identified, and the free energy of association determined from a study of the concentration of the complexes as a function of temperature.

Several other types of measurement, such as nuclear magnetic resonance[26,27] and optical colouration[28], have furnished information on the impurity-vacancy complexes.

Values of the association enthalpy for several divalent ions in NaCl are listed in Table 2.

Theoretical calculations[19,36,37] have been made of the binding energies of some impurity-vacancy complexes in NaCl, Table 3. On the whole, agreement with experiment is good.

TABLE 2. - Values for Association Enthalpy of Divalent Impurity-cation Vacancy Complexes in NaCl

	Ni^{2+}	Co^{2+}	Zn^{2+}	Mn^{2+}	Cd^{2+}	Ca^{2+}	Sr^{2+}
Radius* (Å)	0.78	0.82	0.83	0.91	1.03	1.06	1.27
χ_1(eV) from							
a. conductance measurements	0.32 [29]	0.30 [30]			0.34† [31]	0.31† [32]	
b. impurity diffusion measurements			0.48† [33]	0.71 [34]	0.40 [35]	0.57 [35]	
c. dielectric loss measurements						0.44 [24]	0.45 [24]
d. e.s.r. measurements				0.41 [25]			

* Goldschmidt radii

† Free energy of association

TABLE 3.

Theoretical Estimates of Divalent Cation Impurity-Vacancy Complexes (eV) [37]

	Cd^{2+}	Ca^{2+}	Sr^{2+}
NaCl	0.38	0.38	0.45
KCl	0.32	0.32	0.39

The results indicate that the binding energy should increase with impurity ion size. However, the experimental studies to date, which have been mainly confined to impurity ions of similar or smaller size than the host cation, do not confirm this trend. It has been suggested that in these cases interaction between the impurity ion and the cation vacancy in the next-nearest-neighbour position may be significant.

Perhaps the most important result of these calculations is the prediction that in NaCl the nearest-neighbour complex is the most stable whereas in KCl it is the next-nearest-neighbour pair[19]. This work was done for Sr^{2+} impurity, but the results obtained have been verified indirectly through the application of electron spin resonance to NaCl crystals containing Mn^{2+} impurity.

1.9. Aims of the Present Work

The two most important methods employed in the experimental determination of the parameters governing the concentration and mobility of defects and the interaction between these defects are the measurements of ionic conductance and diffusion coefficients. It is the aim of the present work to use these methods in a detailed study of impurity-vacancy association reactions in single crystals of NaCl.

Theoretical calculations[37] of the impurity-vacancy binding energy indicate that this should increase with increase in impurity ion size. Experimental studies to date, the results of which are listed in table 2., have failed to confirm this trend. This may be due to the fact that the few measurements of the association energy which have been reported were made on systems where the impurity ion was of similar or smaller size than the host cation. In these circumstances the effect of long-range interactions may be extremely significant[19].

The experimental work cited in the literature can be criticised on two grounds; (1) there has been no systematic study of the effects of impurity ion radius over a wide range of ionic sizes, (2) the experiments represent measurements on only a few systems and these have been made using several different techniques. There is some evidence that the discrepancies which do arise are a factor of the experimental methods.

It is therefore proposed to pursue this research along three main lines, (a) to study by conductance methods the association reactions in the following systems ($NaCl - MgCl_2$), ($NaCl - MnCl_2$), ($NaCl - CaCl_2$), ($NaCl - SrCl_2$), ($NaCl - PbCl_2$) and ($NaCl - BaCl_2$). In this way, comparison can be made over a wide range of impurity ion size and polarisability. The relevance of these properties in impurity-vacancy association phenomena can then be evaluated. Since two methods are available from conductance measurements, it should be possible to compare the accuracy of the methods.

(b) to compare the association energy of one impurity ion by several different experimental methods. The system chosen for this study was $NaCl - MnCl_2$ since it is possible to obtain the impurity-vacancy association energy from conductance, dielectric loss, electron spin resonance and Mn^{2+} ion diffusion measurements. Moreover, a previous study of Mn^{2+} ion diffusion in this system has given an exceptionally high value for the free energy of association[34], and is in marked disagreement with the electron spin resonance measurements in the same system. As yet, no conductance measurements have been made on this system.

(c) The significant disagreement between the observed Na^+ ion self-diffusion coefficients, and those calculated from the conductance measurements by means of the Nernst-

Einstein equation, has been attributed to the presence of impurity-vacancy complexes. Since these are neutral species, they would not be expected to contribute to the conductivity, but it has been suggested that they may contribute to Na^+ ion self-diffusion. Although this is generally accepted, there is little experimental evidence to support the assumption. It is therefore proposed to investigate Na^+ ion self-diffusion in pure and Ca^{2+}-doped crystals of NaCl and to compare these with the conductivity measurements. It should be possible to evaluate the importance of associated complexes by studying the temperature dependence of the diffusion.

The theoretical estimates[37] indicate that a significant amount of association should occur in these crystals. However, it has been suggested that the calculations are not applicable to impurity ions of sizes significantly smaller or larger than the host cation. It was decided to extend this work by calculating the binding energy of the Ba^{2+}-vacancy complex and to note any failure of the point-charge model.

Studies of association can also lead to the determination of defect parameters such as enthalpy and entropy of formation of a Schottky defect and the enthalpy and entropy of mobility of these defects. In addition, since association is usually a precursor to precipitation,

studies of these systems can also produce information on the solubility of the impurities.

CHAPTER II

EXPERIMENTAL

2.1. Crystal Growth

From the recent attention given to crystal growing in the literature it is obvious that the subject is rapidly transferring from an art to a science. There is increasing recognition of the fact that measurements made on crystals of unknown purity and perfection are irreproducible. An understanding of the basic crystal growth problems is therefore required and considerably effort has been applied to the control of growth conditions and to the general refinement of growth techniques.

In general, four different methods of growing crystals can be distinguished, depending on the phase from which the crystals grow; they are: (1) growth from the vapour, (2) growth from a supercritical or 'fluid' phase, (3) growth from one or more solid phases and (4) growth from the liquid phase. The latter method is the most convenient for the alkali halides and generally produces larger crystals than any of the other methods.

Crystal Growth from the Liquid Phase

Growth from the melt, where it is possible, is usually preferred by most workers. Crystallisation of a

polycrystalline solid is achieved by a gradual lowering of the temperature of the molten material below the melting point. The melt can be made to solidify in its container by moving it slowly through a temperature gradient[38], or by inducing crystallisation in the centre of the melt, using a cooled seed crystal and allowing it to grow radially outwards[39]. The disadvantages of the melt adhering to the walls of the container on cooling can be overcome by pulling the crystals from the melt[40]. The seed crystal, held in a rotating chuck, is lowered into the molten material and then slowly raised. It is possible to draw a single crystal from the melt with the same crystal structure as the seed.

The growth of crystals from solutions is in principle the same as growth from a molten salt. However, the growth techniques are slightly different. Supersaturation of a solution in a solvent like water is achieved by cooling if the solubility decreases with temperature, or by slow evaporation of the solvent[41]. Single crystal growth can be promoted by suspending a seed crystal in the solution. Growth of crystals by slow evaporation of a supersaturated solution is such a slow process, compared with melt growth, that striations produced by temperature fluctuations are almost undetectable.

2.1(a) Growth from Aqueous Solution

The solubility of NaCl in water is 35.7 gms per 100 ml at room temperature[42], so that in a near saturated solution there is plenty of material available for the growth of crystals. Analar reagent NaCl was used as supplied by British Drug Houses Ltd. 20.00 gms of NaCl were dissolved in 50 ml of distilled water in a 100 ml flask. The rate of growth was then controlled by varying the rate of evaporation of the solvent. Crystals were grown over a period of three days by cooling the saturated solution of NaCl from 70°C to room temperature in a well-lagged Dewar flask.

Alternatively, an even slower growth rate was obtained by transferring the saturated solution at room temperature to a petri-dish suspended over concentrated sulphuric acid in a desiccator. Slow evaporation of solvent was effected by the acid, the first crystals usually appearing after a period of about six days. The crystals were allowed to grow to a size of approximately 0.5 cms on edge before being removed from the solution. In this latter method seeding of the solution promoted crystal growth. Preparation of doped crystals was achieved by incorporating the divalent metallic chlorides in the saturated NaCl solution prior to crystal growth.

Infra-red measurements on these crystals were made using a Unicam S.P.200 Spectrophotometer. The observed spectra showed peaks at 1600 and 3500 cm^{-1} which can be attributed to the occlusion of water in the crystals. To ensure that the observed spectra were not due to surface contamination, the crystals were handled carefully and measurements taken on crystals of varying surface area and thickness. Drying the crystals in vacuum for two hours at 250°C was sufficient to eliminate any water of occlusion.

2.1(b) Growth from the Melt

Two methods of growing crystals from the melt were employed, namely, a modified Stockbarger[38] method and a simple melt-cooling technique.

Growth from the melt was carried out in an atmosphere of dry nitrogen. Strict precautions were taken to ensure complete removal of any moisture present in the starting material. The reagent grade NaCl was contained in a quartz vessel which was attachedto a vacuum line in which a pressure of 10^{-2} mm Hg could be maintained. The temperature was raised to ~ 500°C for a period of two hours and then treated with an atmosphere of HCl gas for a further two hours to drive out any remaining OH^- ions[43]. HCl was produced from the reaction,

$$2NH_4Cl + H_2SO_4 \longrightarrow 2HCl + (NH_4)_2SO_4$$

and is effective in removing surface moisture, which would otherwise lead to the introduction of OH^- ions in the melt as a result of the reaction

$$H_2O + Cl^- \longrightarrow OH^- + HCl$$

After treating with HCl gas the quartz vessel was sealed off under an atmosphere of pure nitrogen, which had been dried by bubbling through concentrated sulphuric acid. The vacuum line and attached reaction vessel are shown in Fig. 8.

In the modified Stockbarger method the quartz vessel containing the reagent measured 3 inches by 1 inch. It was attached by means of a quartz tube to a pulley system operated by an electric motor and placed at the bottom of the furnace. The complete assembly used for crystal growth is shown in Fig. 9.

The furnace was constructed as follows. A core, length 12 inches, diameter 6 inches, resistance 300 ohms, was wound on the outside with nichrome wire of resistance 10 ohms per yard. The additional resistance of the furnace was gradually increased towards the bottom. Asbestos paper was used to cover the extra resistance wire and the core was placed firmly in the centre of a large metal drum. Extensive lagging with tightly packed asbestos wool was essential for good temperature control. Heat was supplied to the furnace via stabilised mains voltage and regulated

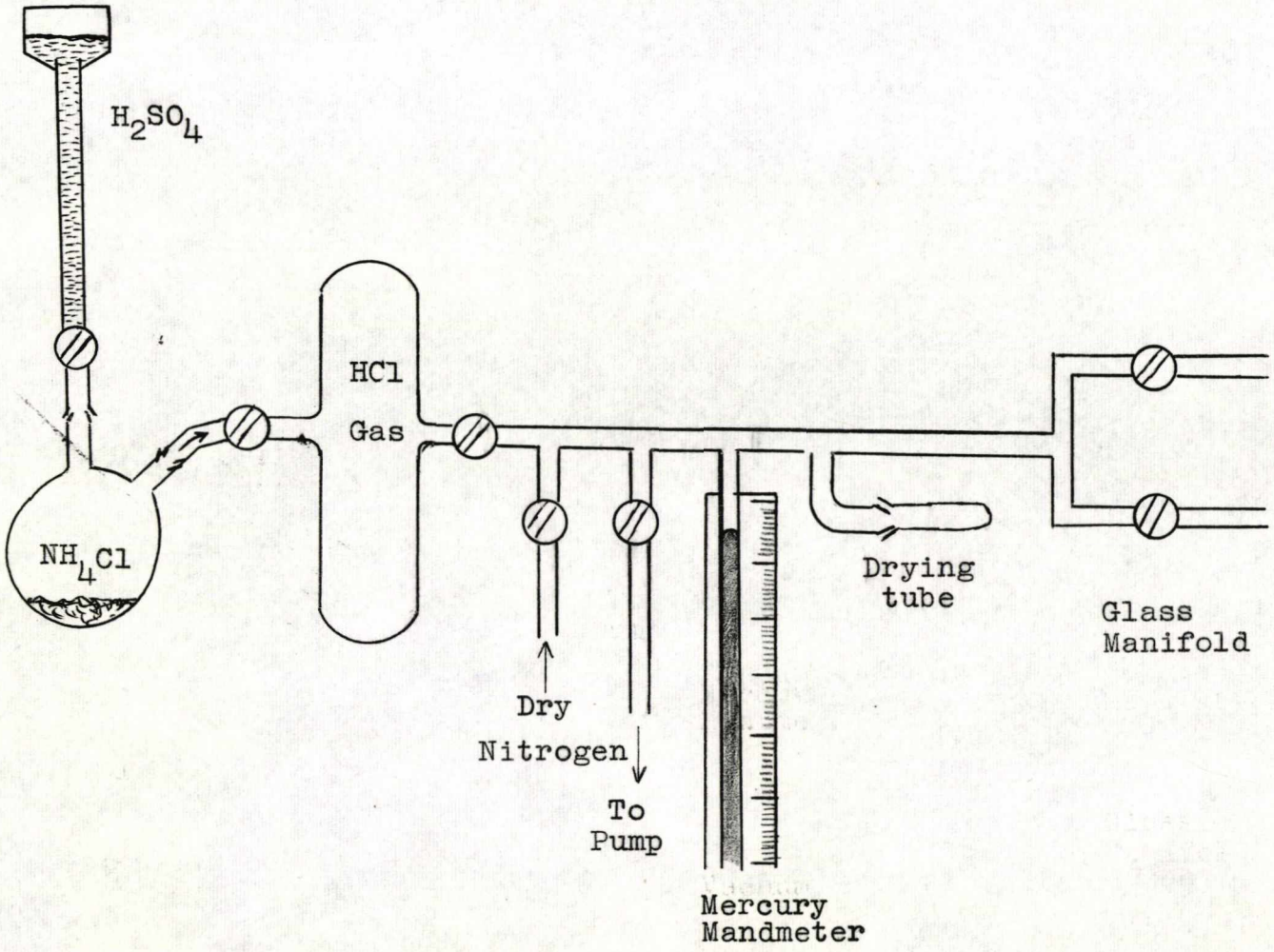

Fig. 8 - Vacuum System

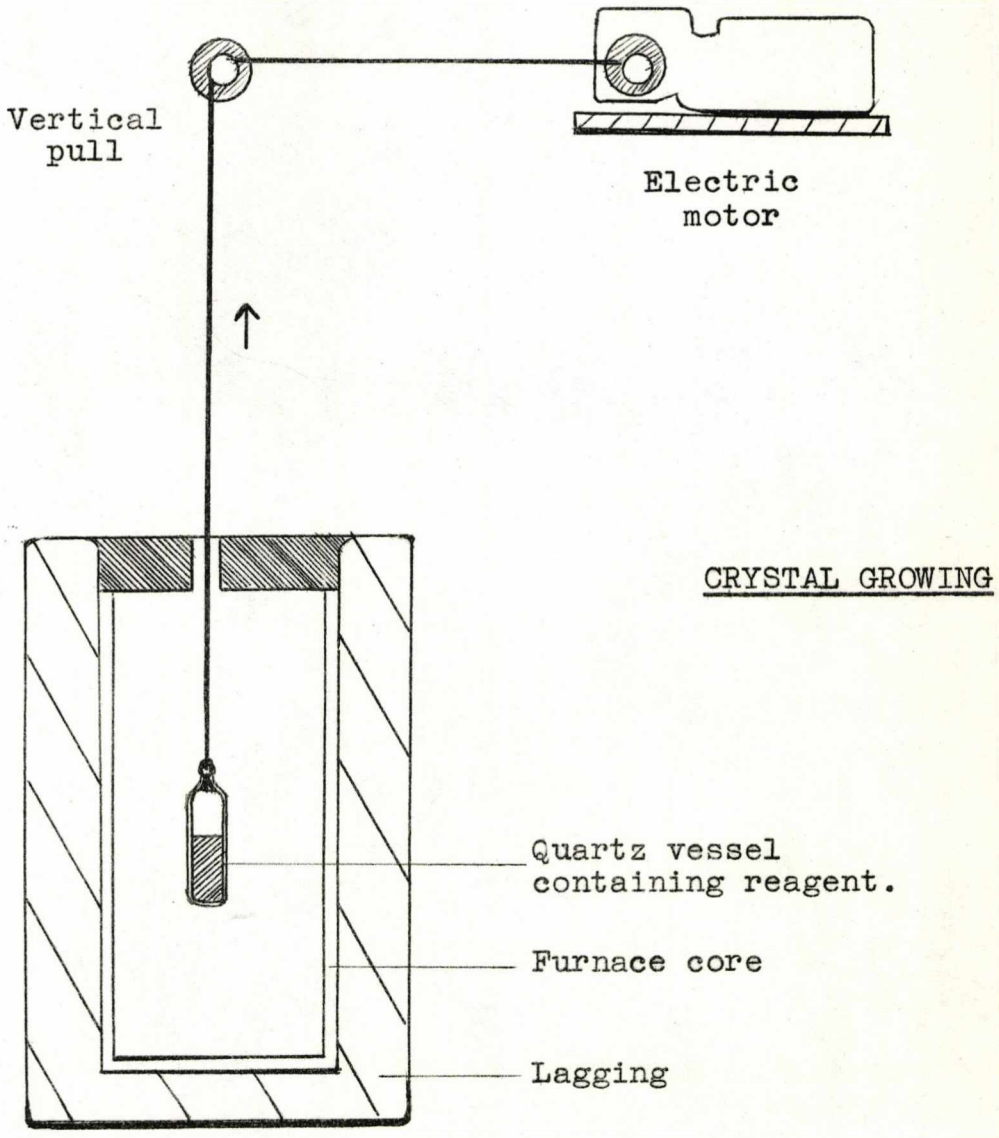

Fig. 9 - Crystal growing furnace.

by means of a manually controlled variac. At the operating temperature of the furnace, that is, in the region of the melting point of NaCl, there was a temperature gradient of ~ 25°C per inch from the bottom to the top.

With the quartz vessel containing the polycrystalline NaCl in position the furnace temperature was raised slowly to 825°C. This temperature was maintained for 30 mins to allow the NaCl to melt. The quartz vessel was then raised through the temperature gradient at a rate of 1 inch per hour. After growth, the crystal was annealed at a temperature of ~ 600°C for 10 hours and then slowly lowered to room temperature over a period of 12 hours.

In general, the specimens obtained from this method of growth were rather small. They were suitable for conductivity work, but inadequate for use in the diffusion studies. As a result, most of the crystals used were grown by a less sophisticated, but nevertheless effective, method in the apparatus shown in Fig. 10.

The furnace was a simple box-type with a maximum power rating of 5 kW. Internal dimensions were, height 6 inches, width 6 inches and depth 12 inches. Refractory castings supported the heavy gauge, internal heater spirals. Built into a control space beneath the furnace was an

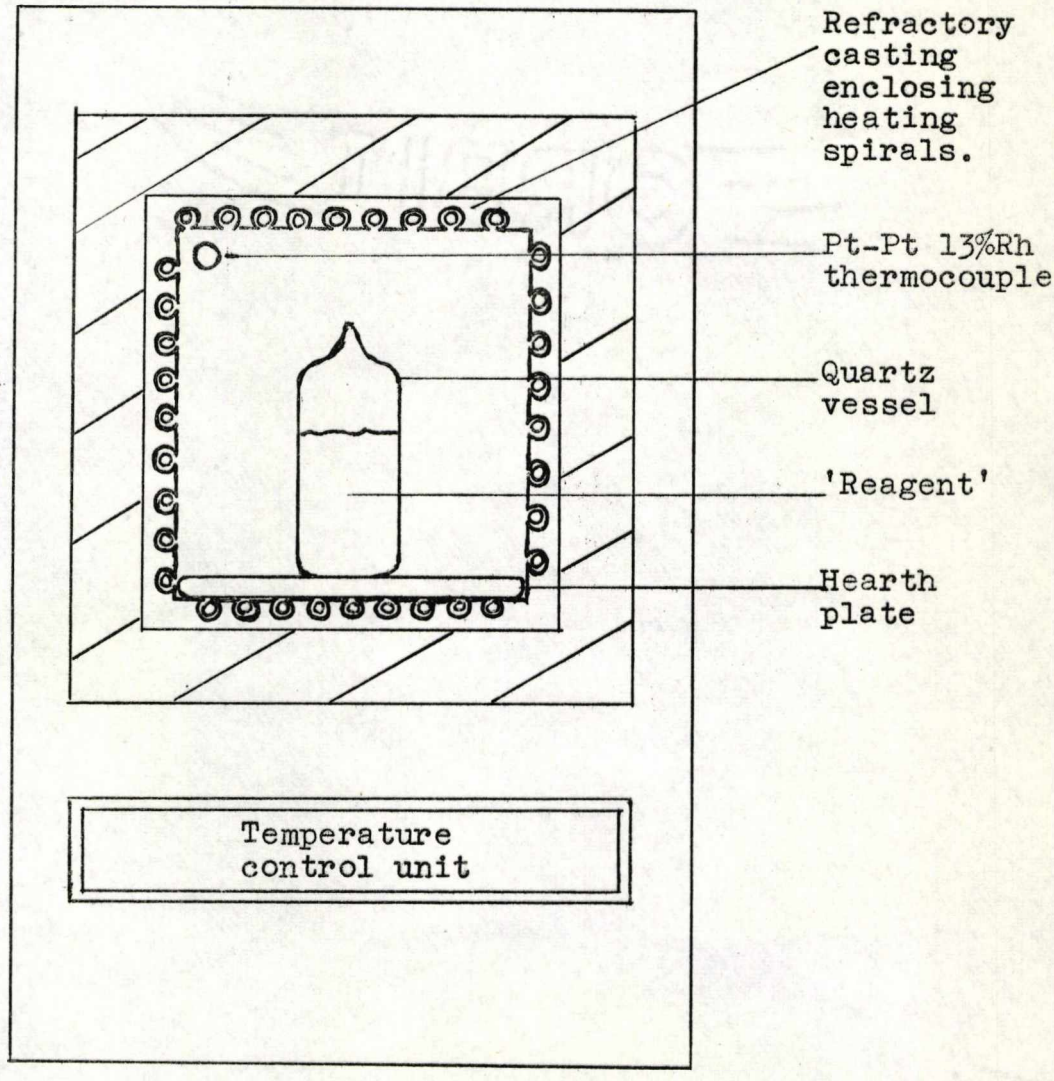

Fig. 10 - Apparatus used for crystal growth from the melt by simple cooling.

automatic proportional temperature control unit. Temperature measurement was by means of a Pt-Pt 13% Rh thermocouple. An energy regulator controlled the rate of heating and cooling.

For this method of growth a larger quartz vessel was used. It measured 3½ inches by 2 inches and had a flat bottom which enabled it to sit upright on the hearth plate in the furnace. Pretreatment of the reagent was carried out as before, and metallic impurities added by selective addition of the corresponding chlorides. The samples were raised to a temperature of 825°C and then allowed to cool from the molten state at a rate of per hour. Annealing of the crystal and the rate of cooling were as described earlier.

The crystal invariably stuck to the quartz vessel on cooling, and, although the centre of the solidified melt tended to be polycrystalline, it was still possible to cleave from the outer portions single crystal specimens large enough for the diffusion work.

2.1(c) Annealing and Quenching of Crystals

The purpose of the annealing experiments was twofold, namely (1) to produce a uniform distribution of impurities in the lattice,[44] and (2) to destroy anionic impurities such as OH^- in the lattice.[43] Annealing of crystals was carried out in quartz tubes which had been degassed. The

atmosphere used for annealing was usually HCl gas, but in a few experiments chlorine gas was employed. The annealing temperature was 700°C and the annealing time was approximately 24 hours.

A non-equilibrium condition can be frozen-in to a crystal lattice by rapid quenching from a high temperature. Crystals were sealed inside a nitrogen-filled pyrex tube and raised to a pre-determined temperature in the range 450 - 500°C. After about one hour the tube was removed from the furnace and plunged into a Dewar flask containing liquid nitrogen. Cooling of the crystal to liquid nitrogen temperature was achieved in approximately 30 seconds.

2.2. Conductivity

The measurement of the temperature dependence of the electrical conductivity in NaCl as a function of the divalent cation impurity concentration provides information on the mobility and concentration of positive ion vacancies, the enthalpy and entropy of impurity-vacancy complexes and the solubility of the impurities in the lattice.

The resistance of a conductor varies directly as its length (d cm) and inversely as its cross-sectional area (A cm^2). Hence,

$$R = \rho \cdot \frac{d}{A} \qquad (2.1)$$

where ρ is the specific resistance, that is, the resistance between opposite faces of a 1 cm cube of the material. The specific conductivity, σ, is defined as the reciprocal of the specific resistance. Hence, from equation (2.1)

$$\sigma = \frac{1}{\rho} = \frac{1}{R} \cdot \frac{d}{A} \qquad (2.2)$$

The factor $^{d}/_{A}$, known as the cell constant, is obtained from the crystal dimensions, which were measured with a micrometer screw gauge. The cross-sectional area, A, is determined by weighing the crystal and dividing the weight by the density of NaCl (2.165 $gm.cm^{-3}$)

$$A = \frac{\text{Volume}}{d} = \frac{\text{Weight}}{\text{Density x } d} \qquad (2.3)$$

The conductivity measurements were made by a standard technique using a Wayne-Kerr Universal a.c. bridge operating at 1592 c.p.s. The bridge is based on the transformer ratio-arm technique and reads out directly the reciprocal resistance and capacitance. Thus, by multiplying the bridge reading, $^{1}/_{R}$, by the cell constant, $^{d}/_{A}$, the specific conductivity, in $ohms^{-1}cm^{-1}$, can be calculated.

2.2(a). Measurement of Conductivity and Temperature

Specimens for conductivity measurements were cleaved plates about 2 mm. thick and 7 mm. on edge. Dag electrode paint (a colloidal suspension of graphite in isopropyl alcohol) was then applied to the crystal faces, which were to be in contact with the electrodes. The electrodes were graphite-coated nickel discs of dimensions 1.50 cms diameter and 1.00 cms thick. Electrical connection to the Wayne-Kerr bridge was made via thick copper wire leads, Fig. 11.

The electrode system was enclosed in a quartz tube which was simply a B45 cone and socket with two capillary tubes acting as electrode supports. A side arm at the lower end of the vessel allowed the introduction of pure nitrogen, dried by passing through concentrated sulphuric acid. The purpose of this was to prevent oxidation of the graphite at higher temperatures. A third capillary tube parallel to the bottom electrode support allowed the introduction of a thermocouple used to measure the crystal temperature.

The quartz vessel was surrounded by an electrically heated furnace, which was made from a cylindrical brass tube, 10 cms high and 6 cms internal diameter. This was wound with nichrome wire (resistance 10 ohms per yard) to give a total resistance of 100 ohms at room

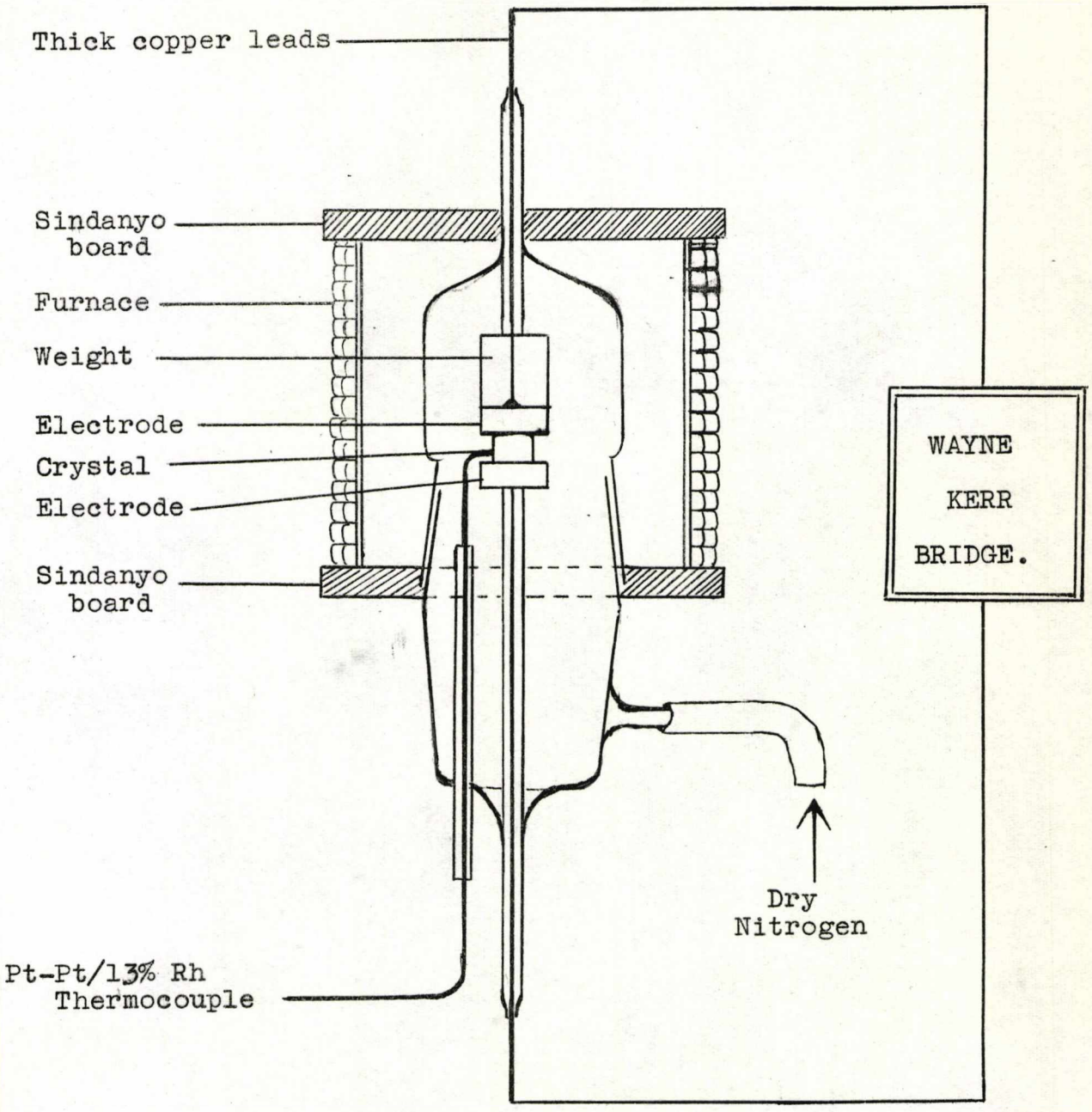

Fig. 11 - Conductivity Cell.

temperature. Asbestos paper and string were used as lagging and two pieces of Sindanyo board, 1 cm thick, enclosed the furnace at top and bottom. This reduced the effect of temperature fluctuations and external draughts to a minimum. Power was supplied to the furnace via a manually controlled variac.

A calibrated Pt-Pt 13% Rh thermocouple was used to measure the crystal temperature. The difference in potential between the 'hot' and the 'cold' end, which was immersed in an ice bath, was determined on a Doran thermocouple potentiometer, type E4223, and converted to degrees centigrade by means of the standard calibration tables[45].

During the conductivity measurements a pressure of 20 gm cm^{-2} was applied to the top electrode by means of a circular brass weight. It should be noted that the absence of any pressure on the top electrode produced serious losses in the magnitude of the measured conductivity. At worst, discrepancies of a factor of two were observed. However, increasing the pressure produced a corresponding increase in the conductivity until it reached a pressure-independent level. The investigation was performed using the brass weight and two similar but lighter nickel weights. The results of this investigation are shown in Fig. 12.

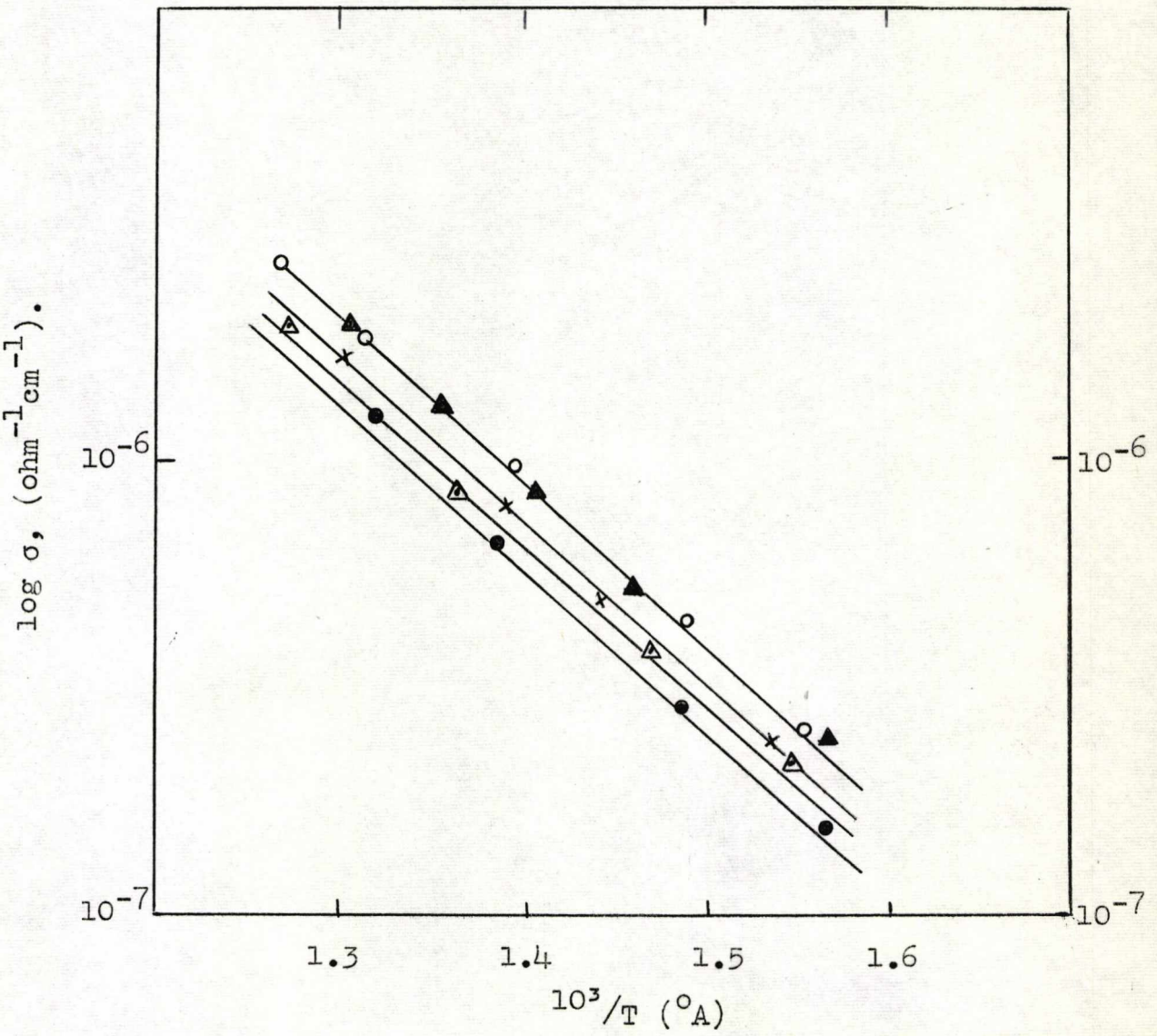

Fig. 12 - log σ as a function of pressure on the top electrode (gm.cm^{-2}).

●– 0; △–5; X–15; ▲–20; 0 – 25.

Measurements of reciprocal resistance were begun at about 10^{-10} mhos (the minimum conductance reading on the Wayne-Kerr bridge). Readings were taken every half-hour in which time the crystal temperature was raised by approximately 15°. At higher temperatures the system came to equilibrium much quicker allowing readings to be taken at twenty minute intervals. Normally, the temperature range covered in the experiments was 150-650°C.

2.2(b) Errors in the Conductivity Measurement

A conductance of 10^{-10} mhos could be measured with an accuracy of about 10%. However, accuracy rapidly increased with increase in conductance so that at all but the lowest values the error was negligible compared to other experimental errors. Temperature measurement and the geometric factor were probably a greater source of error. The weight and thickness of a crystal could be measured with great precision, but any slight non-uniformity in the cleaves would have an effect on the measured conductance. Although the Pt-Pt 13% Rh thermocouple could determine temperature to an accuracy of at least $\pm$ 0.5°C the error involved is probably greater since the thermocouple cannot be in good contact with the crystal.

2.3. Diffusion

In ionic crystals diffusive movements result in the displacement of ions over many interionic distances. According to Fick's[46] first law, the net flux of ions is proportional to the concentration gradient, that is

$$J = -D \text{ grad.} c \qquad (2.4)$$

where J is the number of radioactive atoms crossing 1 cm^2 per sec., D is the diffusion coefficient, and c is the number of radioactive atoms per cm^3.

Fick's law is not often verified directly, but more usually by its consequences. In particular, (2.4) and the conservation condition

$$\text{grad. } J + \frac{\partial c}{\partial t} = 0 \qquad (2.5)$$

yields

$$\frac{\partial c}{\partial t} = D \frac{\partial^2 c}{\partial x^2} \qquad (2.6)$$

assuming the diffusion coefficient D to be independent of c; x is the distance from the face of the crystal. The determination of the diffusion coefficients therefore requires the direct or indirect measurement of the tracer concentration gradient in the sample under investigation.

There are three common methods for the determination of diffusion coefficients employing radioactive tracers, namely, the sectioning, isotope exchange and surface decrease techniques.

(i) The Sectioning Technique

A thin layer of radioactive salt is deposited on one face of a crystal and diffusion allowed to take place. The solution of Fick's Law in this situation states that after time t, the diffusion profile is given by

$$c(x,t) = \frac{c_o}{(\pi Dt)^{\frac{1}{2}}} \exp(-x^2/4Dt) \qquad (2.7)$$

where $c(x,t)$ is the concentration of radioactive ions at a penetration depth x, and c_o is the initial activity per unit area at $t = 0$. This solution is based on the assumption that the migration of radioactive ions is a result of a single diffusion process, since only one diffusion constant has been introduced.

When $\log_{10} c$ is plotted against x^2, a straight line of slope $(-1/4Dt)$ results. The concentration of tracer as a function of penetration depth is determined by measuring the tracer activity in layers of the crystal which are removed by sectioning with a microtome[47,48,49].

(ii) The Isotope Exchange Technique

This method depends upon the rate of exchange between a radioactive tracer incorporated in the crystal and the surrounding gas, the rate of exchange being determined by the rate of the tracer diffusion in the crystal. It is particularly suited to studies of chloride ion diffusion in alkali metal chlorides where the diffusion coefficient at low temperatures is very small.

Harrison, Morrison and Rudham[50] used this technique in the determination of chloride ion diffusion in NaCl. Cl^{36} was incorporated in the lattice and the rate of exchange of the isotope between the solid and the surrounding chlorine gas was measured.

The solution of Fick's Law in this case is given by[51]

$$N(t) = 2A\, c_o \sqrt{\frac{Dt}{\Pi}} \qquad (2.8)$$

where A is the surface area of the specimen, and c_o is the initial uniform concentration of diffusing species in the crystal. A plot of $N^2(t)$ against t gives a straight line of slope $\frac{(4A^2c_o^2)}{\Pi}$ .D.

The advantage of this method is that diffusion measurements over a series of ascending temperatures can be made on the same crystal, so that the activation energy for diffusion may be derived from one experiment. However, it is restricted to situations where the parent element of the ion can be obtained in a gaseous form under reasonable conditions.

(iii) The Surface Decrease Technique

This technique involves the determination of the surface radioactivity before and after diffusion. Diffusion of an α- or β-emitting isotope into a crystal

results in a decrease in activity at the surface because of the absorption of the radioactive particles by the intervening crystal layers. The solution of Fick's Law for this arrangement is given by[53]

$$c(t)/c_o = \{1 - \mathrm{erf}(\mu^2 Dt)^{\frac{1}{2}}\} \exp(\mu^2 Dt) \qquad (2.9)$$

where μ is absorption coefficient of the isotope radiation in the crystal and erf $(\mu^2 Dt)^{\frac{1}{2}}$ is the error function[54].

In the present work the majority of diffusion results were obtained by the sectioning technique. Preliminary investigations were carried out using the surface decrease technique, but owing to several inherent difficulties in the method, which will be discussed later, it was abandoned in favour of the former.

2.3(a) Preparation of Radioactive Material

(i) Sodium-22

Na^{22} is a β^+ (0.511 MeV) and γ (1.274 MeV) emitter of half-life 2.60 years. It was obtained as $Na^{22}Cl$ in aqueous solution; the specific activity was 2.7 c/g Na. A little inactive NaCl was added and the resultant solution evaporated to dryness in a fume cupboard.

(ii) Manganese-54

Mn^{54} is a γ(0.835 MeV) emitter of half-life 314 days. It was obtained as $Mn^{54}Cl_2$ in 0.1N HCl solution. The activity was diluted by the addition of inactive $MnCl_2.4H_2O$ and the solution evaporated to dryness in a fume cupboard.

2.3(b) Deposition of Radioactivity

Two methods of depositing thin films of radioactive $Mn^{54}Cl_2$ and $Na^{22}Cl$ on to the faces of single crystals were employed. These were (i) by evaporation in a vacuum from a heated platinum-clad quartz tube, and (ii) by evaporation of an aqueous methanol solution containing the radioactive salt.

(i) Vacuum Evaporation

The evaporator was specially designed for this operation, and is shown in Fig. 13. It was made from a B35 silica cone and pyrex socket. The protrusion at the bottom of the vessel measured 2.50 cms by 1.00 cm, the inside walls were clad with platinum foil. One of the side-arms at the top led to the air via a U-tube containing silica gel and the other was connected to the vacuum system.

A quartz disc, positioned directly above the platinum-clad tube, had four holes drilled in it, each 2 mm in diameter. This ensured that the evaporated salt

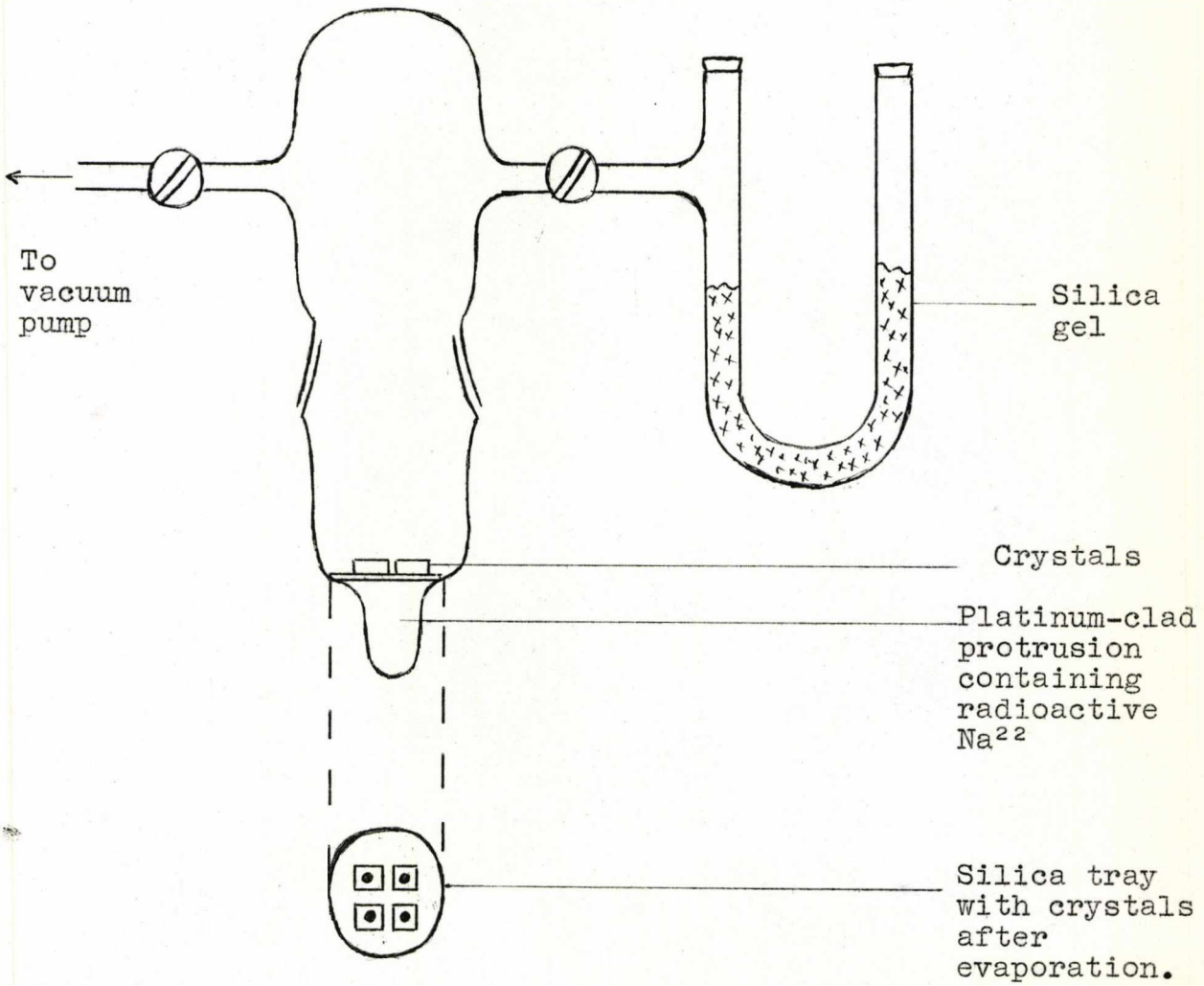

Fig. 13 - 'Evaporator'

was deposited over a circular area on the faces of the crystals.

Evaporation took place quickly in the evacuated vessel (pressure 10^{-2}mm Hg) by heating the protrusion with a bunsen flame, care being taken to prevent overheating. On cooling, the vacuum was released, and the crystals removed to the dry atmosphere of a desiccator containing silica gel.

(ii) Evaporation of Aqueous Methanol Solution

The apparatus is shown in Fig. 14. Deposition from an aqueous methanol solution took place as follows.

Crystals, measuring approximately 1 cm on edge, were placed under an infra-red lamp and warmed slightly before being placed on the tray directly under the 'dropper'. The volume of solution deposited was usually enough to produce a film about 10^{-3} cms thick and was carefully controlled by means of a micro-syringe. The solvent evaporated quickly on the surface of the warm crystal leaving a circular deposit of the radioactive substrate which was approximately 2mm in diameter.

This method was used to deposit thin films of radioactive $Mn^{54}Cl_2$ on single crystals of NaCl. Due to the high temperature instability of $MnCl_2$ vacuum evaporation could not be used. On the other hand NaCl has a much

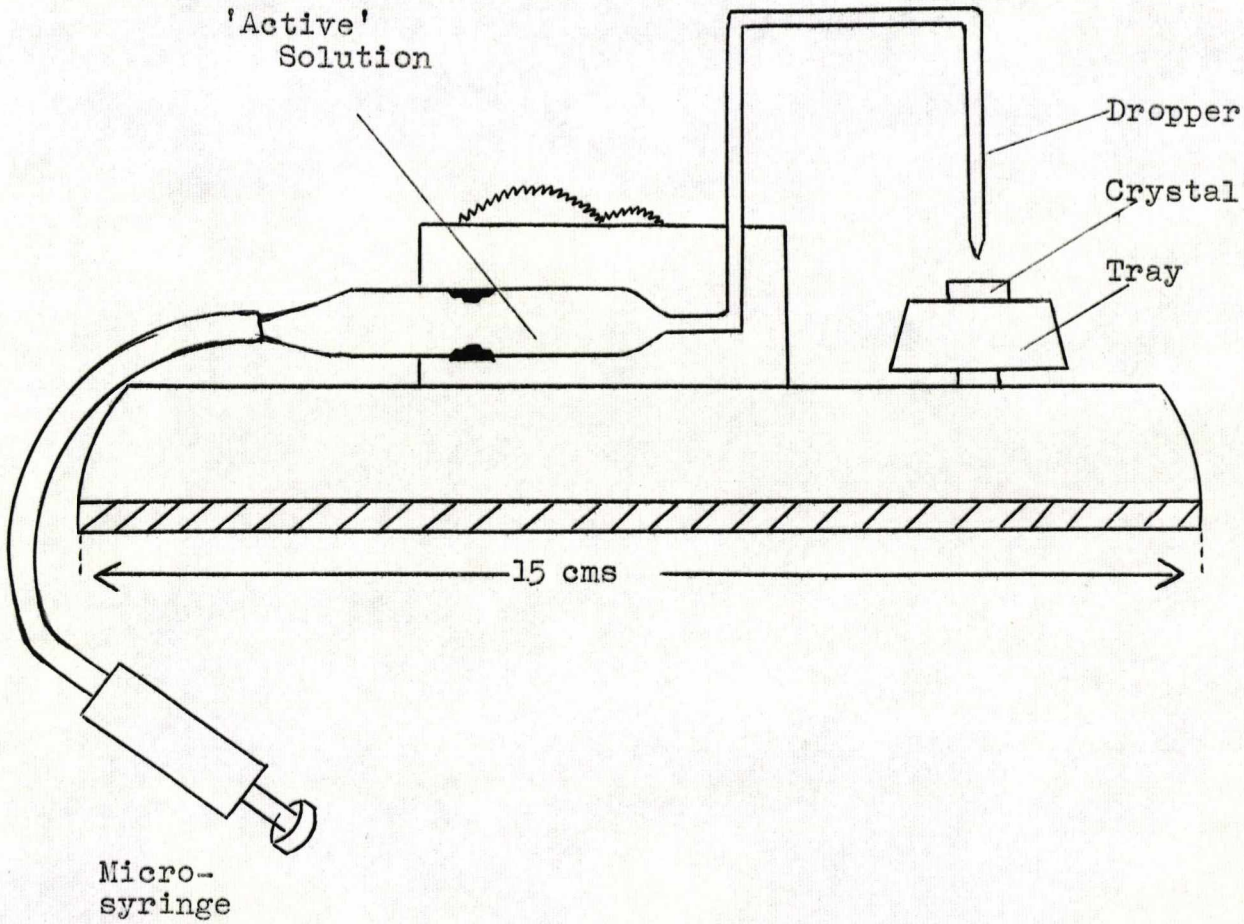

Fig. 14 - Deposition of radioactivity from aqueous solution.

higher melting point and is relatively stable, consequently, it lended itself well to vacuum evaporation.

2.3(c) The Diffusion Cell

Following the evaporation procedure, the crystals were transferred to a constant temperature furnace, where diffusion was allowed to take place for a pre-determined time. During this process the crystals were sealed in a silica diffusion cell, which had first been out-gassed and then filled with an atmosphere of dry nitrogen. The cell was designed to hold four crystals which were placed on a cake-stand arrangement at the bottom of the cell. The complete diffusion cell situated in the furnace is shown in Fig. 15., a distance of 2 cms separated the top and bottom crystals.

Normally, each experiment was carried out with two pure crystals and two impurity-doped crystals in the cell. At the conclusion of a diffusion run, the cell was removed from the furnace and cooled quickly to room temperature. Carrying out the experiments in duplicate provided a check upon the consistency of the data.

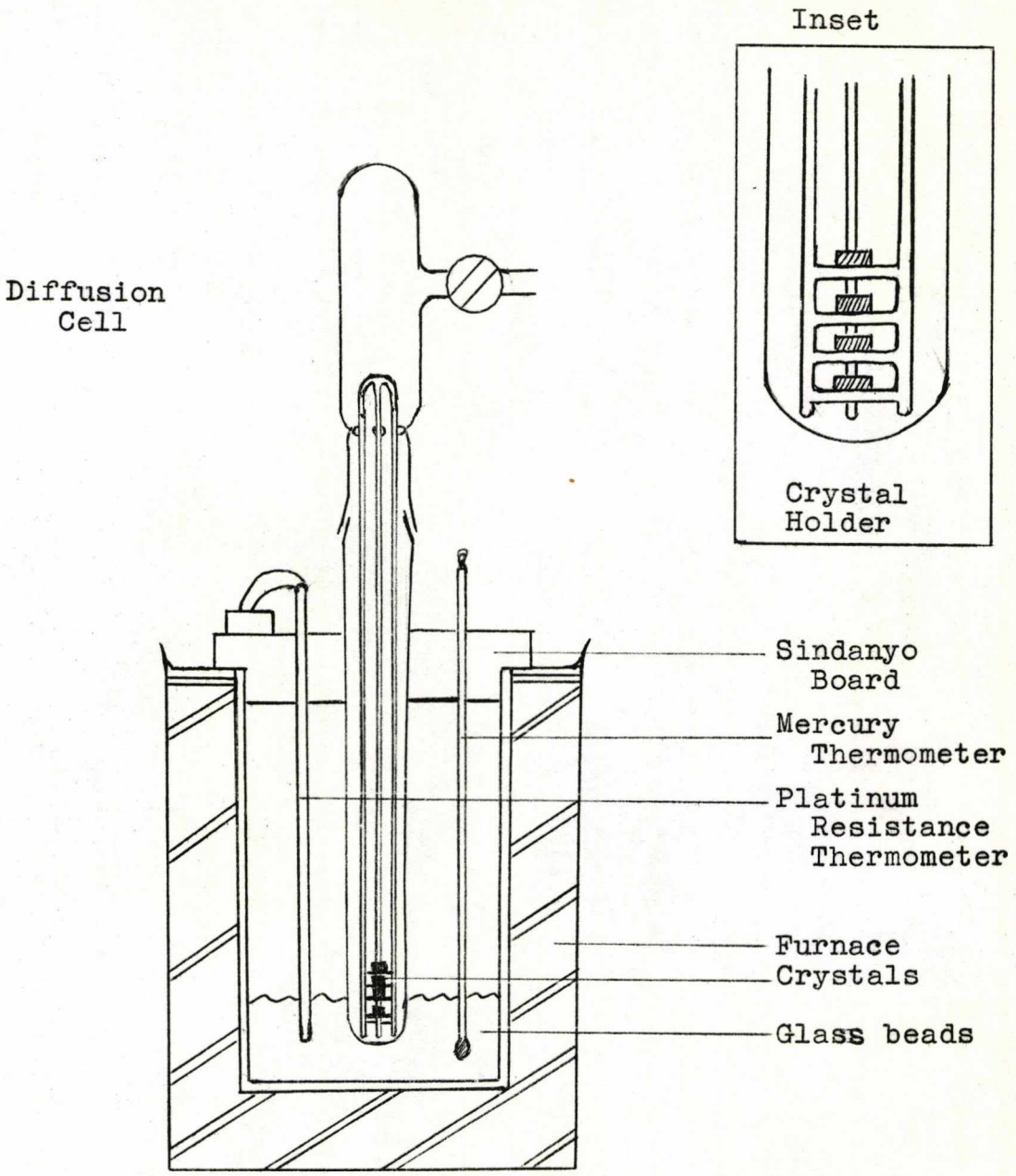

Fig. 15 - Diffusion Furnace and Cell

2.3(d) Temperature-control and Measurement

In order to obtain meaningful results it was essential that good temperature control could be maintained over long periods of time. Using an A.E.I. Ltd. Resistance Thermometer temperature controller, type RT3/R Mk.2, the furnace temperature could be regulated to $\pm$ 1.0°C over periods of up to three weeks.

The RT3/R Mk.2 is a fully proportional temperature controller covering the range 0 - 1200°C. It operates in conjunction with a Platinum Resistance Thermometer temperature sensor. The instrument is in two parts, (a) the Input Unit, and (b) the Power Regulator. A block diagram is shown in Fig. 16. The Input Unit contains the control electronics including its own power supply unit. In operation it delivers a D.C. current signal to the power regulator proportional to the temperature deviation from a set point. The Power Regulator is essentially a Thyristor full-wave power amplifier which has a constant voltage or current output according to requirement. The instrument is fully transistorised.

2.3(e) The Crystal Microtome and Sectioning Technique

The crystals were sectioned with an MSE 9010 Freezing Microtome, slices being taken parallel to the face upon which the radioactive salt had been deposited.

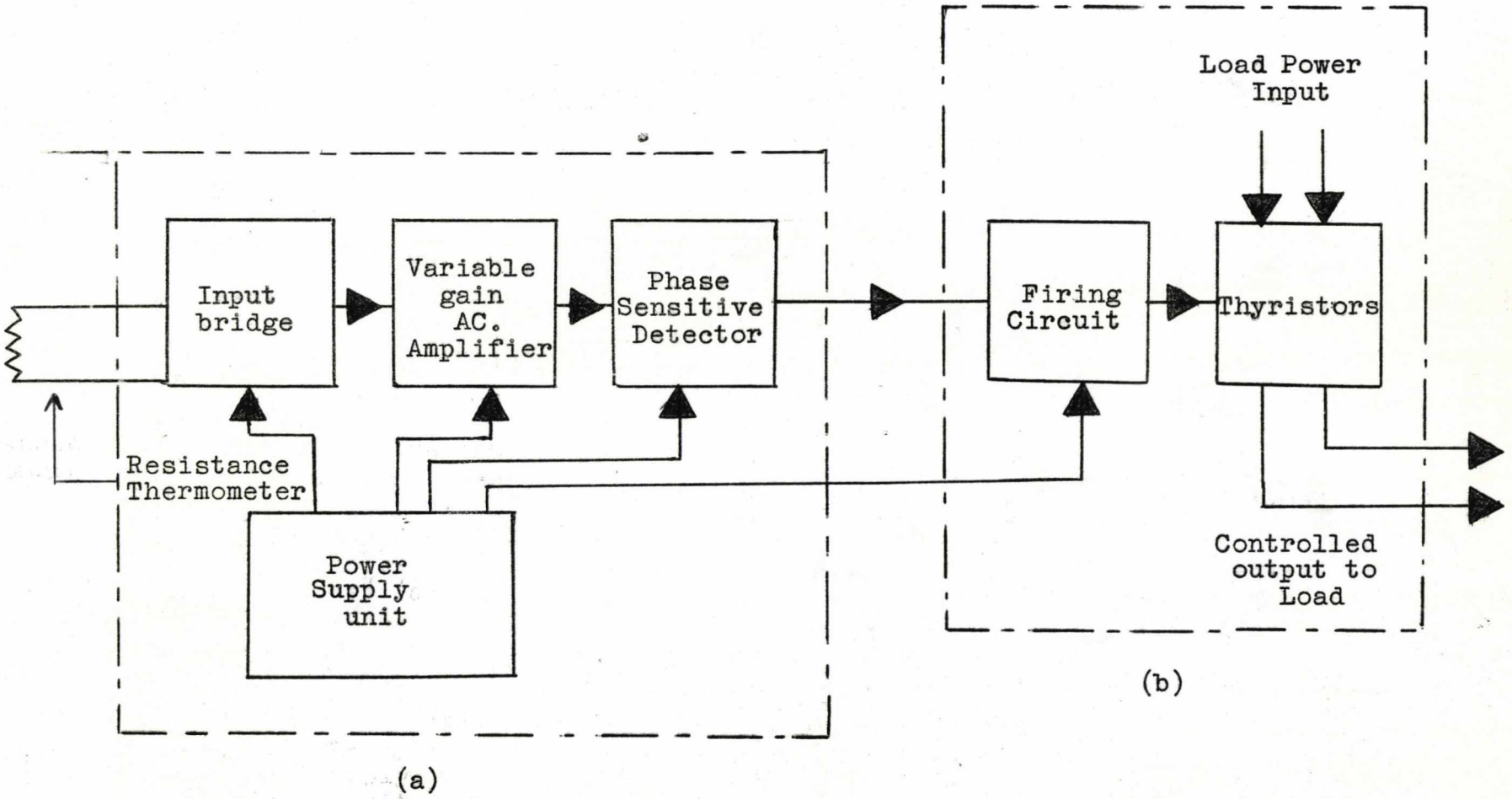

Fig. 16 - Platinum resistance thermometer. Block diagram.

The microtome is shown in Fig. 17.

After diffusion, a crystal was fixed to a brass rod with Araldite adhesive, and the rod clamped tightly in the microtome chuck. The knife was moved by means of a plastic handle attached to it, in a horizontal direction across the face of the crystal. The material removed from the crystal was in the form of a fine powder so that loss of material during the collection procedure could have presented a serious problem. This difficulty was overcome by passing a jet of moist air over the crystal prior to each section. When the crystal surface went just transparent, the knife was drawn across the face of the crystal. Sectioned material simply curled up on itself and fell intact on to an aluminium collection tray directly beneath.

The weight of each section was carefully recorded and an accurate estimate of the section thickness made from prior knowledge of the surface area of the crystal and the density of NaCl. After weighing, the samples were washed into polythene capsules (6 cms x 1.5 cms) and the activity counted in a well-type scintillation counter. To ensure a statistical accuracy of better than one per cent 10,000 or more counts were taken for each section. Each count rate was corrected for background radiation.

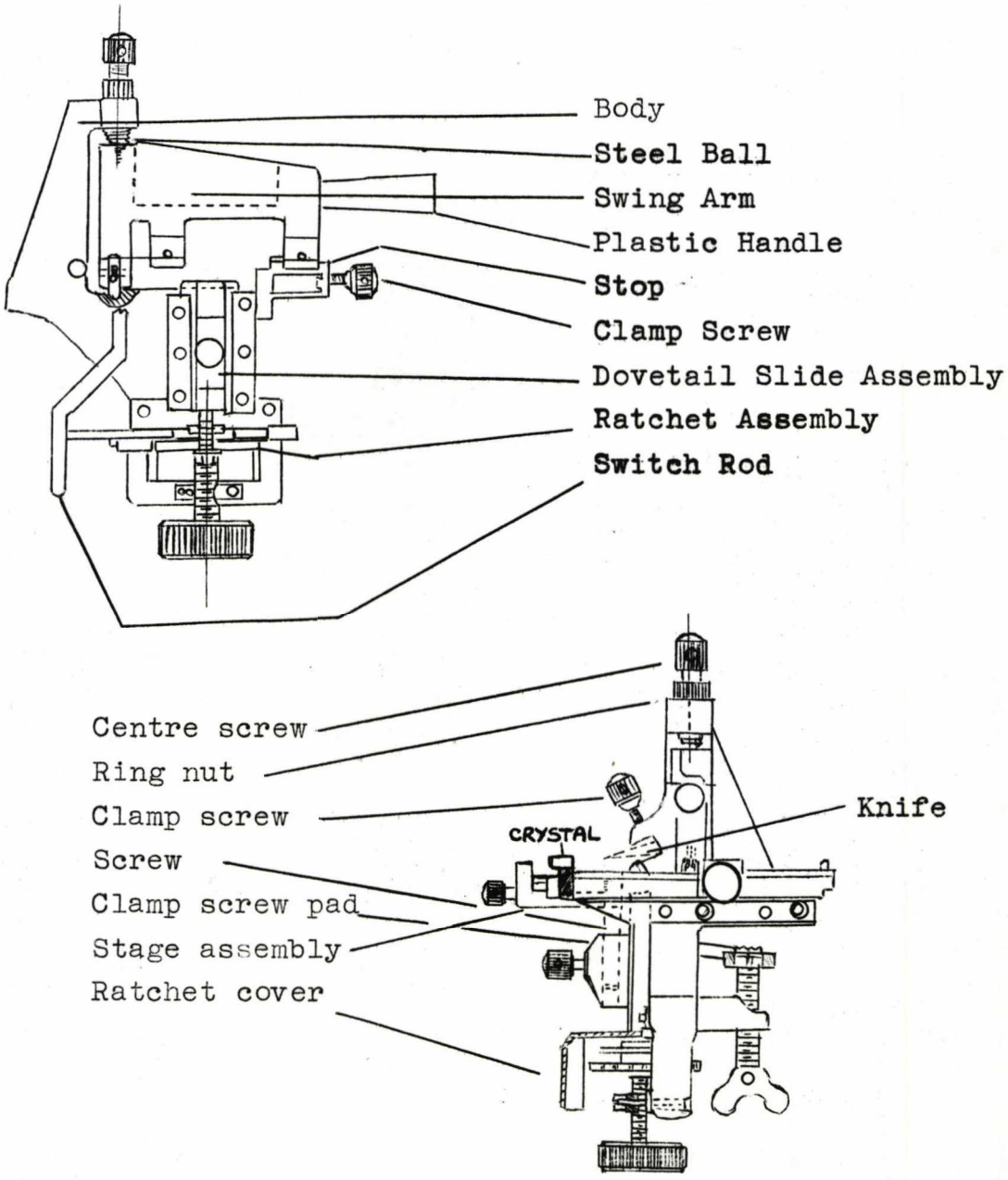

AUTOMATIC LABORATORY MICROTOME

Fig. 17

The accuracy of the sectioning technique in determining diffusion coefficients is critically dependent on the alignment of the knife with the crystal face. The error introduced in the diffusion coefficient due to misalignment of the specimen can be calculated[54]. In the MSE 9010 freezing microtome angular adjustment of the chuck was not possible. However, the brass rod to which the crystal was attached could be clamped in any position required. The crystal was therefore lined up parallel to the cutting edge of the knife and then secured tightly in that position. Slight misalignment of the crystal does not produce serious errors in the measured diffusion coefficient[55].

The minimum section thickness which could be removed by the microtome was 5×10^{-4} cm. Preliminary investigations using a large inactive NaCl crystal showed that the microtome consistently took off the required section thickness.

2.3(f) Surface Decrease Method

Preliminary investigations were made of the self-diffusion of Na^{22} in NaCl, using this method. It was necessary to calculate the absorption coefficient, μ, for the isotope in NaCl. Since it was impossible to prepare thin enough sections of NaCl for this experiment,

standard aluminium absorbers were used and the corresponding absorption in NaCl calculated by comparison of the densities of aluminium and NaCl. The apparatus and counting technique are described as follows.

Radioactivities were determined with a Geiger-Müller counter of window thickness 2.2 mg.cm^{-2}. The working voltage of the counter was 700 volts.

The experimental arrangement is shown in Fig. 18. Counting geometry was made reproducible by positioning the crystals on a brass plate fitted with an L-shaped bracket, which ensured that the active deposit was directly under the counter. Count rates were determined as a function of absorber thickness with the brass plate on the top shelf of the lead castle, that is, with the crystal as close to the counter as possible to eliminate any effect of back-scattered radiation[54]. The absorbers were positioned on the L-shaped bracket between the crystal and counter window. A total count of 10,000 on each sample ensured a statistical accuracy of 1%. A specially prepared standard source of $Na^{22}Cl$ was counted before and after every experiment to enable any corrections for counter fluctuation to be made. Count rates were corrected for dead-time losses and background radiation.

The radiation emitted from Na^{22} is a mixture of β^+ and γ particles. Since only the β^+-radiation was

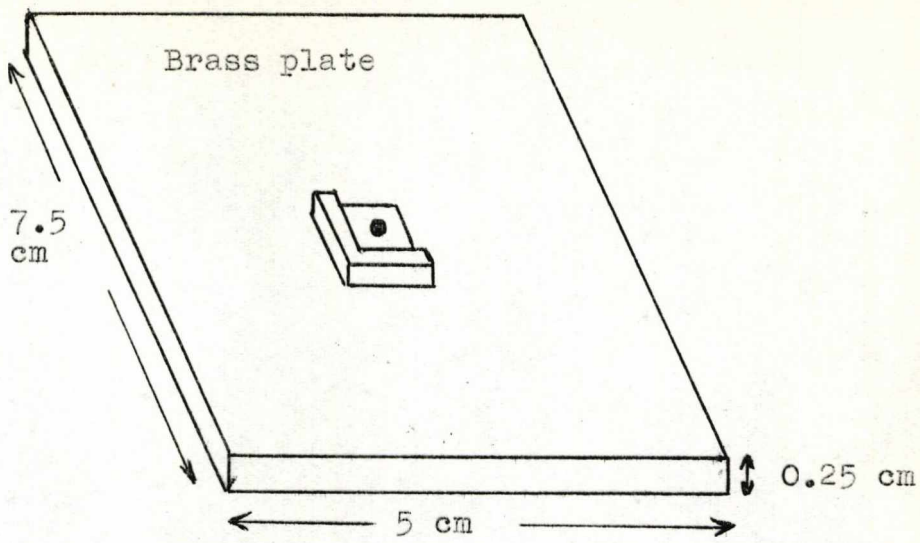

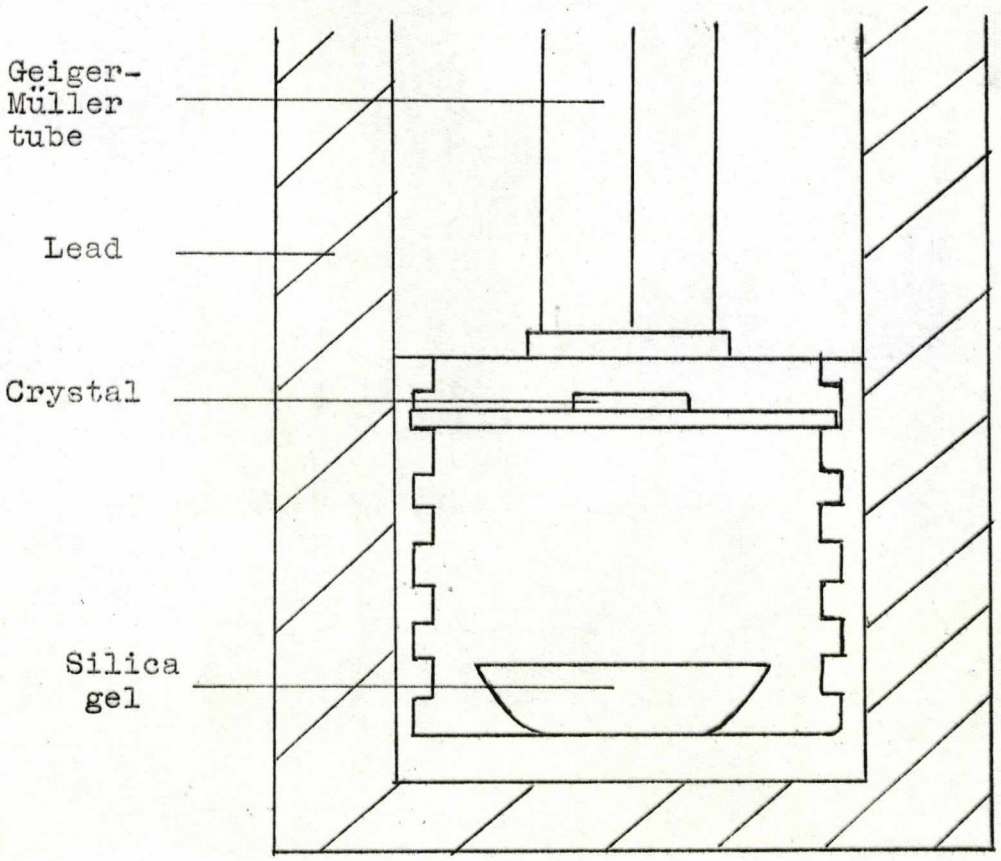

Fig. 18 - Experimental arrangement for 'end-window' counting.

required, the contribution to the total count rate from γ-radiation had to be determined and subtracted. This was done by placing an aluminium absorber of thickness 200 $mg.cm^{-2}$ between the crystal and the counter. The γ count rate should remain constant throughout any experiment, any significant drop at the end of an experiment would indicate loss of material by evaporation and could be corrected for.

Absorption coefficients were determined from plots of log activity (CPM) versus aluminium absorber thickness ($mg.cm^{-2}$). d, the half-thickness, is that weight per square centimetre of absorber which would be required to halve the counting rate, and was calculated from the curve. Experimental results for Na^{22} are plotted in Fig. 19. The absorption coefficient, μ, was calculated in the following way. The absorption of radiation in matter is given by[56]

$$A_d/A_o = \exp(-\mu d) \qquad (2.10)$$

where A_o is initial activity

A_d is activity with absorber of $\underline{d}$ $mg.cm^{-2}$

d is absorber thickness

μ is the absorption coefficient.

Absorption

Coefficient - Na^{22}

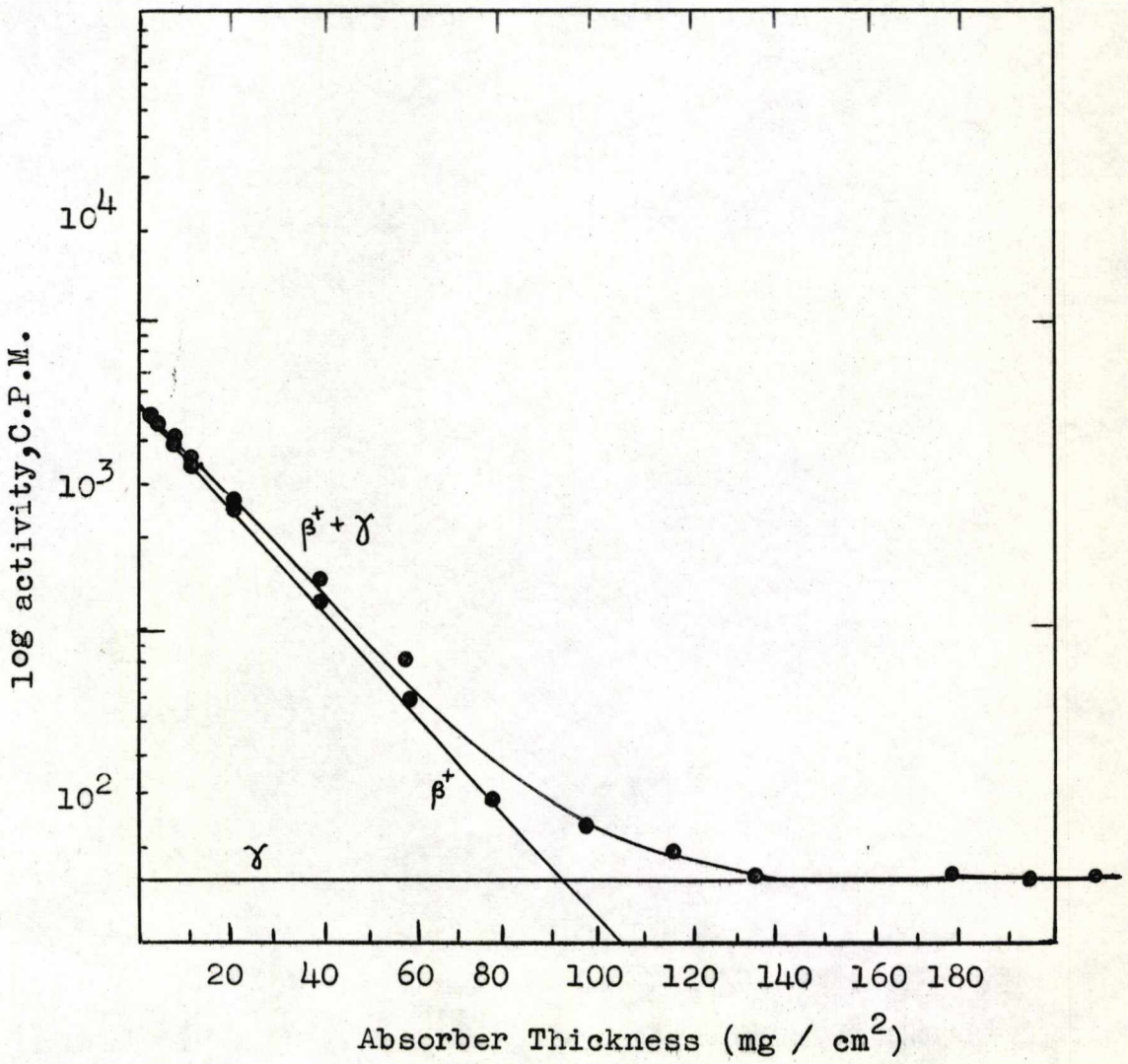

Fig. 19.

TABLE 4

Absorption Coefficient - Na^{22}

Absorber thickness (mg/cm^2)	Activity $\beta^+ + \gamma$ (cpm)	Dead time correction (cpm)	Corrected activity β^+ (cpm)
0.00	5152	5372	5222
1.47	5003	5209	5059
2.94	4780	4967	4817
6.00	4322	4472	4320
11.60	3653	3756	3606
19.40	2668	2715	2565
38.80	1411	1417	1267
58.40	751	744	594
76.40	426	436	286
97.00	247	236	86
116.40	197	186	36
135.80	167	156	6
159.00	161	150	0
178.40	161	150	0
197.80	160	149	1
212.00	161	150	0

$$d = 18.0 \text{ mg/cm}^2$$

$$\therefore \mu_{Na^{22}} = \frac{0.693 \times 2.165}{18.0 \times 10^{-3}} \text{ mg/cm}^2$$

$$= 83.3 \text{ mg/cm}^2$$

$$\mu = \frac{2.303}{d} \times \log \frac{A_d}{A_o} \qquad (2.11)$$

$$= \frac{2.303}{d_{\frac{1}{2}}} \cdot \log 2$$

$$= \frac{0.693}{d_{\frac{1}{2}}} \text{ mg.cm}^{-2} \text{ Al}$$

and converting to cm^{-1} in NaCl (density = 2.165 mg.cm^{-3})

$$\mu = \frac{0.693 \times 2165}{d_{\frac{1}{2}}} \text{ cm}^{-1}$$

Absorption coefficient data for Na^{22} in NaCl is given in table 4.

2.3(g) The Scintillation Counter

The complete assembly was built from units of the fully transistorised A.E.R.E. Harwell 2000 series, and consisted of a well-type thallium activated NaI crystal, whose dimensions were 5 cm x 5 cm., an EMI 9536 A type photomultiplier tube, a 95/0058 - 1/6-type amplifier head, a 95/2151 - 2/6-type amplifier, a 95/2170 - 1/6-type analyser, and a 95/2130 - 2/6-type scaler connected in that order.

The interaction of γ-rays with the crystal produces fast electrons which are readsorbed in the crystal accompanied by the emission of light photons. These are detected by the photocathode surface of the photomultiplier tube and converted into electrical pulses. The

photomultiplier tube acts as a high-gain amplifier, and in successive stages multiplies the number of electrons sufficiently to deliver a pulse at the output, which is large enough to be handled by the remainder of the electronic system.

The main requirement of the amplifier system is to provide a magnified output pulse of defined duration and shape. The amplitude of the output pulse should be proportional to the electrical charge delivered by the nuclear detector. The main amplifier unit provided the bulk of the gain and accommodated the active controls of the complete amplifier assembly.

The pulse-height analyser accepts the pulses from the amplifier and provides output pulses according to whether they fall between two pre-set limits of amplitude, these two limits defining a channel width. The single channel analyser allows the selection of photopeaks corresponding to a particular γ-ray energy. Since the largest pulses are produced by photoelectric absorption, this peak can be used in the determination of γ-ray energies. The photopeaks of Na^{22} and Mn^{54} were selected from their corresponding pulse-height spectra, obtained using a channel width of 0.1 volts. These are shown in Figs. 20 and 21, with the corresponding data in tables 5 and 6.

Pulse-height Spectrum - Na^{22}

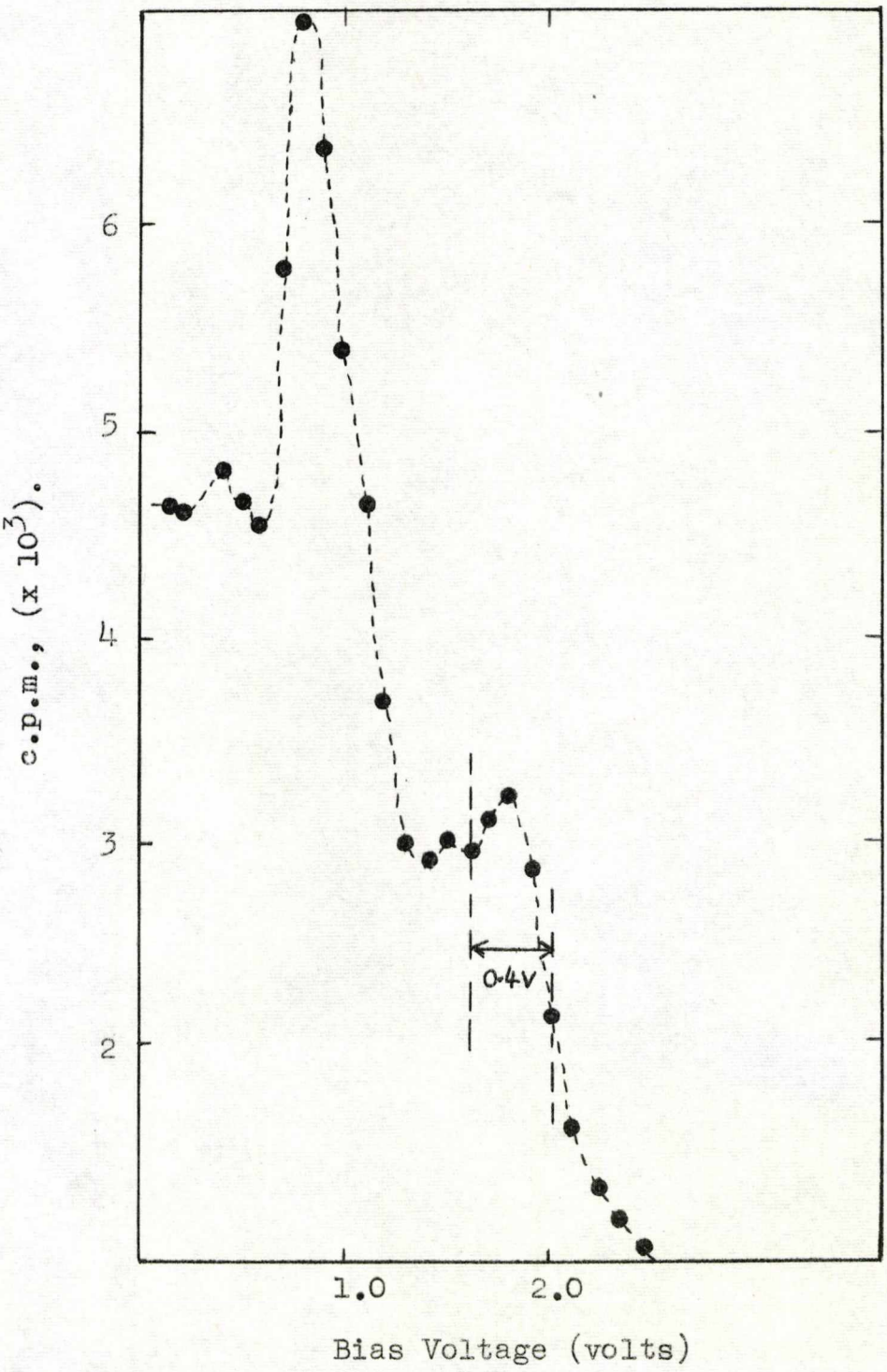

Fig. 20

TABLE 5

Pulse-Height Spectrum of Na^{22}

Bias Voltage (volts)	Corrected Activity (cpm)
0.15	4622
0.20	4577
0.30	4671
0.40	4802
0.50	4646
0.60	4539
0.70	5798
0.80	6977
0.90	6310
1.00	5389
1.10	4597
1.20	3699
1.30	2972
1.40	2916
1.50	2998
1.60	2975
1.70	3125
1.80	3254
1.90	2967
2.00	2185
2.10	1576
2.20	1386
2.30	1182
2.40	1070
2.50	908

Channel width = 0.1v Gain = 38 dB

E.H.T. = 1450v Background activity = 26 cpm.

Pulse - Height Spectrum

Mn^{54}

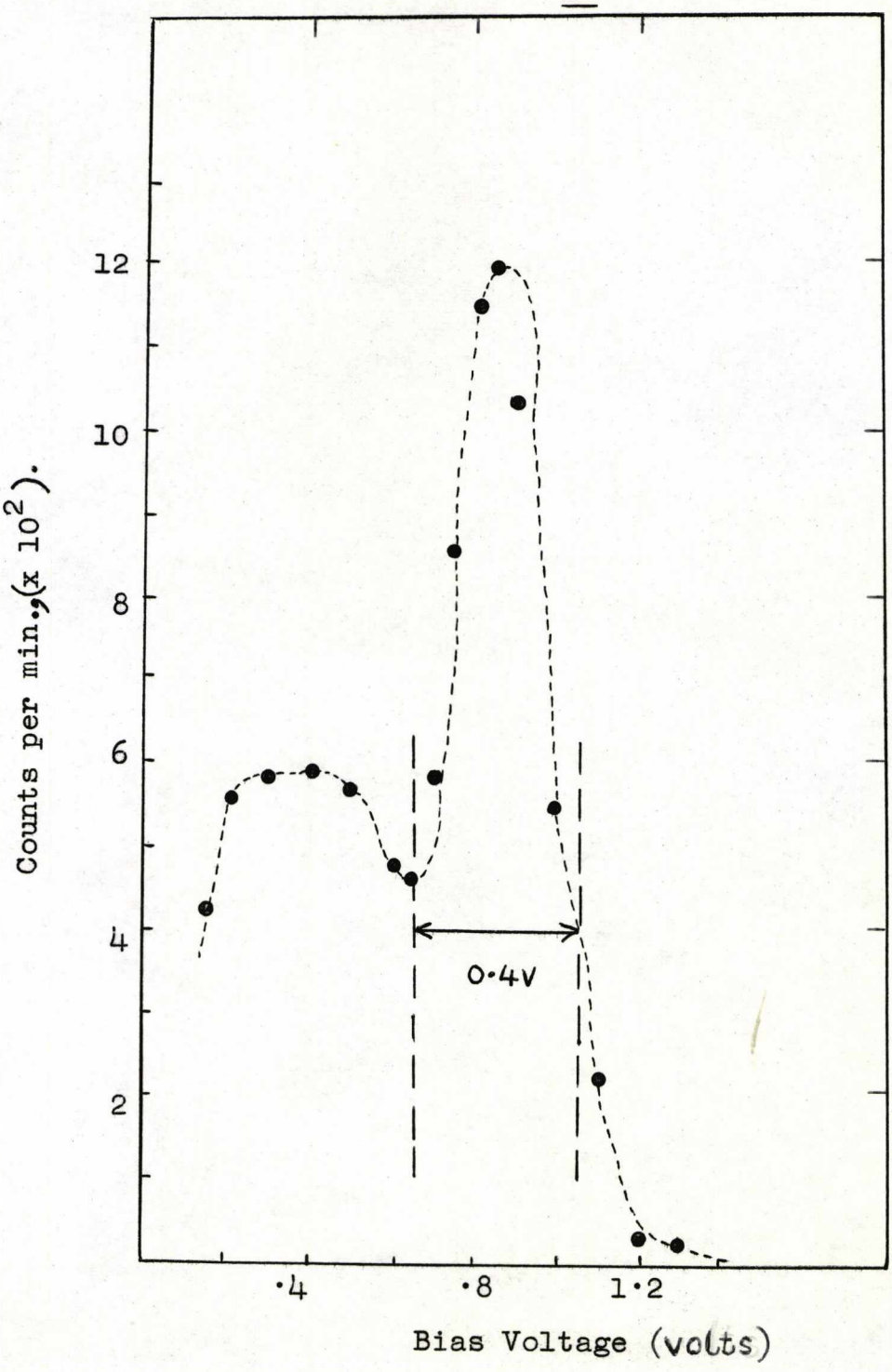

Fig. 21.

TABLE 6

Pulse-Height Spectrum of Mn^{54}

Bias Voltage (volts)	Corrected Activity (cpm)
0.15	423
0.20	559
0.30	585
0.40	593
0.50	570
0.60	476
0.65	464
0.70	581
0.75	854
0.80	1147
0.85	1196
0.90	1035
1.00	545
1.10	220
1.20	29
1.30	17
1.40	13

Channel width = 0.1 v. Gain = 40 dB

E.H.T. = 1450 v. Background activity = 28 cpm.

2.3(h) Trace Analysis

Trace impurities play a major role in a wide variety of physical and chemical processes. In recent years the growing awareness of how significant these trace elements are, and how important it is to detect them accurately has produced refinements and extensions of analyses at the parts per million and even lower concentration levels. The result is a set of new methods and instruments of such a specialised nature that they represent a distinct field of analytical chemistry called trace analysis.

Among the more widely used of the trace-analysis techniques are activation analysis, absorption and emission spectrometry, and x-ray spectrometry. Each method has its advantages and limitations for different applications. Sensitivity, accuracy, precision and selectivity are the criteria used in selecting the appropriate technique. The choice, inevitably, must involve a series of compromises.

Activation analysis, if one uses high fluxes of bombarding particles, offers the most sensitive technique for many elements although the procedure is slower and more cumbersome than the others because the samples must be taken to a reactor for irradiation. In this nuclear analysis method the sample containing the trace element is bombarded so that it becomes radioactive and can be measured. The amount of radioisotope produced in the

sample is directly proportional to the amount of precursor isotope, and is usually measured with a scintillation counter and pulse-height analyser, if γ-rays are emitted. The sensitivity of the method has increased enormously with the high resolutions that are now available with the new lithium-drifted germanium semiconductor detectors. Individual photopeaks now stand out more distinctly over background radiations, allowing one to detect weaker gamma energies than can be measured with NaI scintillation detectors.

For solution analysis, atomic absorption is the most sensitive at very low concentration levels. The solution sample is vapourised in a high-temperature flame. Each of the elements in the vapour phase then absorbs radiation at a discreet number of wavelengths, and these absorption lines are used to identify the elements. Because these absorption lines do not generally overlap, the technique is essentially free from spectral interferences. Moreover, because the atoms must be in the ground state to absorb the radiation, physical effects, such as changes in flame temperature and interactions of excited atoms, have little effect on the analysis. Any element can be measured by atomic absorption spectroscopy if its resonance line is in the part of the spectrum that

the instrument can use and if it can be reduced to the atomic state by a sampling technique.

Optical emission spectroscopy, in which the characteristic line spectra are emitted, rather than absorbed, by elements in flames and discharges, provides a relatively simple and convenient way to detect and determine trace impurities[57]. In most cases, the detection limits are as low as a few parts per million, and under ideal conditions the limits may be as low as a few parts per billion. Unlike chemical analysis methods which are usually less precise at lower concentration levels, optical emission spectrometry show a uniform precision over most of the concentration range.

X-ray fluorescence spectrometry methods are very precise at high levels, that is, more than one per cent of the amount present, and multi-element analysis can be achieved more rapidly with it than with absorption or emission spectrometry.

The basis of the method is that when electrons bombard matter, they react with the atoms, emitting x-rays, the intensity of which depends on the concentration of the element, the matrix in which the element occurs, the concentration and nature of the other elements present, and the thickness of the sample. Thus, by measuring the x-ray spectral lines one can identify trace-element concentrations in the sample. An advantage of x-ray

spectroscopy stems from the fact that the penetration depth of the x-rays into the sample depends on their wavelength and beam strength. By varying these factors, one can regulate the penetration and hence the part of the sample being analysed.

In the present work, it was decided that activation analysis would not be suitable since any bombardment to activate the impurity would also result in the host ions becoming radioactive. One would therefore be dealing with highly radioactive crystals and it is doubtful whether, with the present counting arrangement, there would have been a sufficiently high resolution of the γ-rays. The impurity analyses were therefore made using spectrophotometric techniques. A detailed account of the experimental procedures will now be given.

(i) Spectrophotometric Titration in the Ultra-Violet.

Analyses of traces of alkaline-earth elements present in a large excess of an alkali-halide have been performed successfully using the large absorbance in the ultra-violet at 222 mμ of ethylenediamine tetra-acetic acid[58]. This involves a spectrophotometric titration of a buffered solution of the sample with EDTA.

EDTA or its salts react quantitatively with alkaline-earth ions to produce complexes of high stability. Such

complex-formation reactions are often used as a basis for analytical methods. EDTA is a tetrabasic acid with the formula:

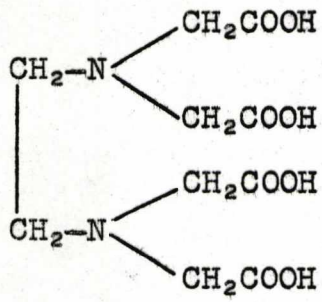

When completely ionised this will react with, for example, Ca^{2+} according to the equation

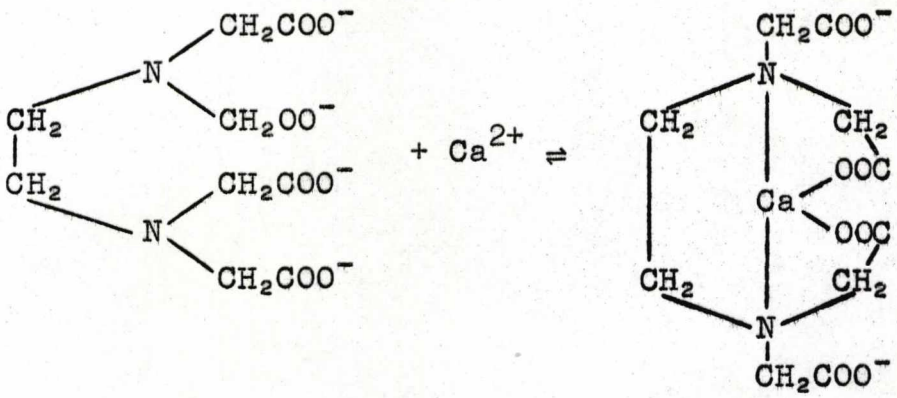

to form a complex with bonds to the calcium atom from both the carboxyl groups and the nitrogen atoms.

Since EDTA is a weak acid it was necessary to make the solution alkaline in order to obtain enough of the completely ionised form for the reaction to take place.

The experimental procedure was as follows. After weighing the sample, it was transferred to a 5 ml volumetric flask, and 10 drops of buffer solution added.

This was diluted to volume, shaken well, and 2 ml transferred to a cell and placed in a Unicam SP 500 spectrophotometer. The absorbance was read at 222 mμ and EDTA of known concentration added in small increments from a 2 ml micro-burette, the absorbance being noted after each addition of reagent. The change in absorbance was small until after the end-point when a sharp rise occurred with increasing amounts of reagent. A blank was prepared in an identical manner but without the sample and dilution corrected for during the titration. The reagents used were prepared as follows:

0.01M EDTA

3.723 gms of dihydrogen disodium ethylene diamine tetra-acetate were dissolved in water and diluted to 1 litre. The solution was standardised against a standard zinc solution.

Buffer Solution

A 1M NH_4Cl-NH_3 buffer of pH 10 was prepared by diluting 5.4 gms of NH_4Cl and 75 ml of ammonia (specific gravity 0.88) to 100 ml.

Standard Zinc Solution

1 gm of pure, granulated zinc was washed with ether to remove any oils present and then dried. The zinc was then washed with 0.5M HCl to remove oxides and finally with de-ionised water. After careful drying 0.626 gms

were weighed out, dissolved in water and made up to 1 litre to give a 0.01M solution.

The EDTA was standardised against the standard zinc solution using xylenol orange as indicator. The colour change was from red to yellow. The strength of the EDTA was calculated using the equation

1 litre 1M EDTA ≡ 65.38 gms Zn.

Spectrophotometric titration in the ultra-violet lends itself well to the determination of traces of alkaline earths in alkali halides. The titration will determine any of the alkaline earths or their sum if a mixture is present. EDTA absorbs more strongly in the ultra-violet than its alkaline earth metal complexes. The method was therefore used for the estimation of Mg^{2+}, Ca^{2+}, Sr^{2+} and Ba^{2+} in the NaCl crystals upon which experiments had been made. Typical titration graphs for the determination of each of these impurities are shown in Figs. 22, 23, 24, 25. The relevant data and sample calculations are listed in the appendix.

The sensitivity of the method is not as high as that possible with the more sophisticated techniques. For example, it was almost impossible to estimate below a concentration level of 20 ppm, especially if the sample was rather small (< 0.10 gms). However, accuracy of

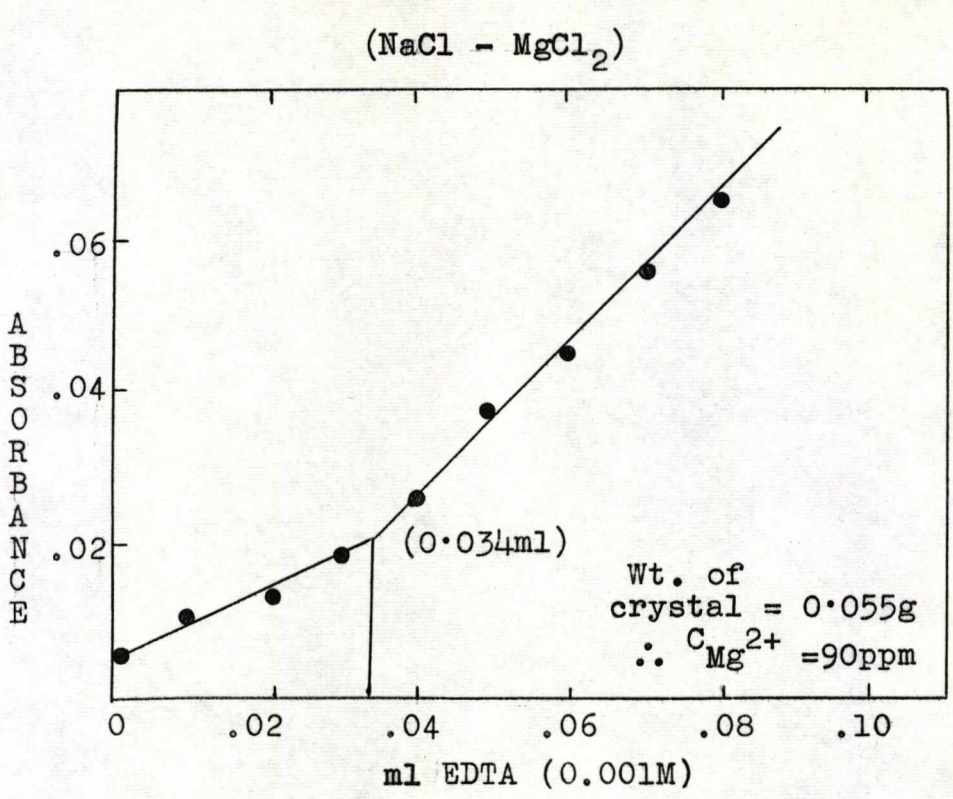
(NaCl - MgCl2)
ABSORBANCE
.06
.04
.02
(0·034ml)
Wt. of
crystal = 0·055g
∴ C Mg2+ =90ppm
0
.02
.04
.06
.08
.10
ml EDTA (0.001M)

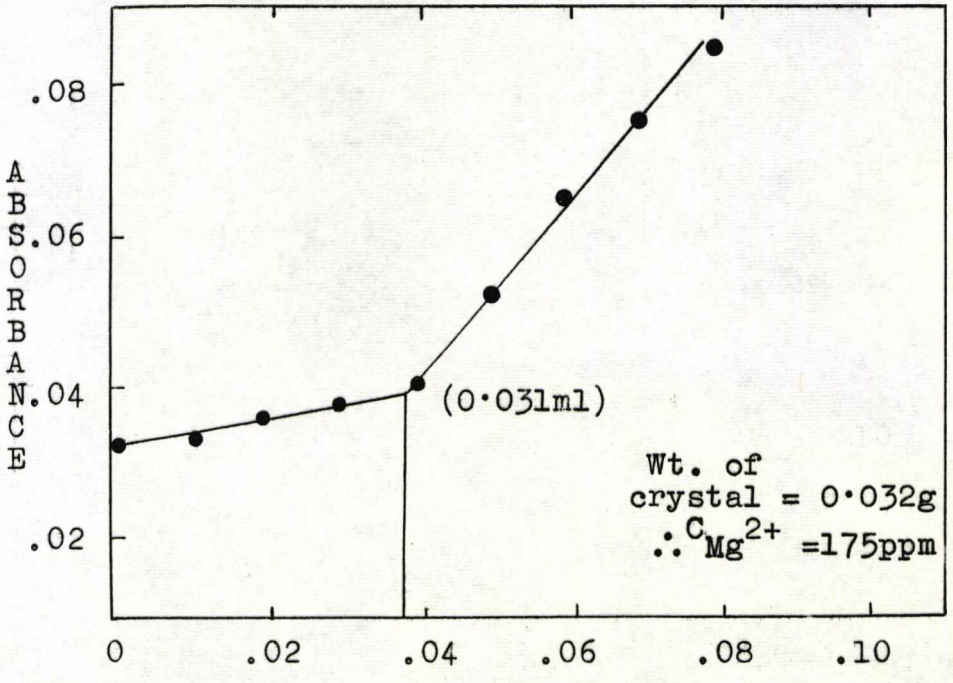
ABSORBANCE
.08
.06
.04
.02
(0·031ml)
Wt. of
crystal = 0·032g
∴ C Mg2+ =175ppm
0
.02
.04
.06
.08
.10

Fig. 22.

($NaCl - CaCl_2$)

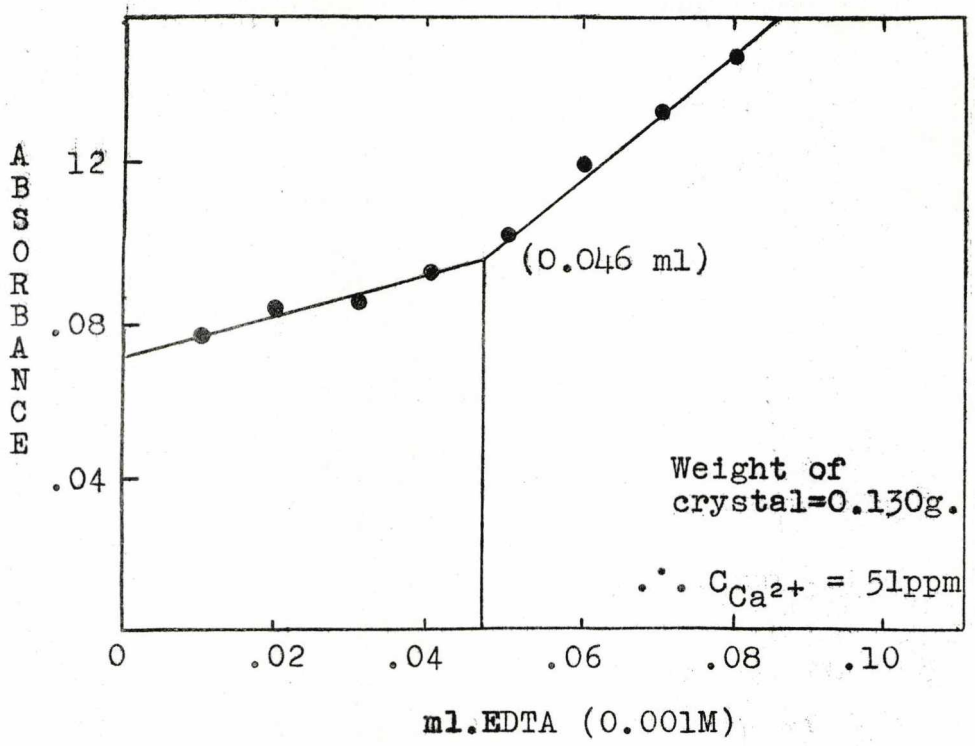

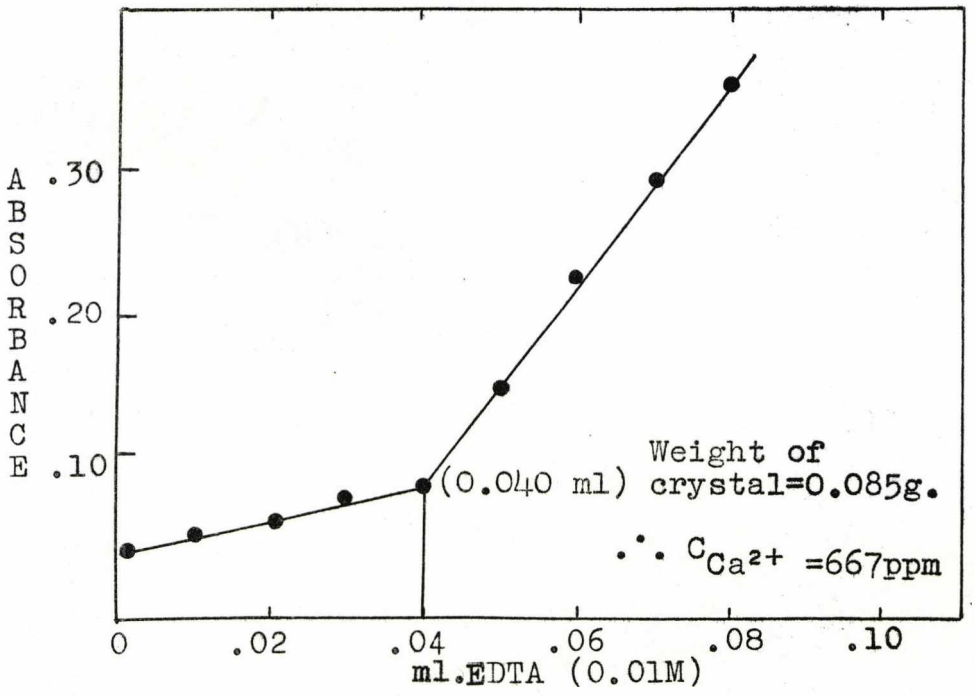

Fig. 23.

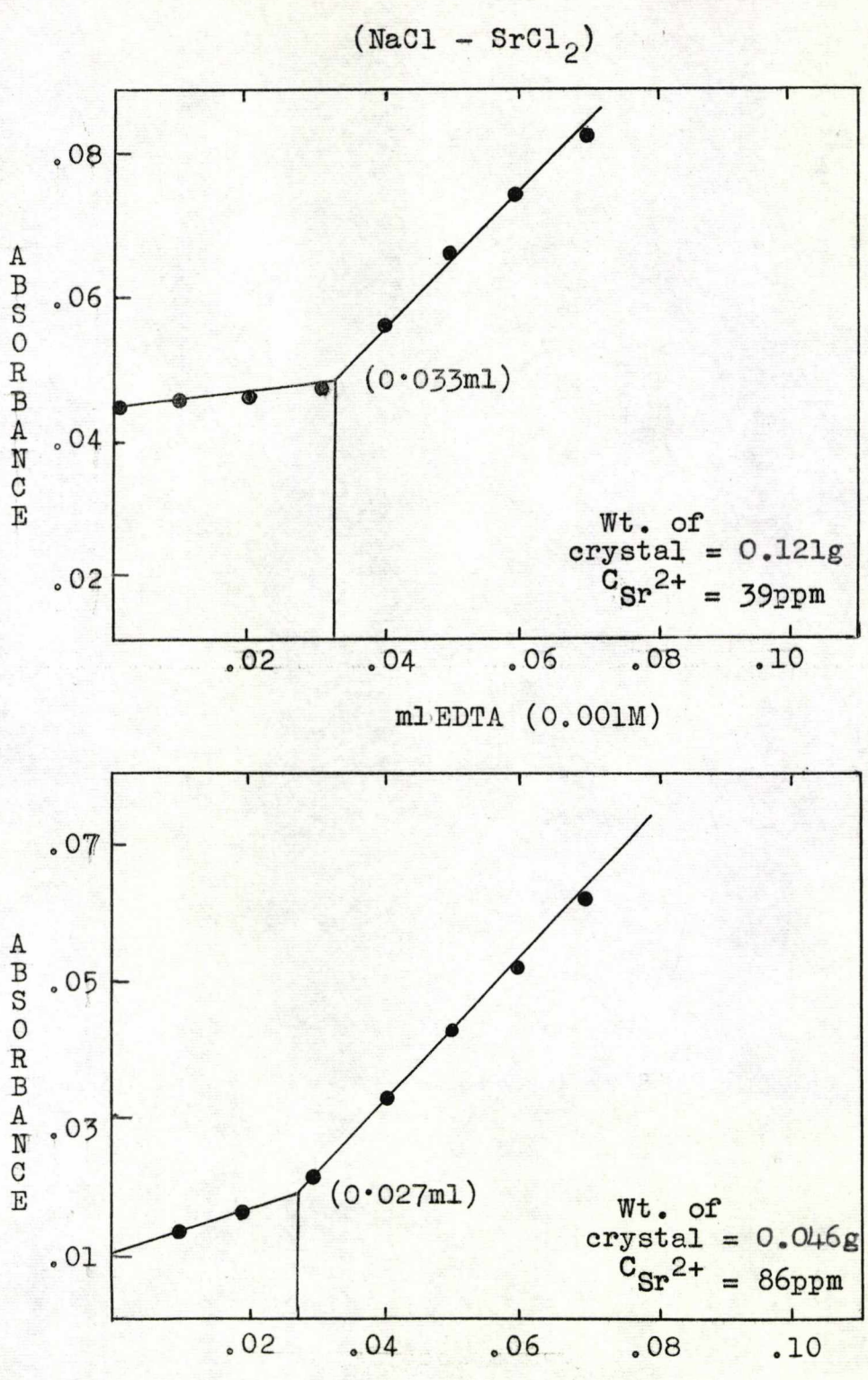
(NaCl - SrCl2)
ABSORBANCE
.08
.06
.04
.02
(0·033ml)
Wt. of crystal = 0.121g
C Sr2+ = 39ppm
.02
.04
.06
.08
.10
ml EDTA (0.001M)
ABSORBANCE
.07
.05
.03
.01
(0·027ml)
Wt. of crystal = 0.046g
C Sr2+ = 86ppm
.02
.04
.06
.08
.10

Fig. 24.

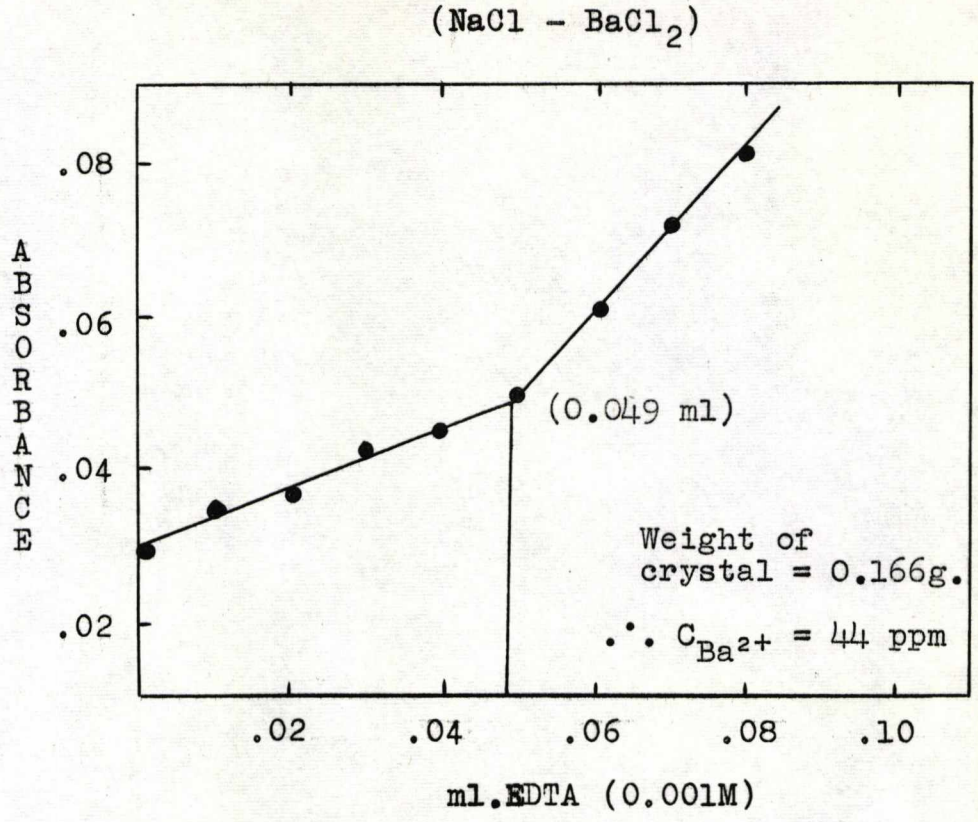
(NaCl - $BaCl_2$)
ABSORBANCE
.08
.06
.04
.02
(0.049 ml)
Weight of crystal = 0.166g.
$\therefore C_{Ba^{2+}}$ = 44 ppm
.02
.04
.06
.08
.10
ml. EDTA (0.001M)

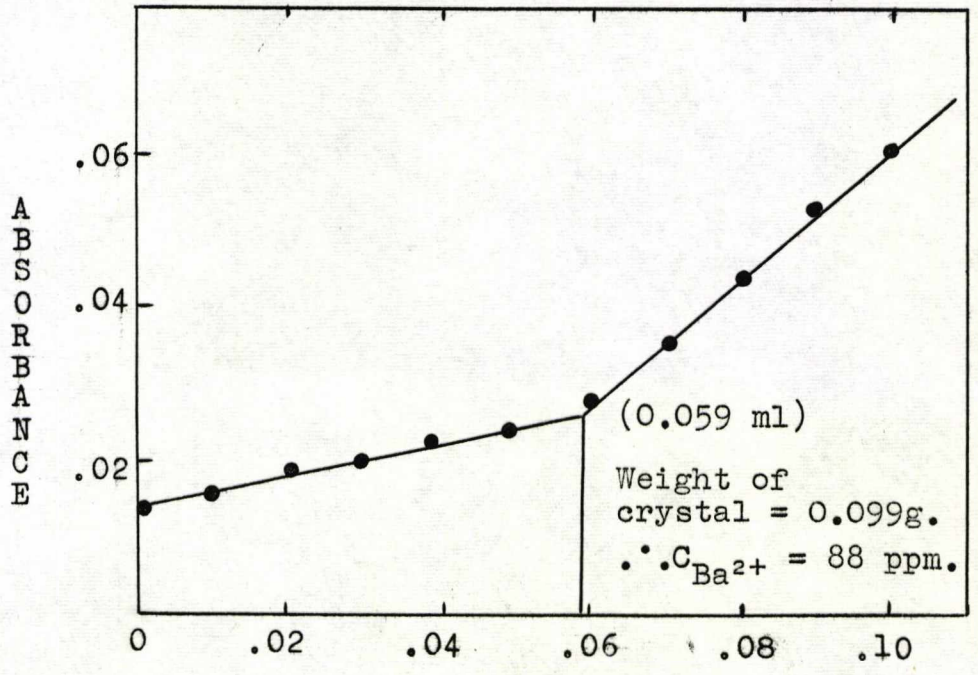
ABSORBANCE
.06
.04
.02
(0.059 ml)
Weight of crystal = 0.099g.
$\therefore C_{Ba^{2+}}$ = 88 ppm.
0
.02
.04
.06
.08
.10

Fig, 25.

Accuracy of the Method

Titration of Calcium Standards

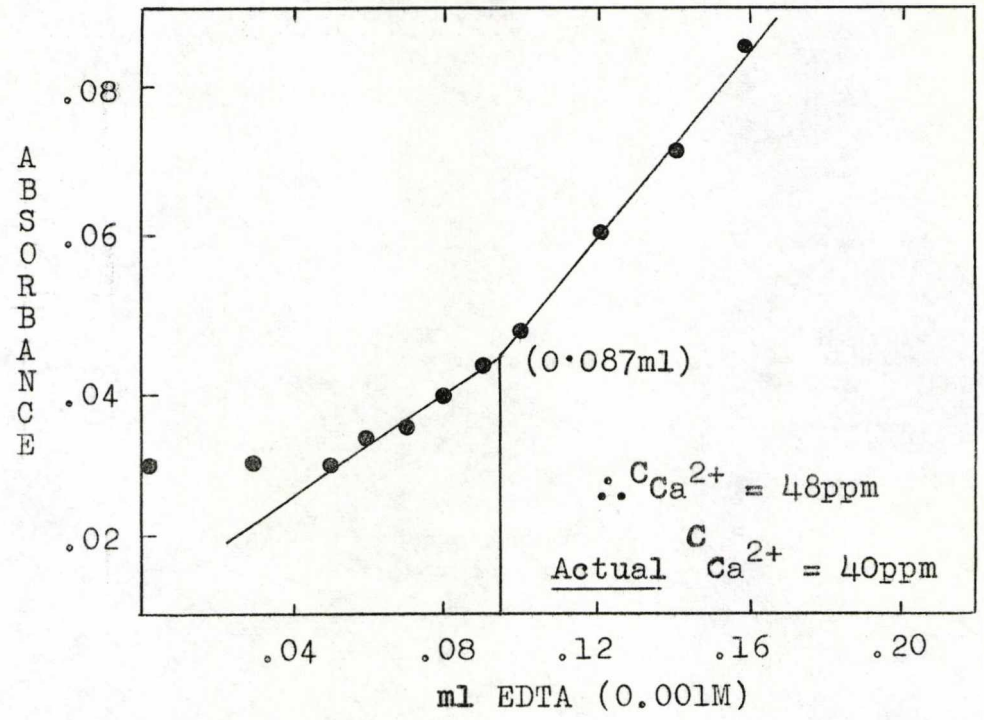

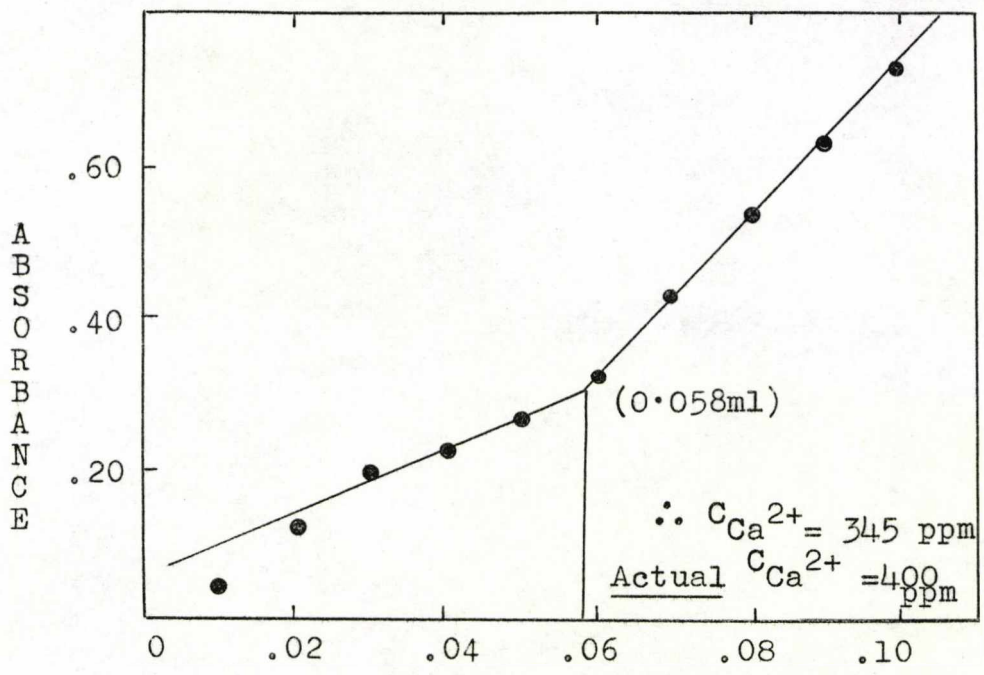

Fig. 26.

measurement increased with concentration of impurity present. The error on a measurement of 100 ppm was estimated to be ± 15 ppm.

A detailed study of the accuracy of the method was made for a series of specially prepared standard solutions of 5% NaCl containing known amounts of Ca^{2+}. These were titrated with EDTA and comparison made between the actual and experimental values of impurity content. Some of these are shown in Fig. 26. Generally speaking the method could determine impurity concentration to within 15% of the actual value.

(ii) Atomic Absorption Spectrophotometry

When a solution is passed as a dispersion of fine droplets into a gas/air flame the elements present are largely converted to the atomic state. Atoms of every element can absorb radiation at different characteristic wavelengths, preferentially by those transitions involving the ground state which result in the resonance lines.

When conditions in the flame are held constant this absorption obeys the same quantitative laws which apply to other forms of solution spectrophotometry, that is:

$$\text{Optical Density} = \log \frac{I_o}{I} \propto \text{concentration}$$

where I_o = incident light intensity

I = transmitted light intensity.

Since the width of atomic absorption lines is extremely small a continuous source is not suitable in an instrument designed to exploit this effect. In order to make the technique sensitive therefore, a hollow cathode discharge lamp is used to provide a source of radiation of extremely narrow band-width specific for the element sought. The cathode of this lamp contains the element in question and emits the characteristic line spectrum in which the resonance lines are prominent.

A monochromator is necessary to select the most sensitive line while rejecting all unwanted radiation. After absorption by the sample a photomultiplier detection system is used to measure the residual transmitted radiation. A block diagram of the Unicam SP 90 Atomic Absorption Spectrophotometer is shown in Fig. 27.

The experimental procedure was as follows. The crystal was dissolved in de-ionised water to give a 1% NaCl solution. This was found to be the maximum concentration permissible which allowed a series of crystals to be estimated without decrease in sensitivity due to unavoidable 'clogging' of the burner by solid NaCl. The solution of the sample was then drawn into the atomiser via a length of flexible polythene capillary tubing, dispersed into droplet form and passed into the cloud chamber. The nominal sample uptake was 3 ml/min

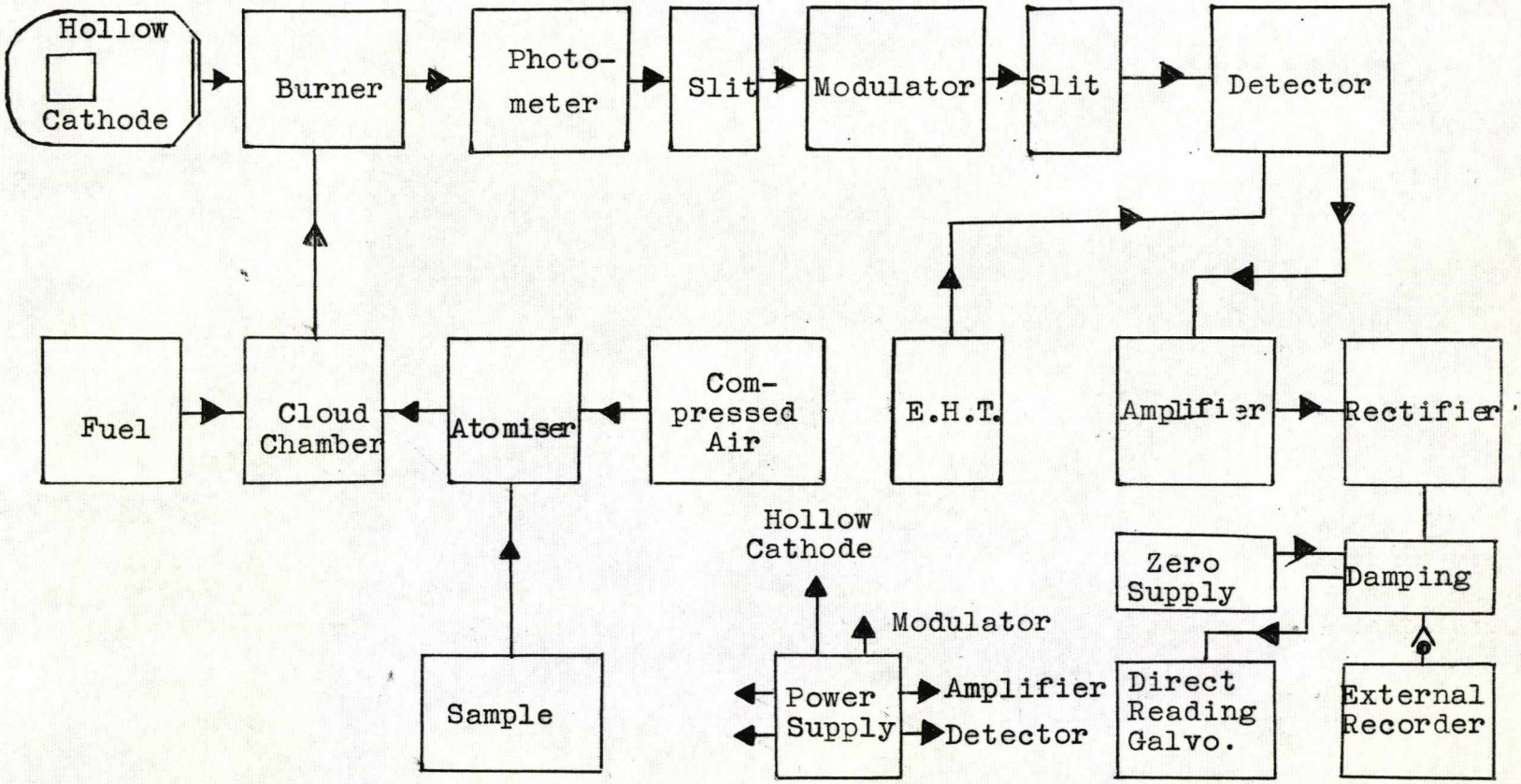

Fig. 27 - Atomic absorption spectrophotometer block diagram.

at an airflow of 5 litres/min. From the cloud chamber an air-fuel mixture carrying an evenly dispersed sample mist was supplied to the 10 cm slot burner, whose height was pre-set by means of a rack and pinion adjustment. The sample was dissociated at the flame temperature into its atomic ground state.

When the SP 90 became available, the elements still to be determined in the present research were Mn and Pb. The method worked well for the determination of Mn, and the optimum conditions are listed below:

Fuel	- Air-propane
Flow Rate	- 450 ccs/min
Gain	- 3
Slit width	- 0.1 m.m.
Burner Height	- 1.5 cms.
Resonance Line	- 279.5 mμ

Before each series of measurements an empirical calibration using a number of standards had to be made. A typical calibration followed by the estimation of some samples of unknown Mn concentration are shown in Fig. 28(a). The calibration graph of % Absorption versus concentration of Mn is shown in Fig. 28(b). The measurements were recorded on a Servoscribe potentiometric recorder, type RE 511.

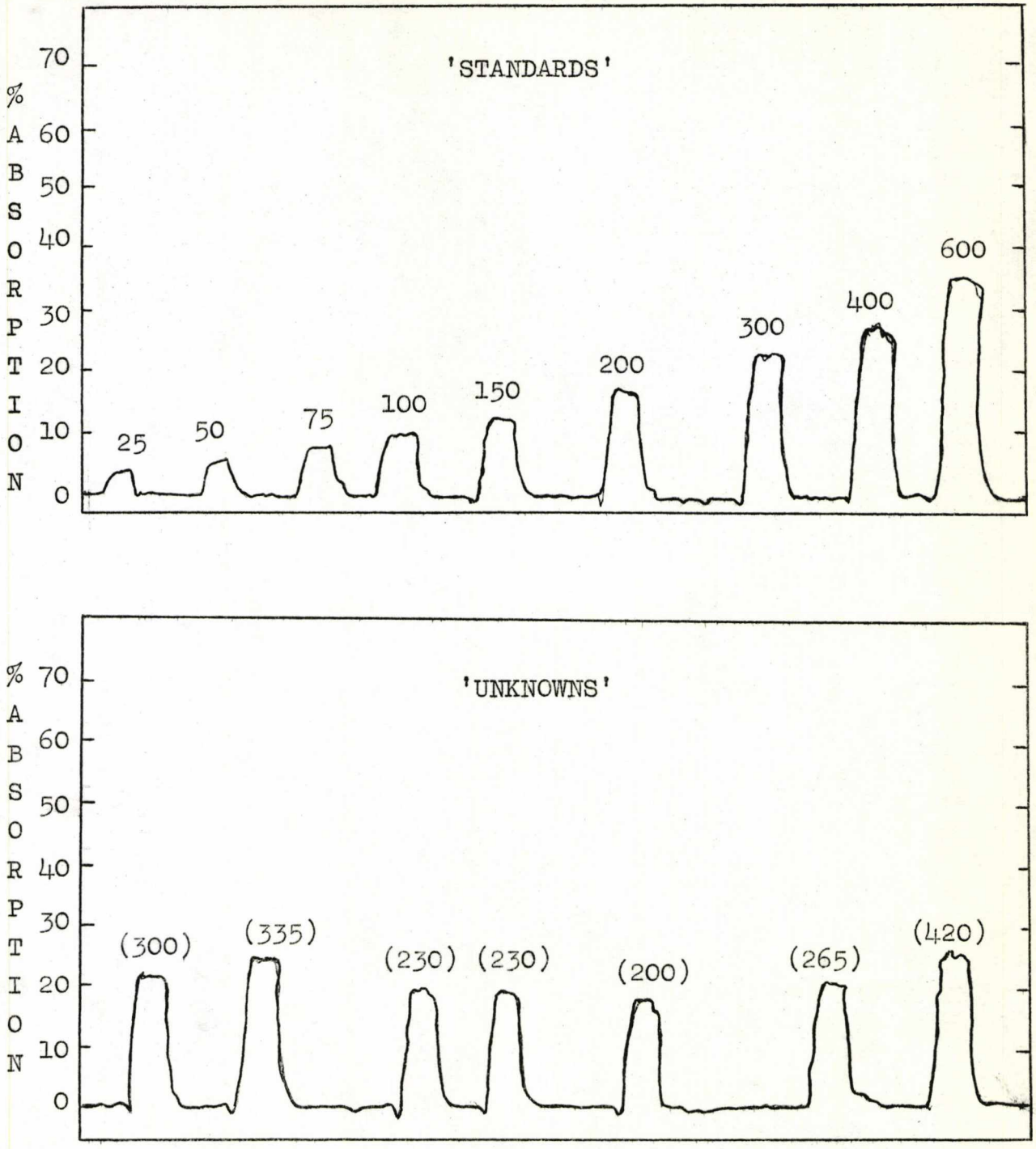

Fig. 28(a) - Trace analysis of Mn^{2+} by atomic absorption spectrophotometry. The figures refer to Mn^{2+} concentrations (m.f. x 10^{-6}).

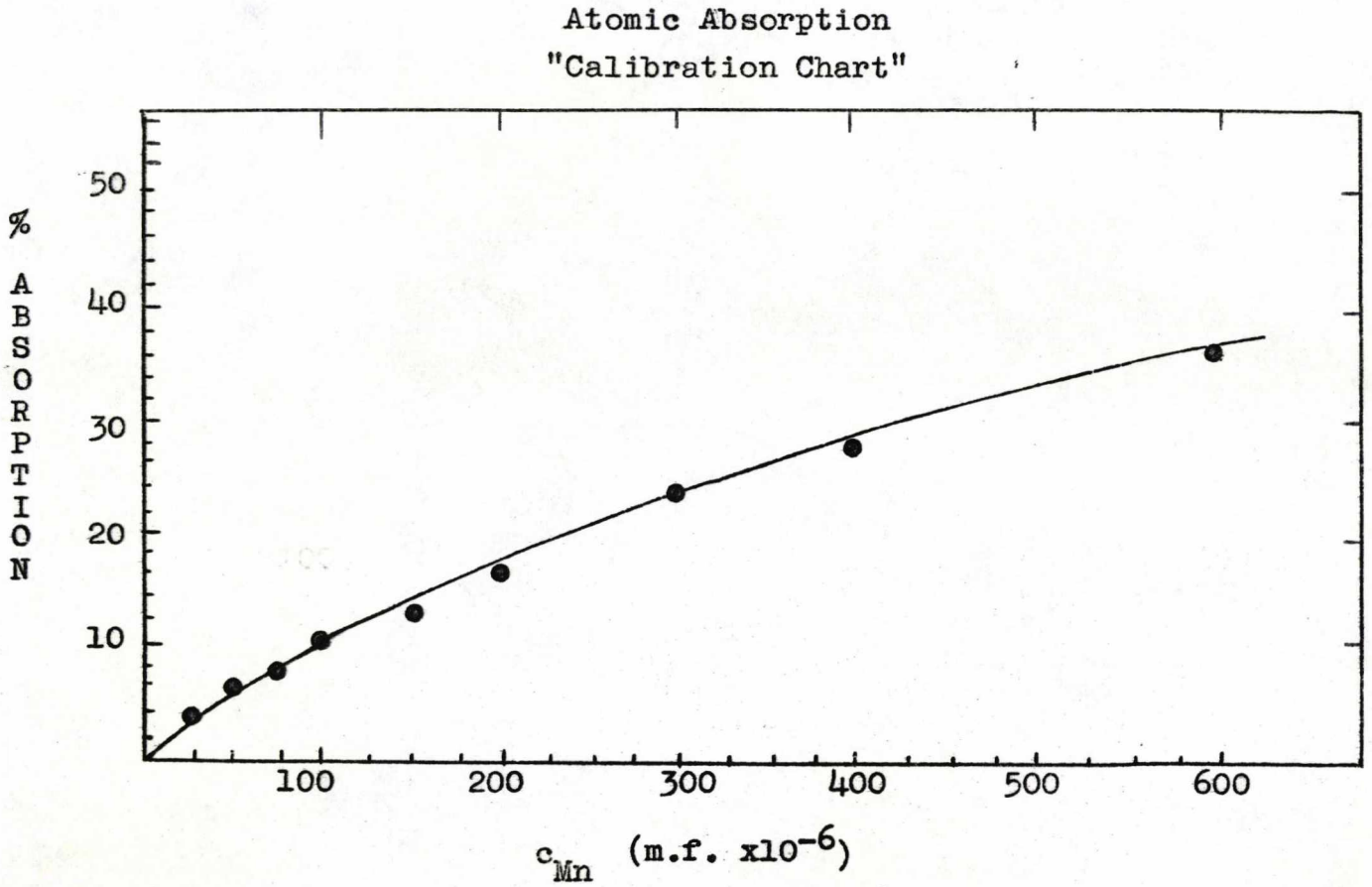
Atomic Absorption
"Calibration Chart"
% ABSORPTION
50
40
30
20
10
100
200
300
400
500
600
c_{Mn} (m.f. x10^{-6})

Fig. 28. (b)

The sensitivity of the method was very good for the detection of Mn, as little as 1 ppm could be estimated accurately. Although specificity is good, the method is not entirely free from contamination. For example, anions and releasing agents for phosphate, sulphate or silicate can depress the absorption because of the stability of their compounds.

Estimation of Pb by Atomic Absorption spectroscopy proved difficult. The lack of response could have been due to the inability to achieve the correct flame conditions. Elements such as Pb are extremely difficult to excite and consequently require very high flame temperatures. The proportion of ground state atoms may have been too small for significant absorption to occur. As a result, the crystals containing Pb impurity were sent to Johnson-Matthey and Co. Ltd., who did a complete spectrographic analysis on them.

CHAPTER III

3. Conductivity Results

Conductivity measurements have been made on pure and doped crystals of NaCl over the temperature range 150-650°C. The added impurities are those listed in the introduction; impurity concentrations varied with the impurity studied, but normally lay within the limits 20×10^{-6} m.f. to 2000×10^{-6} m.f. The results of the conductivity measurements have been plotted as $\log_{10}\sigma$ versus $10^3/T$. Four regions of conductivity can be distinguished in each case, and these have been labelled according to the Dreyfus and Nowick notation[10].

Although in principle the free energies of cation vacancy movement, impurity-vacancy association and impurity solubility can be determined from the apparent activation energies in these regions, the transitions between them usually extended over relatively large temperature ranges. This can cause significant errors in the determination of the free energies. The results have therefore been analysed in terms of the theory developed by Lidiard[18]; this is summarised in the following section.

3.1. Theory of Ionic Conductivity[18]

The general equation relating the mole fractions x_1 and x_2 of positive and negative ion vacancies respectively

to the absolute temperature T is given by

$$x_1 . x_2 = x_0^2 = \exp(-g_s/kT) \qquad (3.1)$$

where x_0 is the mole fraction of thermal vacancies in a pure crystal at temperature T and g_s is the Gibbs free energy associated with the formation of a pair of Schottky defects. The free energy can be divided into entropy, S_s, and enthalpy, h_s, contributions, giving

$$x_1 . x_2 = x_0^2 = \exp(S_s/k)\exp(-h_s/kT) \qquad (3.2)$$

If the mobilities of the complementary defects are μ_1 and μ_2 and the magnitude of their effective charge is q, then the conductivity σ_0 is

$$\sigma_0 = Nq(x_1\mu_1 + x_2\mu_2) \qquad (3.3)$$

where N is the number of ions of the appropriate kind per unit volume.

In a crystal doped with a mole fraction c of divalent cation impurity, the requirement of electrical neutrality is given by

$$x_1 = c + x_2 \qquad (3.4)$$

Equation (3.4) assumes that there is no association between the divalent cation and a cation vacancy in the nearest neighbour position. At lower temperatures,

however, this approximation is not valid, and when allowance is made for association the electroneutrality condition becomes

$$x_1 - x_2 = c - x_k \qquad (3.5)$$

where x_k, the mole fraction of associated pairs, is given by

$$\frac{x_k}{x_1(c-x_k)} = Z_1 \exp(-\eta_1/k)\exp(\chi_1/kT) = K_2 \qquad (3.6)$$

where $Z_1 = 12$, the number of distinct orientations of the associated pair, and η_1 and χ_1 are the entropy and enthalpy of association. Under these conditions the conductivity σ of the doped crystal is given by the following equations:

$$\frac{\sigma}{\sigma_0} = \frac{\xi + \phi/\xi}{1 + \phi} \qquad (3.7)$$

where $\phi = \frac{\mu_2}{\mu_1}$ and $\xi = \frac{x_1}{x_0}$; and

$$\frac{c}{x_0} = (\xi - \frac{1}{\xi})(1 + H\xi) \qquad (3.8)$$

where $H = x_0 K_2$. These equations can be used to interpret experimental results by plotting calculated values of the function $c/(\xi - 1/\xi)$ against values of ξ. According to equation (3.8) a straight line of positive slope, Hx_0, and intercept, x_0, should result if

association occurs. Thus, x_0 and K_2 may be determined as a function of temperature.

The general solution of equation (3.7) requires estimates for the anion-cation mobility ratio . In NaCl, transport number[8] and self-diffusion[11] measurements show that the conductivity is essentially cationic and, on the basis of single vacancy diffusion results[11,15] the maximum value of ϕ would be 0.07 for the temperature range used in the present work. In comparison with the values of ξ, ϕ has been approximated to zero.

3.1(a) Impurity-Vacancy Association

Values of ξ, calculated from the conductivity results in regions II and III, are plotted against the function $c/(\xi - 1/\xi)$ for each divalent impurity. Such plots are a severe test of the experimental data and the results showed appreciable scatter. Consequently, it was experimentally impossible to detect the occurrence of curvature at low values of ξ due to any long-range Coulombic interactions which may have taken place between unassociated defects[18]. In drawing the lines more weight was put on the points at higher ξ values, as they are less susceptible to small errors in the estimated impurity content. In the absence of any noticeable

curvature, the results for the impurity doped crystals were analysed only in terms of nearest-neighbour interactions. Values of K_2 were determined from the slopes of the $c/(\xi - {}^{1}/\xi)$ versus ξ curves and plotted against $10^3/T$.

The conductivity results ($\log_{10}\sigma$ vs. $10^3/T$), σ vs. c plots, $c/(\xi - {}^{1}/\xi)$ vs. ξ plots and plots of $\log_{10}K_2$ vs. $10^3/T$ are presented for each system in the following manner.

	$\log \sigma$ vs. $10^3/T$	σ vs. c	$c/(\xi - {}^{1}/\xi)$ vs.	$\log_{10}K_2$ vs. $10^3/T$
($NaCl-MgCl_2$)	Figs. 29	30	31	32(a)
($NaCl-MnCl_2$)	Figs. 33	34	35	36(a)
($NaCl-CaCl_2$)	Figs. 37	38	39	40(a)
($NaCl-SrCl_2$)	Figs. 41	42	43	44(a)
($NaCl-PbCl_2$)	Figs. 45	46	47	48(a)
($NaCl-BaCl_2$)	Figs. 49	50	51	52(a)

The impurity concentrations associated with each conductivity curve are inserted in the appropriate figures. Three of the plots of $c/(\xi - {}^{1}/\xi)$ versus ξ are shown for each system. Equations describing the association are included in each of the $\log_{10}K_2$ versus $10^3/T$ plots. In order to make a direct comparison of the association in each system, the least squares lines

from the plots of $\log_{10}K_2$ versus $10^3/T$ are shown together in Fig. 53.

3.1(b) Impurity Solubility

In equation (3.8) c is the concentration of impurity substitutionally dissolved in the lattice as unassociated ions. This is generally referred to as the free-impurity solubility and its variation with temperature is given by

$$c = \exp(\eta_i/2k)\exp(-\chi_i/2kT) \qquad (3.9)$$

where η_i and χ_i are the entropy and enthalpy of solution. The conductivity is only affected by the amount of impurity dissolved in the crystal, since precipitated impurity forms a separate phase and as such does not affect the concentration of vacancies in the crystal.

The enthalpy and entropy of free impurity ions were determined from equation (3.9) for each of the impurities studied. The free-impurity solubility 'break' temperature was obtained by extrapolation of the free vacancy region to the solubility region. The variation of 'break' temperature with impurity concentration is shown for each impurity in Fig. 32(b) (for $NaCl-MgCl_2$), Fig. 36(b)(for $NaCl-MnCl_2$), Fig. 40(b)

(for $NaCl-CaCl_2$), Fig. 44(b) (for $NaCl-SrCl_2$), Fig. 48(b) (for $NaCl-PbCl_2$) and Fig. 52(b) (for $NaCl-BaCl_2$). The equations for free-impurity solubility are included in the figures.

($NaCl - MgCl_2$)

Variation of Conductivity with Temperature

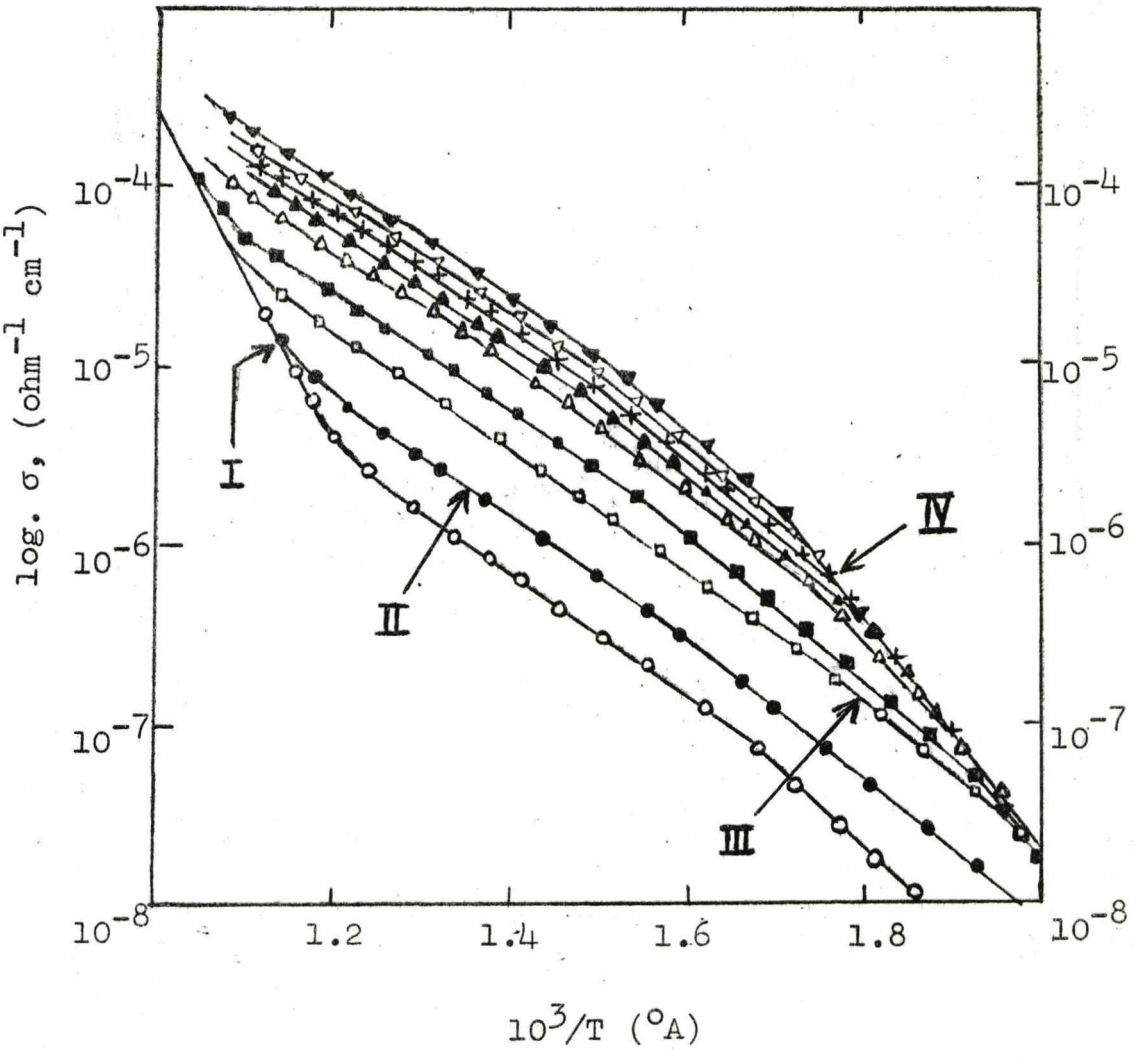

Conc$^{n.}$ Mg^{2+} (m.f. x 10^{-6}):

o 'pure'; ● 20; □ 35; ■ 49; Δ 90;

▲ 94; + 175; ▽ 190; ▼ 223.

Fig. 29

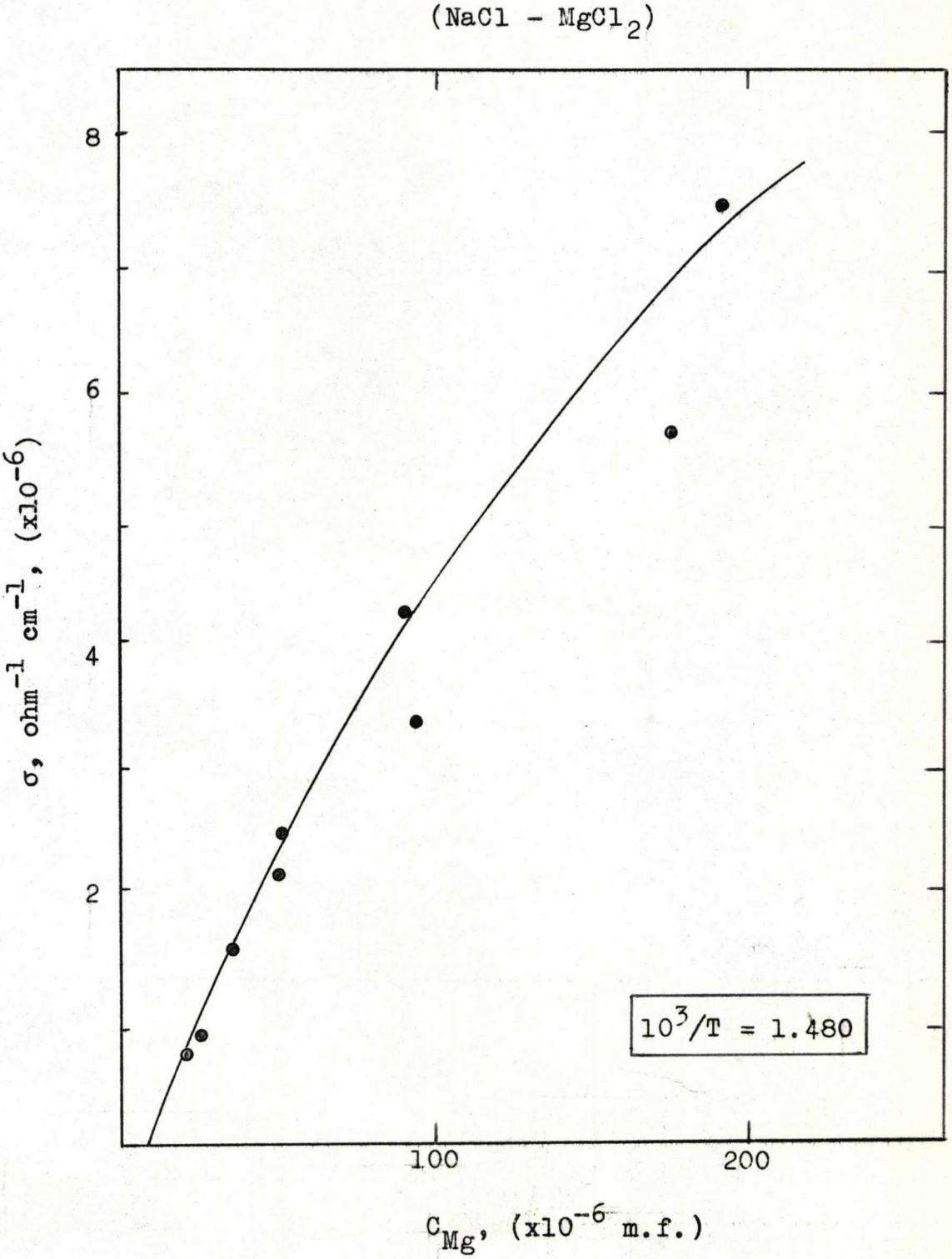

Fig. 30. - Conductivity Isotherm

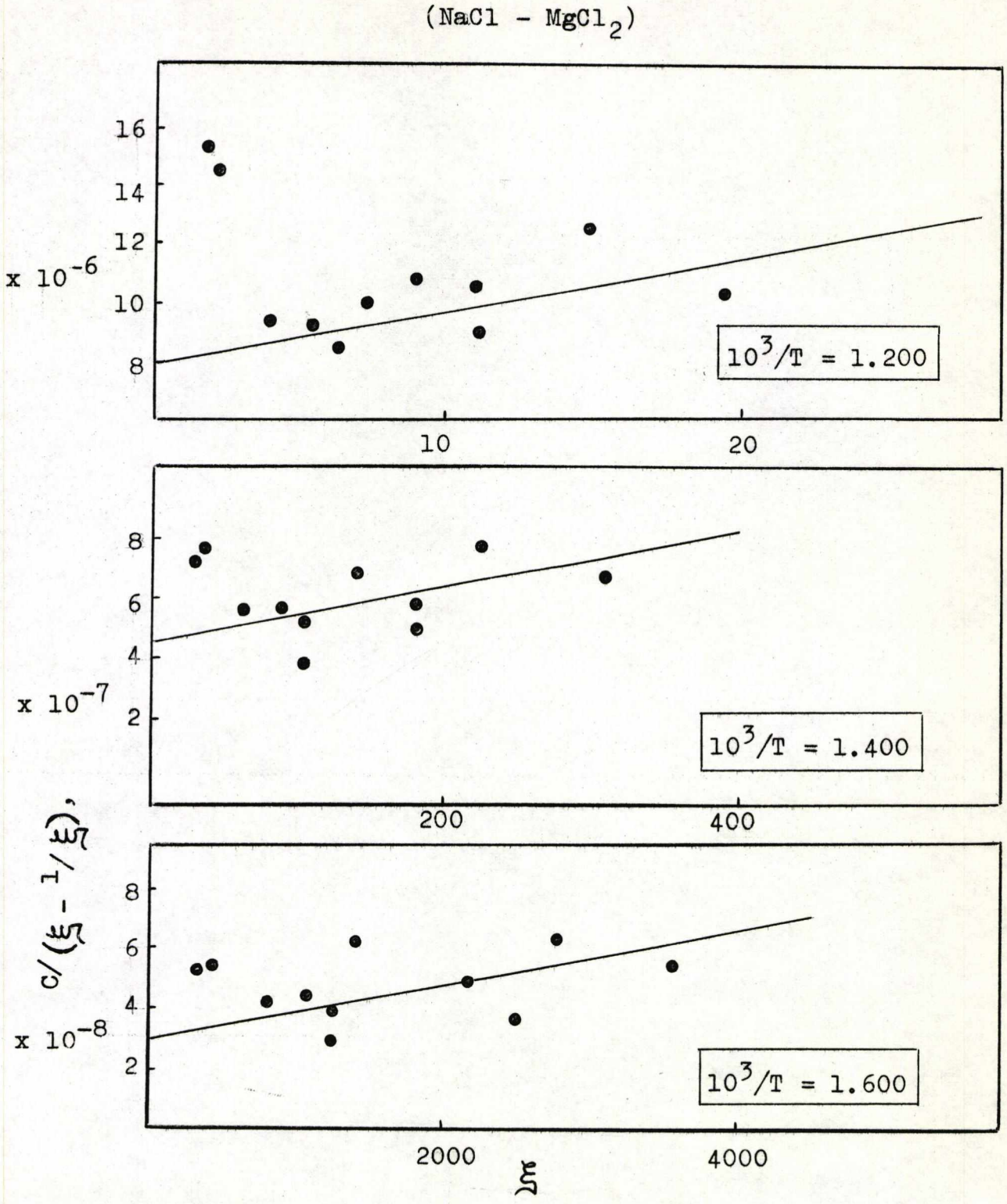

Fig. 31. - $C/(\xi - 1/\xi)$ vrs. ξ

($NaCl - Mg\ Cl_2$)

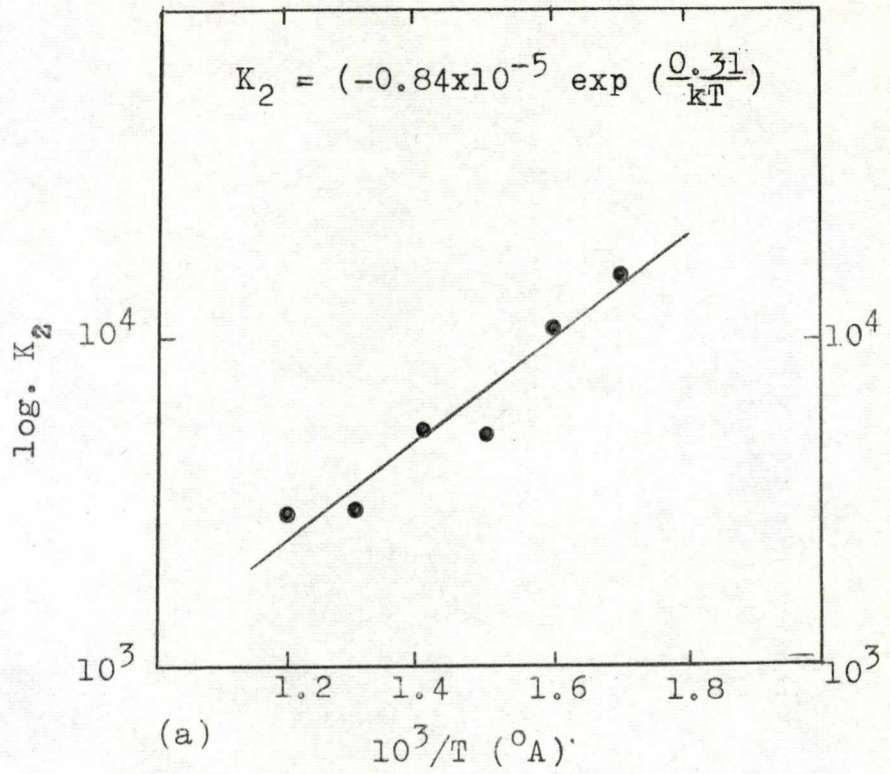

(a)

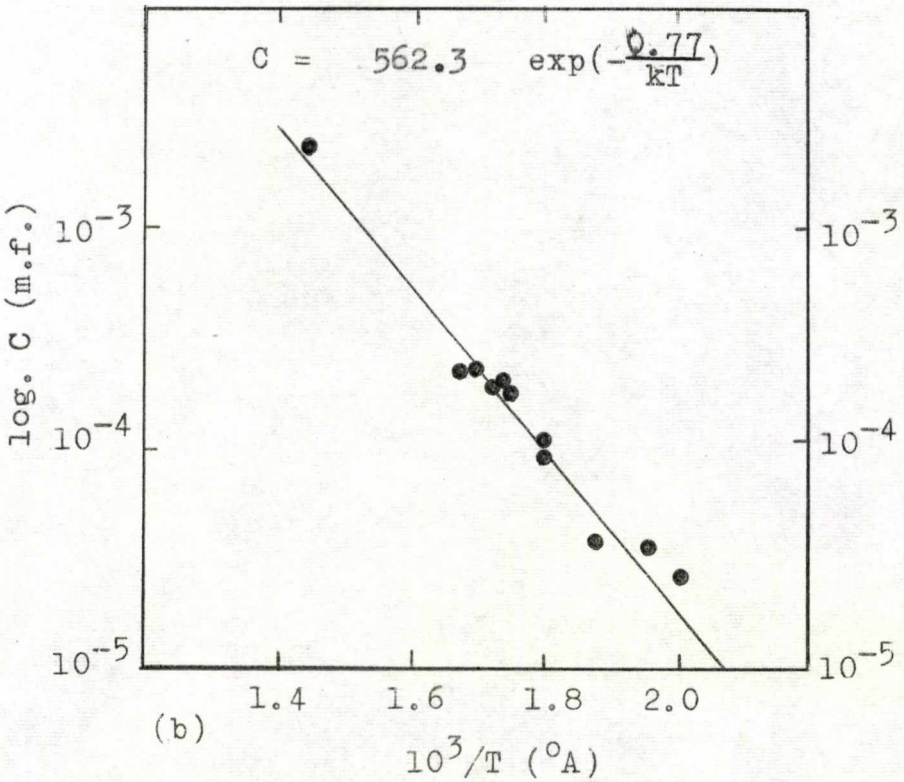

(b)

Fig. 32

($NaCl - MnCl_2$)

Variation of Conductivity with Temperature

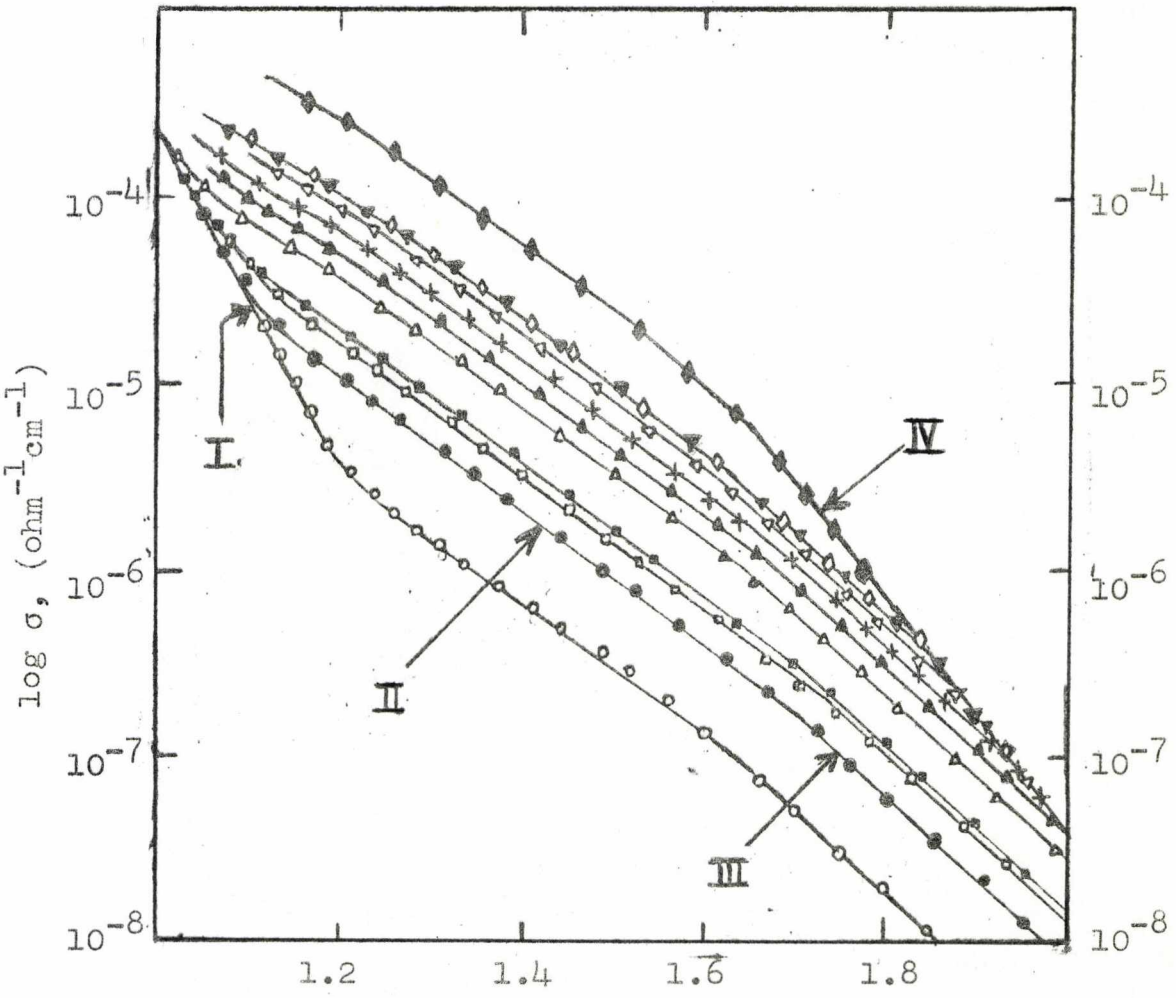

Conc.$^{n.}$ of Mn^{2+} (m.f. x 10^{-6}):

o 'pure; ● 20; □ 45; ■ 55; Δ 90;

▲ 98; + 132; ▽ 202; ▼ 240; ◇ 394; ◆ 600

Fig. 33

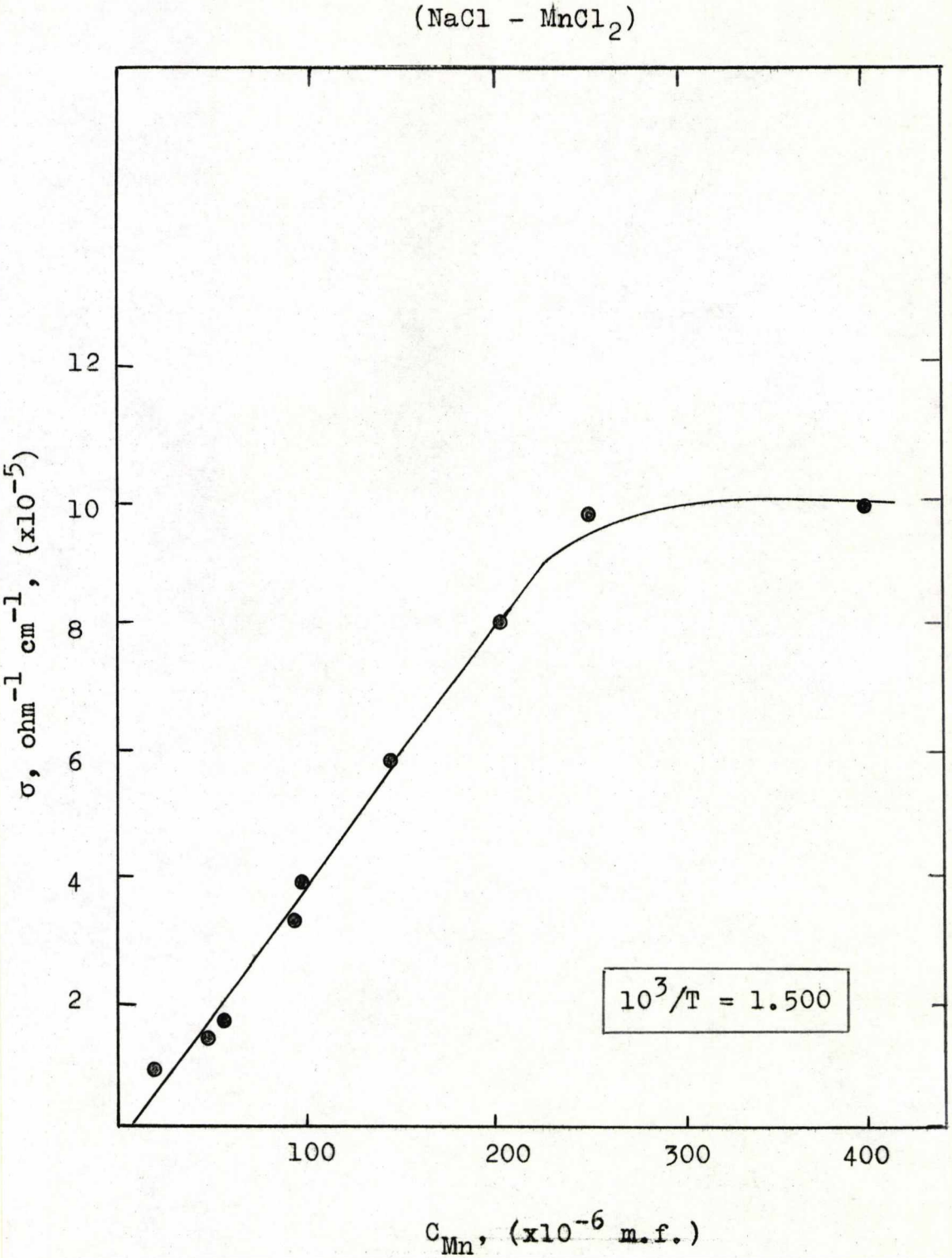

Fig. 34. - Conductivity Isotherm.

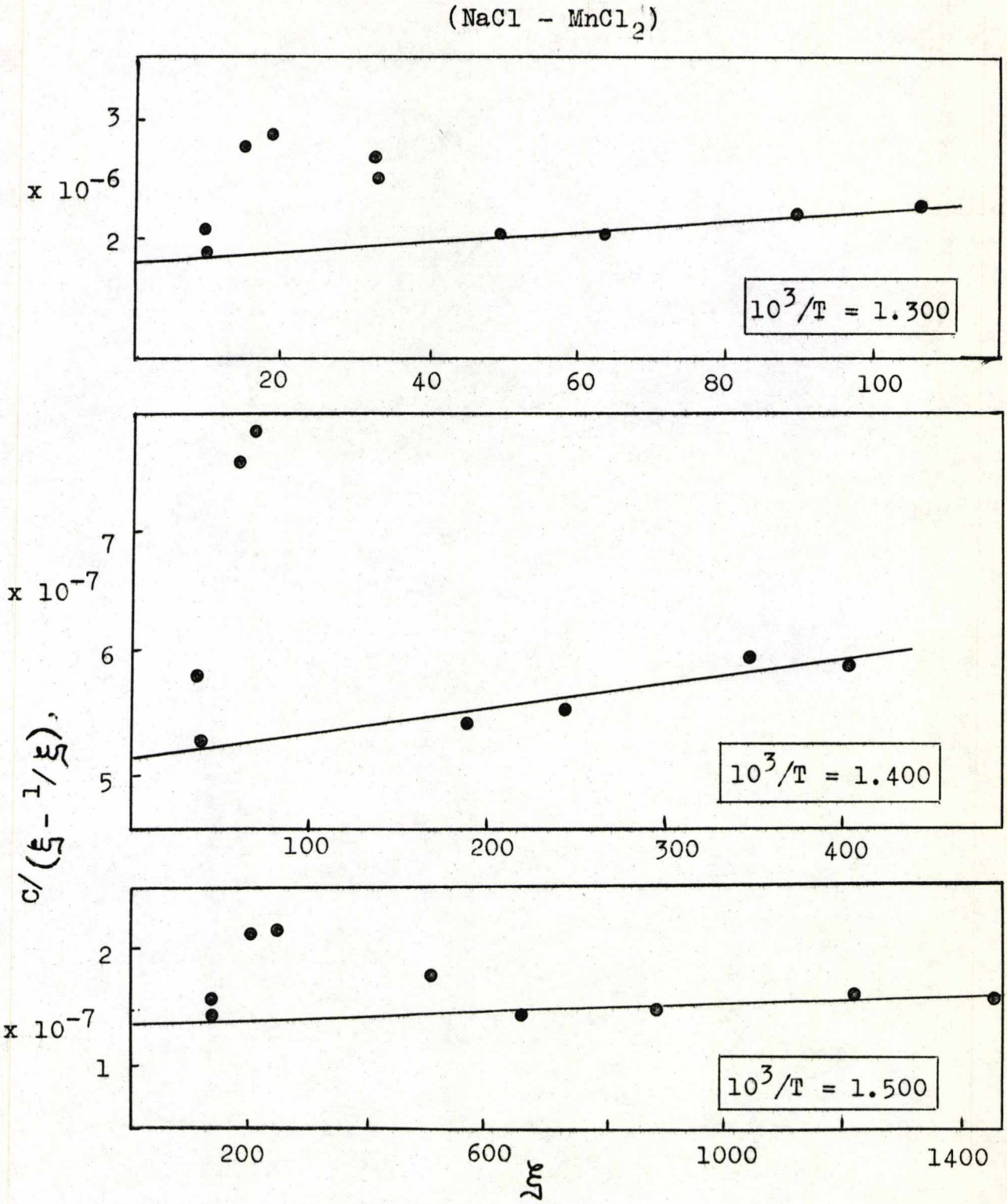

Fig. 35. - $C/(\xi - 1/\xi)$ vrs. ξ

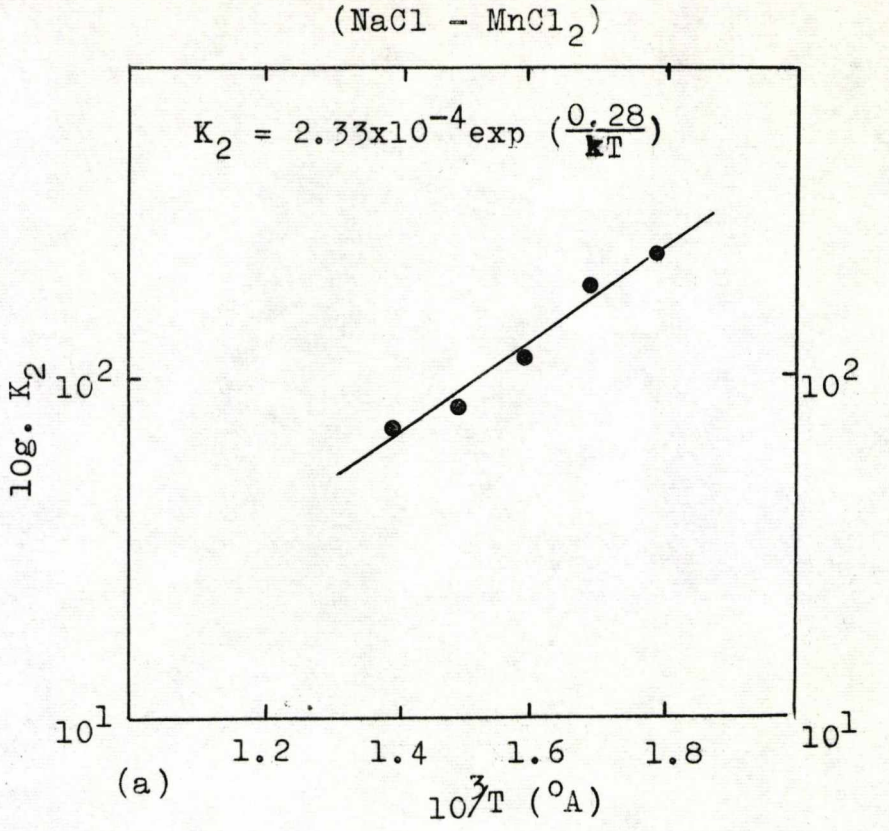
(NaCl - $MnCl_2$)
$K_2 = 2.33 \times 10^{-4} \exp\left(\frac{0.28}{kT}\right)$
log. K_2
10^2
10^1
1.2
1.4
1.6
1.8
(a)
$10^3/T$ (^oA)

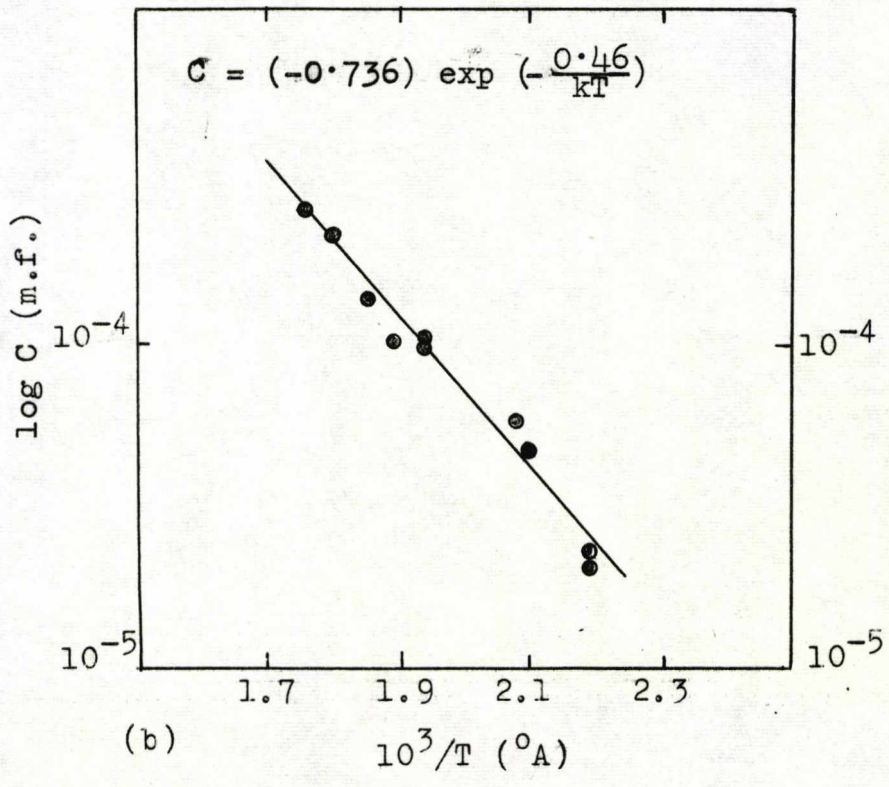
$C = (-0{\cdot}736) \exp\left(-\frac{0{\cdot}46}{kT}\right)$
log C (m.f.)
10^{-4}
10^{-5}
1.7
1.9
2.1
2.3
(b)
$10^3/T$ (^oA)

Fig. 36

($NaCl - CaCl_2$)

Variation of Conductivity with Temperature

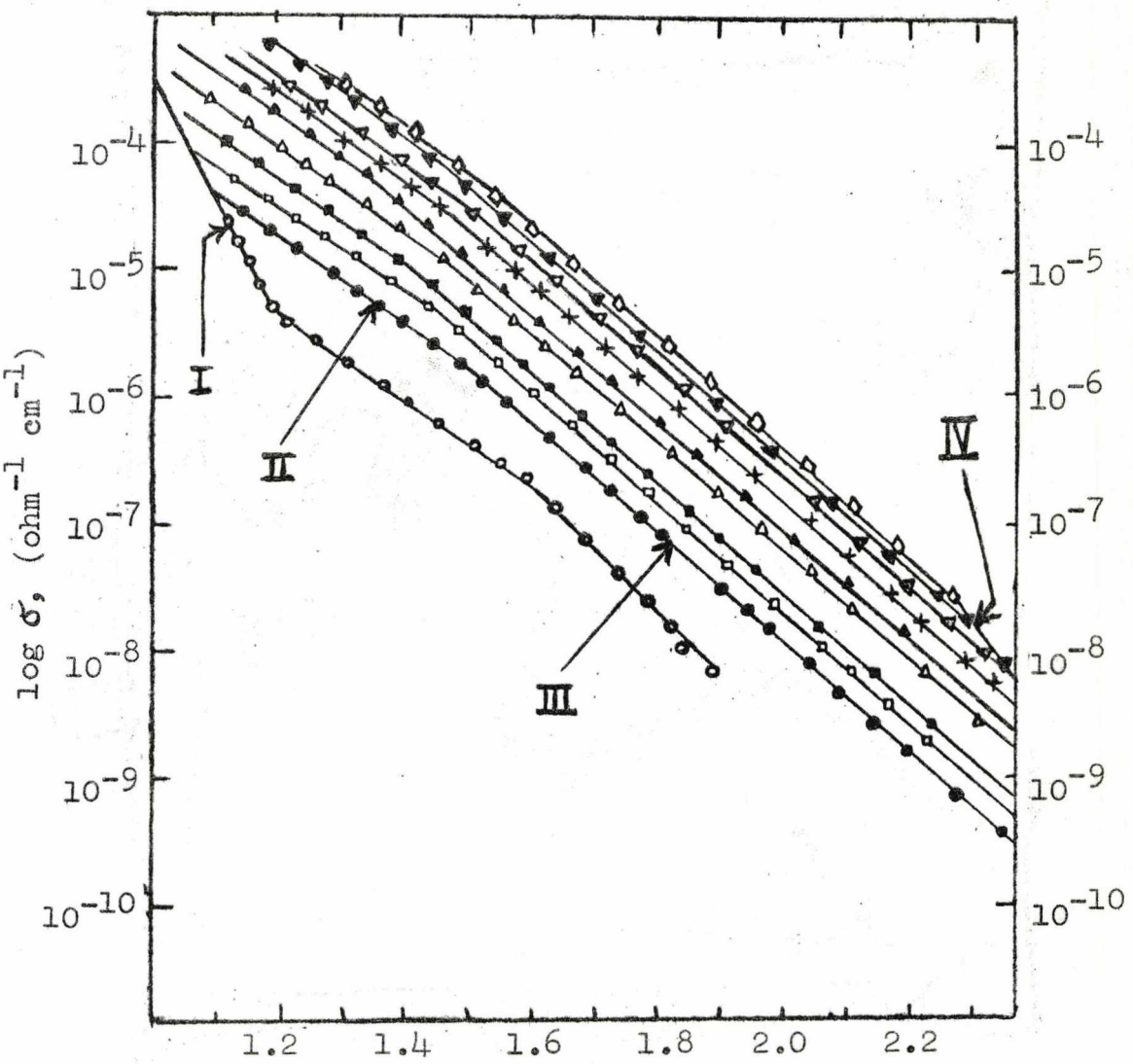

Conc$^{n.}$ Ca^{2+} (m.f. x 10^{-6}):

o 'pure'; • 48; □ 94; ■ 158; Δ 218;

▲ 340; + 455; ▽ 809; ▼ 1160; ◇ 2040

Fig. 37

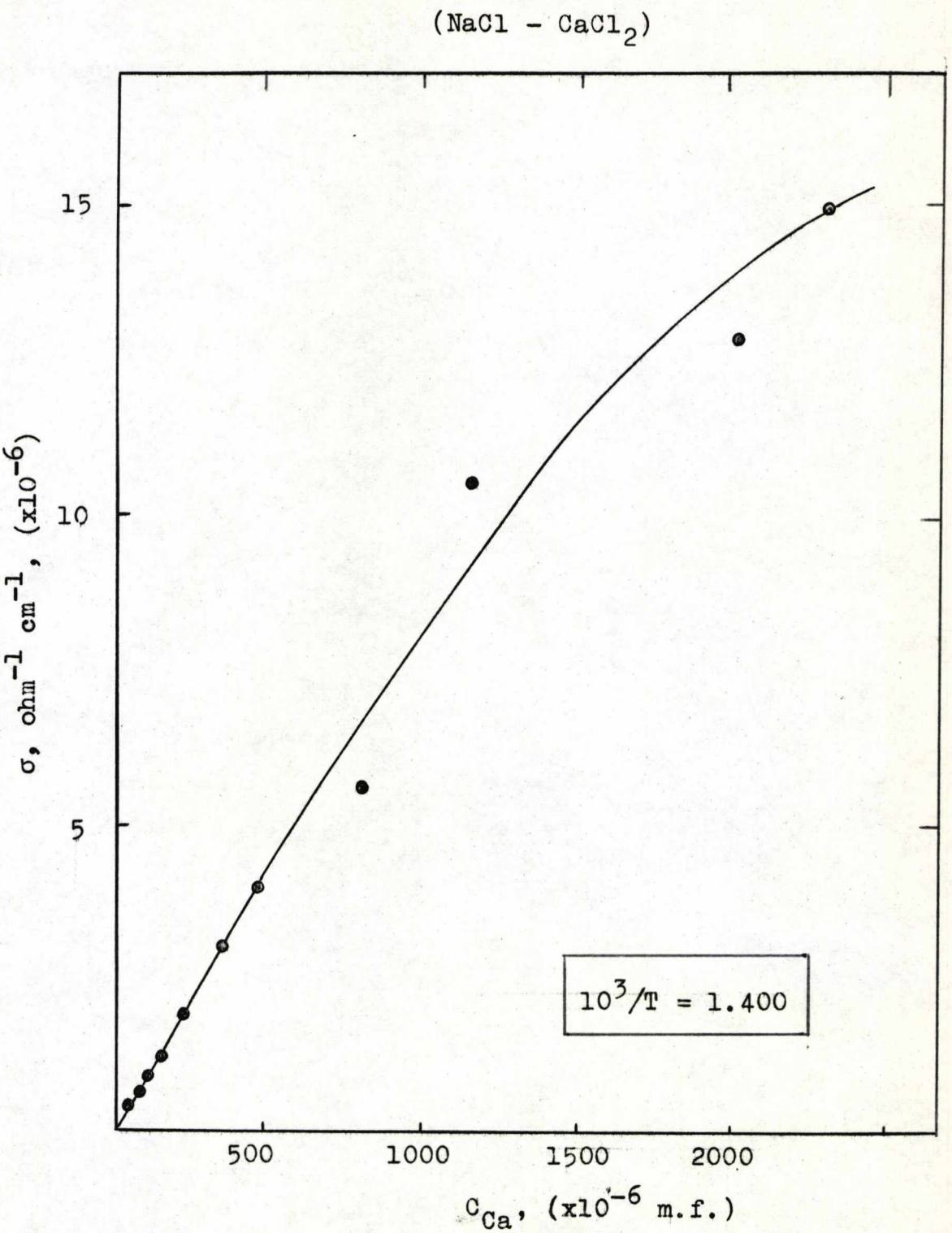

Fig. 38. - Conductivity Isotherm

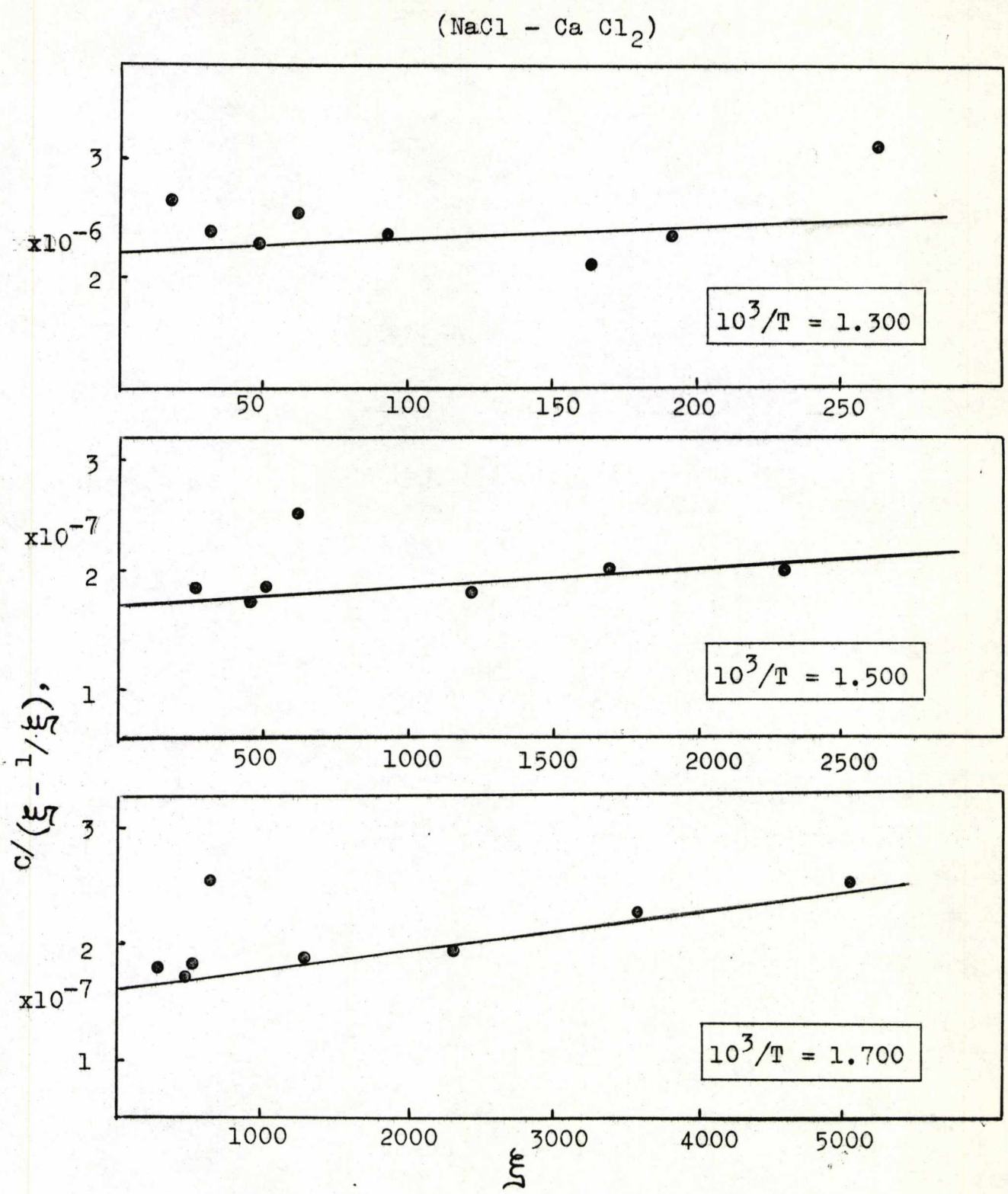

Fig. 39. - $C/(\xi - 1/\xi)$ vrs. ξ

($NaCl - CaCl_2$)

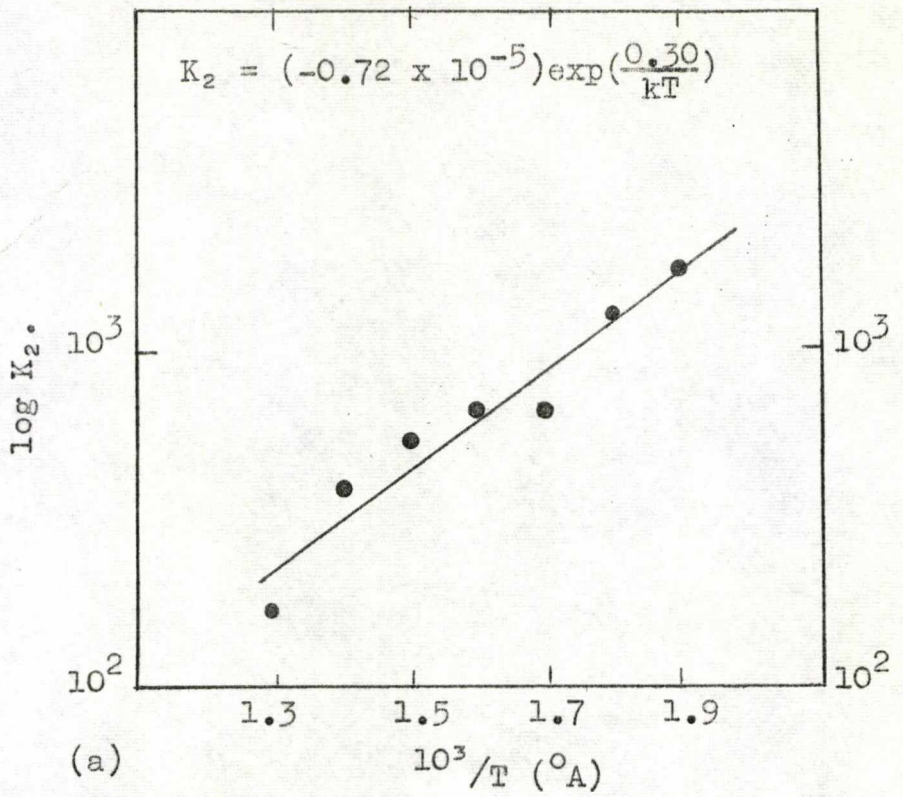

(a)

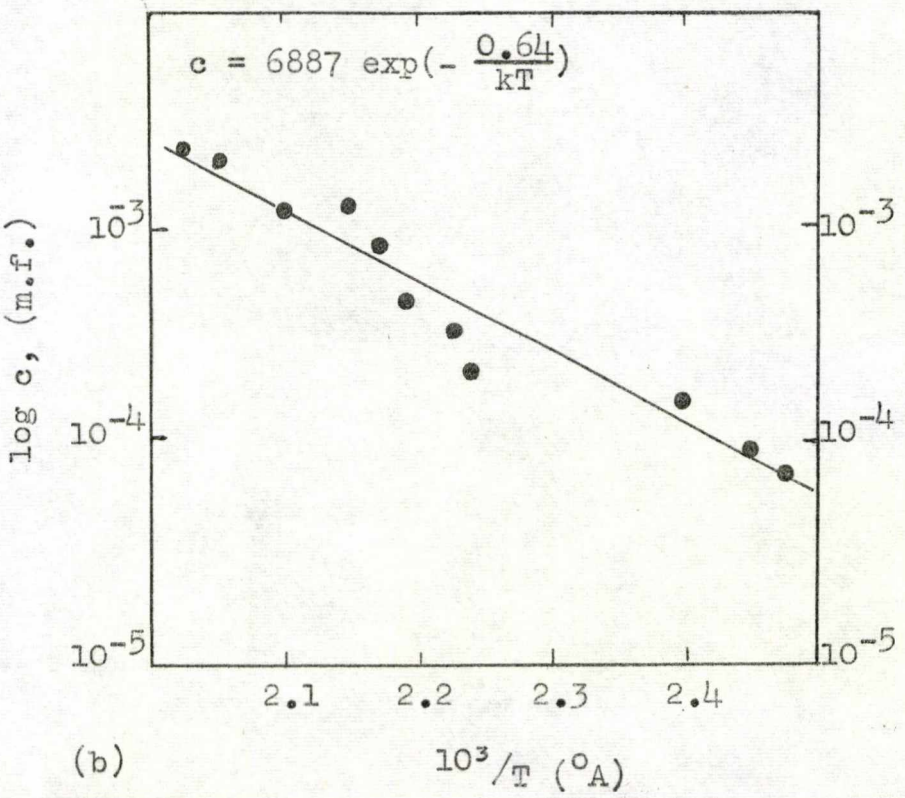

(b)

Fig. 40.

($NaCl - SrCl_2$)

Variation of Conductivity with Temperature

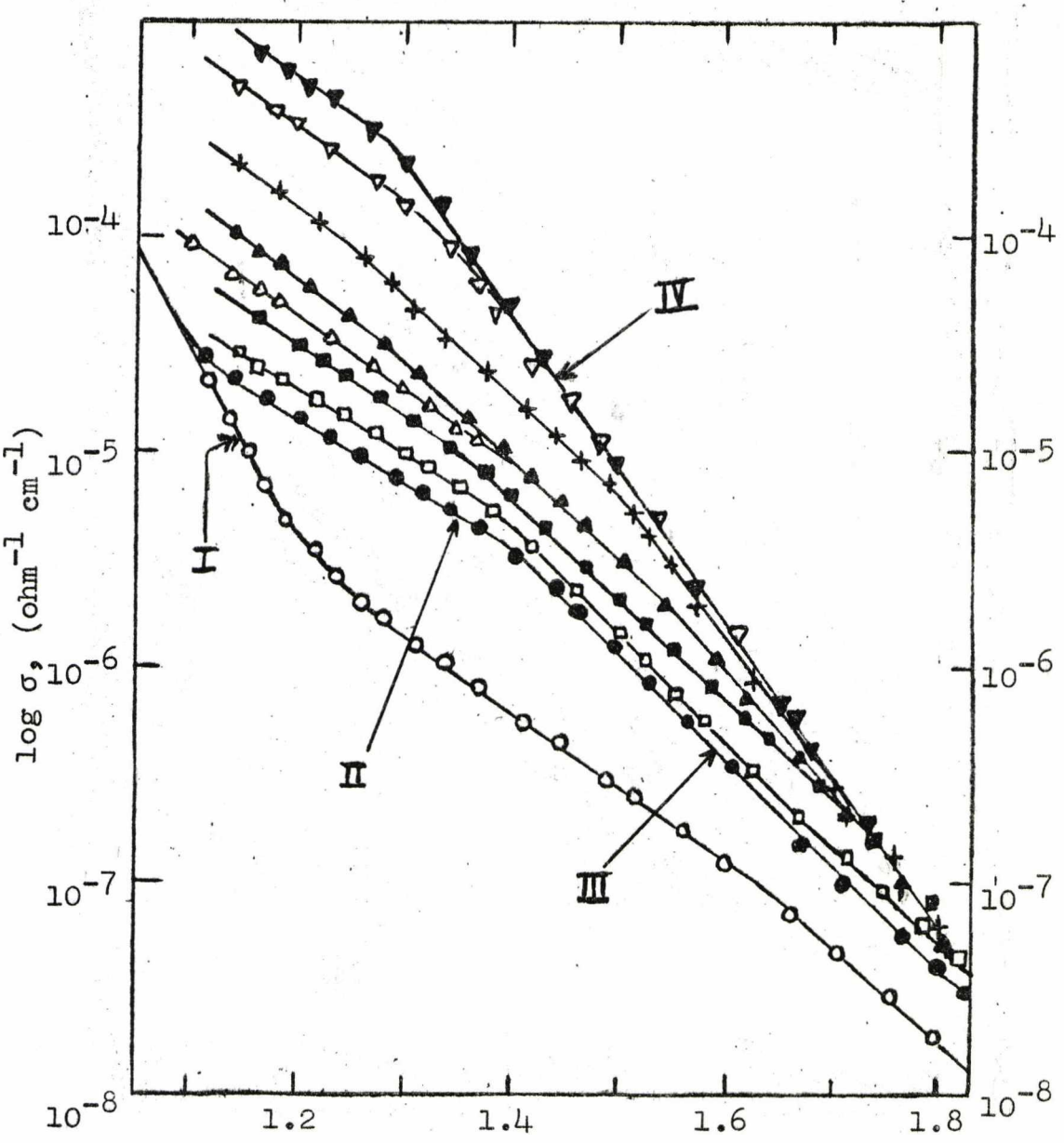

Conc$^{n.}$ of Sr^{2+} (m.f. x10^{-6})

o 'pure'; ● 23; □ 48; ■ 64; Δ 86 (Cl_2 annealed); ▲ 139; + 372: ▽ 1030; ▼ 1680.

Fig. 41

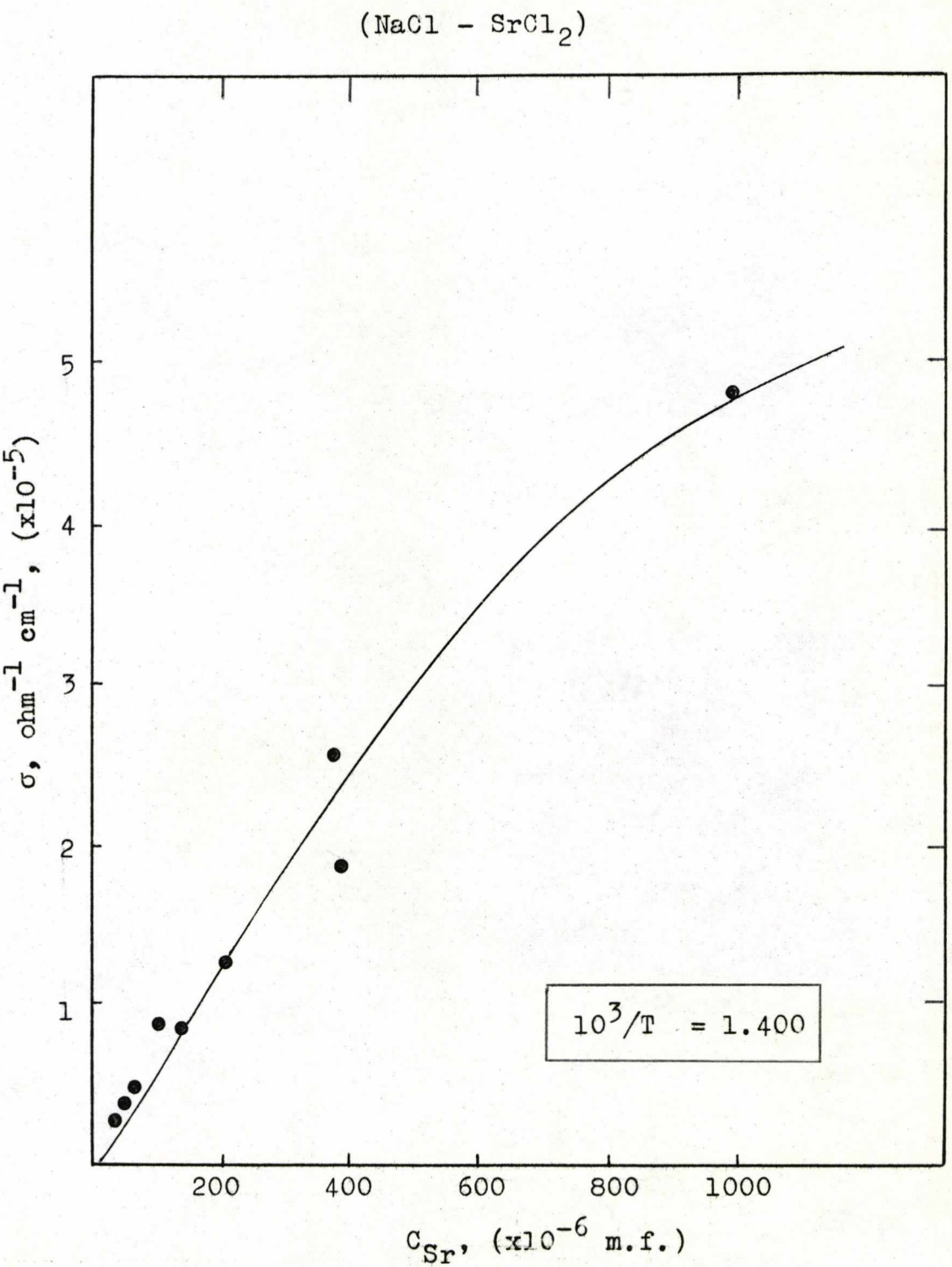

Fig. 42.- Conductivity Isotherm

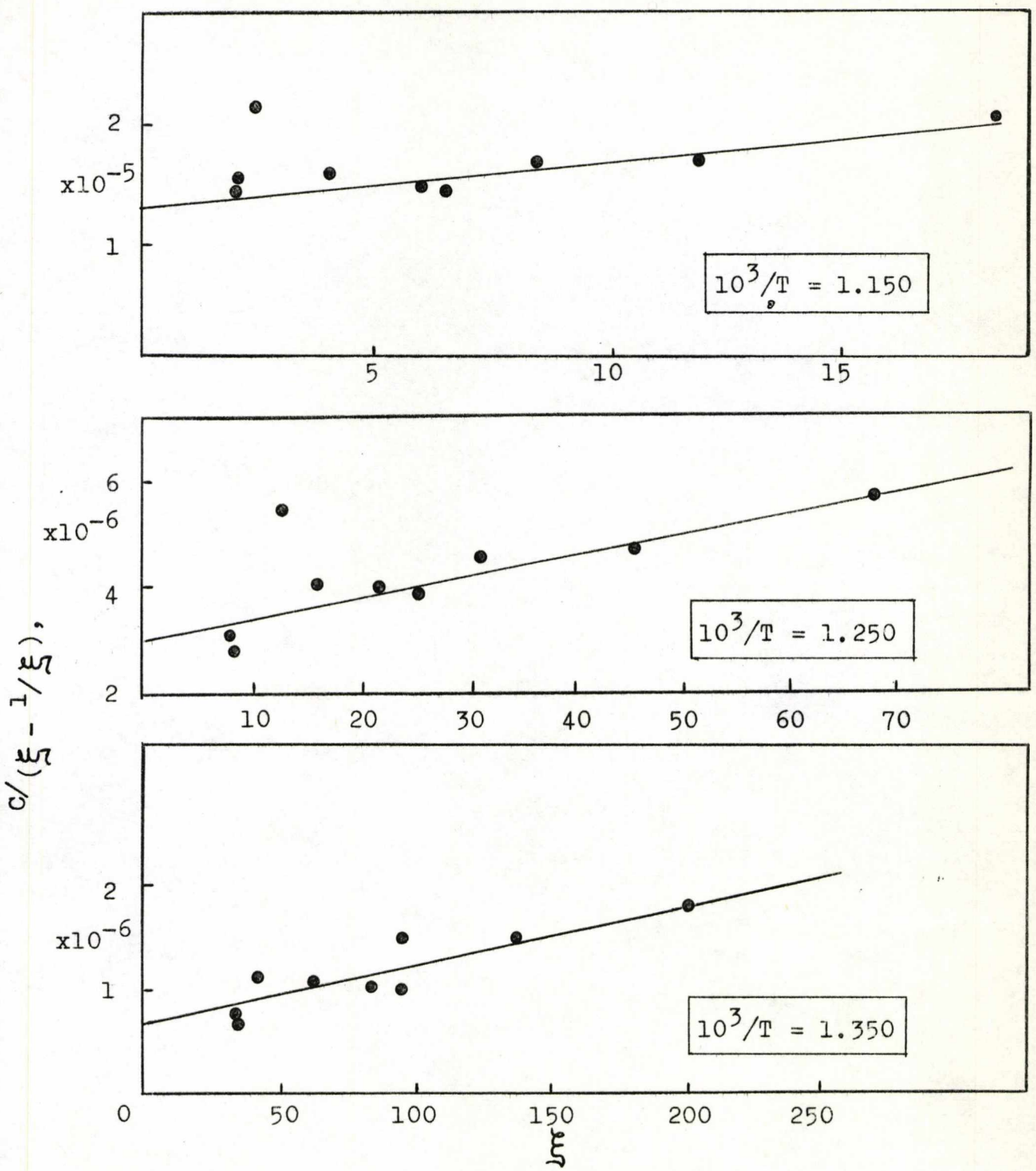

Fig. 43. - $C/(\xi - 1/\xi)$ vrs. ξ

($NaCl - SrCl_2$)

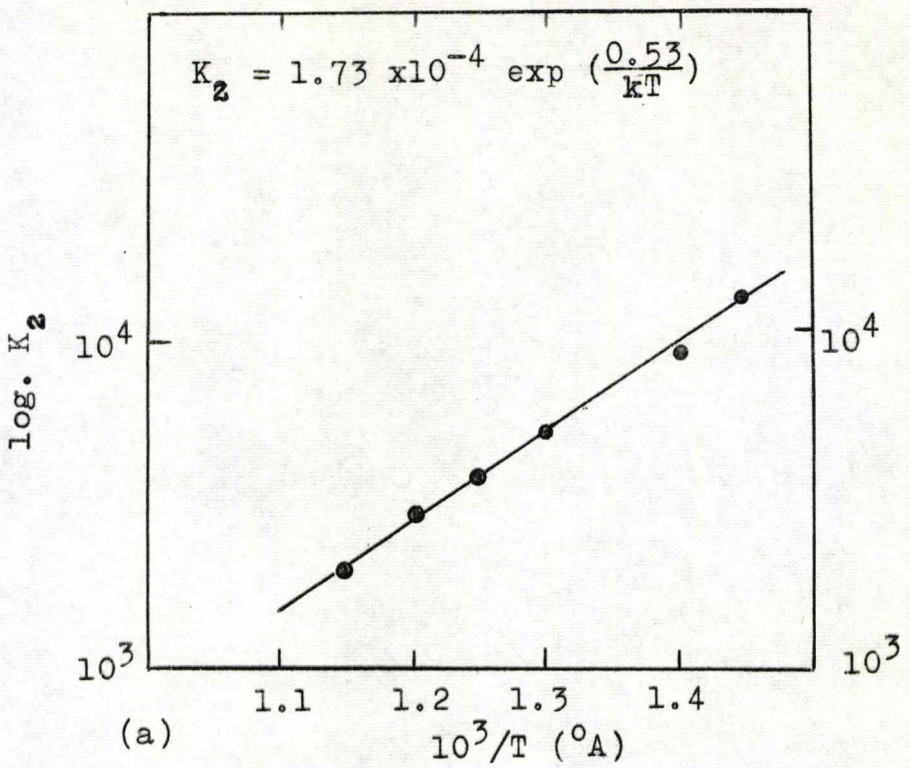

(a)

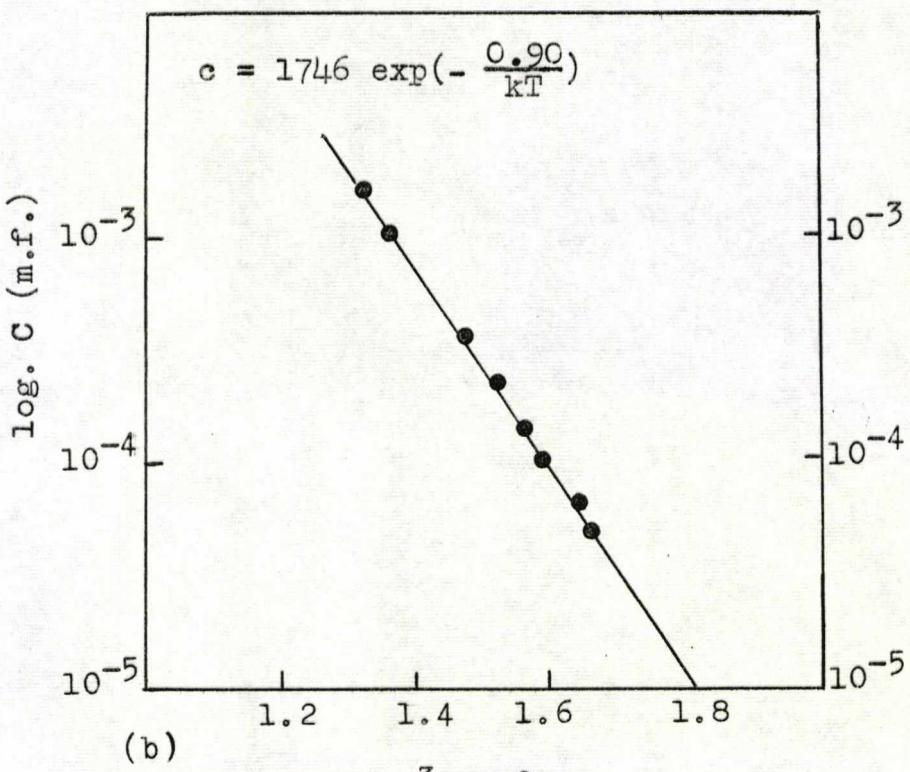

(b)

Fig. 44

($NaCl - PbCl_2$)

Variation of Conductivity with Temperature.

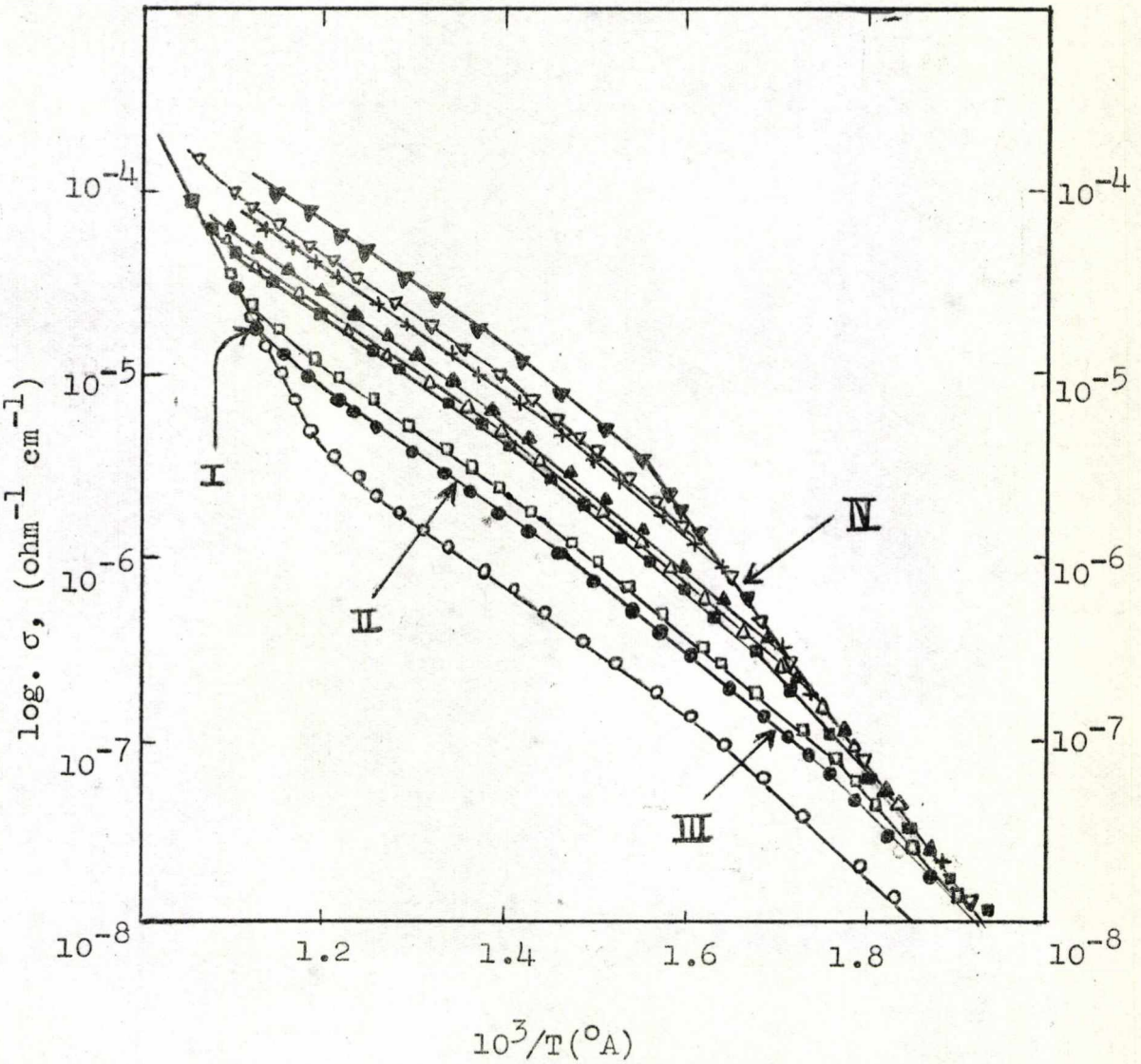

$10^3/T(^oA)$

Conc$^{n.}$ of Pb^{2+} (m.f. x 10^{-6}):

o 'pure'; ● 10; □ 11; ■ 17; Δ 22; ▲ 27;

+ 39; ▽ 42; ▼ 90.

Fig. 45

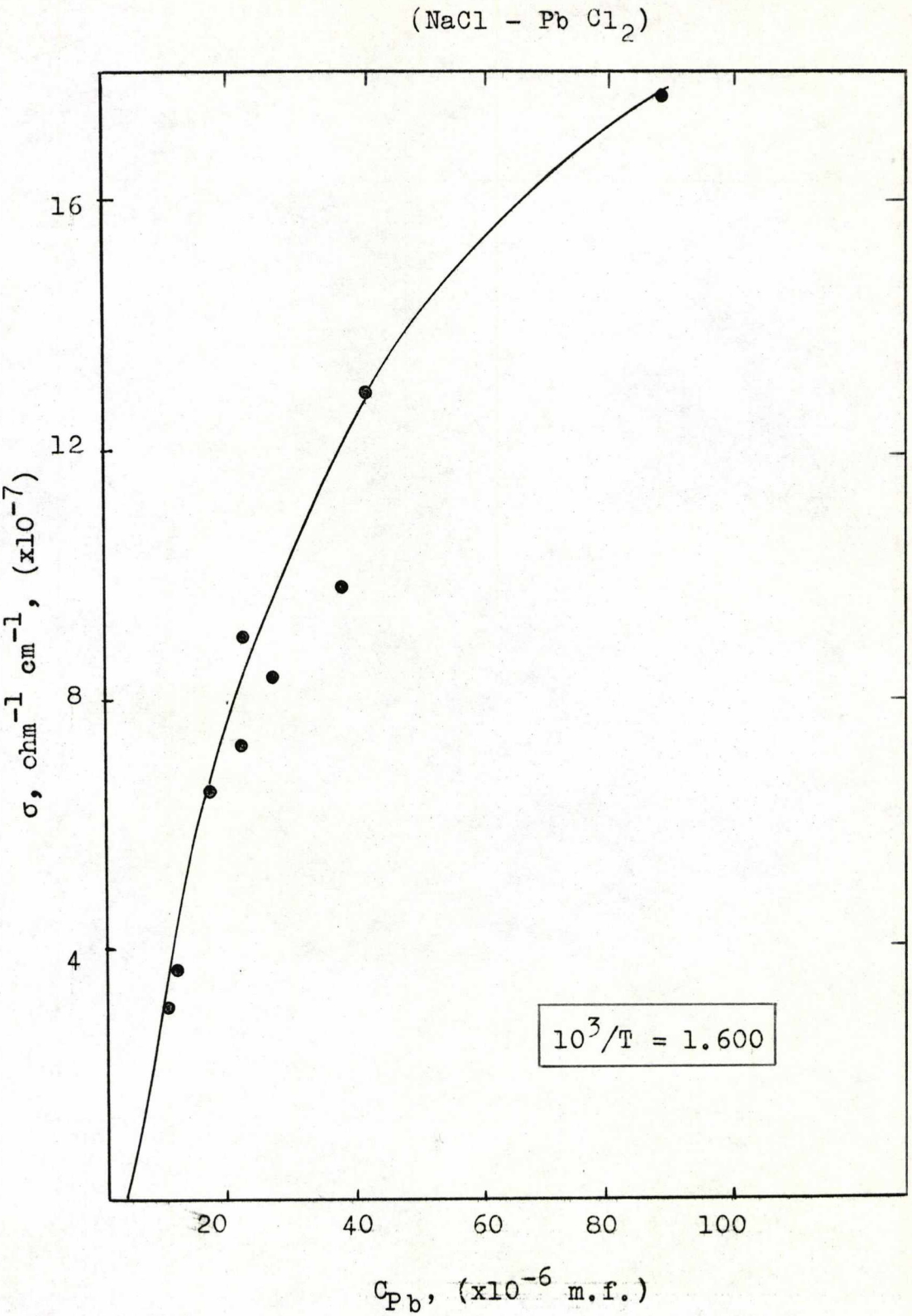

Fig. 46. - Conductivity Isotherm.

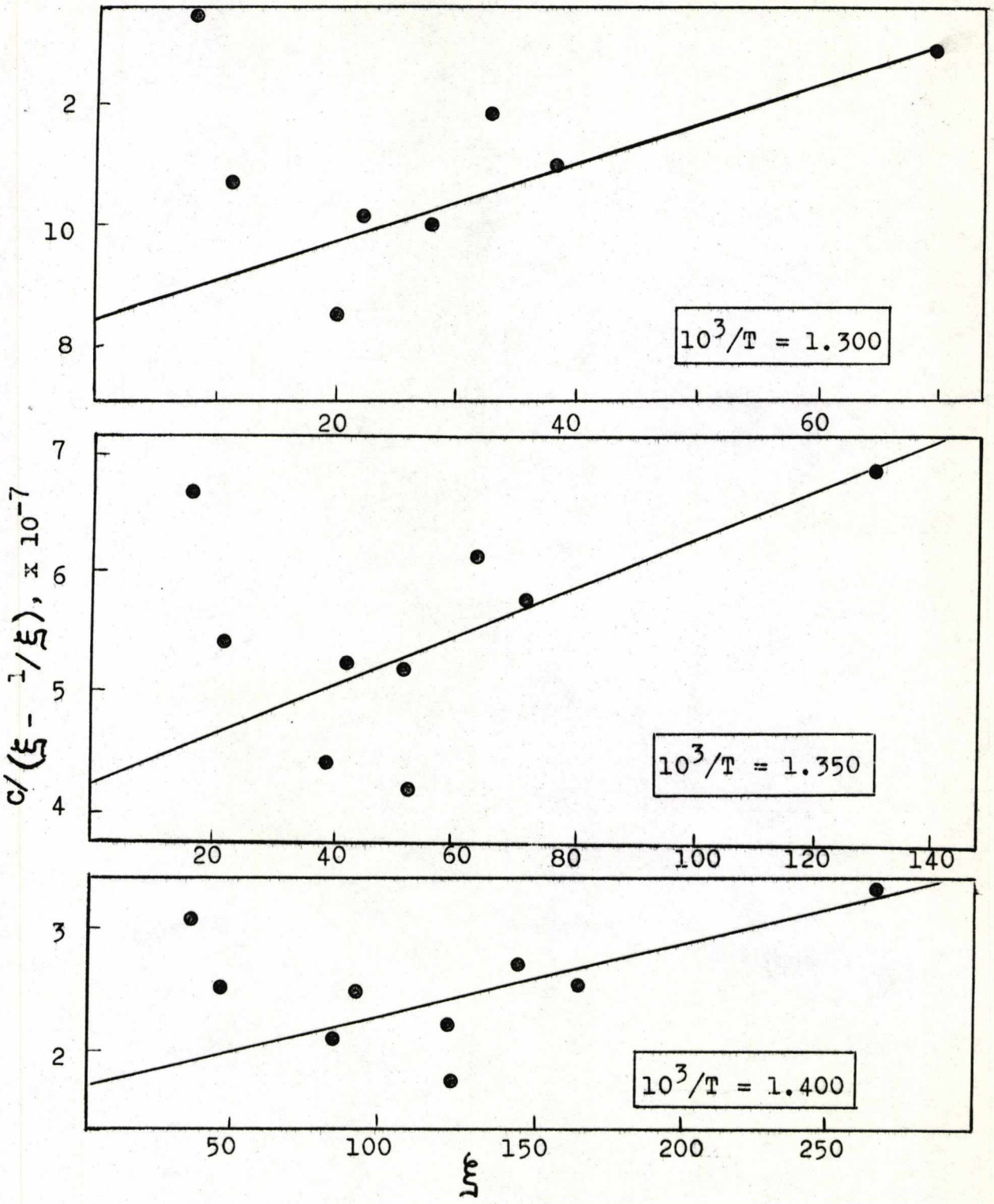

Fig. 47. - $C/(\xi - 1/\xi)$ vrs. ξ

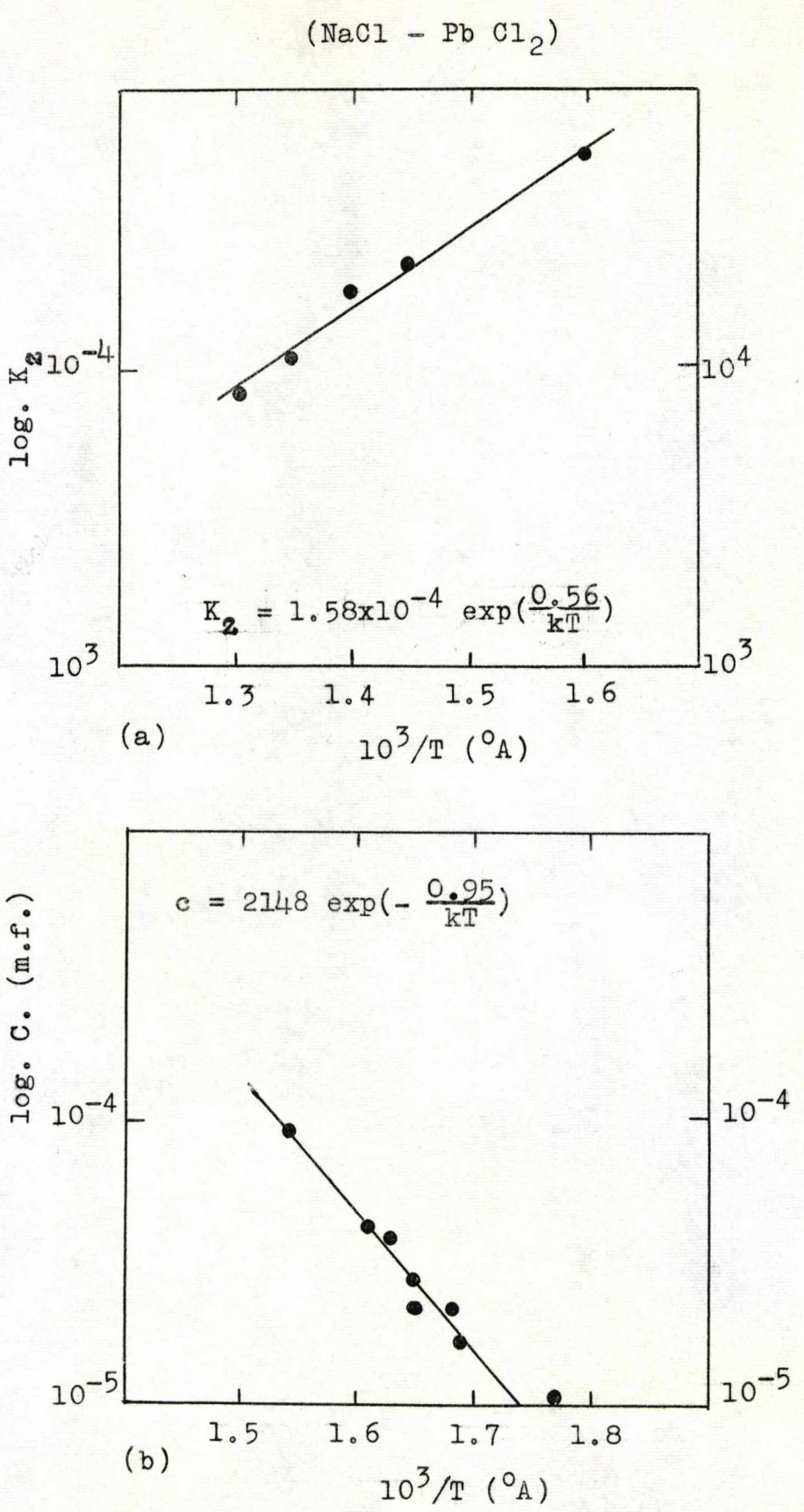
(NaCl - Pb Cl2)
log. K2
10-4
10-3
10-4
10-3
K2 = 1.58x10-4 exp(0.56/kT)
1.3
1.4
1.5
1.6
(a)
10^3/T (°A)
log. C. (m.f.)
c = 2148 exp(- 0.95/kT)
10-4
10-5
10-4
10-5
1.5
1.6
1.7
1.8
(b)
10^3/T (°A)

Fig. 48

($NaCl - BaCl_2$)

Variation of Conductivity with Temperature

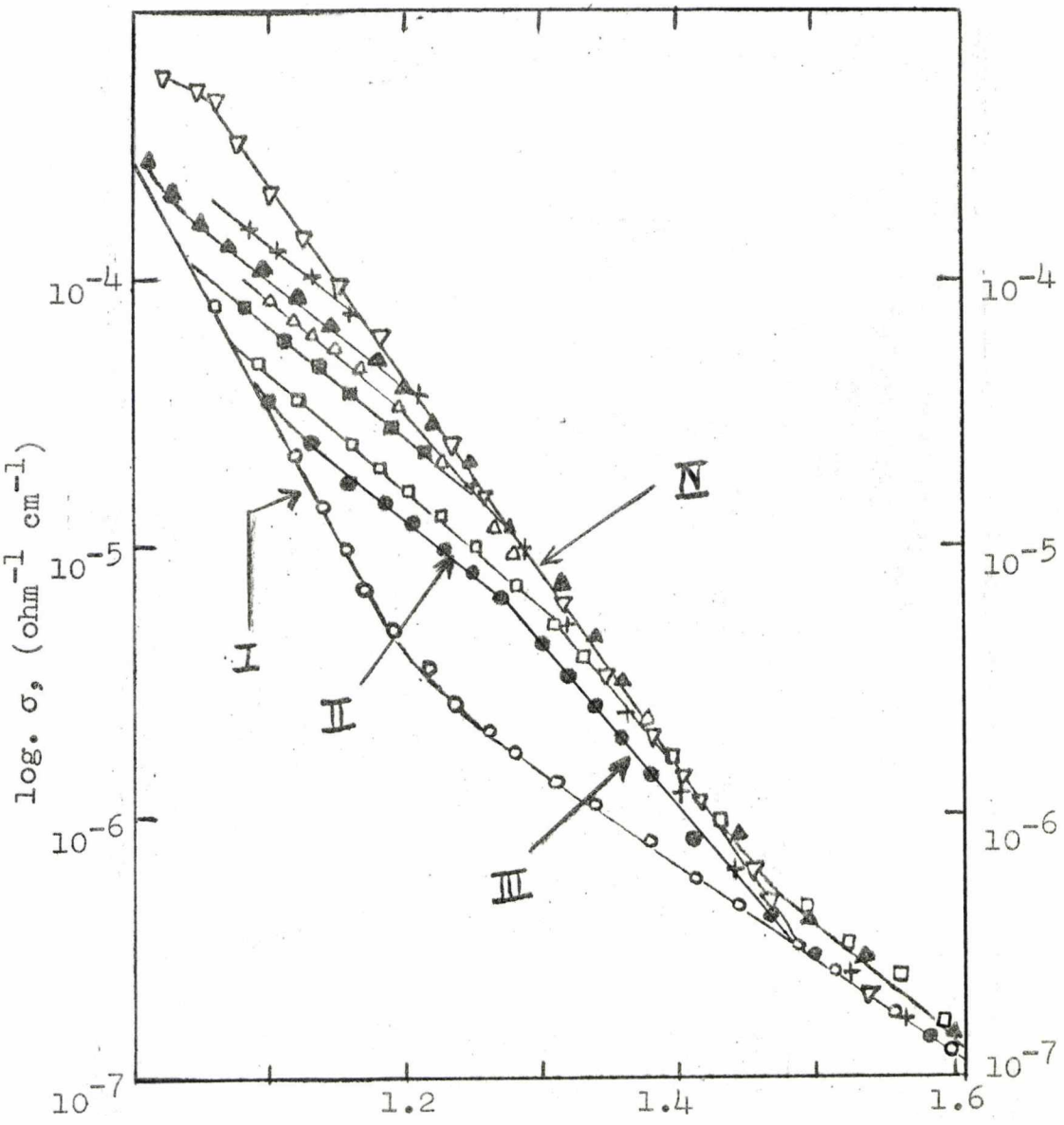

$10^3/T$ (°A)

Conc$^{n.}$ of Ba^{2+} (m.f. x 10^{-6})

o 'pure'; ● 24; □ 45; ■ 53; Δ 82 (Cl_2 annealed); ▲ 123; + 168; ▽ 600.

Fig. 49

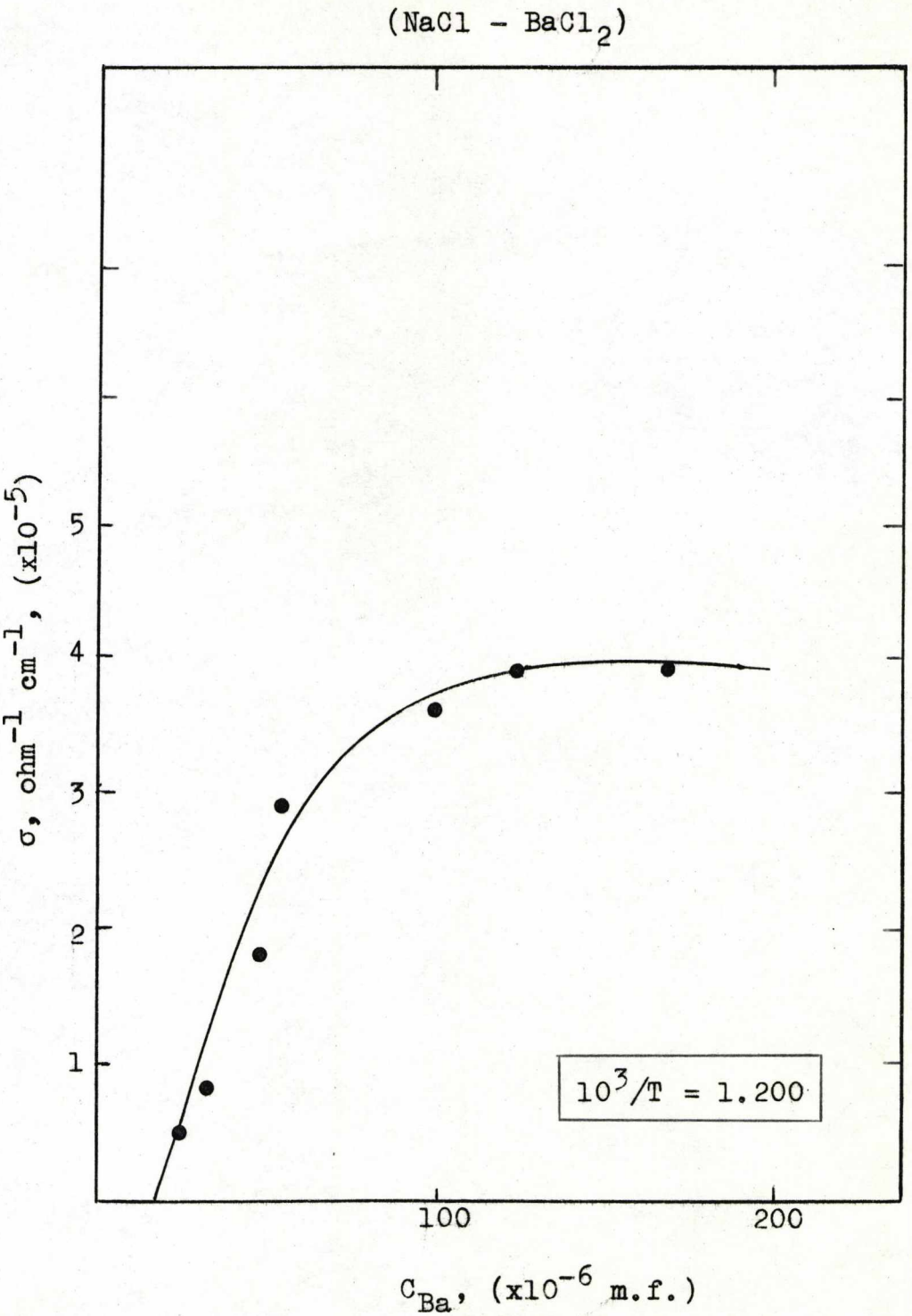

Fig. 50. Conductivity Isotherm.

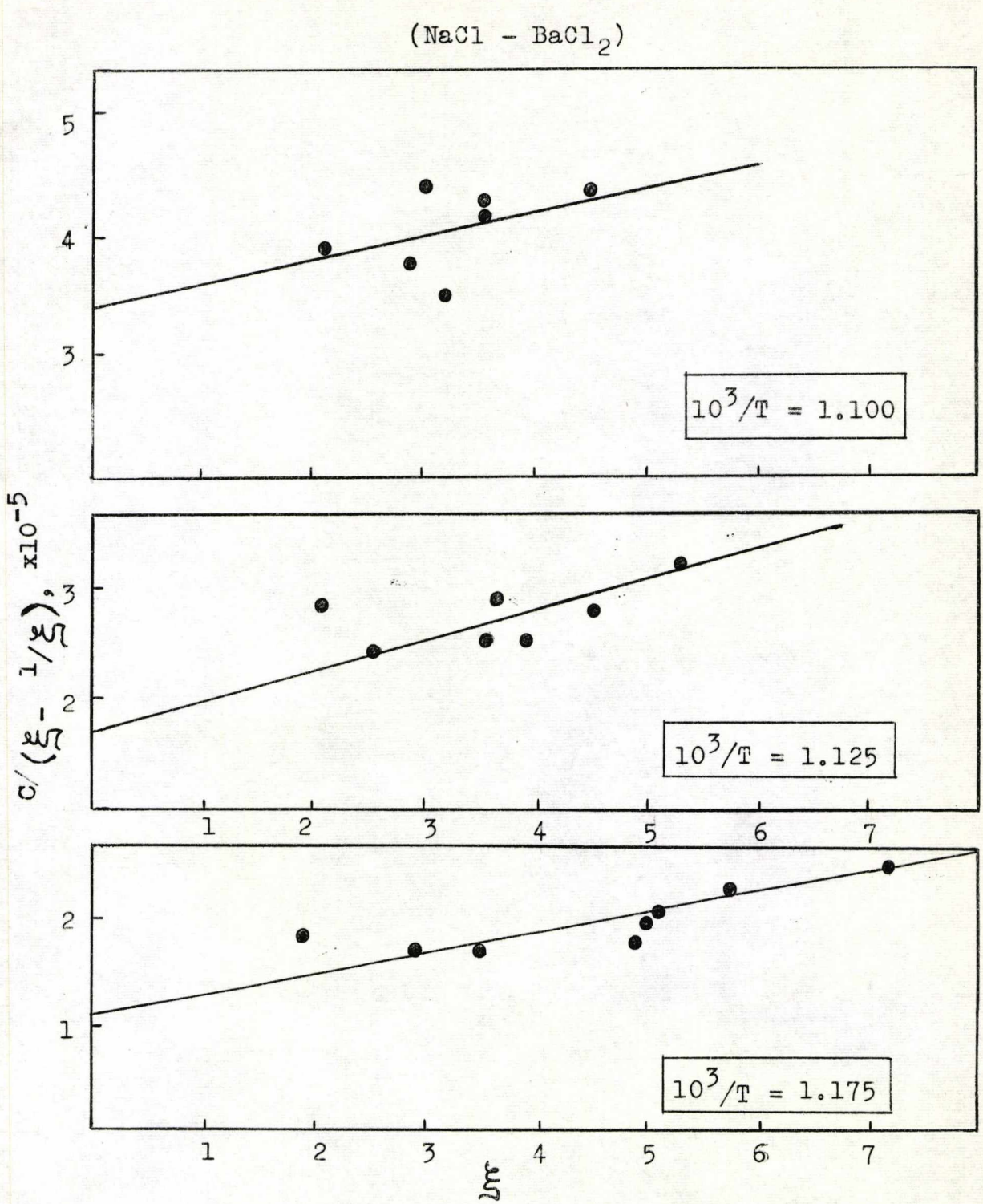

Fig. 51. - $C/(\xi - 1/\xi)$, vrs. ξ

($NaCl - BaCl_2$)

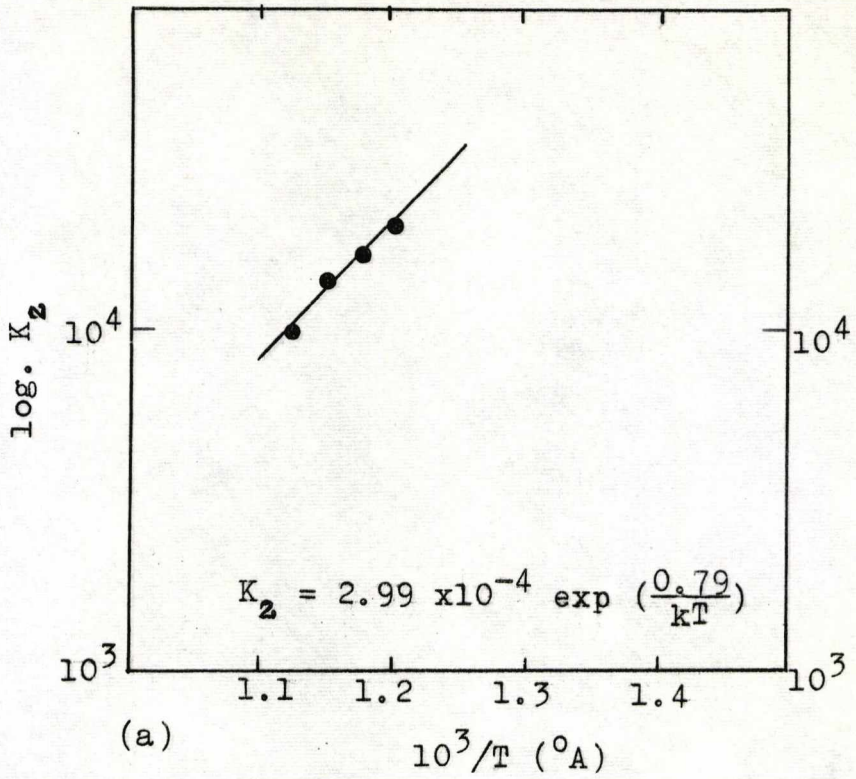

(a)

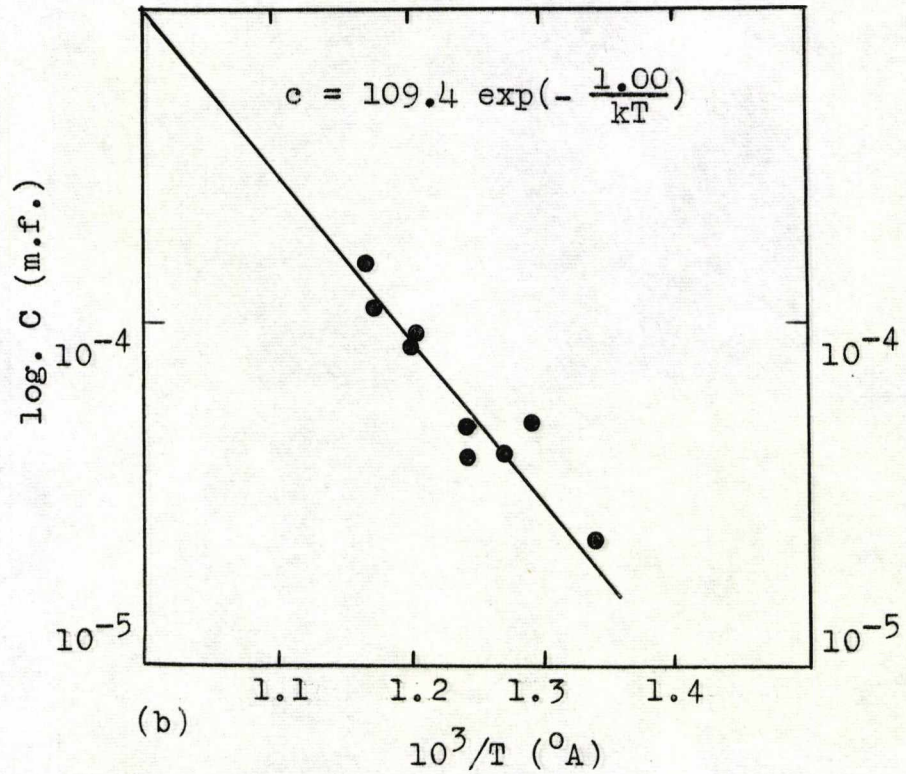

(b)

Fig. 52

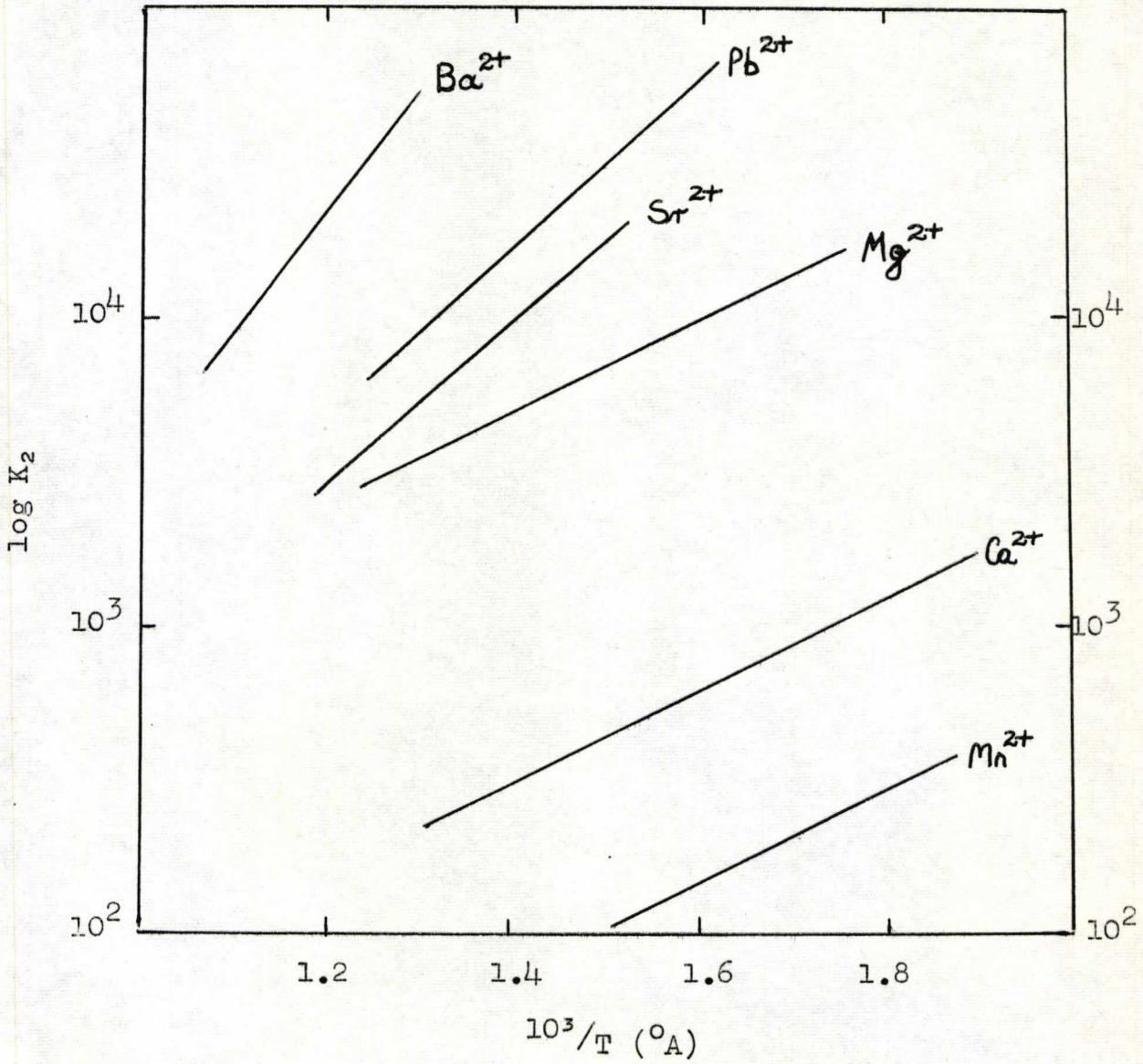

Fig. 53 - Values of the association constant K_2, as a function of temperature, for divalent impurities in NaCl. The straight lines are best, least squares fits.

CHAPTER IV

Diffusion Results

4.1. Self-Diffusion

Measurements of Na^+ self-diffusion in 'pure' and calcium-doped (approx. 50 ppm.) crystals of NaCl have been made over the temperature range 400° - 540°C. The diffusion coefficients were calculated from equation (2.7) by plotting $\log_{10} c$ against x^2. Some of these diffusion profiles are shown in Figs. 54, 55, 56 and 57. Many of these plots are curved upwards near $x^2 = 0$ due to the first few slices showing an abnormally high activity. This almost certainly arose from the fact that the crystal was not perfectly aligned to the cutting edge of the knife. As a result, the first few slices could have contained small quantities of the active material originally deposited on the surface of the crystal. The more reliable points in the interior of the samples were extrapolated to the ordinate and the diffusion coefficients calculated from the slopes. The results are shown as a $\log_{10} D$ versus $10^3/T$ plot in Fig. 58. The plot gives the following equation for Na^+ self-diffusion in 'pure' crystals in this temperature region.

$$D_{(Na^+)} = 1.86 \exp\left(\frac{0.75 \text{ eV}}{kT}\right) \text{cm}^2\text{sec}^{-1}$$

Typical Penetration Plot

Na^{22} in Pure NaCl

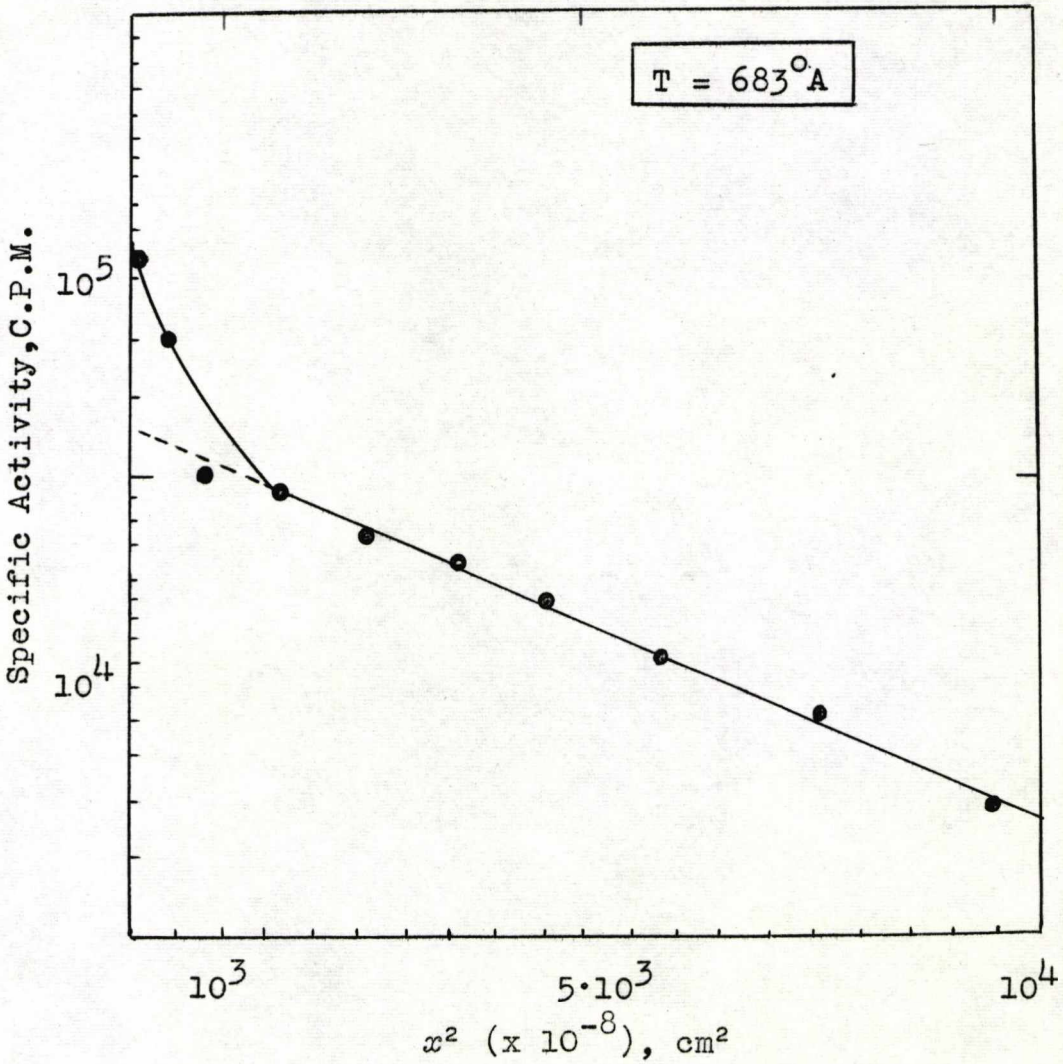

Fig. 54 - Diffusion.

Typical Penetration Plot

Na^{22} in Pure NaCl

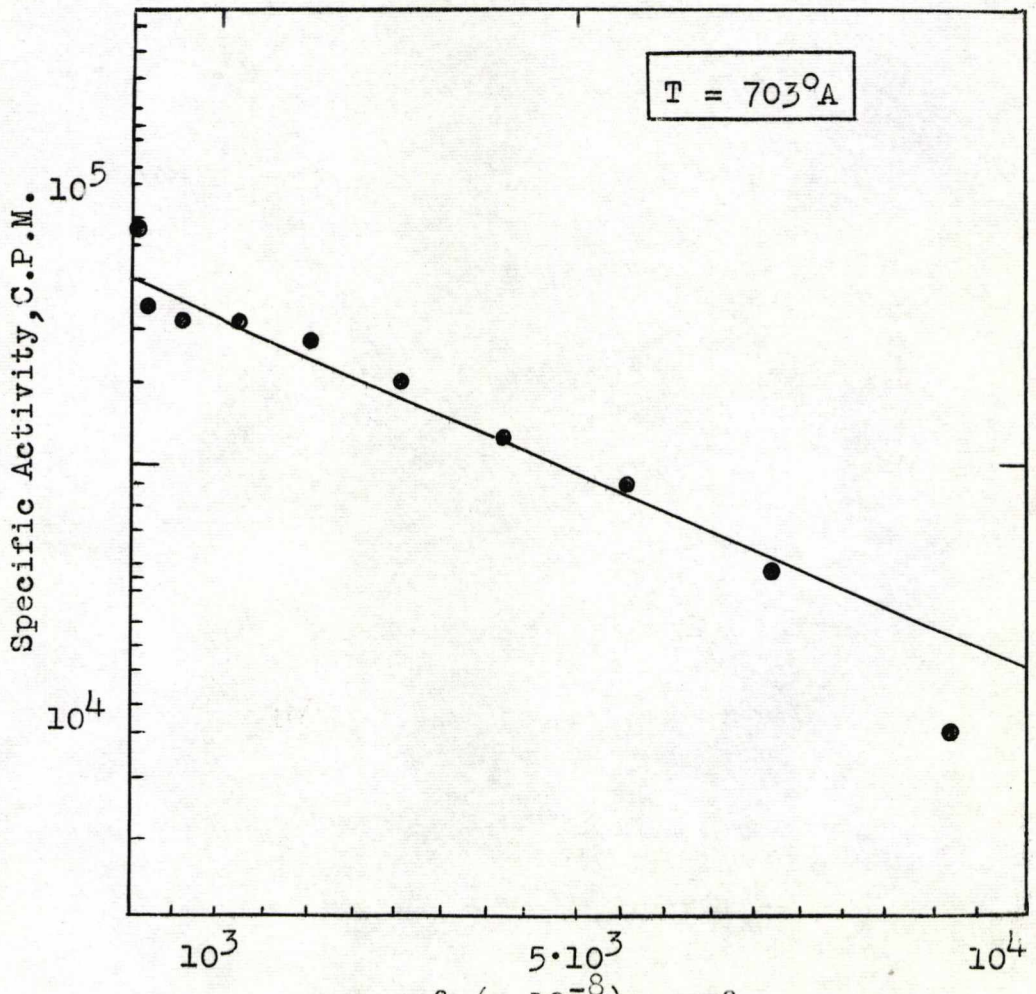

$\Delta t = 1.82 \times 10^6$ secs.

Fig. 55 - Diffusion.

Typical Penetration Plot

Na^{22} in ($NaCl - CaCl_2$)

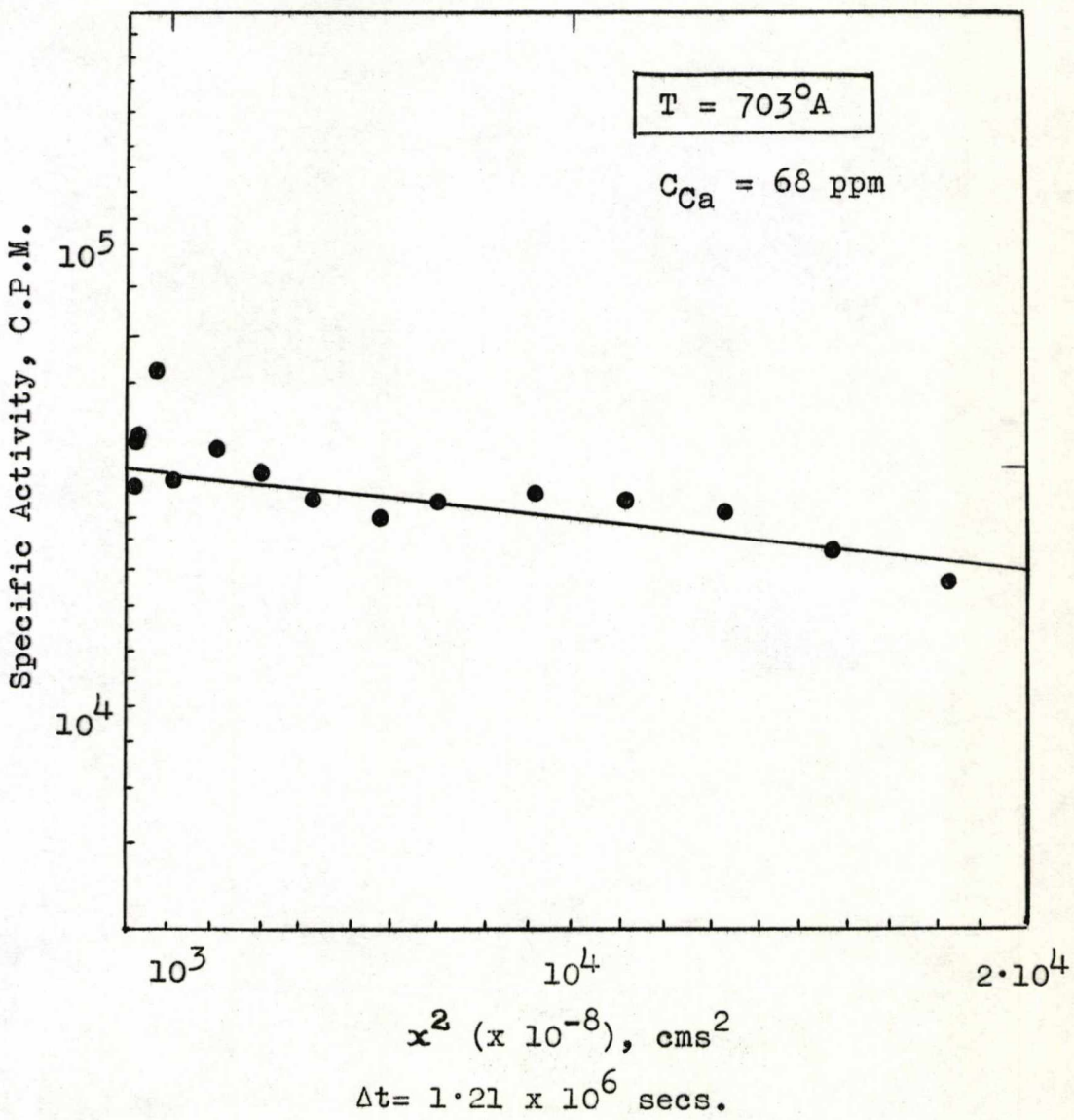

$\Delta t = 1 \cdot 21 \times 10^6$ secs.

Fig. 56. - Diffusion.

Typical Penetration Plot

Na^{22} in ($NaCl - CaCl_2$)

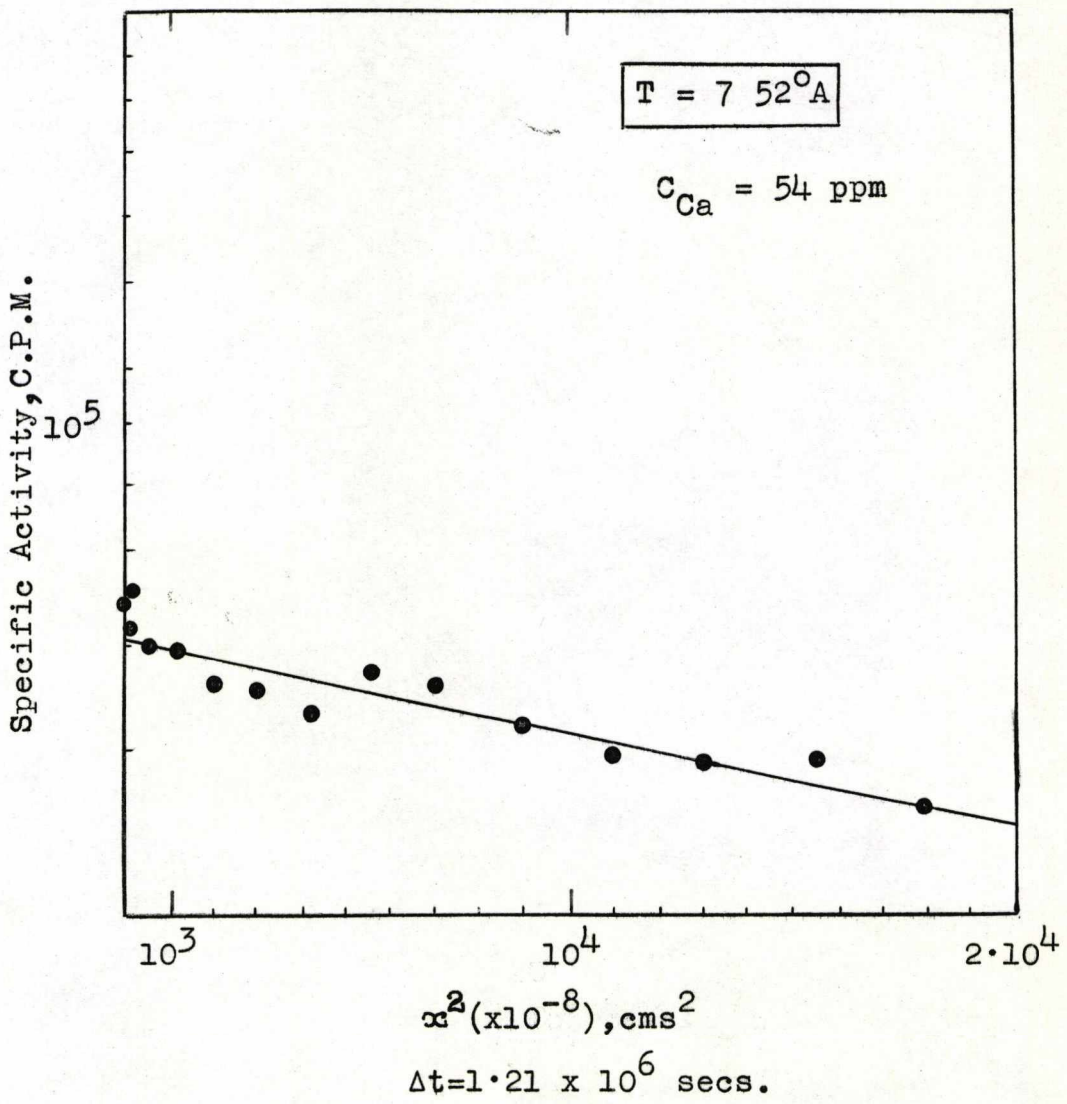

Fig. 57. - Diffusion.

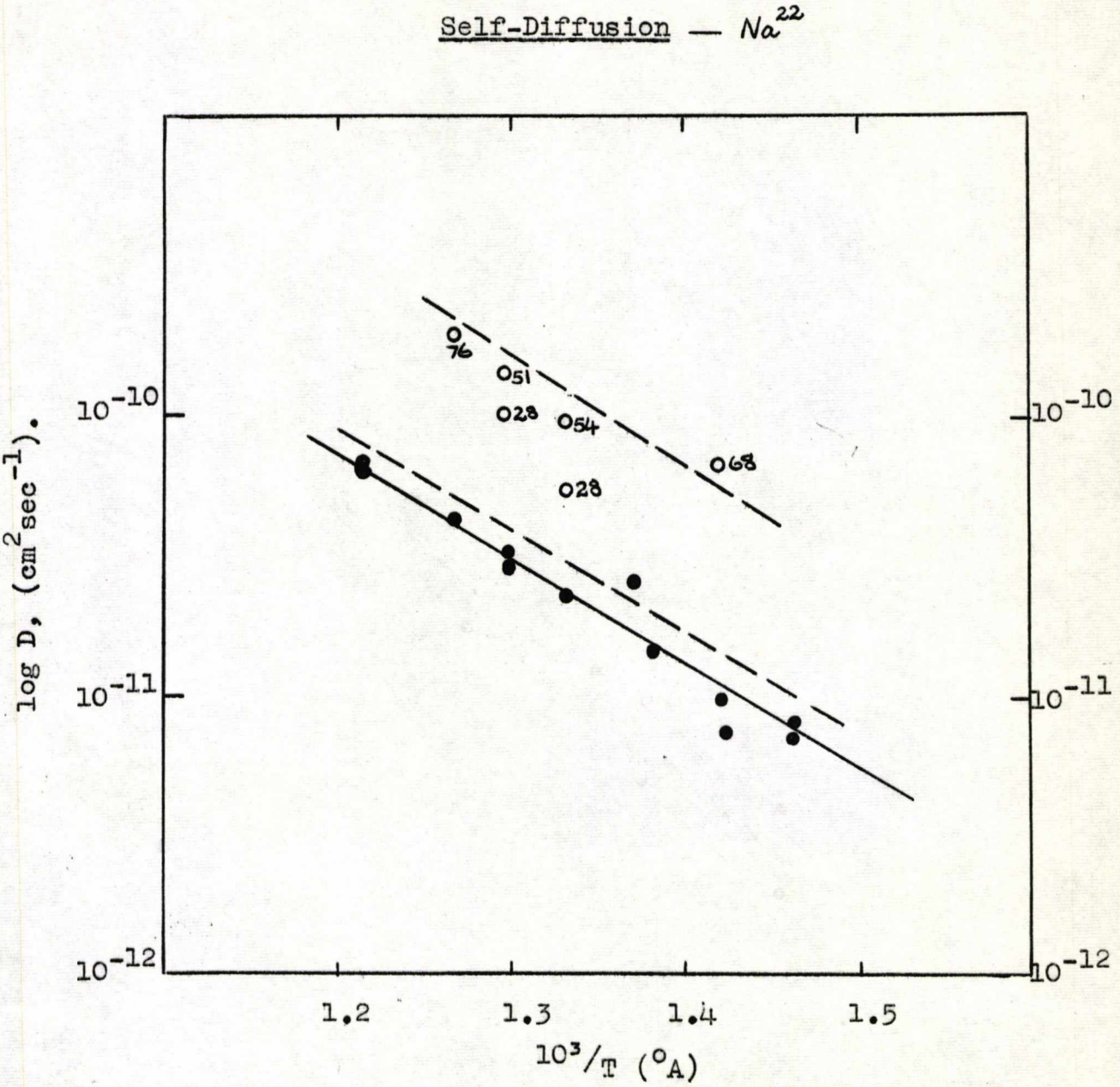

Fig. 58 - Diffusion of Na^+ in 'pure' and Ca^{2+}-doped NaCl. The numbers indicate the concentration of $CaCl_2$ (m.f. x 10^{-6}). The broken lines were calculated from the measured conductivity.

Comparison of the measured and calculated diffusion coefficients was made with a view to testing the validity of the Nernst-Einstein relationship, equation (1.20), and to note the relative contributions of free vacancies and associated impurity-vacancy complexes to the diffusion. The diffusion coefficients, calculated from conductance measurements, are also shown in Fig. 58.

4.2. Impurity-Diffusion

The diffusion of Mn^{++} ions in 'pure' and Mn-doped NaCl single crystals has been studied over the temperature range 400° - 475°C. Some of the penetration profiles are shown in Figs. 59, 60, 61 and 62., the diffusion data is listed in the appendix. The log $_{10}D$ versus reciprocal temperature plot is shown in Fig. 63.

The diffusion coefficients of Mn have been expressed as functions of the impurity concentration, Fig. 64, with a view to determining the free energy of association of the impurity-vacancy complexes. The theory of Lidiard, which relates the impurity diffusion coefficient to the concentration of impurity-vacancy complexes, that is, the degree of association, is given in the following section.

Typical Penetration Plot

^{54}Mn in Pure NaCl

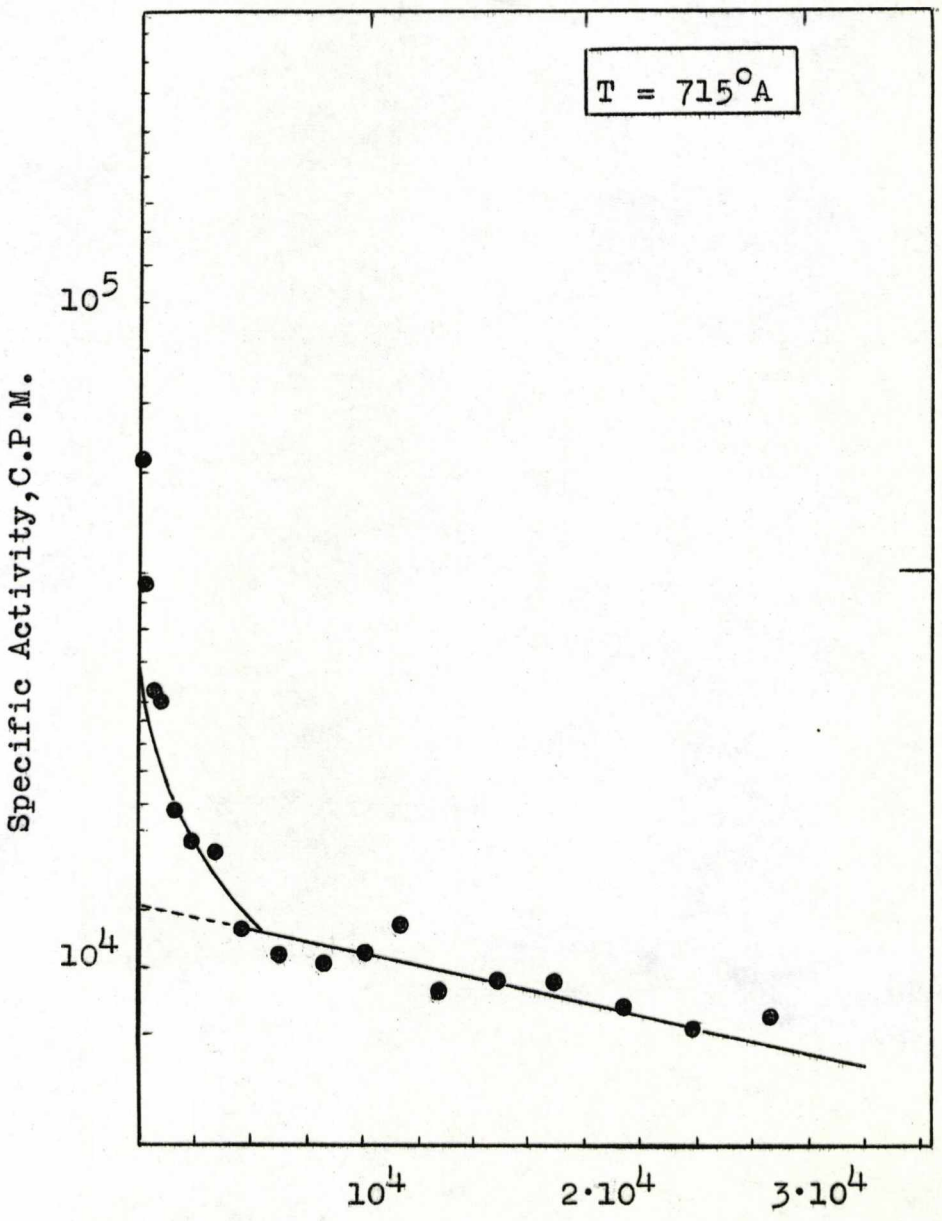

$\Delta t = 2.59 \times 10^5$ secs.

Fig. 59 - Diffusion.

Typical Penetration Plot

^{54}Mn in Pure NaCl

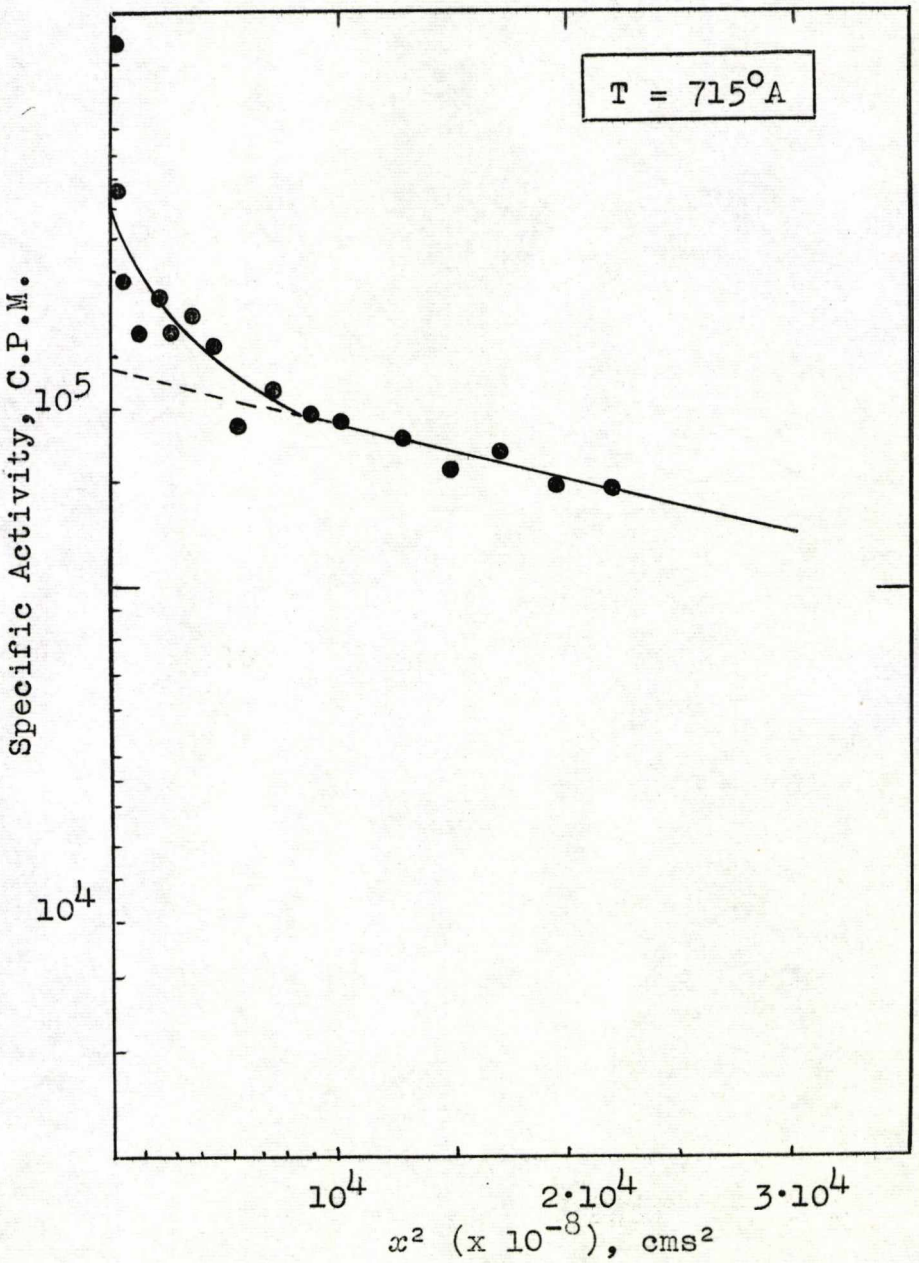

$\Delta t = 2.59 \times 10^5$ secs.

Fig. 60 - Diffusion.

Typical Penetration Plot

Mn^{54} in ($NaCl - MnCl_2$)

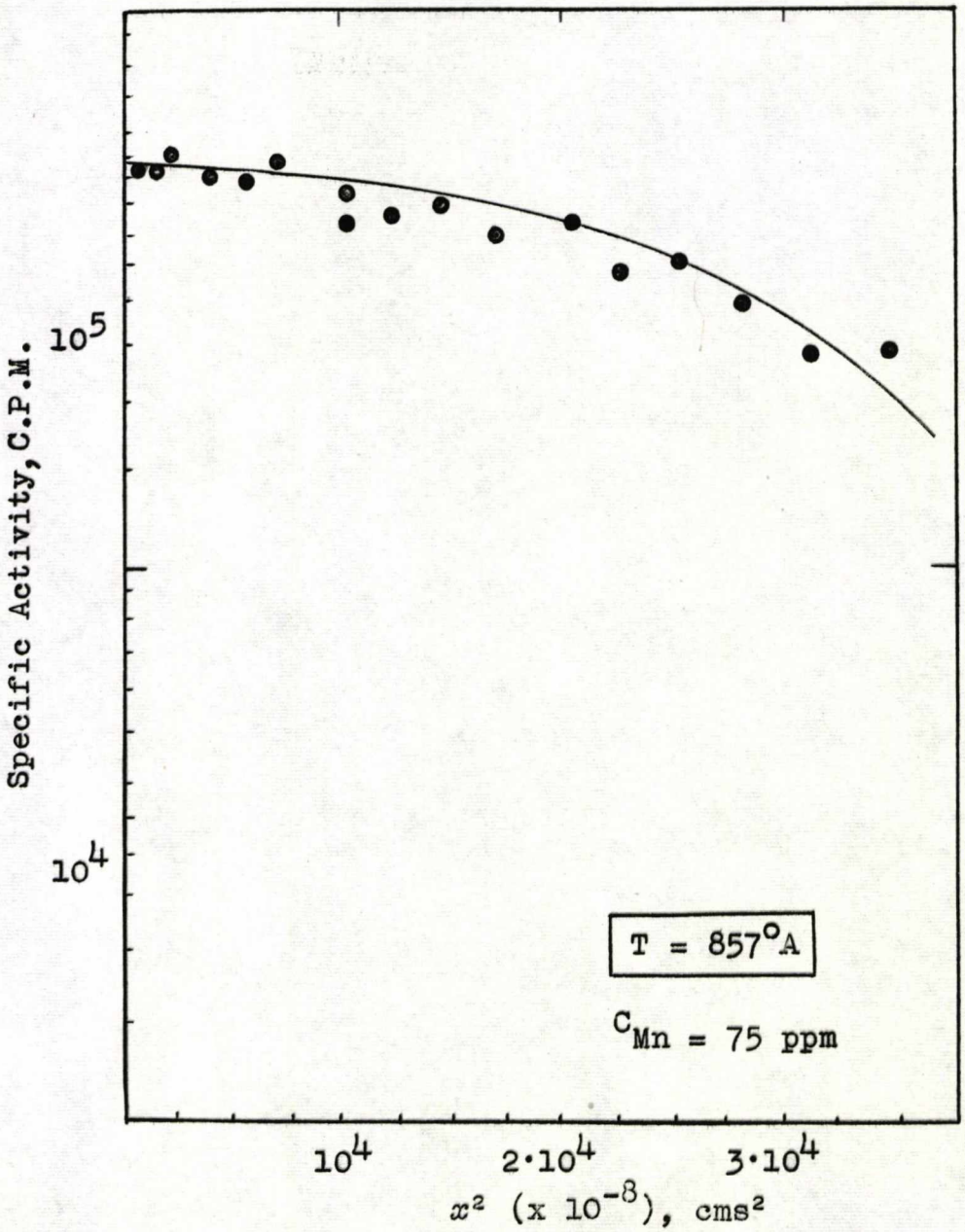

Fig. 61 - Diffusion.

Typical Penetration Plot

Mn^{54} in ($NaCl - MnCl_2$)

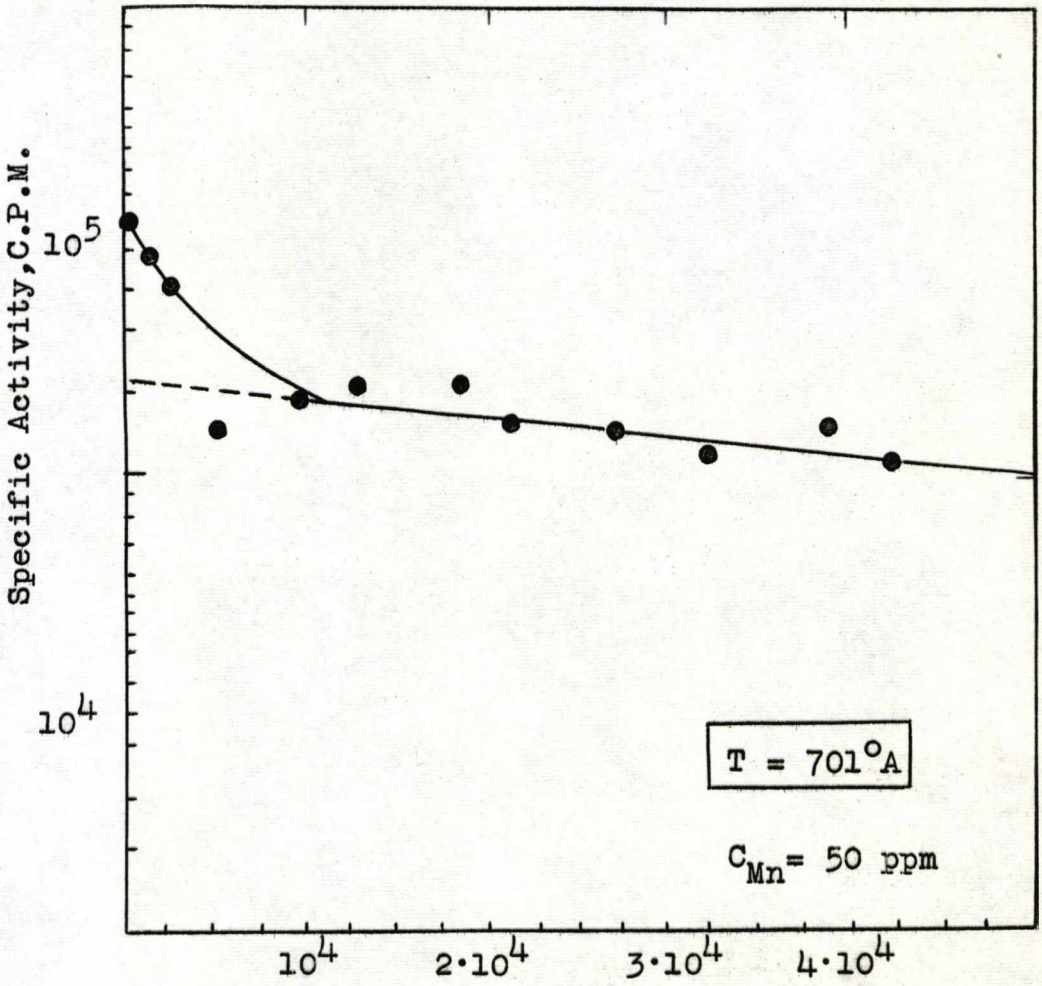

$\Delta t = 3.45 \times 10^5$ secs.

Fig. 62 - Diffusion.

Impurity Diffusion — Mn^{54}

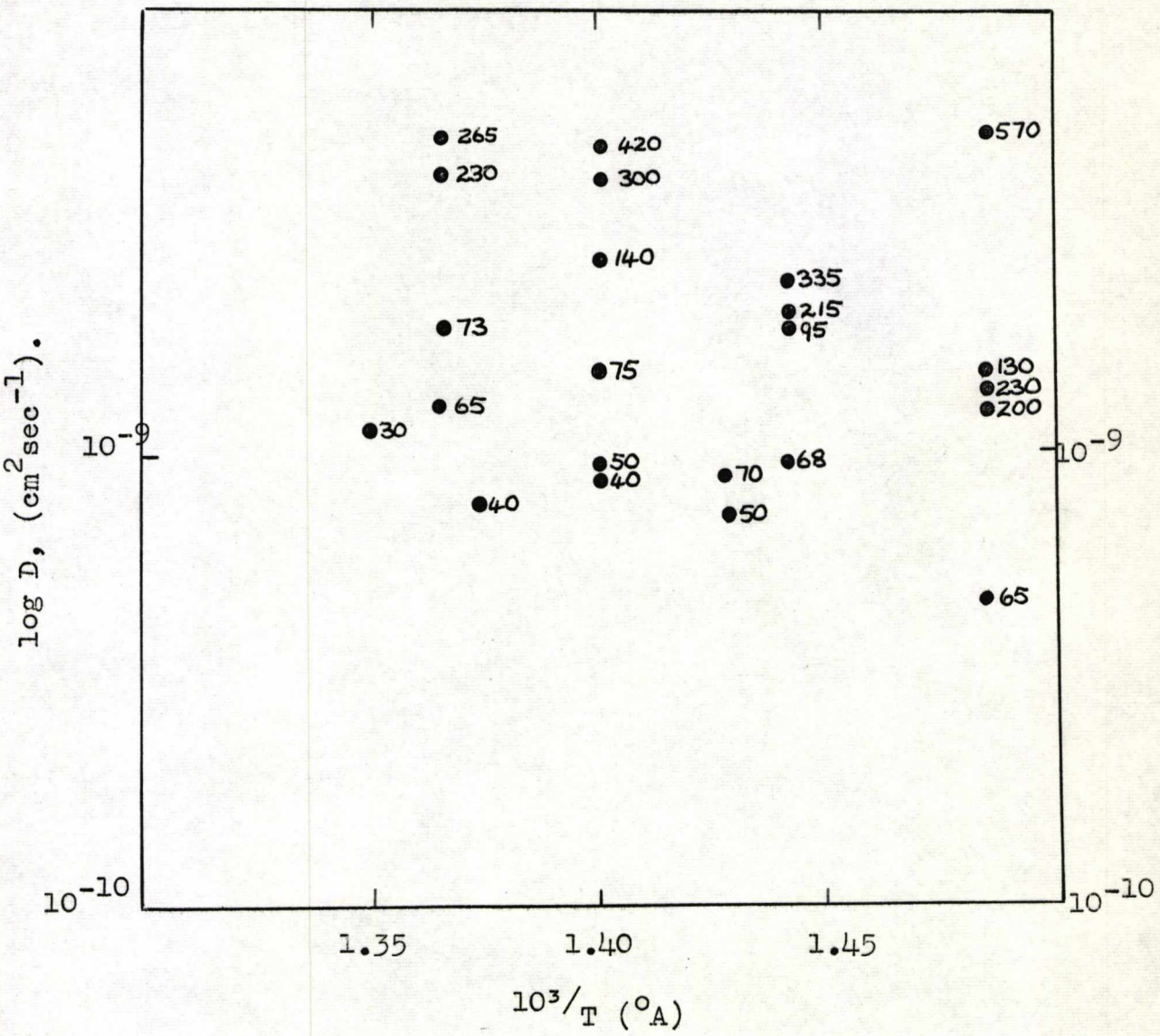

Fig. 63 - Diffusion of Mn^{2+} in NaCl. The numbers indicate the concentration of $MnCl_2$ (in m.f. x 10^{-6}).

Diffusion Isotherms

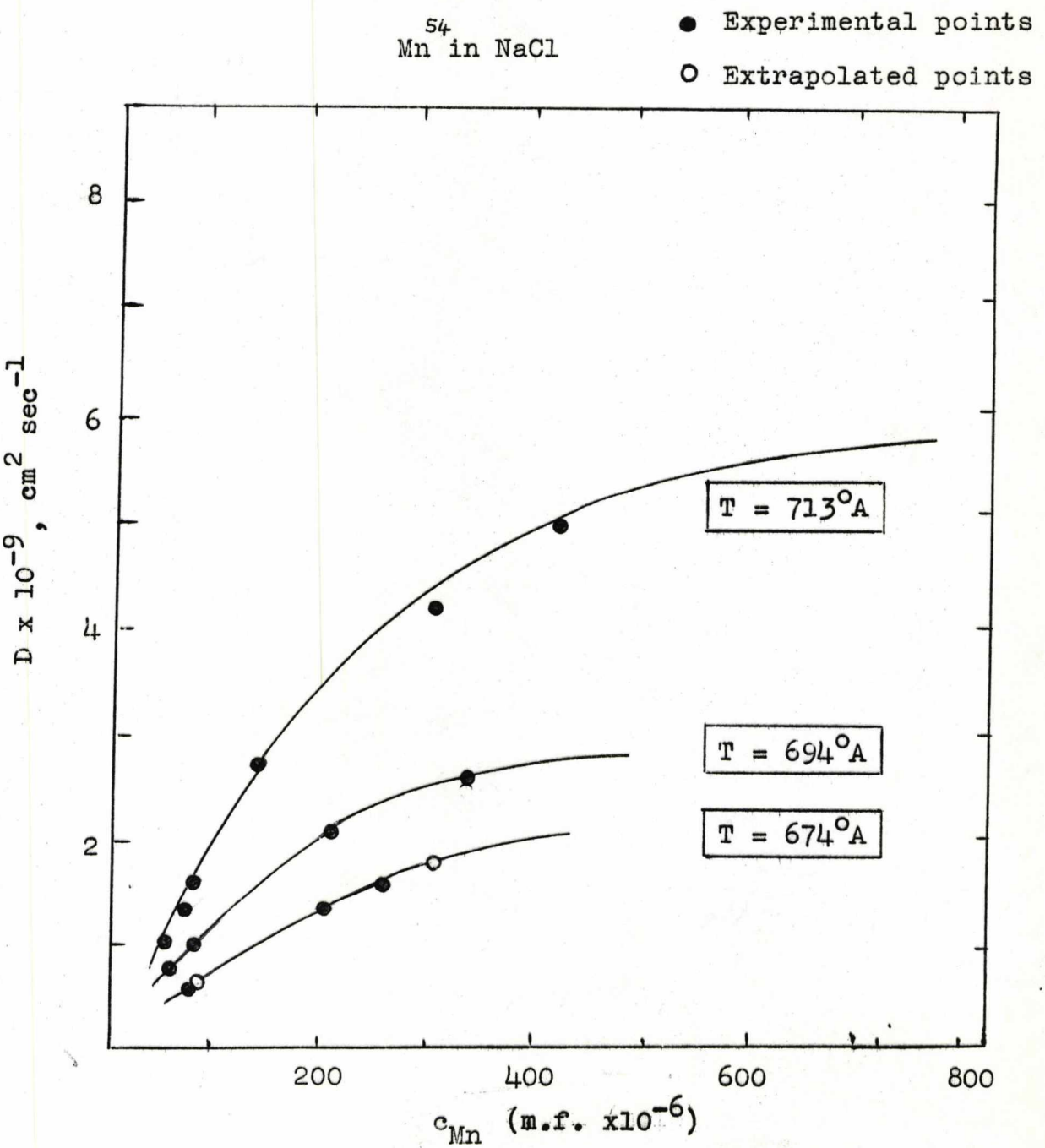

Fig. 64

Impurity Diffusion[18] - Theory

Under conditions of zero impurity concentration gradient, the diffusion coefficient of a radioactive isotope of a divalent impurity ion in a NaCl crystal is given by

$$D = \frac{1}{3} a^2 w_2 p f \qquad (4.1)$$

where a is the smallest distance between two cations in the lattice, w_2 is the frequency with which the impurity ion jumps into a bound cation vacancy, p is the degree of association and 'f' is the correlation factor. The connection between the association energy of an impurity-vacancy complex and the tracer diffusion coefficient, D, is via the degree of association p, which is given by

$$p = \frac{x_k}{c} \qquad (4.2)$$

where x_k is the concentration of nearest-neighbour impurity-vacancy pairs, and c is the concentration of divalent impurity.

The association energy of an impurity-vacancy complex, is deduced by matching plots of p versus c, calculated for a range of values of the association energy, to the experimentally determined values of D. However, steps must first be taken to eliminate the unknowns 'f' and w_2. This is done by 'normalising' D and p and taking

$$\frac{D}{D_c} = \frac{p}{p_c} \qquad (4.3)$$

where D_c is the saturation value of D obtained from diffusion isotherms, and $p_c \approx 1$, i.e., almost total association.

The degree of association, p, is determined from the law of mass action for association. In the simplest case, where the impurity ion and cation vacancy are regarded as associated only when they are nearest neighbours,

$$\frac{p}{(1-p)^2} = z_1 c \exp\left(\frac{W_A}{kT}\right) \qquad (4.4)$$

W_A, the Gibbs free energy of association, is related to the enthalpy, χ_1, and entropy, η_1, of association in the usual way. Equation (4.4) is valid when the concentration c of impurity created vacancies is much greater than the thermal vacancy concentration. It is solved numerically for p and p/p_c as a function of the parameters W_A and c. Curves of p/p_c versus c for different values of W_A are plotted along with experimental values of D/D_c and a direct comparison made. The free energy of association can then be calculated by comparison of the theoretical curves with the experimental points.

Equations (4.2), (4.3) and (4.4) are formally complete, and have been solved numerically for p and

p/p_c as a function of the parameters c_{Mn} and W_A. Curves of p/p_c versus c_{Mn} for different values of W_A are shown in Figs. 65, 66 and 67, along with the experimental values of D/D_{max}.

The experimental points for diffusion at 674°A, Fig. 65, fit well to curve for W_A = 0.30 eV. For 694°A, Fig. 66, the fit to the curve for W_A = 0.35 eV is good, but at 713°A, Fig. 67, one of the experimental points lies well above the calculated line for W_A = 0.35 eV. This discrepancy is probably due to inaccuracy in the estimation of impurity content. The theoretical curves for W_A = 0.25 and 0.40 eV are included in Fig. 65. Comparison of these with the experimental points would indicate that the association energies which have been deduced are accurate to $\pm$ 0.05 eV.

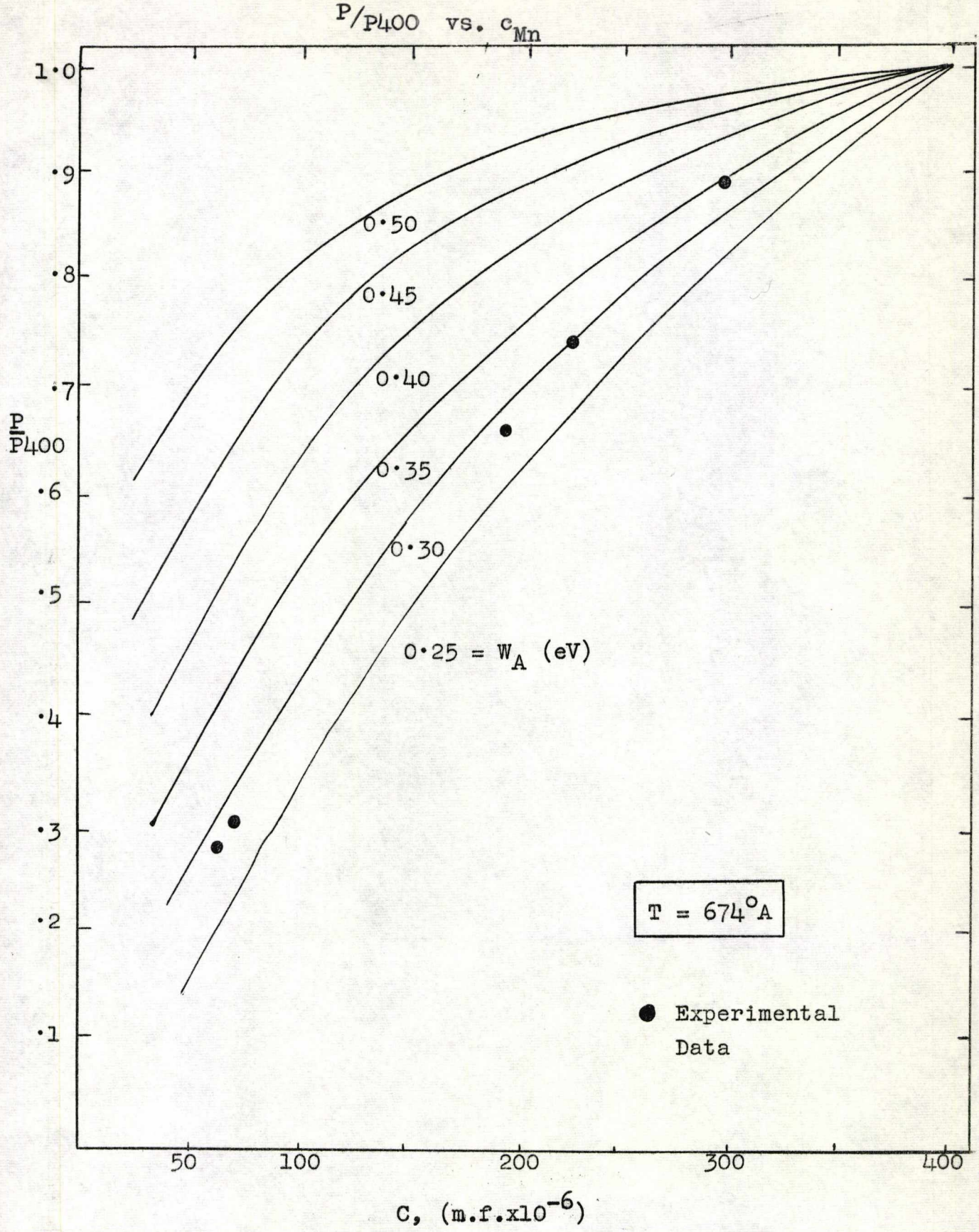
P/P400 vs. c_Mn
1·0
·9
·8
·7
·6
·5
·4
·3
·2
·1
P/P400
0·50
0·45
0·40
0·35
0·30
0·25 = W_A (eV)
T = 674°A
Experimental Data
50
100
200
300
400
C, (m.f.x10^-6)

Fig. 65.

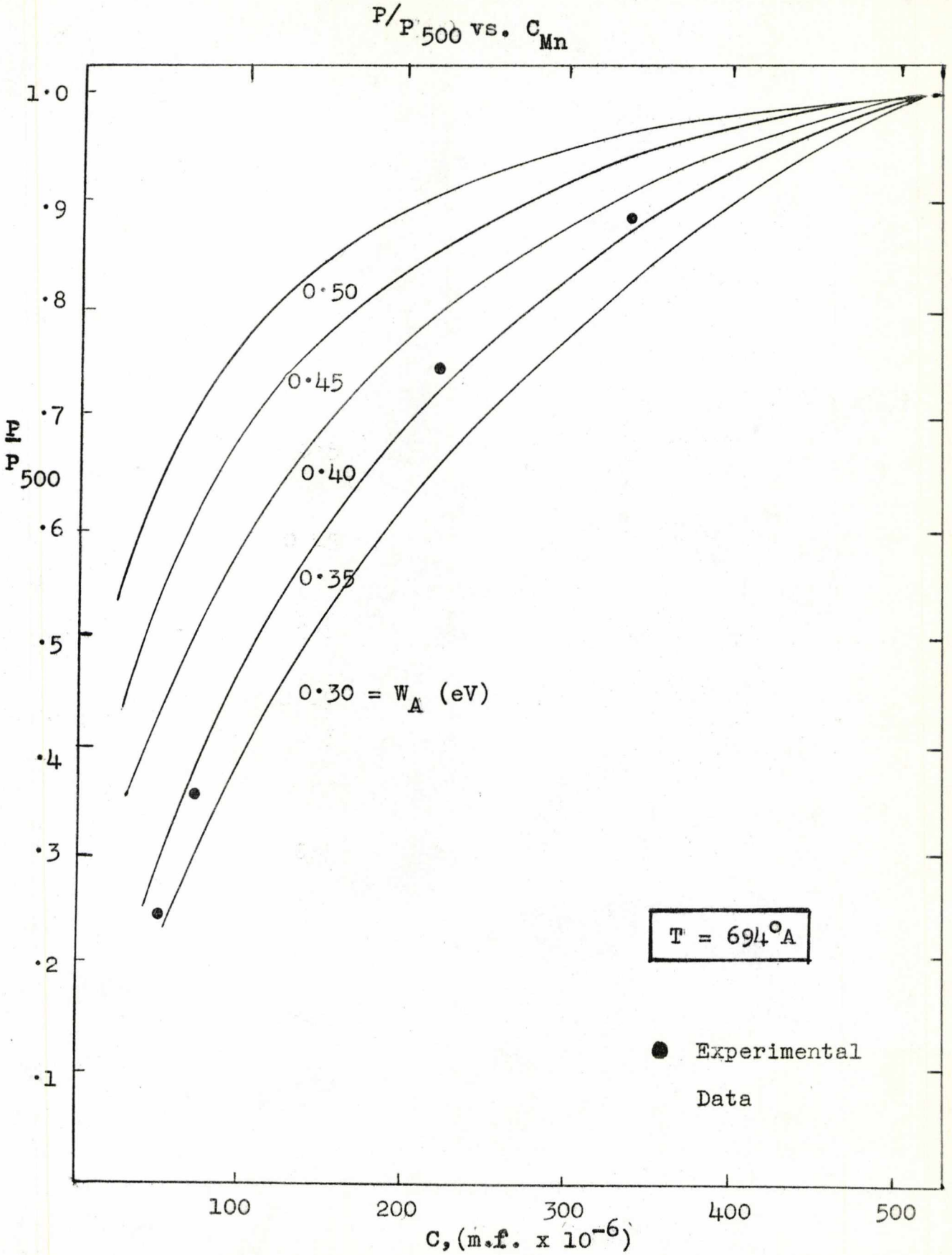
P/P500 vs. CMn
1·0
·9
·8
·7
·6
·5
·4
·3
·2
·1
P/P500
0·50
0·45
0·40
0·35
0·30 = WA (eV)
T = 694°A
Experimental Data
100
200
300
400
500
C, (m.f. x 10-6)

Fig. 66.

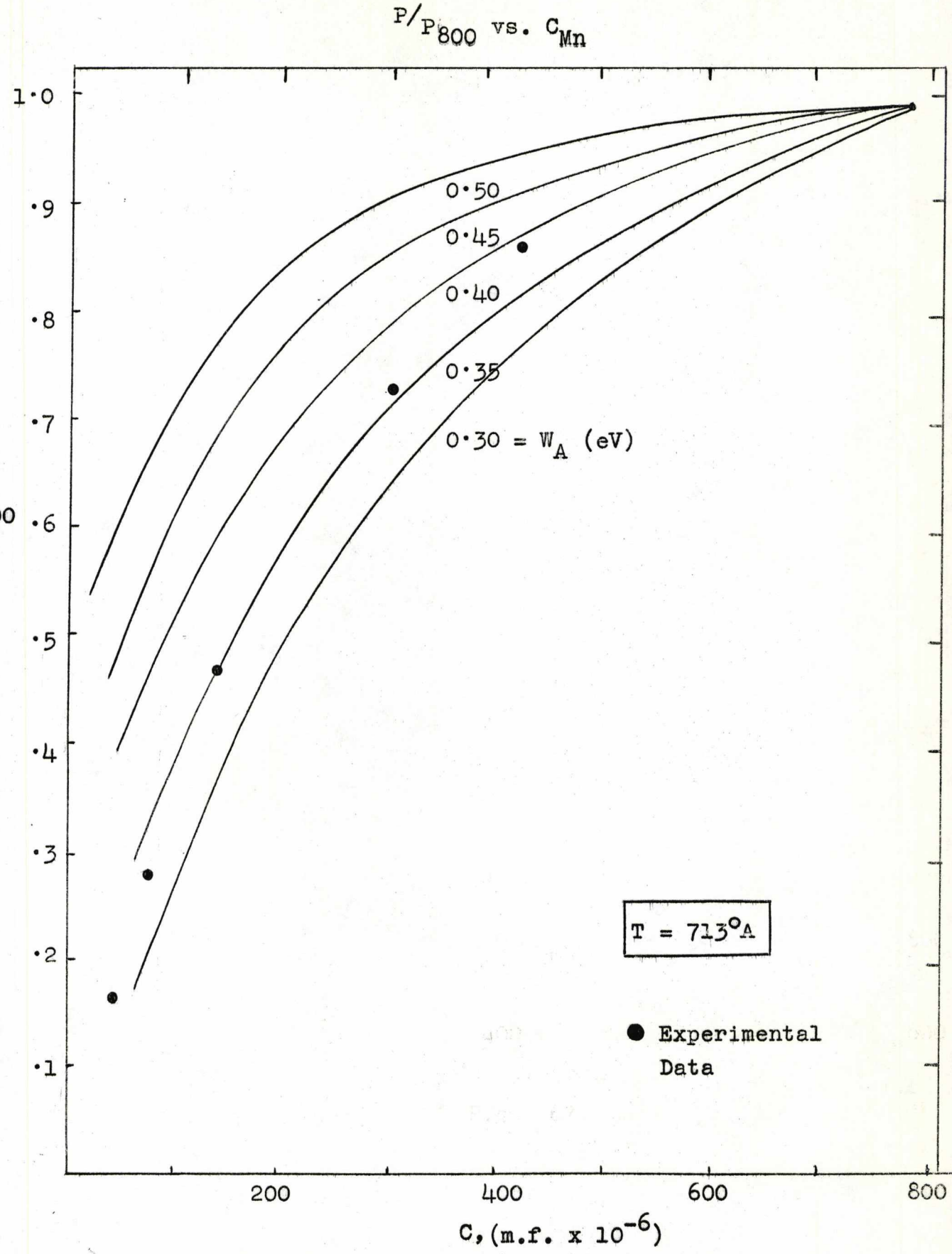
P/P800 vs. CMn
1·0
·9
·8
·7
·6
·5
·4
·3
·2
·1
P/P800
0·50
0·45
0·40
0·35
0·30 = WA (eV)
T = 713°A
Experimental Data
200
400
600
800
C, (m.f. x 10-6)

Fig. 67.

CHAPTER V

Electron Spin Resonance

Electron spin resonance, applied to the study of association, is a powerful technique. It allows the experimental determination of the binding energies of excited states of impurity-vacancy complexes as well as estimates of the ground state of these associations[25].

The spin resonance of a paramagnetic ion present in a crystal is sensitive to its environment. The absorption spectrum indicates the presence of defects in the neighbourhood of a paramagnetic ion because of the corresponding reduction in symmetry of the crystalline electric field acting on the ion. The symmetry of the crystalline electric field depends upon the relative positions of the impurity and vacancy in the crystal, and on the orientation of the crystal relative to the static magnetic field. For an impurity ion, such as Mn^{++}, the state of association and binding energy of the complexes can be determined directly by means of electron spin resonance.

Much is known about the Mn^{++} spin resonance spectrum. In the ground state Mn^{++} has an outer electronic configuration of $3d^5$ and its spin state is described by $^6S_{5/2}$. Splitting of the spectrum due to the interaction of the unpaired electron of the Mn^{++} ion with the

magnetic moments of neighbouring nuclei is relatively small. Mn^{++} has a nuclear spin of $^5/_2$ so that the hyperfine interaction splits each electronic transition into six lines.

The electron spin resonance of Mn^{++} in NaCl has been studied over the temperature range 19.8°C - 182.3°C in crystals containing approx. 40 ppm of Mn.§ The spectra were recorded with the magnetic field along one of the cube axis, that is $\theta = 0^\circ$. Measurements were made at a working frequency of 9270 Mc/sec.

The temperature dependence of the spectrum is shown in Figs. 68, 69 and 70. At room temperature a broad line of half-width 750 gauss is observed. Superimposed on this a weak complex spectrum can be seen. As the temperature is increased the broad line disappears and there is a marked increase in the intensity of the complex spectrum especially in the centre where six central lines gradually emerge.

The spectra are almost identical with those obtained by Watkins[25] on the same system. It must be pointed out however that his measurements were made at the much higher working frequency of 20,000 Mc/sec. The theoretical interpretation of the spectra is discussed in detail in this paper. In the present work, four different spectra for the Mn^{2+} ion in NaCl have been observed. These arise from Mn^{2+} ions in four

§ These measurements were made by Dr. A.L. Porte, (University of Glasgow).

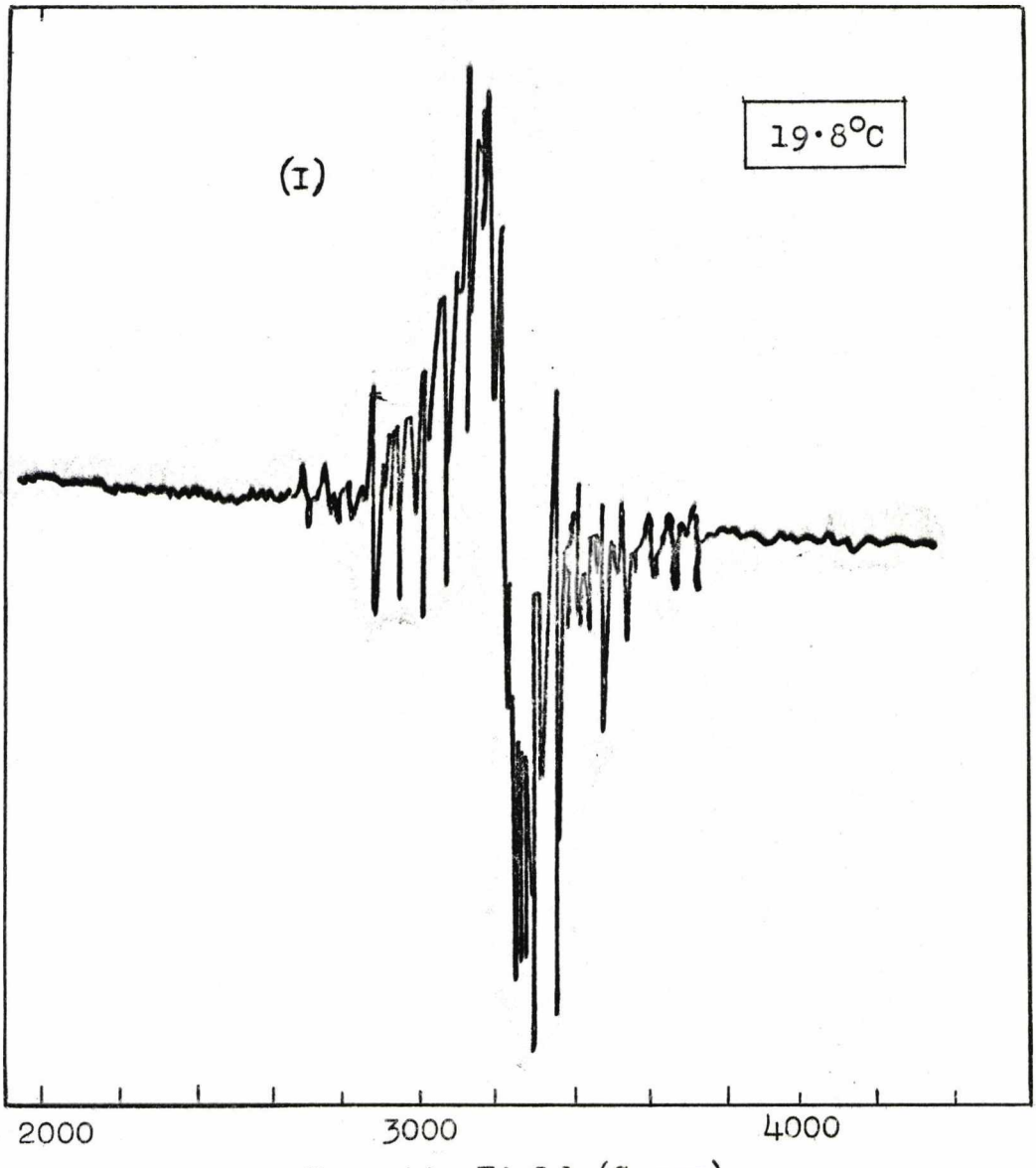

Fig. 68. - The E.S.R. Spectrum of Mn^{2+} in NaCl at a temperature of 19.8°C.

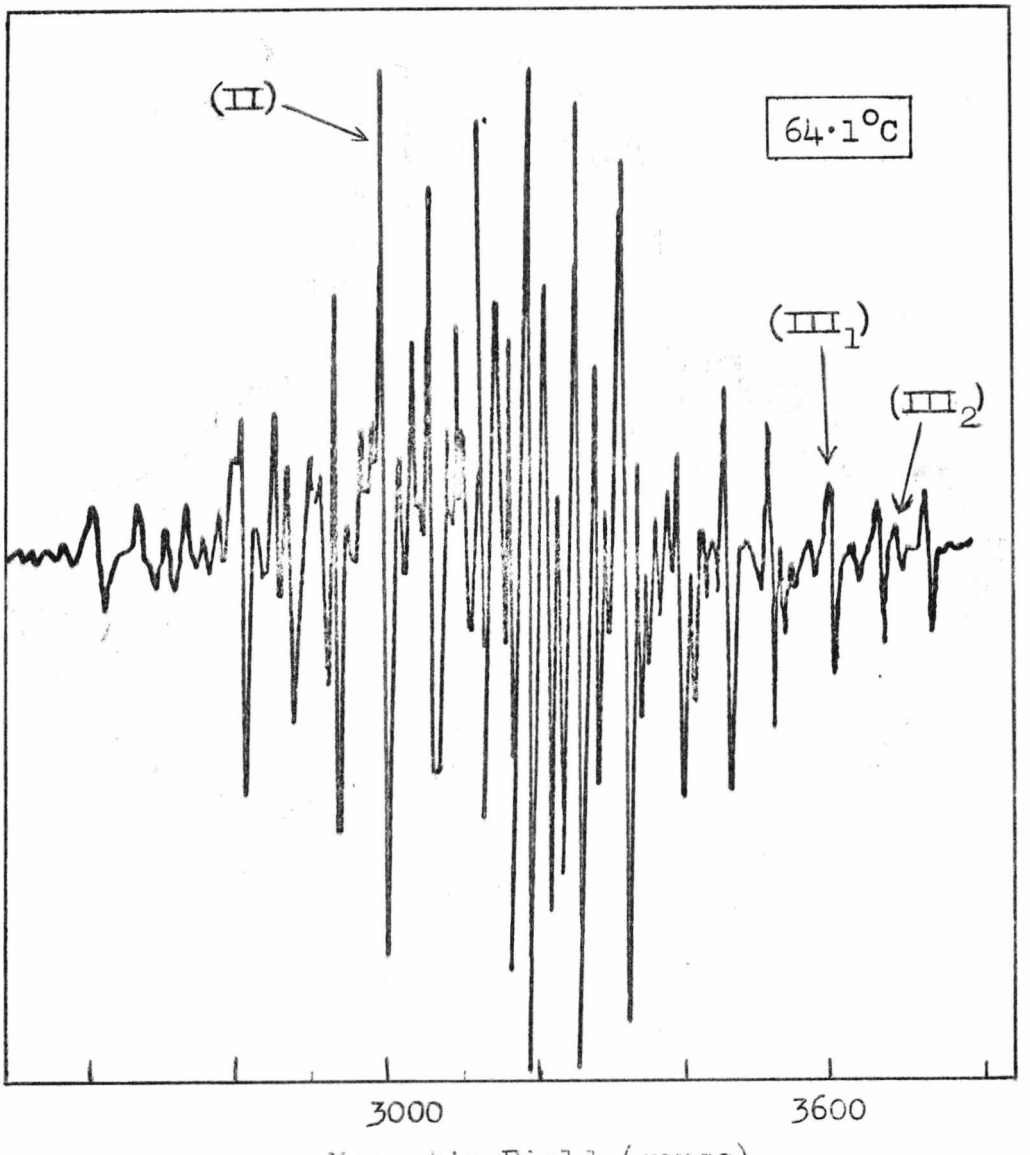

Fig. 69. - The E.S.R. Spectrum of Mn^{2+} in NaCl at a temperature of 64·1°C.

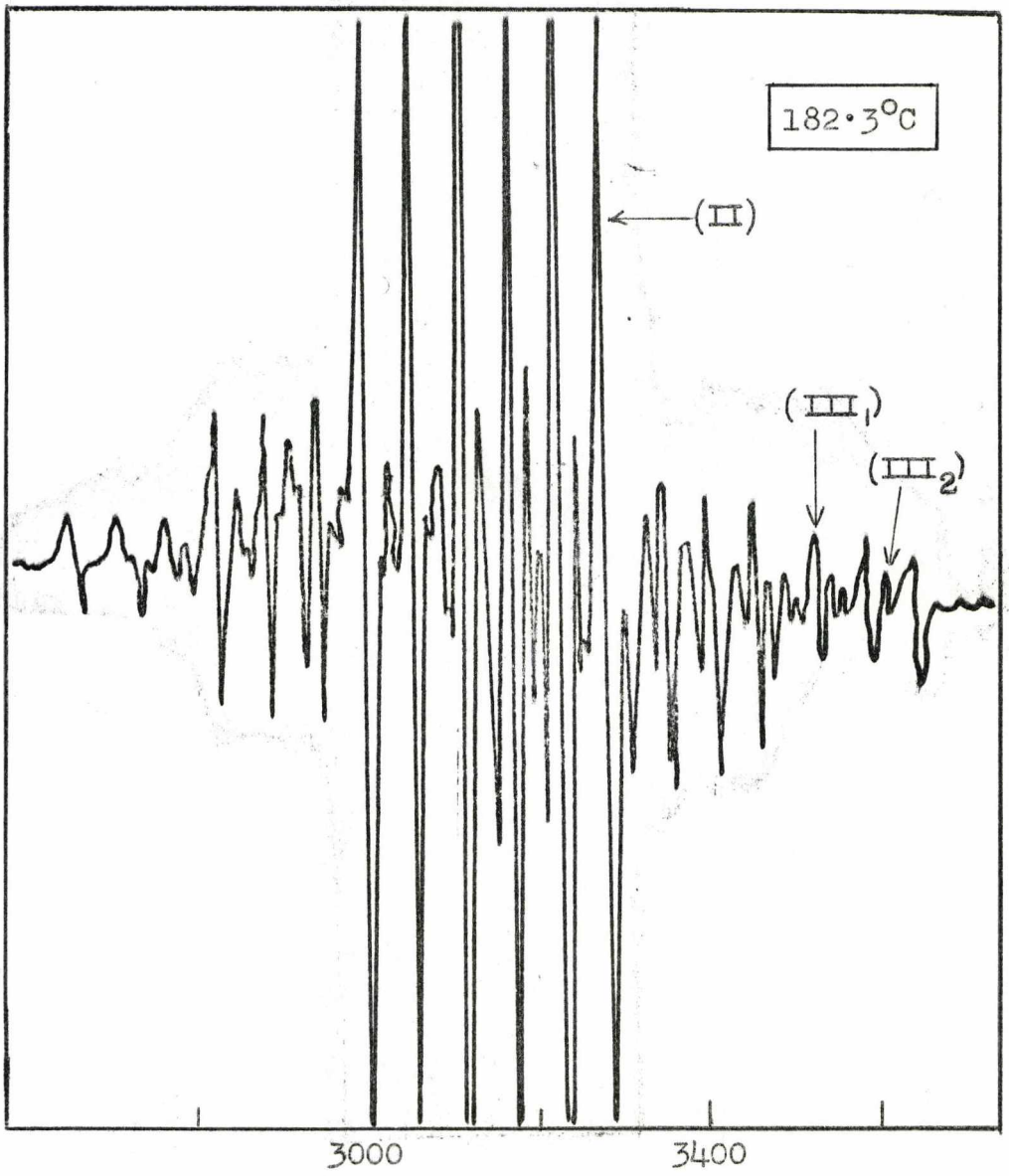

Fig. 70. - The E.S.R. Spectrum of Mn^{2+} in NaCl at a temperature of 182·3°C

distinguishable environments. They have been designated spectrum I, II, III_1 and III_2 according to Watkins'[25] notation. Spectrum (I) arises from Mn^{2+} ions in a precipitated or aggregated state, spectrum (II) from completely isolated Mn^{2+} ions, that is, no defect nearby, spectrum (III_1) from Mn^{2+} ions with a positive ion vacancy in the nearest-neighbour position and spectrum (III_2) from Mn^{2+} ions with a positive ion vacancy in the next-nearest-neighbour position.

Spectrum (II) increases in intensity as the temperature is raised due to an increase in the number of isolated Mn^{2+} ions. The disappearance of spectrum (I) can be attributed to the precipitated Mn^{2+} ions dissolving into the solid. The ionic conductance measurements suggest that Mn is very soluble in the NaCl lattice. This is confirmed by the spin resonance studies since the broad line associated with precipitated Mn^{2+} ions disappears rapidly as the temperature is raised.

The satellite spectra of (III_1) and (III_2) exhibit small changes with increase in temperature. These have been studied in detail since the relative numbers of nearest-neighbour and next-nearest-neighbour pairs can be obtained from measurements of the relative intensities of these spectra. These are given in table 7.

TABLE 7

Relative numbers of nearest-neighbour (n_1) and next-nearest-neighbour (n_2) complexes

n_1/n_2	T°C
7.0	19.8
4.7	41.8
4.6	64.1
4.5	85.5
4.2	102.5
3.6	130.0
3.1	160.6
2.8	183.2

Assuming that a vacancy has the same vibrational frequency in both nearest- and next-nearest-neighbour positions, the ratio n_1/n_2 is given by

$$n_1/n_2 = 12/6 \exp\left(\frac{W_A - W_{A1}}{kT}\right) \qquad (5.1)$$

where 12/6 is the ratio of nearest to next-nearest sites available, and W_A and W_{A1} are the binding energies of these complexes. The value of $(W_A - W_{A1})$ at 19.8°C is calculated to the 0.034 eV. This compares favourably with the value obtained by Watkins[25] at a temperature of 25°C. The difference in binding energies of the two complexes is therefore small, the nearest site being the more stable.

CHAPTER VI

Theoretical Defect Calculations

The theoretical work of Jost[59] showed that, despite the large cohesive forces of ionic crystals, it was possible to obtain reasonable values for defect formation energies by taking into account the large gain in energy due to the polarisation of the lattice by the net charge on the defects. Calculations for these charged defects have mainly been made by various methods derived from the original calculation of Mott and Littleton[60]. They produced a reasonable approximation for estimating the polarisation and displacement fields around the defects by making use of a simple Born ionic model. The model is a two-body potential one, ions interacting through Coulombic forces and repulsion forces due to overlap of the closed electron shells. The polarisation of the lattice is described by assigning dipoles, generated by the electric fields of the defects, to the ions. This results in a fractional displacement of the ions from their equilibrium positions, the relative movement of the ions leading to a distortion of the electron cloud distribution.

The Mott-Littleton approach is to divide the crystal into a region I, containing the defect and its shell of nearest neighbours, and a region II, which is the rest

of the crystal. In region II it is assumed that the displacements and induced moments are so small that a harmonic expansion of the energy can be used. The electrical polarisation of region I is also treated by using a harmonic approximation, the assumptions of harmonicity then leading to a set of linear equations for the equilibrium displacements and moments. These equations can then be solved to give an energy function which is a function only of the displacements in region I. The energy of the crystal in the stable configuration relative to the energy of the perfect crystal gives the work required to produce the defect.

The polarisation of region II contributes significantly to the energy of formation of a defect in ionic crystals. Following Mott and Littleton, most authors since have based their solution for region II upon the fact that the defect is an elastic as well as an electrical singularity. This has led to the inclusion of elastic terms in the region II displacement field, and the effect of deformation dipoles generated by the distortion of electron charge distribution as a result of the relative ionic motion.

Less elaborate calculations are able to give binding energies between divalent cation impurities and cation vacancies in ionic crystals. Since an associated complex

is neutral the large terms contributing to the polarisation of region II disappear. Calculation of the binding energy is done by finding the difference in energy needed to remove a cation from the perfect lattice and from a position neighbouring an existing divalent cation impurity. Here one is calculating the relative energies of two defect configurations rather than an absolute energy. The previous calculations have estimated the divalent impurity-cation vacancy complex binding energy for Cd^{2+} (36,37), Ca^{2+} and Sr^{2+} (37) in NaCl. The results are in reasonable agreement with experimental determinations. The present work extends the previous theoretical calculations to include Ba^{2+}-cation vacancy complexes.

Calculation of the Binding Energy of a Ba^{2+}-Cation Vacancy Complex in NaCl

The work done in removing a Na^{+} ion from the (110), Fig. 71, lattice site to a point at infinity, assuming the Ba^{2+} ion at (000), subtracted from the work done in forming a single cation vacancy at some distant point in the lattice gives the binding energy of the Ba^{2+}-cation vacancy complex. The work to produce a single cation vacancy has been calculated by several workers (60,37,61, 62,63,64).

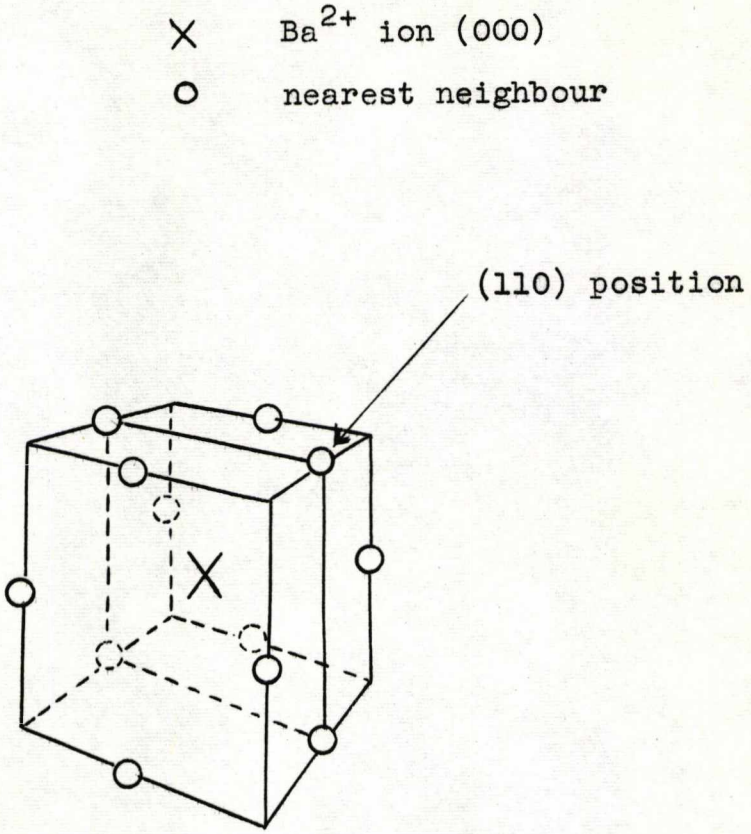

Fig. 71. The twelve nearest cation neighbours to the Ba^{2+} ion in NaCl. When the impurity is part of a complex, one of twelve sites is vacant.

Removal of a Na^+ ion from the (110) position is accompanied by a change in the distortion of the lattice and polarisation of the neighbouring ions. These changes result in a change of potential at the (110) lattice site. In the initial configuration, the lattice distortion is due to the Ba^{2+} impurity ion , whereas, finally, it is due to the impurity-vacancy complex. The changes in lattice distortion as the Na^+ ion is removed from the nearest neighbour position to a Ba^{2+} impurity ion to form an associated complex are shown diagrammatically in Fig. 72. The arrows indicate the direction of ion displacement.

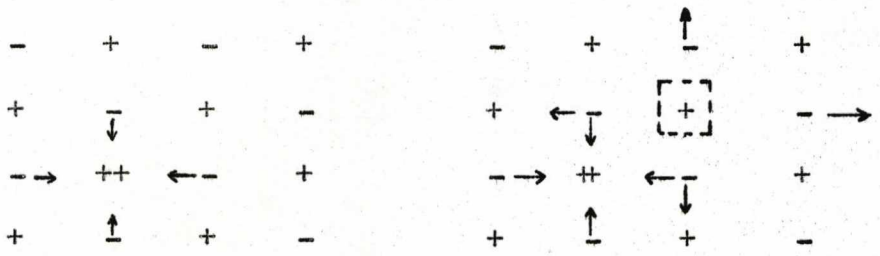

(A) Initial Configuration. (B) Final Configuration.

Fig. 72.

The problem then is to compute the electrostatic and overlap repulsion potentials at the (110) position for each configuration. To do this it is first necessary to determine the polarisation of the lattice, that is the displacements of the surrounding ions and the dipoles induced on them. Using these values the initial

potential at the (110) lattice point can be calculated. The electrostatic potential energy is made up of three terms, (A) for the Initial Configuration;

(i) $V_1^{R.L.}$ - the energy of the lattice, including the contribution of the Ba^{2+} ion,

(ii) $V_1^{DIS.}$ - the correction term for the displacement of the six nearest negative ions, and

(iii) $V_1^{POL.}$ - the polarisation energy due to the dipoles created on the distant ions by displacement and electronic polarisability and on the six nearest neighbours by electronic polarisability alone.

In addition, ϕ_1, is the overlap repulsion energy (a negative contribution), and is due to the six nearest neighbours of the Ba^{2+} ion.

For the final configuration, (B), where the positive ion has been removed, the displacements are different, and the polarisation of distant ions is neglected since the complex is neutral. V_2 and ϕ_2 are computed in the same way as the energies V_1 and ϕ_1. The determination of V_2^{POL}, the polarisation term of V_2, however, is much more complicated due to the low symmetry of the lattice around the complex.

The first step in the calculation therefore is the determination of the lattice polarisation due to the Ba^{2+} ion.

(A)(i) Calculation of the Equilibrium Distortion Around a Ba^{2+} Impurity Ion

The field produced by the extra positive charge of the Ba^{2+} ion polarises the surrounding lattice, the polarisation P at a distance r from (000) being given by(60)

$$P = \frac{1}{4\pi}\left(1 - \frac{1}{K}\right).\frac{e}{r^2} \qquad (6.1)$$

where K is the dielectric constant for NaCl. According to Mott and Littleton the moment is divided in the proportions α_+, α_-, for the electronic and displacement moments respectively. The induced electric moment in one unit cell is $2Pr_o^3$, where r_o is the anion-cation separation. This induced electric moment is composed of a part μ_+ proportional to $\alpha_+ + \alpha$ and a part $\alpha_- + \alpha$. These dipole moments are given by

$$\mu_+ = \frac{\alpha + \alpha_+}{\alpha_+ + \alpha_- + 2\alpha} \cdot \frac{2r_o^3}{4\pi}\left(1 - \frac{1}{K}\right).\frac{e}{r^2},$$

$$= M_+ r_o^3 e/r^2, \qquad (6.2)$$

and

$$\mu_- = M_- r_o^3 e/r^2 \qquad (6.3)$$

where

$$M_{\pm} = \frac{1}{4\Pi}\left(1 - \frac{1}{k}\right) \cdot \frac{\alpha + \alpha_{\pm}}{\frac{1}{2}(\alpha_{+} + \alpha_{-}) + \alpha} \qquad (6.4)$$

The displacement polarisability α can be calculated from

$$\alpha = e^2/p \qquad (6.5)$$

where $-px$ is the restoring force, due to the repulsion between the ions, on any one ion in a uniformly polarised medium when each ion is displaced a distance $\pm x$.

The displacement x of any ion outside the shell of nearest neighbours is given by

$$x = \pm M' r_o^3/r^2 \qquad (6.6)$$

where

$$M' = \frac{1}{4\Pi}\left(1 - \frac{1}{k}\right) \cdot \frac{\alpha}{\frac{1}{2}(\alpha_{+} + \alpha_{-}) + \alpha} \qquad (6.7)$$

In the first-order approximation, the displacements and electric dipole moments of the nearest neighbours to the Ba^{2+} impurity ion are treated as unknowns, those of the more distant ions are computed from equations (6.2), (6.3) and (6.6). They are determined by the requirement that the sum of the electrical and repulsive forces, F_e and F_r respectively, cancels out on each ion. The equations are[36]

$$F_e + F_r = 0 \qquad (6.8)$$

$$me^2 r_{o/\alpha_-} = F_e \qquad (6.9)$$

The displacement is written in the form $x = \xi r_o$, and the induced dipole $\mu = mer_o$. From the symmetry of a NaCl type lattice, it follows that F_e and F_r are in the direction of the lattice lines(100), that is, in the direction of the Ba^{2+} impurity ion. The induced dipole μ is along the direction of the electric field, radially outwards. The electrostatic force on one of the (100) ions inward is[36]

$$F_e = \frac{e^2}{r_o^2}\left\{\frac{1}{(1-\xi)^2} - \frac{(\sqrt{2}+0.25)}{(1-\xi)^2} + \frac{4(1-\xi)}{[1+(1-\xi)^2]^{3/2}}\right.$$
$$+ \frac{1}{(2-\xi)^2} - \frac{2.3713m}{(1-\xi)^3} - (1.965M_+'$$
$$\left. + 0.388M_-') - \xi(1.965 - 0.388)\right\} \qquad (6.10)$$

Of the terms inside the brackets, the first is a result of the net charge acting on the Ba^{2+} ion, the second, third and fourth terms come from the force acting on the (100) ion due to the displacements of the other five nearest neighbours of the impurity ion. The fifth term represents the effect of electronic dipole moments μ of these same five ions. The electronic and displacement dipoles induced on all the other ions of the crystal act on the (100) ion to give term six. The seventh and

last term represents the force on the (100) ion as a result of dipole moments associated with elastic components of the ionic displacements

The repulsive force on one of the (100) ions inward is given by[36]

$$
\begin{aligned}
F_r = \; & -B \exp[-(1 - \xi)r_o/\rho] \\
& +4\, Ad^{-1} (\xi + M'/2\sqrt{2}) \exp[-dr_o/\rho] \\
& +A \exp[-(1 + \xi + M'/4)r_o/\rho] \\
& -2\sqrt{2}\, C \exp[-\sqrt{2}(1 - \xi)r_o/\rho] \\
& +4C\, \eta^{-1} (1 + \xi - 2M'/5\sqrt{5}) \exp[-\eta r_o/\rho] \\
& +4C\, \lambda^{-1} (\xi - M'/3\sqrt{3}) \exp[-\lambda r_o/\rho] \qquad (6.11)
\end{aligned}
$$

where

$$B = 1.125b\, \rho^{-1} \exp[(r_- + r_{Ba^{2+}})/\rho],$$

$$A = b\rho^{-1} \exp[(r_+ + r_-)/\rho],$$

$$C = 0.75\, b\rho^{-1} \exp[2r_-/\rho],$$

and

$$d^2 = (1 + M'/2\sqrt{2})^2 + (\xi + M'/2\sqrt{2})^2,$$

$$\eta^2 = (1 + \xi - 2M'/5\sqrt{5})^2 + (1 - m'/5\sqrt{5})^2,$$

$$\lambda^2 = 2(1 - M'/3\sqrt{3})^2 + (\xi - M'/3\sqrt{3})^2.$$

In the above equations r_+ and r_- refer to the ionic radii of the Na^+ and Cl^- ions respectively. The quantities b and ρ are determined for NaCl from two thermodynamic equations which relate them to experimental data on the compressibility of the ions. The following constants were used throughout the calculation.

C_{++}	= 1.25	r_0(Å)	= 2.815
C_{--}	= 0.75	r_+(Å)	= 0.98
C_{+-}	= 1.00	r_-(Å)	= 1.81
$C_{Ba^{2+}-}$	= 1.125	$r_{Ba^{2+}}$(Å)	= 1.43
ρ (Å)	= 0.345	b (ergs)	= 0.229×10^{-12}

$\alpha.10^{-24}$ (cm^3)	= 4.268
$\alpha_+.10^{-24}$(cm^3)	= 0.410
$\alpha_-.10^{-24}$(cm^3)	= 2.960
$\alpha_{Ba^{2+}}.10^{-24}$($cm^3$)	= 2.50

M'	= 0.0465	A(dynes)	= 0.216
M'_+	= 0.0508	B(dynes)	= 0.895
M'_-	= 0.0788	C(dynes)	= 1.795

κ = 5.62

Tessman, J.R., Kahn, A.H. and Schockley, W., polarisabilities[65].

It is now possible to determine the unknowns m and ξ. By using equation (6.9) the electronic dipole moment on the six anions is eliminated from equation (6.10). Curves of F_e and F_r are plotted as a function of the variable ξ, the equilibrium value of ξ being determined from the point where the sum $F_r + F_e$ vanishes, Fig. 73. The graphical solution of these equations leads to the following results:

$$\xi = 0.0076$$
$$m = 0.096$$

The electrostatic potential at the (110) Na^+ ion to be removed is given by

$$V_1 = V_1^{R.L.} + V_1^{DIS.} + V_1^{POL.}$$

A(i) Calculation of $V_1^{R.L.}$

$V_1^{R.L.}$ is the electrostatic potential of the lattice including the contribution from the Ba^{2+} ion, and is given by[36]

$$V_1^{R.L.} = -e/r_o[\alpha_m - 1/(\sqrt{2} + M'/2)] \qquad (6.12)$$
$$= 5.329 \text{ eV}$$

$\alpha_m = 1.7476$ is the Madelung constant.

A(ii) Calculation of $V_1^{DIS.}$

The electrostatic potential at the (110) lattice position due to the displacements of the six (100) ions

Graphical Solution of λ

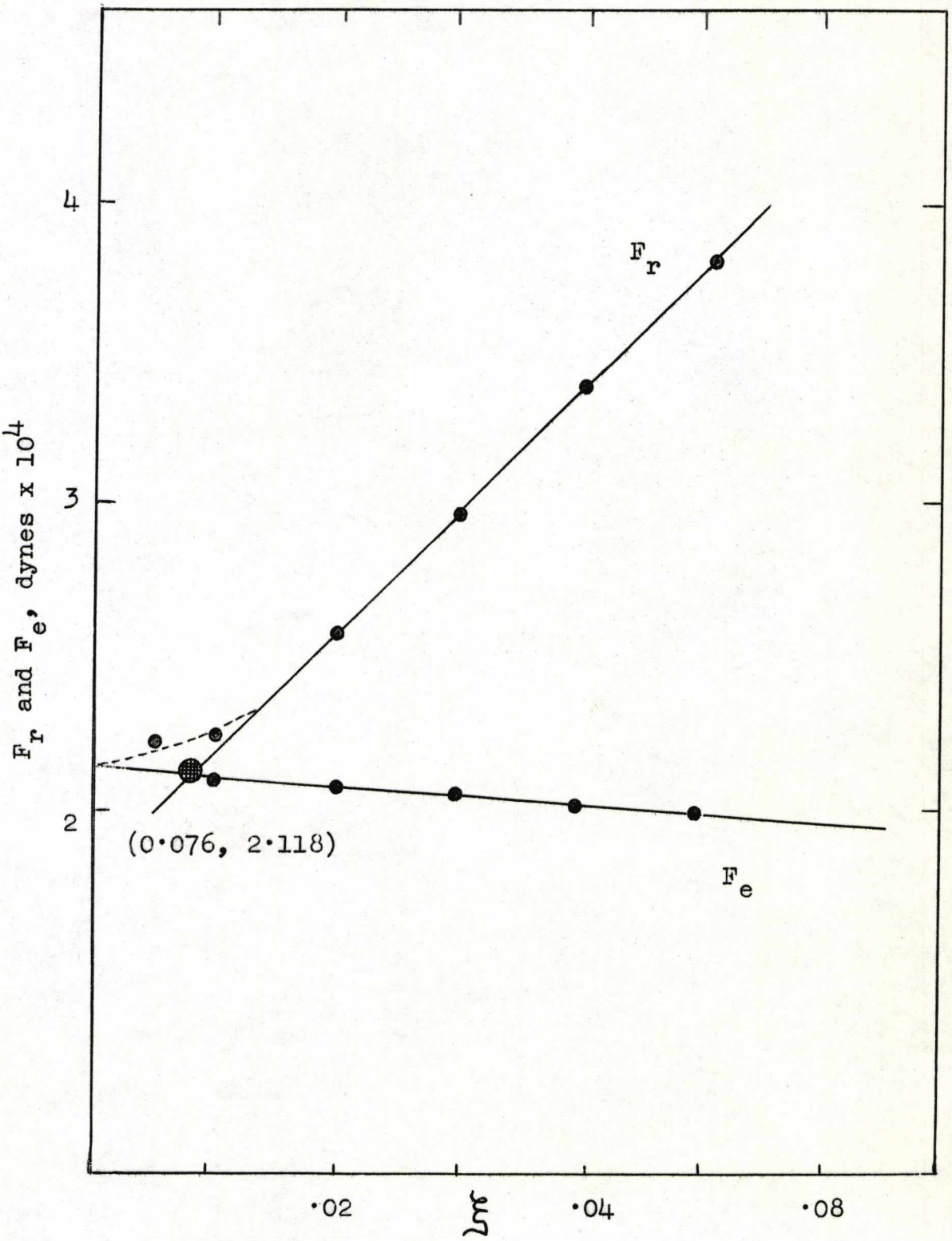

Fig. 73.

is given by[36]

$$V_1^{DIS} = e/r_o[2(1- \frac{1}{(1+\xi^2)^{\frac{1}{2}}} + \frac{1}{\sqrt{3}} - \frac{1}{[2+(1-\xi)^2]^{\frac{1}{2}}} + \frac{1}{\sqrt{5}} - \frac{1}{[1+(2-\xi)^2]^{\frac{1}{2}}}] \quad (6.13)$$

$$= 0.020 \text{ eV}.$$

A(iii) Calculation of V_1^{POL}.

The electrostatic potential due to the induced polarisation of the surrounding lattice is represented by[36]

$$V_1^{POL} = -e/r_o[0.7428m + 4.15M'_+ + 4.29\ M'_-] \quad (6.14)$$

$$= 3.139 \text{ eV}$$

The derivation of this equation requires some explanation. The total potential at (000) due to all the dipoles μ_+ and μ_- is

$$V = -er_o^3[M'_+\Sigma_+ \frac{\cos(\hat{r_+ r_-})}{r_+^2 r_-} + M'_-\Sigma_- \frac{\cos(\hat{r_+ r_-})}{r_+^2 r_-}] \quad (6.15)$$

where r_+ is the distance from the lattice point under consideration to (000), and r_- is the distance from the lattice point to (110). Lattice summations of this type have been carried out by Jones and Ingham[66] in connection with the theory of imperfect gases. Equation (6.15) is slowly converging and the individual terms approach those of the Jones and Ingham series for ions

at distances greater than $4r_o$. For ions outside this sphere the total potential is given by

$$V = -er_o^3 \left[M_+' \sum_{+} \frac{1}{r^4} + M_-' \sum_{-} \frac{1}{r^4}\right] \qquad (6.16)$$

the value of the summation being known. The polarisation potential due to ions inside the sphere was obtained from equation (6.16). Mott and Littleton[60] calculated the potential due to all the dipoles μ_+ and μ_-, and the numerical constants quoted in equation (6.14) are due to them.

A(iv) Calculation of ϕ_1

According to Born and Mayer[67] the repulsive potential function is given by

$$\phi_{(r)} = C_{+-}\, b \exp[(r_+ + r_- - r_o)/\rho] \qquad (6.17)$$

where r_+ and r_- are the Goldschmidt radii[68] of the interacting ions, and the constant C_{+-} is a numerical factor which depends on the charges and electronic structures of the ions[69].

The repulsion potential at the (110) position due to a Ba^{2+} ion at (000) is given by

$$\phi_1 = 2C_{+-}b\left[\exp \frac{r_+ + r_- - r_o(1 + \xi^2)}{\rho} + 2\exp \frac{(r_+ + r_- - r_o)}{\rho}\right]$$

$$= -0.799 \text{ eV}. \qquad (6.18)$$

(B) Calculation of the Equilibrium Distortion Around the Ba^{2+}-Vacancy Complex

The next step in the calculation is the determination of the potential at (110) for the final configuration, which is the Ba^{2+}-vacancy complex. To make an accurate estimation of the lattice distortion around a complex is a formidable problem, due to the low symmetry. In the approximation proposed by Reitz and Gammel[36] a more symmetrical distortion was assumed. This is shown schematically in Fig. 74. For the eight negative ions which are nearest neighbours of either the positive ion vacancy or Ba^{2+} ion only the influence of the nearer defect is considered. There are two negative ions which are nearest neighbours of both defects. The resultant displacement of these two ions is taken as the vector addition of displacements due to both defects.

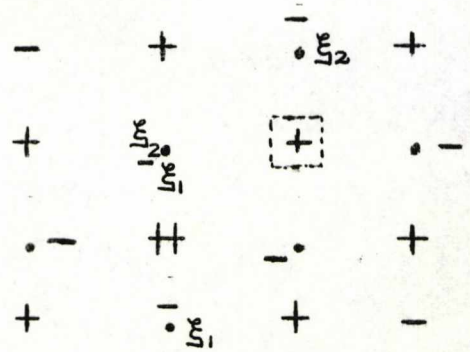

Fig. 74

Since the complex is neutral, polarisation of the distant ions can be neglected, so that the displacements to be used will be different from those computed initially. A value for $x_1 = \xi_1 r_0$ can be obtained by solving once again equations (6.8) and (6.9), this time leaving out the long-range polarisation terms in F_e. Following the same procedure, but this time using Mott and Littleton's equations without the terms in M_+' and M_-', it is possible to arrive at a value for x_2, the displacement of the immediate neighbours of the positive ion vacancy. The displacements obtained were

$$x_1 = 0.010\ r_0,$$

$$x_2 = 0.068\ r_0,$$

from the graphical solutions shown in Figs. 75 and 76.

The electrostatic and overlap potential energies can now be calculated for the final lattice configuration using these new displacements. The electrostatic potential at the (110) lattice can again be written as the sum

$$V_2 = V_2^{R.L.} + V_2^{DIS.} + V_2^{POL.}$$

B(i) Calculation of $V_2^{R.L.}$

$V_2^{R.L.}$, the electrostatic potential of the rigid lattice for the final configuration, is the same as before and is given by equation (6.12)

$$V_2^{R.L.} = 5.329\ eV$$

Graphical Solution of ξ_1

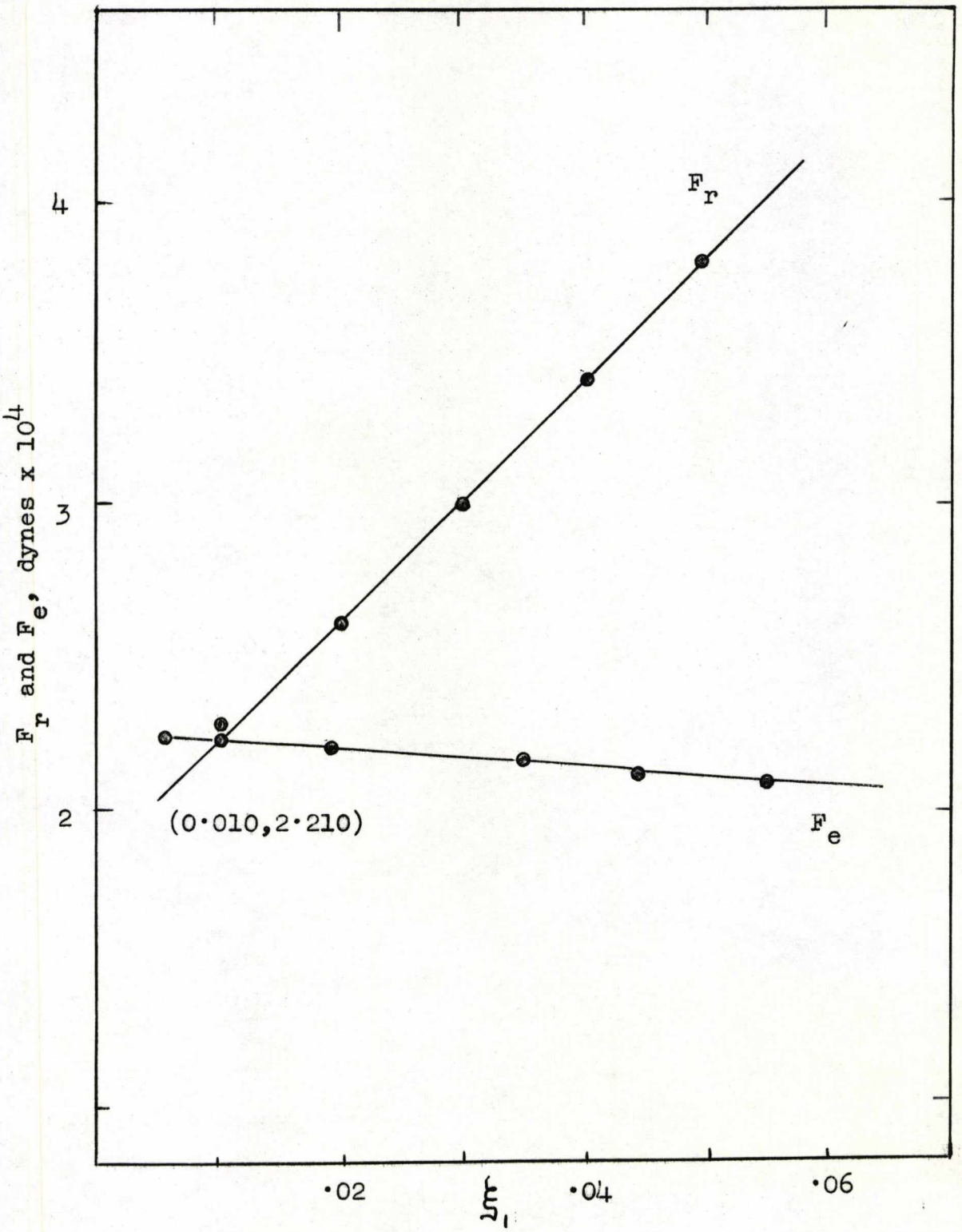

Fig. 75.

Graphical Solution of ξ_2

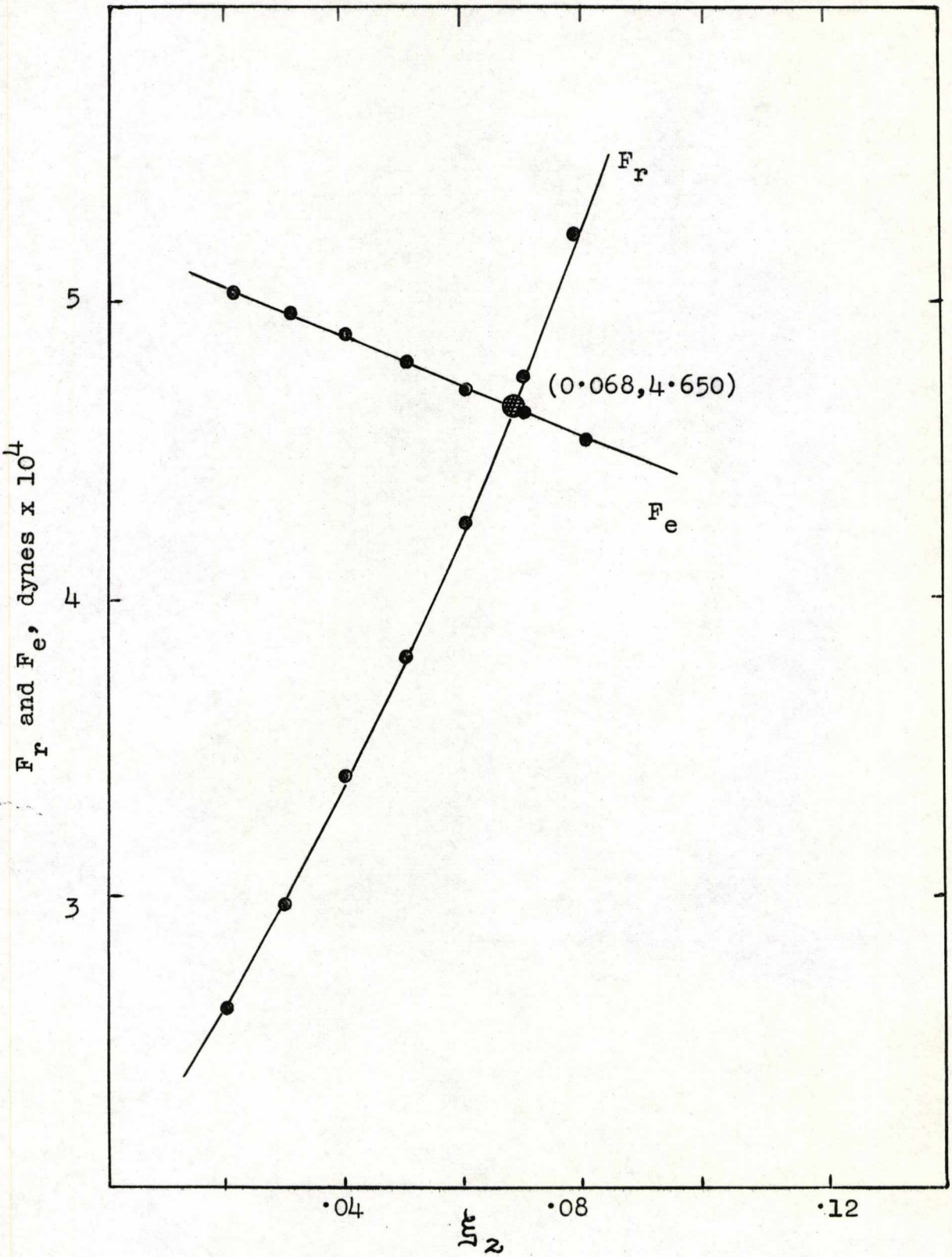

Fig. 76.

B(ii) Calculation of V_2^{DIS}.

V_2^{DIS} is the change in potential due to the displacement of the nearest-neighbour ions and is given by

$$V_2^{DIS} = \frac{e}{r_o} \cdot 2 \left\{ \frac{1}{(1+\xi^2)^{\frac{1}{2}}} - \frac{1}{[(1+\xi_2)^2 + \xi_1^2]^{\frac{1}{2}}} + \frac{1}{[2+(1-\xi)^2]^{\frac{1}{2}}} - \frac{1}{[2+(1-\xi_1)^2]^{\frac{1}{2}}} + \frac{1}{[1+(2-\xi)^2]^{\frac{1}{2}}} - \frac{1}{[1+(2-\xi_1)^2]^{\frac{1}{2}}} + \frac{e}{r_o} \cdot 4 \left[\frac{1}{\sqrt{1}} - \frac{1}{(1+\xi_2)} \right] \right\} \qquad (6.19)$$

$$= -1.923 \text{ eV}.$$

B(iii) Calculation of V_2^{POL}.

V_2^{POL} is the potential at (100) due to the induced polarisation. The dipoles induced on the neighbouring ions are a result of the electric field, **E**, generated by the charges of the defects and displacement dipoles at each of the nearest-neighbour lattice points. The induced dipole at a lattice point is given by

$$\mu_i = \alpha_i . \mathbf{E}. \qquad (6.20)$$

V_2^{POL} is then calculated from

$$V_2^{POL} = e \sum_i \frac{\mu_i \cos\theta_i}{r_i^2}, \qquad (6.21)$$

where r_i is the distance from the (110) position to ion i, and θ_i is the angle between the direction of the induced dipole, μ_i, and that of r_i. The summation is

over the Ba^{2+} ion, the ten ions which are nearest-neighbours of both the impurity and the vacancy, and the second- and third-nearest-neighbours of the vacancy. The contribution from the more distant ions is negligible since the complex is neutral.

An accurate calculation of the polarising field at each of the ions under consideration would be extremely difficult. One has to take into account the effect of deformation dipoles as well as those induced by the charges of the defects. The deformation dipole represents the distortion of electron charge distribution as a result of the relative motion of positive and negative ions against one another, and acts in opposition to the electrically induced dipoles. To simplify the calculation of the lattice distortion around the complex the electric field and the net dipole on each of the surrounding ions was determined as a function of the displaced position of each ion. This approach should be fairly reliable for the very small distortions involved.[70] [Appendix C.]

B(iv) Calculation of ϕ_2

The repulsion potential at the (110) position for the final configuration is given by

$$\phi_2 = -2C_{+-}b \left\{ \exp\left(\frac{r_+ + r_- - r_o[(1+\xi_2)^2 + \xi_1^2]^{\frac{1}{2}}}{\rho}\right) + 2\exp\left(\frac{r_+ + r_- - r_o(1+\xi_2)}{\rho}\right)\right\} \qquad (6.22)$$

$$= -0.458 \text{ eV}.$$

The various contributions to the work to create a positive ion vacancy in the (110) position to the Ba^{2+} ion are now known, and are shown in table 8.

TABLE 8

Contributions to the work W to create a positive ion vacancy in the (110) position to a Ba^{2+} ion.

	Initial Configuration	Final Configuration
Electrostatic:		
$V^{R.L.}$	5.329 eV	5.329 eV
$V^{DIS.}$	0.020	-1.923
$V^{POL.}$	3.139	-2.268
Repulsive:	-0.799	-0.458
	1	2

Total = 4.18 eV

That part of the work which is done against electrostatic forces is given by

$$- e/2 \ (V_1 + V_2) \qquad (6.23),$$

the work done against repulsive forces by

$$- (\phi_1 + \phi_2)/2 \qquad (6.24).$$

Substitution into equations (6.23) and (6.24) gives the total work required to remove the sodium ion. The result is one half the sum of columns 1 and 2. Bassani and Fumi[37] have calculated that the work required to form a single positive ion vacancy in NaCl is 4.65 eV. The binding energy of the Ba^{2+}-vacancy complex is the difference of these two calculated values, that is 4.65 - 4.18 eV, that is, 0.47 eV.

In a similar type of calculation Reitz and Gammel[36] found that the final result was not appreciably affected by slight variations in x_1 and x_2. In addition, they found that the dipole-dipole interactions of the induced dipoles, neglected in this calculation, had little effect on the value of V_2^{POL}, the terms were small and tended to cancel one another out.

The calculated binding energies of impurity-cation vacancy complexes are listed in table 9.

TABLE 9

Binding Energies of Impurity-cation Vacancy Complexes (Theory)

Impurity	Impurity Ion Size (Å)	Binding Energy(eV)
Cd^{2+}	1.03	0.38[37]
Ca^{2+}	1.06	0.38[37]
Sr^{2+}	1.27	0.45[37]
Ba^{2+}	1.43	0.47

The result for the binding energy of the Ba^{2+}-cation vacancy complex is in agreement with the theoretical prediction that the binding energy should increase with the ionic radius of the impurity, and lends support to the assumption that the simple association theory is applicable in a solid such as NaCl.

CHAPTER VII

DISCUSSION

7.1. Conductance Studies of Association

The conductivity curves obtained for each of the systems studied clearly show an intrinsic region (I), an impurity-induced free-vacancy region (II), an association region (III) and a precipitation region (IV). The latter two regions are critically dependent on the concentration and nature of the impurity so that any comparison with previously published work is difficult. However, it should be possible to compare the activation energies in regions I and II with earlier work, tables 10 and 11.

TABLE 10

Activation Energies, ϵ_I, in region I

Reference	ϵ_I (eV)
Etzel and Maurer[31]	1.88
Barr et al.[33]	1.79 ± 0.05
Jain and Dahake[30]	1.92
Present work	1.86 ± 0.03

In region I, there is good agreement in the values of ϵ_I obtained in the present work and those of other workers. However, there are significant variations in the values of ϵ_{II}, the activation energy for mobility of a

TABLE 11

Activation Energies, ϵ_{II}, in region II

Reference	System Studied	Temperature range of the measurements (°C)	ϵ_{II} (eV)
Dreyfus and Nowick (10)	NaCl - $MgCl_2$	< 500	0.75
	NaCl - $MnCl_2$	< 500	0.70
	NaCl - $CaCl_2$	< 500	-
	NaCl - $SrCl_2$	< 500	0.83
	NaCl - $BaCl_2$	< 500	-
	NaCl - $CdCl_2$	< 500	0.79
Jain and Dahake (30)	NaCl - $NiCl_2$	300 - 700	0.75
Jain and Parashar (29)	NaCl - $CoCl_2$	350 - 600	0.75
Kanzaki et al (32)	NaCl - $CaCl_2$	250 - 400	0.85*
Bean (71)	NaCl - $CaCl_2$	160 - 680	0.78
Barr et al (33)	NaCl - $ZnCl_2$	325 - 650	0.65
Etzel and Maurer (31)	NaCl - $CdCl_2$	250 - 400	0.85*
Present work	NaCl - $MgCl_2$	150 - 650	0.70±0.02
	NaCl - $MnCl_2$	150 - 650	0.71±0.01
	NaCl - $CaCl_2$	150 - 650	0.72±0.05
	NaCl - $SrCl_2$	150 - 650	0.70±0.02
	NaCl - $PbCl_2$	150 - 650	0.68±0.01
	NaCl - $BaCl_2$	150 - 650	0.74±0.06

* These values were obtained from analysis of data for the concentration dependence of the conductivity.

cation vacancy. The results of Dreyfus and Nowick[10] in particular, although part of the most systematic study made to date, exhibit marked differences. A possible reason for this may lie in the fact that their measurements were taken over a very limited temperature range (< 500°C). This would also explain the absence of a value for ϵ_{II} in two of the systems they studied, that is (NaCl - $CaCl_2$) and (NaCl - $BaCl_2$). The present work, in which measurements were taken up to a temperature of 650°C, showed that the larger the temperature range over which measurements were taken the less was the variation observed in the values of ϵ_{II}. This would indicate that the transitions from region III to region II are not sharp, but in fact extend over relatively large temperature ranges. The effect of this on the conductivity plots is to produce curvature which in some cases makes the drawing of tangents a rather subjective procedure. This factor underlines the weakness in the method of 'slopes' as used in the determination of association energies and solubility energies, both of which critically depend on accurate estimates of ϵ_{II}.

The apparent activation energy in region III is given by

$$\epsilon_{III} = \epsilon_{II} + W_A/2 \qquad (7.1)$$

where W_A is the free energy of association. Similarly,

the apparent activation energy in region IV can be written as

$$\epsilon_{IV} = \epsilon_{II} + H_s/2 \qquad (7.2)$$

where H_s is the heat of solution. Since the values of $W_A/2$ are in the region of approximately 0.2 eV for a number of impurity ions, the variations observed in the values of ϵ_{II}, table 11, can lead to very significant errors in the determination of W_A. In addition, these 'smeared-out' transitions between the regions also lead to difficulties in the determination of ϵ_{III} and ϵ_{IV}, table 12.

TABLE 12

Activation Energies, ϵ, for Regions III and IV of the Conductivity Plots

System	ϵ_{III}(eV)	ϵ_{IV}(eV)
NaCl - $MgCl_2$	0.83 ± 0.04	1.29 ± 0.04
NaCl - $MnCl_2$	0.89 ± 0.02	1.21 ± 0.01
NaCl - $CaCl_2$	0.89 ± 0.02	1.32 ± 0.10
NaCl - $SrCl_2$	0.95 ± 0.03	1.40 ± 0.10
NaCl - $PbCl_2$	0.83 ± 0.03	1.35 ± 0.05
NaCl - $BaCl_2$	1.23 ± 0.08	1.50 ± 0.10

The present results indicate a slight tendency for the apparent activation energy to increase with impurity content within any one system. Therefore, the

interpretation of region III in terms of association, without considering precipitation, is open to question. In the $NaCl-BaCl_2$ system the association region (III) was completely absent in the majority of the plots. The importance of precipitation in this system was very apparent from the large extent of region IV, which probably obscured region III. The estimates of ϵ_{III}, where it was possible, for the $NaCl-BaCl_2$ system compare favourably with those of Dreyfus and Nowick[10], who experienced the same difficulty. In addition, Dreyfus and Nowick[10] failed to observe a region III for the $NaCl-SrCl_2$ system, although in this case an important factor no doubt was the limited temperature range they employed. Apart from the $NaCl-PbCl_2$ measurements, a definite trend is observed in that the value of ϵ_{III} increases as the impurity ion size increases. In general, the method of slopes is inadequate as a means of determining defect parameters in ionic crystals, and the conductance results have been analysed in terms of the more rigorous theory given in chapter III.

The association enthalpies for each impurity ion deduced from the application of Lidiard's association theory are given in table 13.

TABLE 13

Association Enthalpies from Application of Association Theory to Conductance Measurements

Impurity Ion	Association Energy (eV)
Mg^{2+}	0.31 ± 0.04
Mn^{2+}	0.28 ± 0.03
Ca^{2+}	0.30 ± 0.04
Sr^{2+}	0.53 ± 0.02
Pb^{2+}	0.56 ± 0.08
Ba^{2+}	$\geqslant 0.79$

Comparison with previously reported work can only be made for the Ca^{2+} and Mn^{2+} impurity-vacancy association since these are the only two impurities for which results have been cited in the literature. In general, agreement is good. Kirk and Pratt[72]* arrived at a value of 0.30eV for the association enthalpy of the Mn^{2+} impurity-vacancy complexes, and Kanzaki's[32] value of 0.31eV for Ca^{2+} impurity-vacancy compares well with that obtained in the present work. A complete discussion of these results will be given in a later section.

* We are grateful to Dr. I.M. Boswarva for communicating this result to us prior to its publication.

7.2. Impurity-Diffusion Studies of Association

Values of W_A, the free energy of association, were obtained for Mn^{2+} in NaCl at three different temperatures; the results are shown in table 14.

TABLE 14

Values of the Free Energy of Association, W_A, for Mn^{2+} in NaCl

Temperature °C	W_A (eV)
401	0.30 ± 0.05
421	0.35 ± 0.05
440	0.35 ± 0.05

The average value for the free energy of association of the Mn^{2+}-vacancy complex is 0.33 ± 0.05 eV. The temperature range over which these studies were made is not wide enough to allow any conclusions to be drawn as regards the temperature dependence of W_A.

An anomalously high value for the free energy of association of Mn^{2+} in NaCl has been reported by Murin et al.[34]. They studied the diffusion of Mn^{2+} ions over a temperature range of 450 - 750°C and arrived at a value of 0.71 eV for χ_1, the association enthalpy. It is difficult to suggest a reason for the large discrepancy between their value and that of the present work, in terms of the theory of ion movement. The good agreement between

the present result and those values obtained from ionic conductance and electron spin resonance measurements[25], which will be discussed later, suggests that the value of 0.71 eV for the association enthalpy may be in error. A factor affecting the earlier work could have been the relative purity of the crystals used. Particularly important would be the presence of OH^- ions or other anionic impurities which could form complexes or precipitates with the Mn^{2+} ions. This would result in a lowering of the effective concentration of manganous impurity below that of the concentration determined analytically. This would lead to a corresponding increase in the observed value of χ_1.

7.3. Comparison of the Association Energies deduced from Theoretical Calculations, Ionic Conductivity, Impurity-Diffusion, Dielectric Loss and Electron Spin Resonance Measurements

The theoretical calculations predict that the binding energies of impurity-cation vacancy complexes should increase with the impurity ion size. The work of Bassani and Fumi[37], who calculated the binding energies for Ca^{2+}, Cd^{2+} and Sr^{2+} impurity-nearest-neighbour cation vacancy complexes, has been extended to include the Ba^{2+} impurity-nearest-neighbour cation vacancy complex. The results are shown in table 15.

TABLE 15

Calculated Binding Energies

Impurity Ion	Ionic Radius (Å)	Binding Energy (eV)
Cd^{2+}	1.03	0.38[37]
Ca^{2+}	1.06	0.38[37]
Sr^{2+}	1.27	0.45[37]
Ba^{2+}	1.43	0.47

The binding energy of the Ba^{2+} impurity-vacancy complex confirms the theoretical prediction evident from the results of Bassani and Fumi[37], and suggests that the observed trend may be in fact physically significant. The experimental data now available is not wholely in accord with this assumption. Quantitative estimates of association enthalpies have been made for a wide variety of divalent impurity ions in NaCl[29,30,31,32]. Since the pressure volume work of association-dissociation is small, it is generally assumed that the enthalpy of association is approximately equal to the binding energy. Comparison of the theoretical and experimental estimates is made in table 16.

TABLE 16

Association Enthalpies (eV) of Divalent Impurity-Cation Vacancy Complexes in NaCl

	Mg^{2+}	Ni^{2+}	Co^{2+}	Zn^{2+}	Mn^{2+}	Cd^{2+}	Ca^{2+}	Sr^{2+}	Pb^{2+}	Ba^{2+}
Goldschmidt[68] Radius (Å)	0.78	0.78	0.82	0.83	0.91	1.03	1.06	1.27	1.32	1.43
χ_1 (eV) from										
a. conductance measurements	0.31	0.32[29]	0.30[30]		0.28[72] 0.30	0.34†[31]	0.31†[32] 0.30	0.53	0.56	0.79
b. impurity-diffusion measurements				0.48†[33]	0.71†[34] 0.33	0.40[35]	0.57[35]			
c. dielectric loss measurements							0.44[24]	0.45[24]		
d. e.s.r. measurements				0.41[25]						
e. theoretical binding energies						0.38[37]	0.38[37]	0.45[37]		0.47

† free energy of association.

Results underlined are those of the present work.

Although the agreement in the values of the theoretically estimated binding energies and the measured association enthalpies appears to be reasonable for the Ca^{2+}- and Sr^{2+}-vacancy complexes in NaCl, the discrepancy in the case of the Ba^{2+}-vacancy complex is very large. However, this agreement in the case of Ca^{2+} and Sr^{2+}-vacancy complexes may be somewhat fortuitous. The calculated increase in binding energy in going from the Ca^{2+}-vacancy complex to the Sr^{2+}-vacancy complex is 0.07 eV, yet the observed value is approximately a factor of three greater, table 16.

The ionic model used in these theoretical calculations is a relatively simple one, and the validity of the approach is open to question. This is particularly so when the impurity ion size is significantly different from that of the host ion. In the present work it has been observed that the model gives rise to a somewhat artificial situation in the calculation of the lattice polarisation. In the determination of the displacements of the six Cl^- ions neighbouring the Ba^{2+} ion, the model indicated an inward displacement of these negative ions (see chapter VI). When one considers that a Ba^{2+} ion, on the basis of Goldschmidt[68] radii, has an ionic volume which is

approximately twice that of the Na^+ ion, it seems highly unlikely that it can distort itself sufficiently to fit into the cation vacancy and yet still produce a contraction of the surrounding lattice.

A second feature of the theoretical calculation which may be inadequate is its use of the Goldschmidt ionic radii values. Recent experimental studies of the electron density distribution in crystals of alkali halides[73] indicates that the Goldschmidt radii are too small for the cations and too large for the anions. A new set of ionic radii have been calculated by Fumi and Tosi[62], based on the Born-Mayer model of the crystal and these are in much better agreement with the recent X-ray diffraction data. Calculations of the energy of formation of charged defects in ionic crystals, using Fumi-Tosi radii, have produced higher values than those previously obtained using Goldschmidt radii. These recent results are in better agreement with the experimentally measured values. It is conceivable that the use of Fumi-Tosi radii in the present calculation would have produced a larger value for the binding energy of the Ba^{2+}-vacancy complex. Unfortunately, Fumi-Tosi radii are not available for the alkaline earth cations.

It is therefore suggested that the theoretical calculations of the binding energies are more important from the point of view of the trend in the energies rather than in their absolute values. The calculations of Bassani and Fumi[37] for Cd^{2+}, Ca^{2+} and Sr^{2+}-vacancy complexes and the present calculation for the Ba^{2+}-vacancy complex indicate that, at least for an impurity of similar or larger size than the Na^{+} ion, the binding energy increases as the impurity ion radius increases.

The association energies deduced from the conductance measurements are in agreement with the theoretical prediction, that is, the increase in association energy is apparent when the impurity ion is larger than the host cation. However, for the smaller impurity ions the values of the association energy are remarkably constant. This could be physically significant and could be closely connected with longer range impurity-vacancy interactions.

Theoretical calculations[19] have shown that for Sr^{2+} in KCl the complex between the impurity and a cation vacancy in the next-nearest-neighbour position is more stable than that which has the cation vacancy in the nearest-neighbour position. That the next-nearest-neighbour site should be so stable is at first sight

rather surprising since it is a factor of $\sqrt{2}$ further away from the Sr^{2+} ion than is the nearest-neighbour site. However, when one considers that the Sr^{2+} ion is actually smaller than the host cation (r_{K^+} = 1.33 Å) the situation changes. It is comparable with, for example, the Mn^{2+} ion in NaCl for which definite evidence of next-nearest-neighbour association exists from the electron spin resonance measurements. The stability of the next-nearest-neighbour site can be linked with the inward-relaxation of the lattice surrounding the small impurity ion, as opposed to the pushing-out effect of the large impurity ions. It seems reasonable to assume then that this situation will be representative of any divalent ion which is smaller in size than the host cation.

Direct experimental evidence of long-range interactions from the conductance measurements is very difficult to obtain. According to the Lidiard theory, the plots of $c/(\xi - 1/\xi)$ versus ξ should exhibit gentle curvature towards the horizontal axis at low values of ξ if next-nearest-neighbour association is important. Of the six systems studied in the present work the occurrence of impurity-vacancy association was clearly apparent from the deviation from linearity of the conductivity versus concentration isotherms. However,

in none of the systems was there any definite evidence of long-range interactions occurring. Only in one of the $c/(\xi - 1/\xi)$ versus ξ plots for Sr^{2+} impurity was there any hint of downward curvature. This however was far from being conclusive since it was so small that it could have arisen from slight inaccuracies in the estimation of impurity content. On the basis of the conductivity in 'pure' crystals, the 'background' impurity concentration was estimated to be 4×10^{-6} m.f.; this was included in the value of c. Allowance for an additional 6×10^{-6} m.f. of Sr^{2+} impurity was sufficient to eliminate the curvature completely. Such amounts are within the limits of the accuracy of the analytical method.

Although quantitative analysis of the conductance measurements has failed to reveal the presence of long-range interactions, one cannot rule them out and it should be possible to draw some qualitative conclusions from the results available.

The observed increase in association energy when the impurity ion is larger than the host ion is almost certainly due to the overlap of electron clouds, which leads to a rapid increase in repulsion potential because of the exponential fall-off in electron density at the periphery of an ion. Closed-shell repulsion effects

inevitably lead to an increase in the observed association energy, the presence of a cation vacancy in the nearest-neighbour position leading to a relief of the distortion created by the impurity ion.

When the impurity ion is smaller in size than the host ion a large contraction of the surrounding lattice can be expected. In this situation the effect of a cation vacancy in the nearest-neighbour position to the impurity ion is to increase the distortion already produced by the presence of the impurity ion. When the vacancy is in the next-nearest-neighbour position this distortion may be partially relieved. The polarisation of the negative ion located between the impurity and the cation vacancy, in the next-nearest-neighbour position, will be large because of the large polarisability of the anion itself and the strong electric field due to the charges on the defects. Consequently, one would expect this to increase the stability of the next-nearest-neighbour complex relative to the nearest-neighbour complex.

It is therefore suggested that with impurity ions, which are larger than the host ion, the nearest-neighbour complexes are the most stable, while, with smaller impurity ions, interaction between the impurity and a cation vacancy in the next-nearest-neighbour position may become very significant. Support for this view comes

from dielectric loss measurements on NaCl crystals doped with Mg^{2+}, Zn^{2+}, Mn^{2+}, Ca^{2+} and Sr^{2+} divalent cations[24]. A strong dependence of the jump-frequency on impurity ion size has been observed for the reorientation of impurity-vacancy complexes. The relatively slow reorientation of Sr^{2+} impurity-vacancies could be due to the pushing-out effect of the large impurity ion inhibiting vacancy motion in its vicinity. A cation vacancy in the next-nearest-neighbour position would add to this effect by increasing the distortion. The observed jump-rates decrease with size of the impurity ion until it becomes more or less constant for Zn^{2+} and Mg^{2+} impurity-vacancy complexes. This tendency towards a constant value could be related to the similar situation observed with the association energies. If the increase in jump-rates is associated with an opening up of the lattice in the neighbourhood of a small impurity ion then the pulling-in effect on the six Cl^- ions may be limited due to the rapidly increasing closed-shell repulsions accompanying this inward motion of the negative ions. The jump-rate will then become independent of ion size. Since the stability of the next-nearest-neighbour complex is closely connected with these displacements the same reasoning may account for the constancy in the association energies of the smaller impurity ions.

The changes in vibrational entropy of the surrounding lattice on formation of an impurity-vacancy complex from a separated impurity and a vacancy are very small. Nevertheless the observed changes could be significant, and they do in fact exhibit a dependence on the ionic radius of the impurity ion. In general, complex formation among the smaller impurity ions is accompanied by a negative entropy change, whereas the change is positive for the larger impurity ions. There is good evidence of increasing entropy change with increasing impurity ion size, Fig. 77. Positive and negative entropy changes can be associated with nearest- and next-nearest-neighbour type vacancies respectively. The argument is based essentially on that given earlier to explain the variation in relaxation times with impurity ion size. It was pointed out that large impurity ions may inhibit vacancy motion in the vicinity of the ion. With large impurity ions the vibrational entropy of the surrounding lattice will be increased on complex formation due to the pushing-out effect of the large ion, which produces a decrease in the vibrational amplitudes of the surrounding ions (a decrease in the amplitude of a vibration is accompanied by a corresponding increase in the frequency of that vibration). With the smaller impurity ions, however, the opening up of the lattice due to the pulling in of the Cl^- ions around the impurity makes cation

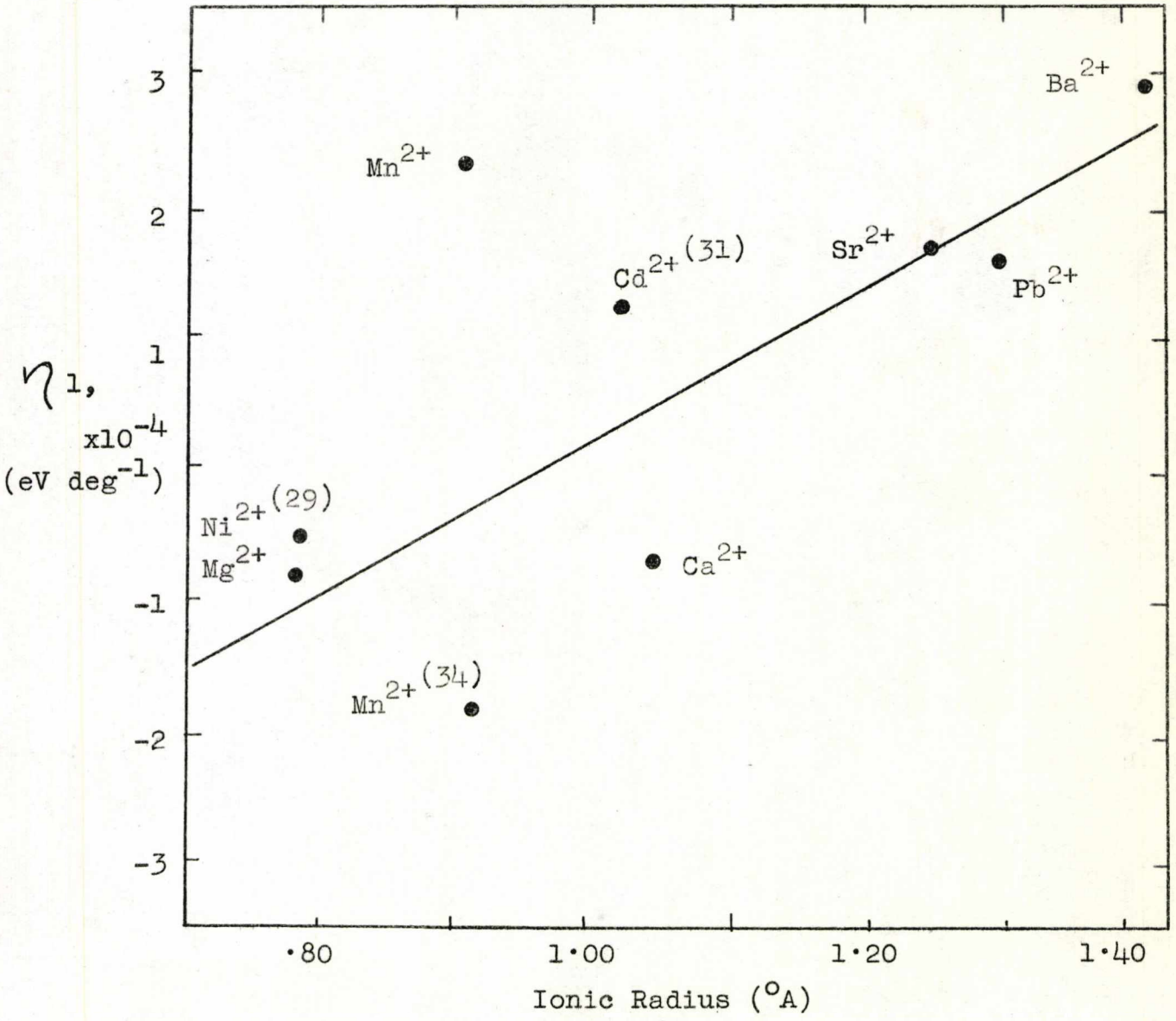

Fig. 77 - Entropy of Association, η_1, as a function of Ionic Radius.

vacancy motion in the vicinity much easier than elsewhere in the lattice. As a result, vibrational amplitudes will tend to increase and vibrational frequencies decrease. Furthermore, the larger the amplitude of a particular vibration the nearer it comes to being a translation, which would not contribute to the observed entropy change. Long-range interactions will promote this effect since they provide an extra possible translation. Hence, the negative changes of entropy can be interpreted as a loss of vibrational entropy of the lattice due to the increased vacancy motion.

Values of the free energy of association obtained from the impurity diffusion studies are rather high in comparison to those of the conductance studies. Since real systems contain unassociated vacancies and impurity ions it is possible that the bond energy of an impurity-vacancy pair may still be considerable at distances greater than the nearest-neighbour distance. That complexes do exist in excited states has already been demonstrated. Whereas this picture of a spread-out impurity-vacancy complex should influence the diffusive movements of the impurity ion, it was neglected in the analysis of the conductance work for reasons stated earlier. Therefore, the higher results obtained from impurity-diffusion studies could be attributed to these long-range interactions since, from the results of the impurity ion diffusion, it is impossible to distinguish

between nearest- and next-nearest-neighbour sites. The validity of this assumption is born out by the results reported from an impurity-diffusion study of the ($NaCl - ZnCl_2$) system[33]. The value of W_A is at least 0.15 eV higher than that which would be expected from theoretical considerations and from comparison with results obtained from the conductance studies on impurity ions of similar size to the Zn^{2+} ion. However, a 'normal' free energy of association, that is approximately 0.33 eV, was obtained from the data of Barr et al.[33] when next-nearest-neighbour association was included in the calculation.

It is likely that direct comparison of results from impurity-diffusion and conductance studies is only meaningful in systems where there is not a significant energy difference between the ground state and the first excited state of the complex, or, if excited states are present, the next-nearest-neighbour sites are less stable than the nearest-neighbour sites. This approach was followed in the present work and the ($NaCl - MnCl_2$) system studied by both methods with a view to comparing the association enthalpy of the nearest-neighbour complex from conductance studies with the free energy of association of the Mn^{2+} ion from impurity diffusion studies. The electron spin resonance measurements made on the ($NaCl - MnCl_2$) system indicate that the nearest- and next-nearest-neighbour

positions are in fact bound to the Mn^{2+} ion with the same energy, table 7. In addition, Watkins[25] has studied the spectrum of Mn^{2+} in NaCl as a function of temperature, and obtained a value of 0.41 eV for the association enthalpy. It should be interesting to compare this result with those from the analysis of conductance and impurity diffusion data.

There is good agreement between the two values obtained in the present work, table 16. Watkins'[25] result, although slightly higher, nevertheless indicates that this approach is valid, and that the simple association theory is in fact applicable to such systems. The predicted increase in association energy with impurity ion size, however, is confined to ions of size larger than the host cation. For impurity ions of size smaller than the host cation the association energy is essentially constant due to the increasing importance of long-range interactions. Due to the large relaxation of the lattice around a small impurity ion, next-nearest-neighbour association becomes dominant. It should be noted that Lidiard[18], who analysed the conductance data of Etzel and Maurer[31] for the system ($NaCl - CdCl_2$), included the effect of long-range interactions and this led to an increased value of the association energy.

7.4. Self-Diffusion Studies of Association

Although associated pairs are electrically neutral, it is generally assumed that the migration of these pairs can affect the magnitude of the self-diffusion coefficient but not that of the conductivity. In the present work, the self-diffusion coefficient of the Na^+ ion was studied over the temperature range 400-540°C. Self-diffusion in 'pure' crystals of NaCl is given by the equation

$$D_{Na^+} = 1.86 \exp(-\frac{0.75}{kT}) \qquad (7.3)$$

The activation energy for diffusion has a value of 0.75 eV.

The self-diffusion coefficients calculated from the measured conductivity in both 'pure' and Ca^{2+}-doped NaCl crystals are compared with the experimental values in Fig. 58. At first sight the validity of the Nernst-Einstein relationship for crystals containing approximately 50 ppm of Ca^{2+} impurity seems rather surprising. However, the theoretical calculation of the degree of association at a temperature of 440°C (Fig. 67), for an association energy of 0.30 eV is shown to be appreciably less than 10%. Since the estimated errors in the measurements of the diffusion coefficients are $\pm$ 15%, the agreement between the observed and calculated diffusion coefficients is within the limits of accuracy of the experimental method. As such, no definite conclusions can be drawn as regards the relative contribution of associated complexes to the diffusion.

The 'pure' crystals used in the present study were as received from Hilger and Watts. Normally, these crystals contain approximately 10 ppm of divalent cationic impurities. The validity of the Nernst-Einstein relationship for these crystals suggests that the divalent impurities are not highly associated. This is in marked contrast to the results of Mapother, Crooks and Maurer[11] who studied the self-diffusion of Na^+ ions in NaCl and NaBr. The calculated self-diffusion coefficients from their work were a factor of two lower than the directly measured self-diffusion coefficients. The failure of the Nernst-Einstein relationship was explained in terms of association between divalent cationic impurities and cation vacancies. This explanation would be valid only in the case of highly associated impurities which could contribute to the diffusion, but not the conductivity.

It is interesting to note that the increase in magnitude of the diffusion coefficients due to approximately 50 ppm of Ca^{2+} impurity is in good agreement with the observed increase in conductivity, table 17.

Table 17 - Relative Increase in Diffusion and Conductivity due to approximately 50 ppm Ca^{2+}

Temperature $10^3/T(^\circ A)$	Increase in Conductivity	Increase in Diffusion
1.300	6.8	6.0
1.400	6.8	6.0

This confirms the assumption that self-diffusion and ionic conductivity are both due to the same mechanism, that is the migration of single vacancies (in the absence of appreciable association).

7.5. Impurity Solubility

The effect of impurity dissolution or precipitation is usually recognised on the $\log_{10} \sigma$ versus $10^3/T$ plots by the superimposition of conductivities of crystals containing different impurity concentrations. In equilibrium, the conductivity of a crystal in this region (IV) depends only upon the temperature and type of impurity. In the present work, the conductivities were measured as a function of increasing temperature since these correspond to equilibrium (the time to reach equilibrium on cooling the crystal is considerably longer, depending on the solubility of the impurity in the lattice).

The free-impurity solubility for each of the impurities studied in NaCl was calculated by Haven's method[74], by extrapolation of the free vacancy region (II) to the solubility region (IV). This 'break' temperature corresponds to the temperature at which NaCl is saturated with divalent impurity. The variation of 'break' temperature with impurity concentration for each system studied is shown in Fig. 78. The least squares lines give the following equations for the free-impurity solubility:

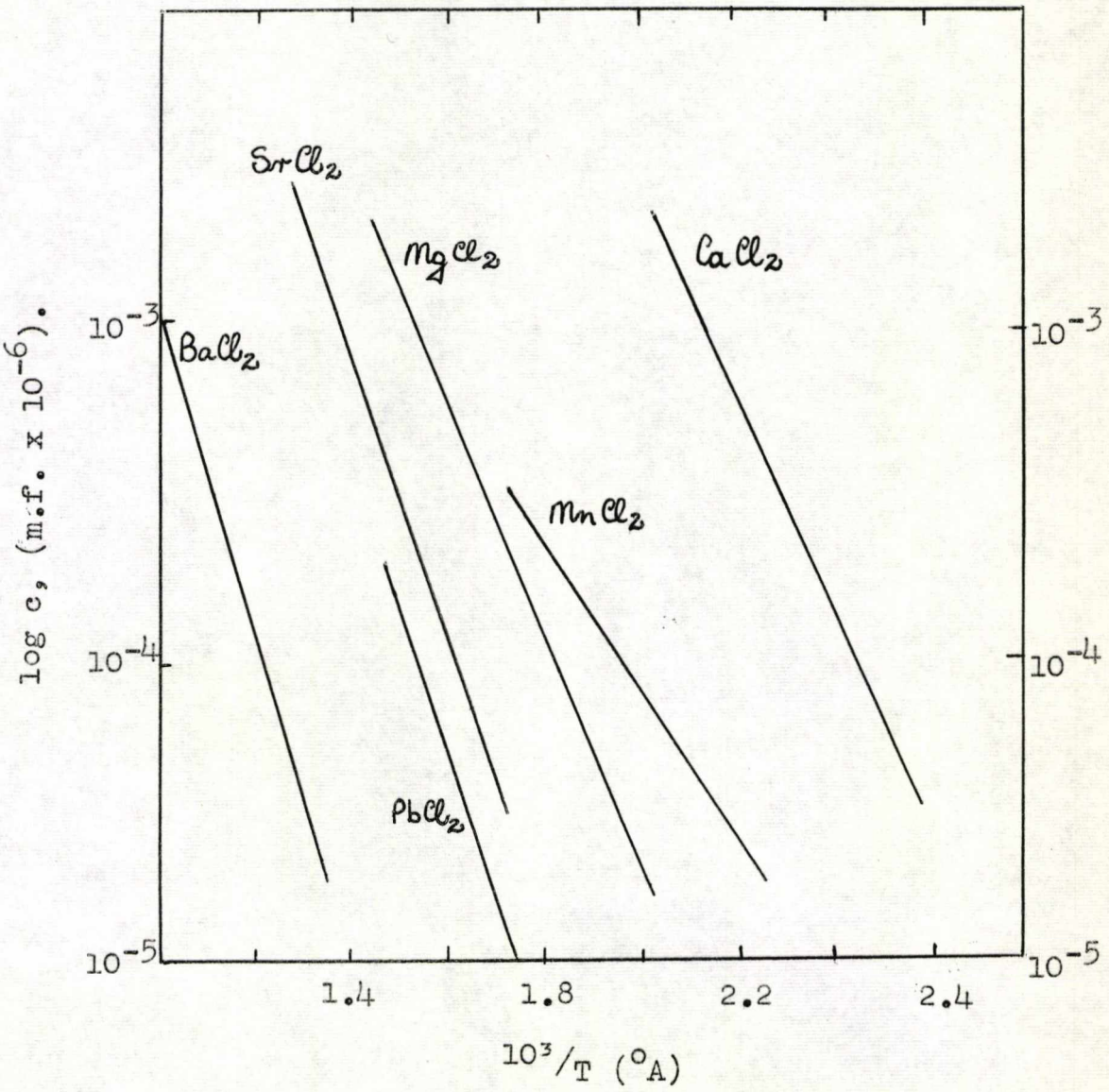

Fig. 78 - The free-impurity solubility of divalent impurities in NaCl. The straight lines are best, least squares fits.

$$c(\text{m.f. } MgCl_2) = 562 \exp\left(-\frac{0.77 \text{ eV}}{kT}\right) \quad (7.4)$$

$$c(\text{m.f. } MnCl_2) = (-0.74) \exp\left(-\frac{0.46 \text{ eV}}{kT}\right) \quad (7.5)$$

$$c(\text{m.f. } CaCl_2) = 6887 \exp\left(-\frac{0.64 \text{ eV}}{kT}\right) \quad (7.6)$$

$$c(\text{m.f. } SrCl_2) = 1746 \exp\left(-\frac{0.90 \text{ eV}}{kT}\right) \quad (7.7)$$

$$c(\text{m.f. } PbCl_2) = 2148 \exp\left(-\frac{0.95 \text{ eV}}{kT}\right) \quad (7.8)$$

$$c(\text{m.f. } BaCl_2) = 109 \exp\left(-\frac{1.00 \text{ eV}}{kT}\right) \quad (7.9)$$

The energy of solubility of these impurity ions shows a curious dependence on ionic radius, Fig. 79. To interpret this variation, the main factors which determine the solubility in ionic crystals must be considered, these are:

(1) Madelung energy,

(2) Polarisation energy,

(3) Repulsion energy.

The second factor usually favours the solubility, whereas the first and last are against it. The Madelung energy of an impurity ion and a Na^+ ion vacancy in the dissolved state is much the same as that of two Na^+ ions, so that any loss of Madelung energy on dissolving an impurity ion should not be very significant. A means of gaining energy is provided by the polarisation of the

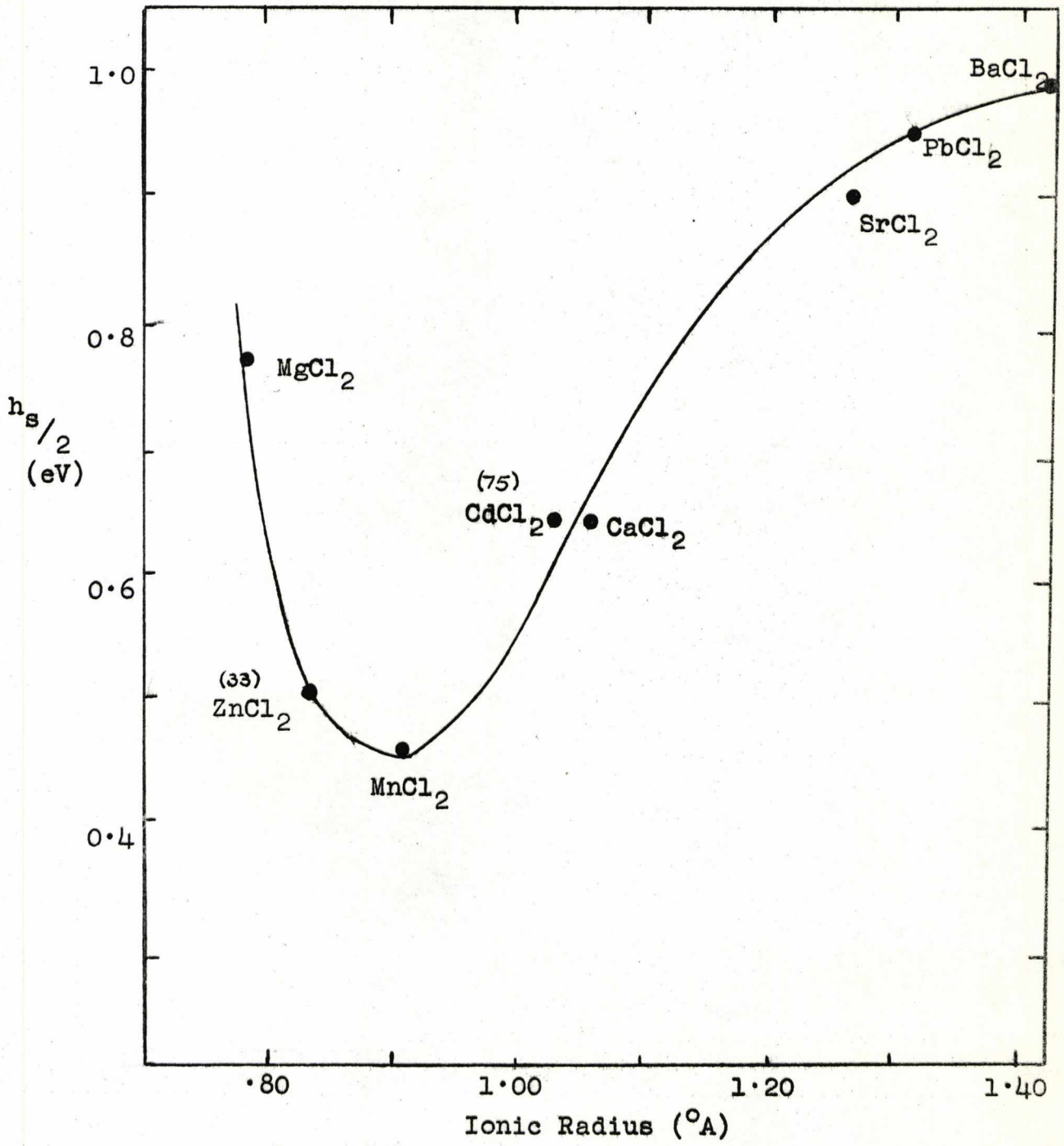

Fig. 79 - Solution Energy, $h_{s/2}$, as a function of Ionic Radius.

solvent lattice by the introduction of the doubly-charged impurity ion. The gain in polarisation energy should increase as the impurity ion size decreases. A possible explanation of the low solubility of Sr^{2+}, Pb^{2+} and Ba^{2+} compared to the smaller impurity ions such as Mn^{2+} could be that any gain in polarisation energy may not be sufficient to overcome the large repulsion energy created by the overlap of impurity ion and Cl^- ion charge clouds. Repulsion due to overlap of charge clouds decreases in importance as the size of the impurity ion approaches that of the ion it is replacing, that is the Na^+ ion. The remarkably high solution energy of Mg^{2+} is probably due to a combination of overlap and covalent effects. A significant amount of covalency may exist for the Mg^{2+} ion which, being very small, will draw the surrounding Cl^- ions in on top of each other and increase anion-anion repulsion. Again, this effect should become less significant as the impurity ion size increases towards that of the Na^+ ion. It is noteworthy that the Mn^{2+} ion which is more comparable in size to the Na^+ ion has the lowest solubility energy of all the ions studied in the present work.

There are very few other experimental results available for solubilities in NaCl. Haven[75], however, has quoted some values for NaCl, table 18.

Table 18 - Solubility of Divalent Cation Impurities in NaCl

Reference	Impurity Ion	Solubility (eV)
Haven[75]	Mn^{2+}	0.44
	Cd^{2+}	0.62
	Ca^{2+}	0.32
Barr et al.[33]	Zn^{2+}	0.49
Present Work	Mg^{2+}	0.77
	Mn^{2+}	0.46
	Ca^{2+}	0.64
	Sr^{2+}	0.90
	Pb^{2+}	0.95
	Ba^{2+}	1.00

Haven's[75] result for Ca^{2+} and Barr's[33] for Zn^{2+} are rather low in comparison with the results of the present work. However, there is excellent agreement in the value for Mn^{2+}. As was pointed out in section (7.2), much of the earlier work was influenced by the relative purity of the crystals used. Anionic impurities such as OH^- were often present and no doubt were responsible for some of the 'odd' results obtained. A recent study[76] of the effect of OH^- ions on the defect properties of NaCl crystals has shown that OH^- ions tend to be present in crystals doped with alkaline earth ions.

On the other hand, a crystal lattice containing Mn^{2+} ions was found to be relatively free of OH^- ions if normal precautions were taken during the growth process. In the light of this, the agreement between the solubility energies deduced from the present work and those reported earlier is in general reasonable. It should be noted that the work of Barr et al.[33] was hampered by the high vapour pressure of $ZnCl_2$ which tended to diffuse out of the crystal at high temperatures (> 560°C).

It is therefore suggested that the solubility of divalent cations in NaCl is critically dependent on the size of the impurity ion and, to a lesser extent, its polarisability. The gain in polarisation energy is only significant when the impurity ion is of similar size to the host cation, that is, when repulsion effects are at a minimum. The greater the misfit around the impurity ion the greater is the distortion produced, and the higher is the solubility energy of that ion.

The free energies of solution obtained from the difference in activation energies in conduction regions II and IV, are significantly lower than those obtained from equation (3.9).

7.6. Energy of Formation of a Schottky Defect and Mobility of a Cation Vacancy

Values of x_o, the mole fraction of Schottky defects in a pure crystal, were determined from the intercepts of the $c/(\xi - 1/\xi)$ versus ξ plots. When log x_o is plotted against reciprocal temperature a straight line is obtained, Fig. 80. A least squares method was used to find the best straight-line fit of the results. The values of x_o obtained from the ($NaCl - PbCl_2$) system were omitted from the least-squares analysis as they were anomalously low. The estimated impurity content of these crystals was consistently a factor of two lower than that indicated approximately by the magnitude of the conductivity, and, as they had been analysed independently by Johnson-Matthey and Co., the results of the analyses could not be readily checked against one of the more conventional laboratory methods of analysis. The slope of the least squares line in Fig. 80 is 1.10 $\pm$ 0.01 eV, so that the corresponding enthalpy of formation of a Schottky defect is 2.20 $\pm$ 0.02 eV. This result compares well with the experimental value of 2.34 eV obtained by Jain and Dahake[30], and the theoretical figure , W_S = 2.14 eV, for the energy of formation of a Schottky defect calculated by Boswarva and Lidiard[77]. The theoretical calculation employed the Born-Mayer-Verwey[14] repulsion potential

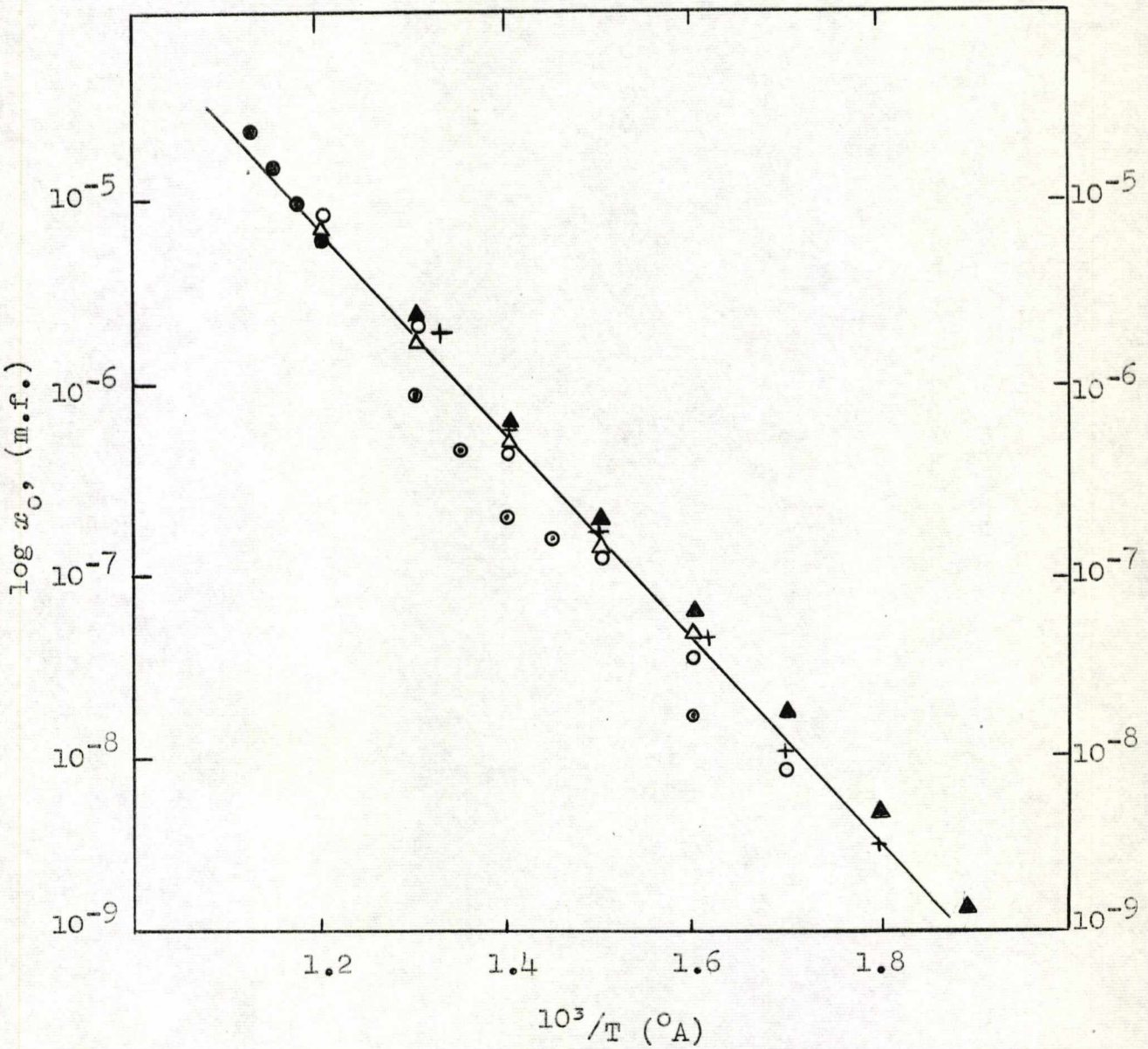

Fig. 80 - Thermal vacancy concentration, x_o, as a function of temperature. Points are obtained from conductivity measurements on NaCl containing divalent impurities.

O $MgCl_2$; + $MnCl_2$; ▲ $CaCl_2$; △ $SrCl_2$; ⊙ $PbCl_2$; ● $BaCl_2$.

approach and included Van der Waal's terms.

The vibrational entropy change accompanying the formation of a Schottky defect is given by the equation [79]

$$S_S = 2kz \ln (V/V') \qquad (7.10)$$

The pre-exponential factor in the equation for x_o (equation 3.2) leads to a value of 5.83×10^{-4} eV deg^{-1} for S_S, the vibrational entropy of a Schottky defect. If it is assumed that only the thermal vibrations of nearest-neighbours of a vacancy are altered, then it is possible to calculate the ratio of the frequencies of the perfect lattice ions (V) to those surrounding the vacancy (V') from equation (7.10). Substituting into equation (7.10) for S_S, k, the Boltzmann constant and z = 12, a value of 1.33 is obtained for (V/V'). This result is in excellent agreement with the value of 1.32 for NaCl quoted by Etzel and Maurer [31].

From equation (1.16) it follows that

$$\sigma = Nq_1\mu_1 x_o \xi \qquad (7.11)$$

Values of μ_1 were calculated for a wide range of impurity concentrations and the mean value found at a series of different temperatures. The plot of log $(\mu_1 T)$ versus $10^3/T$, Fig. 81, gave a straight line of slope 0.76 $\pm$ 0.01 eV, corresponding to the enthalpy of mobility of a cation

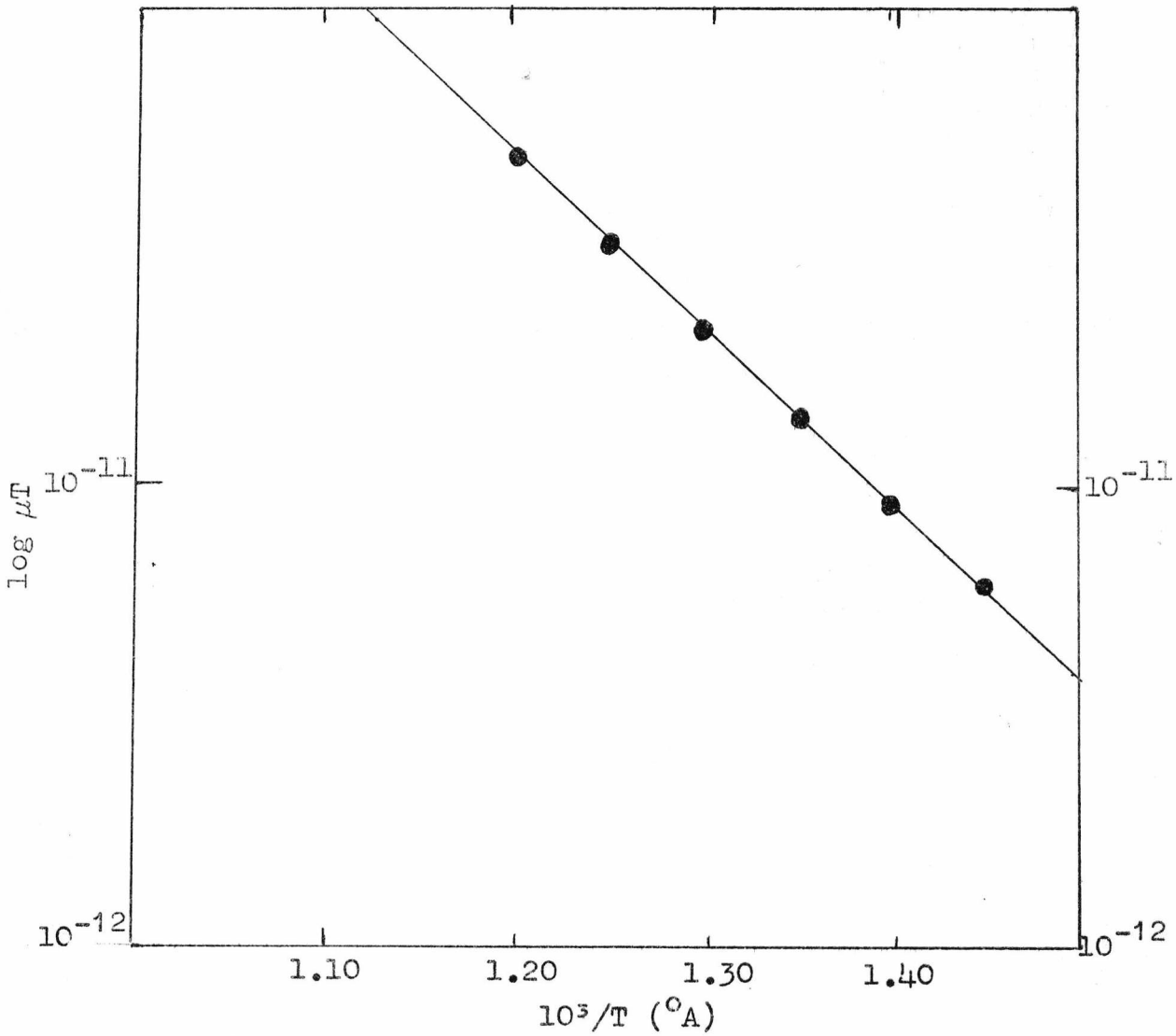

Fig. 81 - Values of μT, calculated from the conductivity measurements, as a function of temperature. The straight line is a best least squares fit.

vacancy. There is good agreement between this value and those obtained from recent studies of divalent cation-doped NaCl systems[10,30,71,78].

It is worth noting that this value for the enthalpy of mobility of a cation vacancy obtained from the analysis of conductance data is in satisfactory agreement with the 0.75 eV deduced from the experimental self-diffusion studies. This is further evidence that the ionic conductivity and self-diffusion of the Na^+ ion are both due to the same mechanism, that is, the migration of single vacancies.

APPENDIX

A. Estimation of Impurity Content by Spectrophotometric Titration.

B. Diffusion Data for the Penetration Profiles.

C. Calculation of the Polarisation Potential at the (110) Lattice Position due to the Ba^{2+}-cation Vacancy Complex.

A. Estimation of Impurity Content by Spectrophotometric Titration

Typical Calculation

Weight of crystal ($NaCl-CaCl_2$) = 0.1386g.

Titration 'end-point' = 0.092 ml.

Molarity of EDTA = 0.001 M.

1 litre 1M EDTA $\equiv$ 40.08 g Ca^{2+}

$\therefore$ 1 ml 0.001M " $\equiv$ 4.01×10^{-5} g Ca^{2+}

$\therefore$ 0.092ml 0.001M " $\equiv$ 3.69×10^{-6} g Ca^{2+} in 2 ml.

$\equiv$ 9.23×10^{-6} g Ca^{2+} in 5 ml.

$\equiv$ 2.50×10^{-5} g $CaCl_2$ in 5 ml.

$$\therefore \quad Ca^{2+}/Na^{+} = \frac{2.50 \times 10^{-5} \times 58.49}{111.08 \times 0.1386}$$

$$= 94 \times 10^{-6} \text{ m.f. (or 94 ppm)}$$

The complete set of results for Mg^{2+}, Ca^{2+}, Sr^{2+} and Ba^{2+} impurities are given in table 19.

TABLE 19

Impurity Ion	Wt. of crystal(g)	'End-Point' (ml)	Molarity EDTA (M)	Conc^{n}. of Impurity ($\times 10^{-6}$ m.f.)
Mg^{2+}	0.1558	0.028	0.001	20
	0.0669	0.012	0.001	26
	0.0768	0.184	0.001	35
	0.1800	0.060	0.001	49
	0.0551	0.034	0.001	90
	0.1242	0.079	0.001	94
	0.0317	0.038	0.001	175
	0.0624	0.081	0.001	190
	0.1020	0.155	0.001	223
Sr^{2+}	0.1404	0.023	0.001	23
	0.2046	0.070	0.001	48
	0.1514	0.069	0.001	64
	0.0461	0.027	0.001	86
	0.2230	0.023	0.0093	139
	0.2065	0.032	0.0093	207
	0.1960	0.054	0.0093	371
	0.0930	0.070	0.0093	1030
	0.0700	0.090	0.0093	1680
Ba^{2+}	0.0666	0.010	0.001	24
	0.1658	0.049	0.001	45
	0.1367	0.050	0.001	53
	0.0444	0.025	0.001	82
	0.1846	0.016	0.010	123
	0.0583	0.068	0.001	168
	0.0712	0.029	0.010	600

TABLE 19 (continued)

Impurity Ion	Wt. of Crystal(g)	'End-Point' (ml)	Molarity EDTA (M)	Conc^{n}. of Impurity (x 10^{-6} m.f.)
Ca^{2+}	0.1576	0.030	0.001	28
	0.1980	0.038	0.001	28
	0.1336	0.044	0.001	48
	0.1300	0.046	0.001	51
	0.1063	0.038	0.001	54
	0.1322	0.062	0.001	68
	0.1110	0.058	0.001	76
	0.1055	0.065	0.001	88
	0.1386	0.092	0.001	94
	0.0275	0.030	0.001	158
	0.2010	0.033	0.0093	218
	0.1595	0.040	0.0093	340
	0.2436	0.076	0.010	455
	0.1077	0.065	0.0093	809
	0.1209	0.096	0.010	1160
	0.0380	0.053	0.010	2040
	0.1212	0.039	0.050	2320

B. Diffusion Data for the Penetration Profiles

TABLE 20

(i) Self-Diffusion - $Na^{22}/NaCl$

Crystal - 'Pure' NaCl
Δt - 1.82×10^6 secs.
T - 410°C

Diffusion Distance (x) (μ)	Specific Activity (cpm) x 10^4
11.63	287
11.63	201
11.63	101
10.80	92
9.14	73
9.97	64
4.99	53
11.63	40
10.80	29
9.97	18
9.97	12
9.14	5

$D = 6.94 \times 10^{-12} cm^2 sec^{-1}$

Crystal - 'Pure' NaCl
Δt - 1.82×10^6 secs.
T - 410°C

Diffusion Distance (x) (μ)	Specific Activity (cpm) x 10^4
11.18	367
12.90	397
12.04	303
12.90	294
11.18	223
10.32	157
15.48	114
14.62	98
13.76	69
10.32	39
14.62	18
12.90	11

$D = 7.54 \times 10^{-12} cm^2 sec^{-1}$

Crystal - 'Pure' NaCl
Δt - 8.64×10^5 secs.
T - 518°C

x (μ)	(cpm) x 10^4
8.04	395
9.50	383
13.15	315
13.15	334
12.42	312
12.42	268
12.42	255
13.15	209
12.86	188
12.86	155
13.15	94
12.42	45
12.42	22

$D = 3.80 \times 10^{-11} cm^2 sec^{-1}$

Crystal - 'Pure' NaCl
Δt - 1.21×10^6 secs.
T - 479°C

x (μ)	(cpm) x 10^4
~ 10	500
~ 10	276
~ 10	294
~ 10	272
~ 10	235
~ 10	171
~ 10	209
~ 10	172
~ 10	172
~ 10	94
~ 10	136
~ 10	32

$D = 2.06 \times 10^{-11} cm^2 sec^{-1}$

Crystal - 'Pure' NaCl
Δt - 1.82×10^6 secs
T - 450°C

Diffusion Distance x (μ)	Specific Activity (cpm) x 10^4
~ 10	384
~ 10	335
~ 10	282
~ 10	282
~ 10	272
~ 10	251
~ 10	228
~ 10	251
~ 10	190
~ 10	213
~ 10	119
~ 10	97
~ 10	80

$D = 1.36 \times 10^{-11} cm^2 sec^{-1}$

Crystal - 'Pure' NaCl
Δt - 1.21×10^6 secs
T - 500°C

Diffusion Distance x (μ)	Specific Activity (cpm) x 10^4
~ 10	748
~ 10	569
~ 10	499
~ 10	462
~ 10	515
~ 10	426
~ 10	340
~ 10	345
~ 10	322
~ 10	281
~ 10	206
~ 10	85
~ 10	89
~ 10	38

$D = 2.84 \times 10^{-11} cm^2 sec^{-1}$

Crystal - 'Pure' NaCl
Δt - 1.21×10^6 secs
T - 500°C

x (μ)	(cpm) x 10^4
~ 10	190
~ 10	140
~ 10	134
~ 10	113
~ 10	124
~ 10	113
~ 10	88
~ 10	90
~ 10	84
~ 10	36

$D = 2.95 \times 10^{-11} cm^2 sec^{-1}$

Crystal - 'Pure' NaCl
Δt - 6.05×10^5 secs
T - 540°C

x (μ)	(cpm) x 10^4
~ 10	513
~ 10	286
~ 10	268
~ 10	280
~ 10	273
~ 10	244
~ 10	207
~ 10	197
~ 10	172
~ 10	141
~ 10	128
~ 10	122

$D = 5.40 \times 10^{-11} cm^2 sec^{-1}$

Crystal - 'Pure' NaCl
Δt - 6.05×10^5 secs
T - 540°C

Diffusion Distance x (μ)	Specific Activity (cpm) x 10^4
~ 10	162
~ 10	143
~ 10	162
~ 10	151
~ 10	138
~ 10	139
~ 10	130
~ 10	130
~ 10	122
~ 10	136
~ 10	103
~ 10	107
~ 10	92

$D = 5.82 \times 10^{-11} cm^2 sec^{-1}$

Crystal - 'Pure' NaCl
Δt - 1.82×10^6 secs
T - 430°C

Diffusion Distance x (μ)	Specific Activity (cpm) x 10^4
~ 10	325
~ 10	456
~ 10	429
~ 10	407
~ 10	246
~ 10	221
~ 10	191
~ 10	182
~ 10	130
~ 10	98

$D = 9.10 \times 10^{-12} cm^2 sec^{-1}$

Crystal - 'Pure' NaCl
Δt - 6.05×10^5 secs
T - 430°C

x (μ)	(cpm) x 10^4
~ 10	331
~ 10	229
~ 10	205
~ 10	208
~ 10	186
~ 10	151
~ 10	112
~ 10	90
~ 10	59
~ 10	26
~ 10	17

$D = 7.05 \times 10^{-12} cm^2 sec^{-1}$

Crystal - (NaCl - $CaCl_2$)
Δt - 1.21×10^6 secs
T - 500°C

x (μ)	(cpm) x 10^4
~ 10	214
~ 10	262
~ 10	218
~ 10	283
~ 10	239
~ 10	205
~ 10	231
~ 10	224
~ 10	243
~ 10	199
~ 10	91

$D = 1.28 \times 10^{-10} cm^2 sec^{-1}$

$c_{Ca} = 51 \times 10^{-6}$ m.f.

Crystal - ($NaCl-CaCl_2$)
Δt - 1.21×10^6 secs
T - 500^oC

Diffusion Distance x (μ)	Specific Activity (cpm) x 10^4
~ 10	282
~ 10	349
~ 10	392
~ 10	314
~ 10	339
~ 10	341
~ 10	342
~ 10	277
~ 10	302
~ 10	262
~ 10	286
~ 10	237
~ 10	253
~ 10	204

$D = 8.92 \times 10^{-11} cm^2 sec^{-1}$

$c_{Ca^{2+}} = 28 \times 10^{-6}$ m.f.

Crystal - ($NaCl-CaCl_2$)
Δt - 1.21×10^6 secs
T - 500^oC

Diffusion Distance x (μ)	Specific Activity (cpm) x 10^4
~ 10	222
~ 10	209
~ 10	231
~ 10	200
~ 10	198
~ 10	181
~ 10	177
~ 10	168
~ 10	187
~ 10	182
~ 10	164
~ 10	153
~ 10	148
~ 10	149

$D = 8.55 \times 10^{-11} cm^2 sec^{-1}$

$c_{Ca^{2+}} = 54 \times 10^{-6}$ m.f.

Crystal - ($NaCl-CaCl_2$)
Δt - 1.82×10^6 secs
T - 430^oC

x (μ)	(cpm) x 10^4
~ 10	111
~ 10	117
~ 10	163
~ 10	96
~ 10	111
~ 10	99
~ 10	86
~ 10	78
~ 10	84
~ 10	89
~ 10	85
~ 10	80
~ 10	67
~ 10	56

$D = 5.53 \times 10^{-11} cm^2 sec^{-1}$

$c_{Ca^{2+}} = 68 \times 10^{-6}$ m.f.

Crystal - ($NaCl-CaCl_2$)
Δt - 8.64×10^5 secs
T - 518^oC

x (μ)	(cpm) x 10^4
9.10	142
10.40	146
11.87	158
10.40	158
11.87	155
11.87	128
10.40	149
11.87	145
10.40	129
9.10	120
11.87	158
10.40	96
13.20	131
13.20	128
9.10	92

$D = 1.75 \times 10^{-10} cm^2 sec^{-1}$

$c_{Ca^{2+}} = 76 \times 10^{-6}$ m.f.

(ii) Impurity-Diffusion - Mn^{54}/NaCl

In the present work a vast amount of diffusion data was accumulated. To list all of the data would be tedious and serve no real purpose. Consequently, the following table (21) includes only the data relating to penetration profiles which were ultimately used in the determination of the free energy of association for the Mn^{2+} - cation vacancy complex, that is, those results which were analysed in terms of the simple association theory. In addition a few results of Mn^{54} diffusion in 'pure' NaCl are included, since these were made to provide a means of comparing the results of the present work with those cited in the literature.

Crystal - 'Pure' NaCl
Δt - 2.59×10^5 secs
T - 442°C

Diffusion Distance x (μ)	Specific Activity (cpm) x 10^4
7.02	162
7.02	96
10.53	64
6.32	61
11.93	39
7.72	34
10.53	32
11.23	23
11.23	22
12.64	21
7.72	22
7.72	24
9.13	18
11.23	19
8.42	19

$D = 5.26 \times 10^{-10}$ $cm^2 sec^{-1}$

Crystal - 'Pure' NaCl
Δt - 2.59×10^5 secs
T - 455°C

Diffusion Distance x (μ)	Specific Activity (cpm) x 10^4
5.04	140
6.72	65
5.88	69
8.40	62
9.24	66
5.04	54
6.72	55
4.20	50
6.72	53
10.04	58
6.72	50
10.92	55
4.20	44
5.88	44
11.76	52

$D = 6.76 \times 10^{-10}$ $cm^2 sec^{-1}$

Crystal - ($NaCl-MnCl_2$)
Δt - 1.91×10^5 secs
T - 440°C

x (μ)	(cpm) x 10^4
14.49	39.9
10.63	13.2
11.59	6.4
7.73	10.8
11.59	8.3
10.63	8.2
10.63	8.7
6.76	7.1
11.59	6.9
5.80	7.3
13.52	6.9
11.59	6.7
12.56	6.6
8.69	6.1
11.59	6.3

$D = 1.58 \times 10^{-9}$ $cm^2 sec^{-1}$

$c_{Mn^{2+}} = 75 \times 10^{-6}$ m.f.

Crystal - ($NaCl-MnCl_2$)
Δt - 1.91×10^5 secs
T - 440°C

x (μ)	(cpm) x 10^4
19.40	75.8
20.37	30.6
21.34	14.6
21.34	16.8
22.31	16.4
22.31	18.4
8.73	19.0
9.70	20.5
9.70	20.5
10.67	24.7
10.67	13.8
4.85	17.9
12.61	14.5
11.64	16.4
9.70	12.7

$D = 2.71 \times 10^{-9}$ $cm^2 sec^{-1}$

$c_{Mn^{2+}} = 140 \times 10^{-6}$ m.f.

Crystal - ($NaCl-MnCl_2$)
Δt - 1.91×10^5 secs
T - 440°C

Diffusion Distance x (μ)	Specific Activity (cpm) x 10^4
13.92	43.8
13.22	26.4
13.22	15.1
14.62	12.6
13.22	13.7
13.22	10.9
9.74	10.7
9.74	10.0
8.35	8.4
9.74	8.2
9.05	8.5
9.74	7.7
6.26	8.2
6.96	8.0
7.66	7.7

$D = 4.20 \times 10^{-9}$ $cm^2 sec^{-1}$

$c_{Mn^{2+}} = 300 \times 10^{-6}$ m.f.

Crystal - ($NaCl-MnCl_2$)
Δt - 1.91×10^5 secs
T - 440°C

Diffusion Distance x (μ)	Specific Activity (cpm) x 10^4
17.20	19.7
14.65	20.9
13.74	20.5
13.38	21.7
5.73	19.2
7.64	13.2
6.37	13.8
7.01	12.5
10.83	12.1
8.92	10.2
7.01	19.9
5.73	11.8
8.92	9.1
7.01	9.4
11.46	9.6

$D = 5.05 \times 10^{-9}$ $cm^2 sec^{-1}$

$c_{Mn^{2+}} = 420 \times 10^{-6}$ m.f.

Crystal - ($NaCl-MnCl_2$)
Δt - 2.59×10^5 secs
T - 442°C

x (μ)	(cpm) x 10^4
7.91	86.7
6.78	83.2
7.35	44.0
10.17	34.2
9.61	23.8
8.48	18.9
-	-
10.17	13.7
9.04	16.6
6.22	16.7
9.61	16.7
9.61	13.1
7.35	14.6
7.91	12.0
9.04	13.6

$D = 9.25 \times 10^{-10}$ $cm^2 sec^{-1}$

$c_{Mn^{2+}} = 40 \times 10^{-6}$ m.f.

Crystal - ($NaCl-MnCl_2$)
Δt - 2.59×10^5 secs
T - 442°C

x (μ)	(cpm) x 10^4
12.98	134.4
9.52	63.3
8.65	45.3
8.65	32.9
8.65	27.5
9.52	21.2
8.65	16.8
14.71	12.9
8.65	12.0
13.84	13.0
8.65	15.0
15.57	13.2
8.65	13.3
8.65	11.5
6.92	9.8

$D = 9.52 \times 10^{-10}$ $cm^2 sec^{-1}$

$c_{Mn^{2+}} = 50 \times 10^{-6}$ m.f.

Crystal - ($NaCl-MnCl_2$)
Δt - 2.59×10^5 secs
T - 421°C

Diffusion Distance x (μ)	Specific Activity (cpm) x 10^4
15.40	66.2
18.12	83.6
9.06	61.0
9.06	70.1
18.12	71.8
12.68	16.7
7.25	18.8
12.68	16.2
10.87	22.0
7.25	20.8
10.87	20.9
5.44	20.5
9.97	13.4
9.06	12.2
8.15	14.0

$D = 1.01 \times 10^{-10}$ $cm^2 sec^{-1}$

$c_{Mn^{2+}} = 68 \times 10^{-6}$ m.f.

Crystal - ($NaCl-MnCl_2$)
Δt - 2.59×10^5 secs
T - 421°C

Diffusion Distance x (μ)	Specific Activity (cpm) x 10^4
8.71	126.2
15.68	83.2
12.19	59.0
10.45	64.2
10.45	62.2
10.45	52.2
8.71	52.8
10.45	53.9
13.94	40.0
6.97	34.8
15.68	33.8
8.71	23.8
6.97	21.5
13.94	20.9
12.19	20.3

$D = 2.02 \times 10^{-9}$ $cm^2 sec^{-1}$

$c_{Mn^{2+}} = 95 \times 10^{-6}$ m.f.

Crystal - ($NaCl-MnCl_2$)
Δt - 2.59×10^5 secs
T - 421°C

x (μ)	(cpm) x 10^4
11.60	66.6
12.28	44.1
11.12	37.8
11.60	24.8
4.68	40.1
5.85	13.2
5.85	15.9
5.85	17.5
4.09	13.4
7.02	10.8
7.02	10.6
8.19	9.5
5.85	10.0
8.77	11.1
5.27	10.3

$D = 2.05 \times 10^{-9}$ $cm^2 sec^{-1}$

$c_{Mn^{2+}} = 215 \times 10^{-6}$ m.f.

Crystal - ($NaCl-MnCl_2$)
Δt - 2.59×10^5 secs
T - 421°C

x (μ)	(cpm) x 10^4
10.75	68.0
9.22	51.6
10.75	32.4
9.22	26.3
8.45	23.6
9.22	18.5
7.68	15.9
7.68	15.5
6.91	15.6
7.68	15.0
6.91	16.0
10.75	12.1
7.68	13.5
9.98	15.0
9.22	14.8

$D = 2.46 \times 10^{-9}$ $cm^2 sec^{-1}$

$c_{Mn^{2+}} = 335 \times 10^{-6}$ m.f.

Crystal - ($NaCl-MnCl_2$)
Δt - 3.45×10^5 secs
T - 401°C

Diffusion Distance x (μ)	Specific Activity (cpm) x 10^4
7.57	87.4
9.08	76.7
7.57	62.4
7.57	58.0
6.81	41.9
9.08	38.9
5.29	33.0
9.08	19.8
7.57	14.2
9.08	12.0
7.57	12.5
9.84	7.7
10.59	10.4
8.33	8.2
10.59	7.9

$D = 5.28 \times 10^{-10}$ $cm^2 sec^{-1}$

$c_{Mn^{2+}} = 65 \times 10^{-6}$ m.f.

Crystal - ($NaCl-MnCl_2$)
Δt - 3.45×10^5 secs
T - 401°C

Diffusion Distance x (μ)	Specific Activity (cpm) x 10^4
10.41	132.6
11.66	66.9
11.66	46.1
11.66	32.6
10.41	33.9
11.66	22.3
10.41	35.6
10.41	32.6
5.20	26.6
6.25	23.0
9.37	17.8
5.20	23.8
6.25	17.7
12.49	17.7
5.20	25.2

$D = 1.55 \times 10^{-9}$ $cm^2 sec^{-1}$

$c_{Mn^{2+}} = 130 \times 10^{-6}$ m.f.

Crystal - ($NaCl-MnCl_2$)
Δt - 3.45×10^5 secs
T - 401°C

x (μ)	(cpm) x 10^4
14.22	22.4
14.22	22.3
14.77	16.5
12.03	10.3
8.75	8.1
7.11	7.7
13.13	7.1
8.75	7.3
8.21	6.8
6.02	6.6
7.66	7.9
13.13	6.5
9.85	6.6
10.94	6.2
10.39	5.9

$D = 1.26 \times 10^{-9}$ $cm^2 sec^{-1}$

$c_{Mn^{2+}} = 200 \times 10^{-6}$ m.f.

Crystal - ($NaCl-MnCl_2$)
Δt - 3.45×10^5 secs
T - 401°C

x (μ)	(cpm) x 10^4
13.16	28.2
17.11	14.2
13.82	9.8
11.84	9.4
10.53	8.7
9.87	8.3
7.24	8.3
8.55	8.4
7.24	8.3
10.53	8.0
5.92	8.4
6.58	6.8
7.90	7.1
9.21	5.2
7.90	3.9

$D = 1.50 \times 10^{-9}$ $cm^2 sec^{-1}$

$c_{Mn^{2+}} = 230 \times 10^{-6}$ m.f.

Crystal - ($NaCl-MnCl_2$)
Δt - 3.45×10^5 secs
T - 428°C

Diffusion Distance x (μ)	Specific Activity (cpm) x 10^4
8.04	116.2
22.33	35.7
18.75	29.9
11.61	25.3
33.04	12.4
17.86	14.4
14.29	15.6
25.00	15.5
12.50	12.8
16.07	12.8
17.86	11.1
14.29	12.4
18.75	10.7
11.61	14.8
13.39	12.1

$D = 7.72 \times 10^{-10}$ $cm^2 sec^{-1}$

$c_{Mn^{2+}} = 50 \times 10^{-6}$ m.f.

Crystal - ($NaCl-MnCl_2$)
Δt - 3.45×10^5 secs
T - 428°C

Diffusion Distance x (μ)	Specific Activity (cpm) x 10^4
12.93	154.3
12.93	86.6
14.54	38.6
16.16	21.5
17.78	18.9
8.08	17.0
9.69	17.1
21.01	15.3
9.69	15.9
11.31	16.4
8.08	17.9
12.93	16.1
14.54	15.4
12.93	13.1
11.31	13.6

$D = 9.38 \times 10^{-10}$ $cm^2 sec^{-1}$

$c_{Mn^{2+}} = 70 \times 10^{-6}$ m.f.

All the count rates (cpm) listed in the preceding tables have been corrected for 'background' radiation.

C. Calculation of the Polarisation Potential at the (110) Lattice Position due to the Ba^{2+}-Cation Vacancy Complex

$$V_2^{POL} = e \sum_i \mu_i \cos\theta_i / r_i^2$$

V_2^{POL} was computed as follows. The polarising field E produced by the charges of the defects was calculated at each lattice point under consideration. The induced dipole at a lattice point is given by

$$\mu_i = \alpha_i E.$$

Values of μ_i and θ_i, the angle between the direction of μ_i and that of r_i, are then substituted into the equation for V_2^{POL}. The summation was over the Ba^{2+}, the ten nearest-neighbours of the complex, and second and third nearest-neighbours of the (110) position.

The calculation of the field due to an electric dipole is an easy problem that does not involve integration since only point charges are concerned. The dipole producing the electric field in this case is made up of the extra positive charge on the Ba^{2+} ion and the effective negative charge on the positive ion vacancy. To illustrate the approach the calculation of

the field at three different positions in the lattice is made. Consider the field of the dipole along its axis and perpendicular to the axis from the centre of the dipole, Fig. 82.

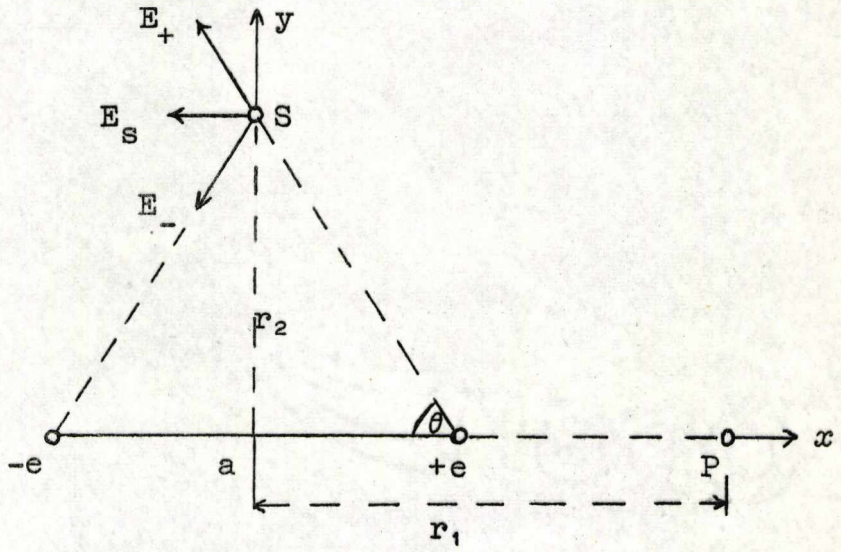

Fig. 82 - Calculation of the field of a dipole of moment $p = ea$.

The field at P at a distance of r_1 from the centre of the dipole is given by

$$E_p = \frac{e}{(r_1 - a/2)^2} - \frac{e}{(r_1 + a/2)^2}$$

$$= \frac{2r_1 ae}{(r_1^2 - a^2/4)}$$

At S the fields due to +e and -e are designated as E_+ and E_-, respectively. Their y components cancel, while their x components add to yield the resulting field E_s. Thus

$$E_s = |E_+| \cos\theta + |E_-| \cos\theta$$

or

$$E_s = \left\{ \frac{e}{[r_2^2 + (a/2)^2]} + \frac{e}{[r_2^2 + (a/2)^2]} \right\} \frac{a/2}{[r^2+(a/2)^2]^{\frac{1}{2}}}$$

$$= \frac{ea}{[r_2^2 + (a/2)^2]^{3/2}}$$

Whenever s was situated reasonably far from the dipole, that is r > a, Fig. 83, the following approximated expressions were used in the evaluation of E.

$$E_r = \frac{2p \cos\theta}{r^3}$$

and

$$E_\theta = \frac{p \sin\theta}{r^3}$$

where E_r and E_θ are the components of E in two perpendicular directions. The magnitude and direction of the total field can then be obtained by simple vector addition of the two perpendicular components. The expressions were obtained using the relationship between potential gradient and electric fields, that is the expression for the potential at P is differentiated with respect to r.

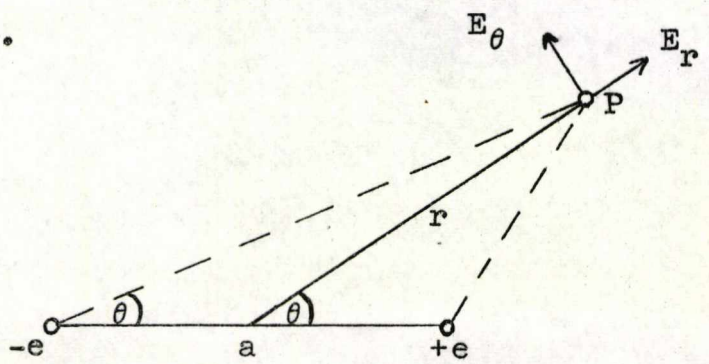

Fig. 83

Wherever necessary, the 'cosine' rule was used to determine the exact positions of the ions under consideration. In table 22, the electrostatic field, E, and the magnitude and direction of the induced dipoles are shown. This is followed by the final stages in the calculation of V_2^{POL}.

TABLE 22

Ion Position	Field, E, dynes/statcoulomb x10^6	Induced Dipole dynes/cm^3/statcoulomb x 10^{-18}	θ_i
(100) and (010)	0.782	2.315	42°3'
(111) and (11-1)	0.274	0.811	61°27'
(120) and (220)	0.149	0.441	30°39'
(-100) and (0-10)	0.167	0.494	20°0'
(001) and (00-1)	0.308	0.911	45°53'
(011), (01-1), (101) and (10-1)	0.428	0.176	45°0'
(211), (21-1), (121) and (12-1)	0.198	0.081	28°27'
(200) and (020)	0.309	0.127	34°43'
(220)	0.227	0.093	0°
(021), (02-1), (201) and (20-1)	0.148	0.438	70°11'
(221) and (22-1)	0.147	0.435	42°33'
(000)	0.303	0.758	0°

$$V_2^{POL} = -e \sum \frac{\mu_i \cos\theta_i}{r_i^2}$$

$$= - \frac{4.803 \times 10^{-10} \times 6.25 \times 10^{11}}{(2.815)^2 \times 10^{-16}}$$

$$\left[\frac{2 \times 2.315 \times 0.707 \times 10^{-18}}{(1 + 0.068)^2 + (0.010)^2} + \frac{2 \times 0.811 \times 0.478 \times 10^{-18}}{(1.068)^2} \right.$$

$$+ \frac{2 \times 0.441 \times 0.860 \times 10^{-18}}{(1.068)^2} + \frac{2 \times 0.494 \times 0.939 \times 10^{-18}}{[1 + (2-0.01)^2]}$$

$$+ \frac{2 \times 0.911 \times 0.696 \times 10^{-18}}{[2 + (1-010)^2]} + \frac{4 \times 0.176 \times 0.707 \times 10^{-18}}{2}$$

$$+ \frac{4 \times 0.081 \times 0.879 \times 10^{-18}}{2} + \frac{2 \times 0.127 \times 0.479 \times 10^{-18}}{2}$$

$$\left. + \frac{0.093 \times 10^{-18}}{2} + \frac{4 \times 0.438 \times 0.338 \times 10^{-18}}{3} \right.$$

$$\left. + \frac{2 \times 0.435 \times 0.737 \times 10^{-18}}{3} + 0.379 \times 10^{-18} \right]$$

$$= - 0.379 \, [2.867 + 0.679 + 0.664 + 0.187$$

$$+ 0.425 + 0.124 + 0.143 + 0.061$$

$$+ 0.047 + 0.196 + 0.214 + 0.379] \text{ eV}$$

$$= - 0.379 \times 5.986 \text{ eV}$$

$$= - 2.268 \text{ eV}.$$

REFERENCES

1. Schottky, W., Z. Phys. Chem., B29, 335 (1935).

2. Frenkel, J., Z. Physik, 35, 652 (1926).

3. Van Beuren, H.G., "Imperfections in Crystals", North Holland Publishing Co., Amsterdam, 1960.

4. Burton, W.K., Cabrera, N., and Frank, F.C., Nature, 163, 398 (1949).

5. Lehovec, K., J. Chem. Phys., 21, 1123 (1953).

6. Eshelby, J.D., Newey, C.W., Pratt, P.L. and Lidiard, A.B., Phil. Mag., 3, 75 (1958).

7. Koch, E. and Wagner, C., Z. Phys. Chem., B338, 295 (1937).

8. Tubandt, C., Handbuch der Experimental physik, 12, 383 (1932).

9. Mott, N.F. and Gurney, R., "Electronic Processes in Ionic Crystals", 2nd Edition (Oxford, 1948), p.43.

10. Dreyfus, R.W. and Nowick, A.S., Phys. Rev., 126, 1367 (1962).

11. Mapother, D., Crooks, H.N. and Maurer, R., J. Chem. Phys., 18, 1231 (1950).

12. Aschner, J.F., Thesis, University of Illinois (1954).

13. Chemla, M., Thesis, University of Paris (1954).

14. Born, M., Mayer, J. and Verwey, E.J.W., Rec. Trav. Chim. Pays. Bas., 65, 521 (1946).

15. Barr, L.W., Morrison, J.A. and Schroeder, P.A., J. Appl. Phys., 36, 624 (1965).

16. Fuller, R.G., Phys. Rev., 142, 524 (1966).

17. Laurance, N., Phys. Rev., 120, 57 (1960).

18. Lidiard, A.B., Handbuch der Physik (S. Flügge), Springer-Verlag (Berlin, 1957), XX, p.246.

19. Tosi, M.P. and Airoldi, G., Nuovo Cim., 8, 584 (1958).

20. Breckenridge, R.G., J. Chem. Phys., 16, 959 (1948).

21. Haven, Y., J. Chem. Phys., 21, 171 (1953).

22. Dryden, J. and Meakins, R., Disc. Far. Soc., 23, 39 (1957).

23. Watkins, G.D., Phys. Rev., 113, 91 (1959).

24. Dreyfus, R.W., Phys. Rev., 121, 1675 (1961).

25. Watkins, G.D., Phys. Rev., 113, 79 (1959).

26. Reif, F., Phys. Rev., 100, 1597 (1955).

27. Satoh, M., J. Phys. Soc. Japan, 20, 1008 (1965).

28. Camagni, P., Chiorotti, G., Furai, F.G. and Guilotto, L., Phil. Mag., 45, 225 (1954).

29. Jain, S.C. and Parashar, D.C., Indian J. Pure Appl. Phys., 3, 154 (1965).

30. Jain, S.C. and Dahake, S.L., Indian J. Pure Appl. Phys., 2, 71 (1964).

31. Etzel, H.W. and Maurer, R.J., J. Chem. Phys., 18, 1003 (1950).

32. Kanzaki, K., Kido, K., Tamura, S. and Oki, S., J. Phys. Soc. Japan, 20, 2305 (1965).

33. Barr, L.W., Rothman, S.J., Rowe, A.H. and Selwood, P.G., Phil. Mag., 14, 501 (1966).

34. Lure, B.G., Murin, A.N. and Brigevich, R.F., Sov. Phys. Solid State, 4, 1432 (1963).

35. Murin, A.N., Banasevich, S.N. and Grushko, Yu S., Sov. Phys. Solid State, 3, 1762 (1962).

36. Reitz, J.R. and Gammel, J.L., J. Chem. Phys., 19, 894 (1951).

37. Basanni, F. and Fumi, F.G., Nuovo Cim., 11, 274 (1954).

38. Stockbarger, D.C., Rev. Sci. Instr., 10, 205 (1939).

39. Kyropoulos, S., Z. Anorg. Chem., 154, 308 (1926).

40. Czochralski, J., Z. Phys. Chem., 92, 219 (1918).

41. Corwin, J.F., J. Phys. Chem., 62, 1086 (1958).

42. "Handbook of Chemistry and Physics", Chemical Rubber Publishing Co., 46th Edition (1965-66), p.B-222.

43. Barr, L.W., Private Communication.

44. Schneider, E.E. and Caffyn, J.E., "Defects in Crystalline Solids", The Physical Society, London, 1955, p.261.

45. "Handbook of Chemistry and Physics", Chemical Rubber Publishing Co., 46th Edition (1965-66), p.E-84.

46. Fick, A., Pogg. Ann., 94, 59 (1855).

47. Chemla, M., Ann. de Phys., 1, 959 (1956).

48. Laurent, J.F. and Benard, J., J. Phys. Chem. Solids, 3, 7 (1957).

49. Laurent, J.F. and Benard, J., J. Phys. Chem. Solids, 7, 218 (1958).

50. Harrison, L.G., Morrison, J.A. and Rudham, R., Trans. Far. Soc., 54, 106 (1958).

51. Carslaw, H.S. and Jaeger, J.C., "Conduction of Heat in Solids", 2nd Edition (Oxford, 1959).

52. Leymonie, C. and Lacombe, P., "Symp. on Solid State Diffusion", North Holland Publishing Co., Amsterdam, p.37 (1958).

53. Jost, W., "Diffusion", Academic Press, N.Y., p.62 (1952).

54. Shirn, G.A., Wajda, E.S. and Huntington, H.B., Acta Met., 1, 513 (1953).

55. Barr, L.W., Private Communication.

56. Cook, G.B. and Duncan, J.F., "Modern Radiochemical Practice", (Oxford), p.79 (1952).

57. Welsh, A., Spectrochim. Acta., 7, 108 (1958).

58. Parry, E.P. and Dolman, G.W., J. Anal. Chem., 36, 1783 (1964).

59. Jost, W., J. Chem. Phys., 1, 466 (1933).

60. Mott, N.F. and Littleton, M.J., Trans. Far. Soc., 34, 485 (1938).

61. Brauer, P., Z. Naturforsch, 7a, 732 (1952).

62. Tosi, M.P. and Fumi, F.G., J. Phys. Chem. Solids, 25, 45 (1964).

63. Kurosawa, T., J. Phys. Soc. Japan, 13, 153 (1958).

64. Scholz, A., Physica Stat. Solidi, 7, 973 (1964).

65. Tessman, J.R., Kahn, A.H. and Schockley, W., Phys. Rev., 92, 890 (1953).

66. Jones, J.E. and Ingham, A.E., Proc. Roy. Soc. London, A107, 636 (1925).

67. Born, M. and Mayer, J., Zeits f. Phys., 75, 1 (1932).

68. Goldschmidt, V.M., Norske Vid. Akad. Oslo, Skr., Math. Nat. Kl., 2 (1926).

69. Pauling, L., Z. Kristallogr., 67, 377 (1928).

70. Boswarva, I.M., Private Communication.

71. Bean, C., Thesis, University of Illinois (1952).

72. Kirk, D. and Pratt, P.L., to be published.

73. Fumi, F.G. and Tosi, M.P., J. Phys. Chem. Solids, 25, 31 (1964).

74. Haven, Y., Rec. Trav. Chim., 69, 1505 (1950).

75. Haven,Y., Rept. Conf. Defects Crystalline Solids, Bristol, p.261 (1954).

76. Pratt, P.L., Private Communication.

77. Boswarva, I.M. and Lidiard, A.B., to be published.

78. Kobayashi, K. and Tomiki, J., J. Phys. Soc. Japan, 15, 1982 (1960).

79. Vineyard, G.H. and Dienes, D.J., Phys. Rev., 93, 265 (1954).